Bone morphogenetic proteins 9 & 10 in pulmonary arterial hypertension

Joshua Hodgson

Christ's College, University of Cambridge

November 2019

This dissertation is submitted for the degree of Doctor of Philosophy

Preface

This dissertation is the result of my own work and includes nothing which is the outcome of work done in collaboration except as declared in the Preface and specified in the text.

It is not substantially the same as any that I have submitted, or, is being concurrently submitted for a degree or diploma or other qualification at the University of Cambridge or any other University or similar institution except as declared in the Preface and specified in the text. I further state that no substantial part of my dissertation has already been submitted, or, is being concurrently submitted for any such degree, diploma or other qualification at the University of Cambridge or any other University or similar institution except as declared in the Preface and specified in the text

It does not exceed the prescribed word limit for the relevant Degree Committee.

Abstract

Joshua Hodgson
Bone morphogenetic proteins 9 & 10 in pulmonary arterial hypertension

Pulmonary arterial hypertension (PAH) is a rare disease initiated by dysfunction of the pulmonary vascular endothelium. Mutations in *BMPR2*, which encodes the type-II bone morphogenic protein (BMP) receptor BMPR-II, explain the majority of heritable PAH. BMPR-II forms a signalling complex, with ALK1 and endoglin, specific to endothelial cells which maintains vascular quiescence. BMP9 and BMP10 are the high affinity ligands for this signalling complex. Administering exogenous BMP9 has been shown to reverse disease in animal models of PAH, so the Morrell group is investigating the use of BMP9 as a therapy for PAH. Nonetheless, mutations in *GDF2*, which encodes BMP9, or *BMP10* had not been conclusively associated with PAH. BMP9 and BMP10 are produced as inactive *ProBMPs*, which are processed by proteases to leave an active, non-covalent Pro:BMP complex of the prodomains and growth-factor domain. The circulating levels of processed and unprocessed BMP9 and BMP10 published in current reports are inconsistent. There is also some evidence circulating BMP9 and BMP10 may be co-complexed and otherwise coregulated. BMP9 is highly expressed in livers, and high doses can regulate lipogenesis and glucogenesis *in vitro* and *in vivo*. BMP9 deficiency is reported to protect against hepatic fibrosis and damage after inducement with severe surgical and chemical interventions. In contrast, BMP9 deficient animals do not appear to develop a phenotype reminiscent of PAH.

Recently, the Morrell group discovered loss-of-function mutations in *GDF2* were associated with PAH with genome-wide significance in a rare-variant analysis. Most of the identified mutations were missense. To validate their effect *in vitro*, I compared a selection of those predicted to be pathogenic *in silico* to those predicted to be benign. Pathogenic variants were poorly secreted due to destabilisation of the interaction between the prodomains and growth-factor domain, reducing their activity. Patients carrying loss-of-function *GDF2* mutations had reduced circulating levels of both BMP9 and BMP10. Data from a combination of ELISAs, immunoprecipitations and activity assays suggested that active BMP9 circulates in healthy people, whilst inactive, unprocessed BMP10 circulates at higher levels. Circulating levels of BMP9 and BMP10 were tightly correlated, and data from immunoprecipitations and size-exclusion chromatography suggests they may circulate in macromolecular complexes. Exogenous BMP9 administered to mice was rapidly cleared from the circulation but was able to bind the lungs and activate signalling there, further demonstrating its therapeutic utility. Hepatic transcriptomes from *Gdf2* knockout mice showed evidence of reduced lipogenesis and oxidative metabolism, confirming a role for endogenous BMP9 in metabolism. We developed a protocol to measure pulmonary vascular leak in BMP9 deficient mice.

Contents

Abbreviations

ActRIIA	Activin receptor 2a: a type-II receptor for BMP9 & BMP10.
ACVRL1	Gene which encodes ALK1
ALK1	Activin like kinase receptor I. High affinity receptor for BMP9 & BMP10
ALK1-Fc	ALK1 conjugated to the Fc (constant) region of human IgG. Forms a dimer
ALP	Alkaline phosphatase. A hepatic enzyme released into serum after damage
ALT	Alanine aminotransferase. A hepatic enzyme released into serum after damage
AMC	A fluorophore which is quenched if bound to a peptide
AST	Aspartate aminotransferase. A hepatic enzyme released into serum after damage
BMP9	Bone morphogenetic protein 9 – specifically the growth factor domain.
BMPR2	The gene which encodes BMPR-II
BMPR-II	Bone morphogenetic protein receptor 2: a type-2 receptor for BMP9 & BMP10
BRE	*BMP response element*. Gene regulatory element from *ID1* promoter which binds activated SMAD proteins
BRE-HMEC1	HMEC1 cells transduced with *BRE:luciferase*
BSA	Bovine serum albumin
CADD	Combined annotation dependent depletion. A score that increases with predictions of deleteriousness. Includes sequence conservation, in silico predictions of disrupted protein structure, sequence DNAse hypersensitivity, transcription factor binding etc. Higher score = more deleterious
CHX	Cycloheximide. A translation inhibitor
Col1a1, 4a4	Genes encoding type-I and type-IV collagen respectively
EBM2	Endothelial cell basal media (Lonza)
EDTA	Ethylenediaminetetraacetic acid. Chelates multivalent cations
ELISA	Enzyme linked immunosorbent assay
ENG	Endoglin. A type-3 receptor for BMP9 & BMP10
FBS	Foetal bovine serum
GDF2	Growth and differentiation factor two. The name of the gene encoding BMP9 in mouse, humans, rat, zebrafish etc. *GDF2* is homologous to *Dorsalin* in birds.
GFD	Growth factor domain. The active, c-terminal domain of BMP9 or BMP10
hAEC	Human aortic endothelial cells. A primary, mortal cell line.
HEK-EBNA	Human embryonic kidney cells with the Epstein Barr virus gene EBNA
HEY	Hairy/enhancer of split related, a marker of Notch & BMP9 signalling

HHT	Hereditary haemorrhagic telangiectasia
HMEC1	Human microvascular endothelial cells. An immortalised line (Ades et al. 1992)
HPAH	Hereditary pulmonary arterial hypertension
ID1, ID2	Inhibitor of DNA binding 1/2. Genes encoding transcription factors ID1 and ID2 which are directly upregulated by BMP signalling
IP	Immunoprecipitation
IPAH	Idiopathic pulmonary arterial hypertension
KO	Genetic knockout
LPS	Lipopolysaccharide: derived from *E. coli*. Triggers inflammatory responses
ME1	Gene encoding malic enzyme 1 required for fatty-acid biosynthesis
PAECs	Pulmonary arterial endothelial cells (Lonza)
PAH	Pulmonary arterial hypertension
pBMP9	Pro-BMP9. May be unprocessed, in which case pBMP9 is inactive, or processed with the prodomain and growth factor domain associated non-covalently
PBS	(Dulbecco's) Phosphate buffered saline
PBST	Phosphate buffered saline supplemented with 0.05% (v/v) tween-20
PFO	Patent foramen ovale
PreProBMP9	Unprocessed BMP9 with signal peptide still present
Pro:BMP9	The non-covalent complex of BMP9 and its prodomains
ProBMP9	Unprocessed BMP9
qPCR	Quantitative polymerase chain reaction
RDW	Red cell distribution width. Percentage deviation in mean cell volume
RIPA	Cell lysis buffer with low detergent strength
SDS	Cell lysis buffer with high detergent strength
SFM	Serum free media
SMAD	*Mothers against dpp homologue:* downstream intermediates of BMP signalling
SVC	Superior vena cava
TBST	Tris-buffered saline supplemented with 0.05% tween-20
v/v	Volume of solute in volume of solvent
w/v	Weight of solute in volume of solvent
WBC	White blood cell count
WT	Genetically wildtype

Introduction

1.1. Basics of pulmonary arterial hypertension

Pulmonary hypertension refers to conditions where the mean blood pressure of pulmonary arteries increases from the normal value of 14 ± 3 mmHg at rest. Recent guidelines reduced the threshold for diagnosing pulmonary hypertension from 25 mmHg to 20 mmHg (Simonneau et al. 2013; Simonneau et al. 2019). Pulmonary arterial hypertension (PAH) specifically refers to conditions caused by obstructions in the arteries and arterioles, leading to increased pulmonary vascular resistance (>3 mmHg per L/min) and excludes pulmonary hypertension caused by left-heart dysfunction (pulmonary arterial wedge pressure must be <15 mmHg)(Galiè et al. 2016; Archer, Weir, and Wilkins 2010). PAH is known as class 1 pulmonary hypertension (table 1)(Simonneau et al. 2019).

1. Pulmonary arterial hypertension (PAH)——~16% of PH cases
   - 1.1. Idiopathic PAH (IPAH). *No known cause* ——30-50% of PAH
   - 1.2. Heritable PAH (HPAH) ——~5% of PAH
     - 1.2.1. *BMPR2* mutations ——~70% of HPAH
     - 1.2.2. *ALK1, ENG, SMAD9, CAV1,* or *KCNK3* mutations
     - 1.2.3. Unknown mutation with family history
   - 1.3. Drug and toxin induced PAH. *Anorexigens, amphetamines, SRC/ABL inhibitors, interferon therapy* ——~6% of PAH
   - 1.4. Disease associated PAH
     - 1.4.1. Connective tissue disease ——15-30% of PAH
     - 1.4.2. HIV infection ——1-6% of PAH
     - 1.4.3. Portal hypertension. *Usually associated with cirrhosis.*-5-10% of PAH
     - 1.4.4. Congenital heart disease ——10-23% of PAH
     - 1.4.5. Schistosomiasis ——20% of PAH if prevalent
   - 1.5. PAH that responds to calcium channel blockers in the long-term-~7% of PAH
   - 1.6. PAH with obvious venous/capillary involvement
   - 1.7. Persistent PH of the newborn

Table 1. World Health Organisation classifications of pulmonary hypertension (bold numbers = classification). Proportions of patients affected by different forms of the disease collated from Sionneau *et al.* 2019; Örem 2017; Lau *et al*. 2017; and Porres-Aguilar *et al*. 2012.

The division between heritable and idiopathic PAH is often unclear without genetic testing since they are often clinically and pathologically indistinguishable, and causal mutations may be found after screening idiopathic cases. Additionally, *BMPR2* mutations have been found in patients with anorexigen and congenital heart disease associated PAH, illustrating how multiple factors might contribute to disease (Ma and Chung 2017). This thesis will focus on type 1.1 and 1.2 PAH.

PAH is a rare disease (15-26 cases/million)(Peacock et al. 2007). PAH was most commonly diagnosed at 25-40 years-of-age, although mean age-of-diagnosis has increased recently to 50-65 as the number of elderly patients investigated has increased (Örem 2017;

Lau et al. 2017). Nonetheless, paediatric cases are also reported, albeit at lower frequency (~2 cases/million). Paediatric PAH often occurs alongside heterogeneous comorbidities and has some distinct genetic associations (Peacock et al. 2007; Ma and Chung 2017). PAH is generally regarded as being much more common in females (2.3 females : 1 male), although the sex difference is variable between cohorts, and may be reduced as the number of elderly patients identified increases (Örem 2017; Lau et al. 2017). Except for these factors, and those listed in table 1, hypoxia (exposure to high altitude), pollution and obesity are being investigated as risk factors for PAH (Sofianopoulou et al. 2019).

Preclinical disease may evolve for some time before manifesting clinical symptoms. The pulmonary circulation initially compensates for disease effectively and people are not routinely screened for PAH. The right ventricle compensates for increasing pulmonary vascular resistance by hypertrophy to contract with enough force to maintain cardiac output. This leads to progressively worsening pulmonary pressures and increased ventricular strain (figure 1). The peak-cardiac output attainable during exercise falls as the heart becomes dilated and pulmonary resistance increases.

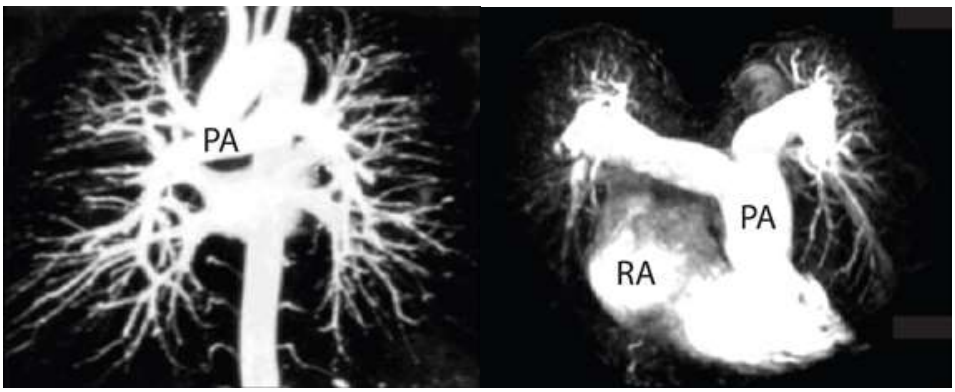

Figure 1. MRI angiograms of chest. Left: healthy person. Right: PAH patient showing obliterated distal pulmonary arteries, pressure over-loaded proximal pulmonary arteries and distended right-heart. PA = pulmonary artery, RA = right atrium. Adapted from Sutendra and Michelakis (2013).

Patients typically present with progressive unexplained breathlessness, fainting, chest-pain, tiredness and reduced ability to exercise (table 2). Diagnosis is via right-heart catheterisation of patients with suspect echocardiograms, but at this point, patients usually have substantial heart and vascular disease. Maximal cardiac output gradually falls as the right ventricle fails, until patients are unable to cope with normal activities. Additionally, patients may develop oedema as venous pressure increases as a result of volume overload. Patient prognosis is best predicted by how quickly their cardiac output deteriorates, but 50% mortality occurs ~3 years after diagnosis without treatment, and after ~6 years with current treatments (Lau et al. 2017; Thenappan et al. 2007; Benza et al. 2012).

World Health Organisation functional classes of pulmonary hypertension:

1. Patients with PH but without any limitation on ordinary physical activity
2. PH patients comfortable at rest, but with some undue symptoms from ordinary activity
3. PH patients comfortable at rest, but with undue symptoms from less than ordinary activity
4. Patients unable to carry out any activity without symptoms. Signs of heart failure.

Table 2.

PAH patients are primarily prescribed vasodilators which reduce pulmonary arterial resistance and increase cardiac output, including nitric oxide potentiators, endothelin-receptor antagonists and prostacyclin analogues (Lau et al. 2017; Jasińska-Stroschein and Orszulak-Michalak 2017). Additionally, ~5% of PAH patients sustain a long-term vasodilatory response to Ca^{2+} channel blockers, which substantially improves their prognosis. A potentially curative treatment route is heart-lung transplant. However, due to the demands of the operation, only carefully selected patients are suitable. Lung transplants themselves have a poor long-term prognosis, so survival (50% after 5 years) is not much improved.

1.2. Aetiology of pulmonary arterial hypertension

1.2.1. Genetic disposition to pulmonary arterial hypertension

Pulmonary arterial hypertension can afflict several members of sequential generations in some families (Dresdale, Michtom, and Schultz 1954). In 2000, researchers identified that familial PAH was associated with loss-of-function mutations in *BMPR2* (International PPH Consortium 2000; Deng et al. 2000). Subsequent analyses found 53-86% of familial PAH cases, and 14-35% of patients regarded as idiopathic, are explained by >400 different *BMPR2* mutations (Ma and Chung 2017; Archer, Weir, and Wilkins 2010; Soubrier et al. 2013).

BMPR2 encodes a type-II receptor for the transforming growth-factor beta (TGFβ) superfamily of ligands. PAH-associated mutations are heterozygous loss-of-function and include rearrangements, copy number variants, frameshifts, missense and nonsense variants throughout the gene (Thomson et al. 2000; Cogan et al. 2005, 2006; Aldred et al. 2006). Truncating mutations (~70% of PAH-associated *BMPR2* mutations) lead to haploinsufficiency, whilst missense mutations either cause retention within the endoplasmic reticulum or abolish activity (Rudarakanchana et al. 2002; Sobolewski et al. 2008). *BMPR2* mutation carriers are diagnosed younger than idiopathic PAH patients, and have worse haemodynamics, functional class and survival, highlighting the importance of BMPR-II signalling in both the initiation and progression of PAH (Rosenzweig et al. 2008; Evans et al. 2016).

BMPR2 mutations are not highly penetrant: approximately 20-30% of carriers develop disease (Ma and Chung 2017; Machado et al. 2005; Aldred et al. 2010). This indicates

additional genetic or environmental factors must influence disease development. For example, in a longitudinal study, *BMPR2* mutation penetrance was higher in females (~42%) than males (~14%)(Larkin et al. 2012). Patients carrying mutations in multiple PAH-associated genes have been reported, but this requires validation with large cohorts (Pousada, Baloira, and Valverde 2016). Intriguingly, BMPR-II protein levels and downstream intermediaries, are downregulated in *BMPR2* mutation carriers, idiopathic cases of PAH and inducible animal models of PAH (Archer, Weir, and Wilkins 2010; Ramos et al. 2008; Long et al. 2015). Hence non-genetic or epigenetic suppression of BMPR-II signalling could play a role in PAH.

More rarely, heritable PAH is associated with loss-of-function mutations in other components of the BMPR-II signalling pathway (see 1.3.1)(Ma and Chung 2017; Miyazono, Kamiya, and Morikawa 2010; Machado et al. 2009). These include: *ACVRL1*, which encodes activin receptor-like kinase-1 (ALK1)(Harrison et al. 2003; Gräf et al. 2018); *ENG*, which encodes endoglin—a co-receptor (Chaouat et al. 2004); and *SAMD1, SMAD4* and *SMAD9*, which encode downstream signalling intermediates of BMPR-II (Nasim et al. 2011; Shintani et al. 2009; Drake et al. 2011; Gräf et al. 2018). Most recently, *GDF2*, which encodes the ligand BMP9, and *BMP10*, which encodes a ligand with a very similar structure to BMP9, mutations were found to cause PAH (Wang et al. 2016; Eyries et al. 2019; Wang et al. 2019; Gräf et al. 2018). Notably, *ACVRL1* mutation carriers have an even earlier mean age of diagnosis, worse haemodynamics and faster disease progression than *BMPRR2* mutation carriers (Girerd et al. 2010). *Bmpr2, Acvrl1* and *Smad9* heterozygous knockout mice may spontaneously develop PAH-like hypertension and/or vascular remodelling (Long et al. 2015; Huang et al. 2009; Jerkic et al. 2011; Beppu et al. 2004). However, only a minority of mice may be affected (Hong et al. 2008). This may be exacerbated by inflammatory stimuli or combined *Bmpr2/Smad9* mutation (Long et al. 2015; Song et al. 2005).

Rare, causal mutations in genes without clear links to BMPR-II signalling have also been reported in PAH. Examples include: *CAV1,* which encodes caveolin 1, an architectural protein of the plasma membrane that can modulate TGFβ signalling (Austin et al. 2012); *KCNK3,* which encodes a potassium channel facilitating smooth-muscle polarisation and vasodilation (Ma et al. 2013); and *TBX4*, mutations in which are predominately associated with paediatric PAH (<10% children versus ~0.1% of adults), have a milder prognosis than IPAH, and may co-present with other conditions like small patella syndrome (Zhu et al. 2019; Navas et al. 2016; Kerstjens-Frederikse et al. 2013).

Recently, whole-genome and exome sequencing studies of large cohorts of PAH patients and controls have been undertaken (Gräf et al. 2018; Wang et al. 2019; Zhu et al.

2019; Eyries et al. 2019). These studies have confirmed the association of *BMPR2, ACVRL1, ENG, SMAD9, KCNK3,TBX4,* and *GDF2* with PAH. Notably, *GDF2* loss-of-function was highly significantly associated with PAH, and this was driven by missense mutations predicted to disrupt protein structure *in silico* (Gräf et al. 2018; Wang et al. 2019; Zhu et al. 2019).

Novel genes were putatively associated with PAH in one or more of these studies: *AQP1*, which encodes aquaporin 1, the water channel; *ATP13A3*, which encodes a transmembrane ATPase (also implicated in Barozzi *et al.* 2019); *SOX17*, which encodes a transcription factor active in endothelial cells during development; *KDR,* which encodes vascular endothelial growth-factor receptor-II; *KLK1,* which encodes kallikrein 1, and is produced by endothelial cells for systemic blood pressure regulation and vascular remodelling; *GGCX,* which encodes an enzyme associated with coagulation disorders; and *BMP10*.

Gräf *et al.* and Wang *et al.* used burden tests to associate genes with disease because each individual variant is so rarely found within PAH. Therefore, the association of novel genes with PAH rests on *in silico* predictions of variants' deleteriousness and their rarity in control cohorts. To validate these findings, the Morrell group has undertaken to experimentally determine the effects of putatively pathogenic variants in *ATPA13A3, SOX17, AQP1* and *GDF2.*

Not all coding variation was reported in these studies due to technical and stochastic factors. For example, two patients carrying large deletions including *GDF2* were not reported in Gräf *et al.* because current technologies are not efficient at detecting structural variation. Similarly, the frequency of PAH cases associated with mutations in each gene varies between cohorts. This could reflect different ethnicities, environments and inclusion criteria, or be due to random variation.

The contribution of rare non-coding variants to PAH has not been explored fully because it is difficult to determine their pathogenicity and many previous studies have used exome sequencing. Common variants are expected to have small effect-sizes, so it is difficult to gather sufficiently large cohorts of PAH patients to identify them. Nonetheless, genome-wide association studies have been carried out for PAH, identifying risk loci close to a *SOX17* enhancer (Rhodes et al. 2019); *HLA-DPA1/DPB1* encoding the MHC-II complex (Rhodes et al. 2019); and *CBLN2*, encoding cerebellin 2, which is highly expressed on pulmonary vascular endothelial cells (Germain et al. 2013).

In summary, *BMPR2* loss-of-function mutations are by far the largest contributor to heritable PAH. Nonetheless, identifying other genes involved in PAH through human genetic studies will refine our understanding of disease pathways, aid the identification of druggable

targets, and help provide an explanation for patients suffering from unexplained PAH (Morrell, Aldred, et al. 2019). Most PAH-associated genes are in the BMP9/ALK1/BMPR-II signalling pathway, making this a preeminent potential therapeutic target.

1.2.2. Environmental triggers of pulmonary arterial hypertension

Environmental triggers of PAH are diverse even though they generally cause histologically indistinguishable disease. An inflammatory milieu may be important: infections and autoimmune diseases create highly inflammatory environments, disrupt endothelial integrity, and can lead to PAH in a high proportion of patients. In genetically predisposed animals and cells, lipopolysaccharide, 5-lipoxygenase and tumour necrosis factor-α induced inflammation can exacerbate PAH-like phenotypes (Kiskin et al. 2018; Soon et al. 2015; Hurst et al. 2017; Song et al. 2005; Tian et al. 2019).

An initial pressure overload may trigger the development of pulmonary vascular lesions that lead to the development of lasting PAH. Congenital heart disease leads to PAH in 15-30% of patients because blood shunting at high pressure from the left-ventricle to the right-ventricle leads to over-loading of the pulmonary vasculature. Correcting the heart defect does not necessarily prevent the escalation of PAH, which indicates some positive-feedbacks or a common cause for both morbidities (Brida and Gatzoulis 2018). For example, *BMPR2* mutations are found in 6% of combined PAH-CHD cases (Roberts et al. 2004).

Similarly, ~7% of patients with hepatic portal vein hypertension develop PAH, perhaps because blood shunts into the right-heart, over-loading the pulmonary vasculature (Porres-Aguilar et al. 2012). In small cohort studies, around three-quarters of portopulmonary hypertension resolved after liver transplant (Ashfaq et al. 2007; Hollatz et al. 2012). Hepatic cirrhosis also releases various inflammatory signals, and inhibits BMP9 secretion, which could contribute to PAH (Nikolic et al. 2019; Upton unpublished).

1.2.3. Pathobiology of pulmonary arterial hypertension

Human samples necessarily come from late-stage disease. Small arteries (<200 μm) from these patients show thickening and fibrosis of the intima (concentric intimal fibrosis). Additionally, medial smooth-muscle cell layers become expanded with disorganised cells, thickened extracellular matrices and fibrosis (figure 2). These changes lead to greatly narrowed vessel lumens (Archer, Weir, and Wilkins 2010; Hoeper et al. 2013). Plexiform lesions, which are tangles of small channels found adjacent to small arteries, comprised of proliferative endothelial, smooth-muscle and fibroblast cells, are found distally to vessel branch-points in ~50% of PAH patients (Tuder et al. 2007).

There is compelling evidence that endothelial dysfunction underlies the earliest stages of PAH (Budhiraja, Tuder, and Hassoun 2004; Xu and Erzurum 2010; Toshner et al. 2009). Endothelial cell-specific knockout of *Bmpr2* is sufficient to predispose mice to a PAH-like phenotype including pulmonary hypertension and vascular remodelling (Hong et al. 2008). Intriguingly, a patient with congenital heart disease associated PAH was found to have a *SMAD9* deletion in pulmonary artery endothelial cells, but not other pulmonary cell-types (Drake et al. 2015). A wave of endothelial cell apoptosis is believed to be among the earliest events in PAH. This may facilitate the expansion of metabolically dysfunctional, angiogenic endothelial cells which stain strongly for markers of hyper-proliferation (Cool et al. 1999; Xu and Erzurum 2010).

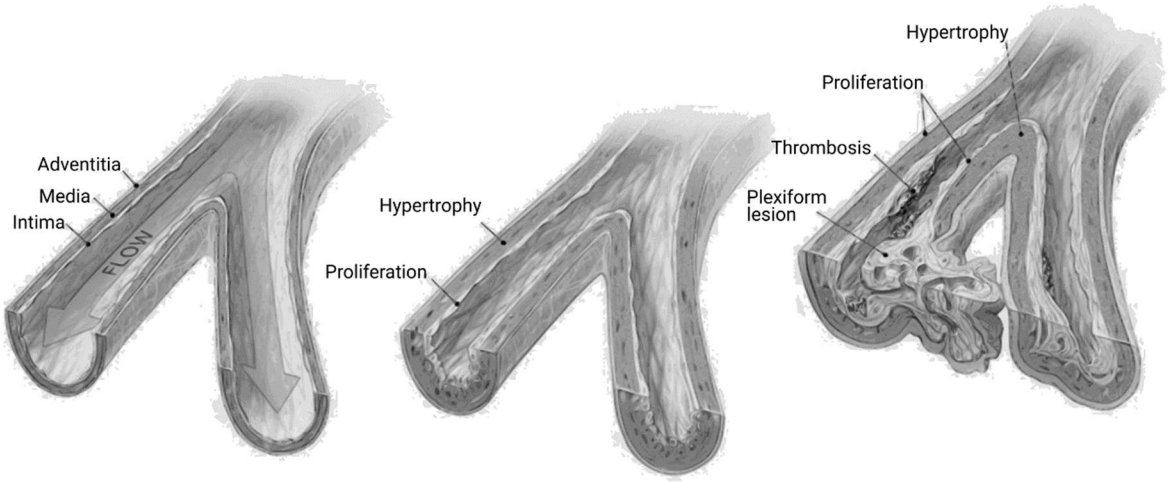

Figure 2. Vessel pathology in pulmonary arterial hypertension. **Left:** healthy pulmonary artery, **middle:** early stages of intimal dysfunction and wall thickening, **right:** advanced disease with intimal and adventitial proliferation, media thickening and angiogenic plexiform lesions. Redrawn from Gaine (2000).

In PAH, endothelial cells over-produce vasoconstrictive paracrines, such as endothelin-1 and serotonin, which drives smooth-muscle cell constriction and proliferation (Budhiraja, Tuder, and Hassoun 2004; Eddahibi et al. 2006). Endothelial cells also downregulate vasodilatory paracrines, such as prostacyclin, vasoactive intestinal peptide and nitric oxide, which removes anti-proliferative signals (Budhiraja, Tuder, and Hassoun 2004). Additionally, endothelial cells from PAH patients, or with *BMPR2* mutations, form monolayers with reduced integrity which may allow serum factors and inflammatory cells to egress into the smooth-muscle and fibroblast layers (Rabinovitch 1999; Burton et al. 2011).

Pulmonary artery smooth-muscle cells and fibroblasts express *BMPR2*, but at lower levels than pulmonary artery endothelial cells. In smooth-muscle cells, BMPR-II signalling is anti-proliferative, anti-hypertrophic, and pro-apoptotic (Tajsic and Morrell 2011). Mice expressing *Bmpr2* truncating transgenes only in smooth muscle can develop PAH

spontaneously (West et al. 2008). Thus BMPR-II signalling in smooth-muscle protects against PAH, but it is not ALK1-mediated and is more responsive to ligands other than BMP9 (Lagna et al. 2006; Yu et al. 2008; Morrell et al. 2001; Long et al. 2015). Dysfunctional endothelial cell signalling is believed to be the preeminent factor driving smooth-muscle and fibroblast cells to remodel pulmonary arteries through growth, migration and extracellular matrix synthesis (Tajsic and Morrell 2011).

In summary, the lesions found in PAH are complex and profoundly dysfunctional. However, an initial endothelial dysfunction, in response to impaired BMPR-II signalling, inflammation or pressure overload, appears to trigger progressive vessel remodelling. Pulmonary arteries become obliterated, constricted and fibrotic. BMP9 signalling on endothelial cells is a key way to study PAH development *in vitro*.

1.2.4. Overlap between PAH & HHT

Several genes involved in BMP9 signalling are associated with the disease hereditary haemorrhagic telangiectasia (HHT). HHT is a dysplasia of the vasculature consisting of poorly muscularised, dilated and tortuous arterioles and venules in the mucosa, hands, brain, spine, gut, liver and lung (figure 3)(Abdalla and Letarte 2006). This is driven by endothelial cell dysfunction. Some reports suggest plexiform lesions found in PAH are derived from bronchopulmonary anastomoses (Galambos et al. 2016) which could be compared to the arteriovenous anastomoses of HHT. Thus, there is genetic and phenotypic overlap between PAH and HHT (Vorselaars et al. 2015; Faughnan, Granton, and Young 2009).

Loss-of-function mutations in *ACVRL1* (Tørring et al. 2014); *ENG* (Tørring et al. 2014; Saito et al. 2017), *SMAD4* (Tørring et al. 2014; Gallione et al. 2006); and *GDF2* (Wooderchak-Donahue et al. 2013; Hernandez et al. 2015) are reported in HHT-like syndromes (table 3). *ACVRL1* and *ENG* mutations cause HHT much more often than PAH (Shovlin 2014). However, HHT (125-200 cases/million) is much more common than PAH.

Some HHT patients (<1%), including a high proportion (<20%) of *ACVRL1* mutation carriers, also suffer from PAH (McDonald et al. 2015; Harrison et al. 2003; Vorselaars et al. 2015). The histology and haemodynamics of HHT-PAH is often indistinguishable from classical PAH (Harrison et al. 2003; Prigoda 2006; Abdalla et al. 2005; Faughnan, Granton, and Young 2009). Notably, 7/9 of *ACVRL1* mutation carrying PAH patients manifested with HHT after PAH so longitudinal reassessments are needed to describe the co-incidence of disease (Girerd et al. 2010). Nevertheless, some argue *GDF2* mutations do not cause HHT based on the weak evidence mutations are not found in all cohorts (Tørring et al. 2016).

Classification of hereditary haemorrhagic telangiectasia:
HHT1. *ENG* mutations. *80% lead to premature STOP codons* ——————<50% of HHT
HHT2. *ACVRL1* (ALK1) mutations. *~50% missense, rest loss-of-function*——<40% of HHT
HHT3. Unknown gene linked to 5q31.3-q32
HHT4. Unknown gene linked to 7p14
HHT5. *GDF2* mutations. *Loss-of-function missense*————————————~1.6% of HHT
JPHHT. *SMAD4* mutations. Combined juvenile polyposis-HHT. *Loss-of-function*-1-2% of HHT

Table 3. Details were collated from Ma and Chung 2017; Abdalla and Letarte 2006; and McDonald et al. 2015.

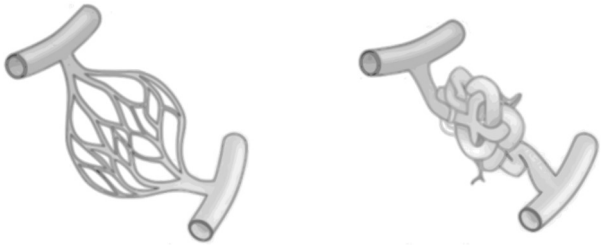

Figure 3. Arteriovenous malformations in hereditary haemorrhagic telangiectasia. Left: normal blood vessel architecture. Right: arteriovenous malformation showing tortuous vessels, dilated pre-capillaries and capillary bypass. Redrawn from Crist *et al*. (2019).

1.3. BMP9, BMP10/ALK1/BMPR-II/Endoglin signalling

1.3.1. Receptor activation

Endothelial cells are constitutively stimulated by circulating BMP9 via the ALK1/BMPR-II/endoglin complex (David et al. 2008). BMPR-II is expressed on numerous cell-types, but its expression is strong in pulmonary artery endothelial cells. BMPR-II is a type-II receptor serine/threonine kinase with low affinity for BMP2,4,7,9 and 10. ALK1is a type-I receptor serine/threonine kinase with high affinity for BMP9 and BMP10, most highly expressed by endothelial cells, especially in arteries proximal to the heart, and is particularly highly expressed by pulmonary artery endothelial cells (David et al. 2007; Mahmoud et al. 2009; Seki, Yun, and Oh 2003; Corti et al. 2011; Panchenko et al. 1996). Endoglin is almost exclusively expressed by endothelial cells, highly expressed on pulmonary artery endothelial cells, and can bind BMP9 and BMP10 with very high affinity (Saito et al. 2017; Mahmoud et al. 2009). Endoglin does not appear to have catalytic activity, and can be expressed at the cell surface, with a small intracellular domain, or cleaved and released into the blood.

It is difficult to crystallise tertiary BMP9 signalling complexes and aspects of BMP9 signalling have been inferred from other ligands/receptors which may behave differently. Nonetheless, the relative affinities and binding surfaces of each receptor lead to the following model of BMP9 and BMP10 signalling (figure 4):

1. Active BMP9 and BMP10 are dimers in non-covalent complexes with their prodomains (Bidart et al. 2012; Jiang et al. 2016).

2. At the apical surface of endothelial cells, two molecules of ALK1 form a high affinity complex with one BMP dimer. Two molecules of endoglin are likely present in the receptor complex (Alt et al. 2012; Barbara, Wrana, and Letarte 1999; Blanco et al. 2005). This may take place near the primary cilium and caveolae (Goetz and Anderson 2010; Vion et al. 2018).
3. Two molecules of BMPR-II or ActR-II are then recruited (Upton et al. 2009). The BMP9/10 prodomains must be displaced to allow BMPR-II binding, and there is some evidence prodomains are released from the cell-surface (Kienast et al. 2016; Jiang et al. 2016).
4. BMPR-II phosphorylates the cytoplasmic side of itself and ALK1. The cytoplasmic tail of endoglin may become phosphorylated, and this may facilitate activation of the complex (Morris et al. 2011; Blanco et al. 2005). The receptor complex then recruits and phosphorylates receptor regulated SMADs, predominantly SMAD-1/5/9 complexes, but sometimes SMAD-2 (Miyazono, Kamiya, and Morikawa 2010; Upton et al. 2009). These complex with the common partner SMAD-4 and translocate to the nucleus.
5. The SMADs behave as weak transcriptional activators/repressors, acting in concert with cell-type specific factors to drive responses characteristic of the ligand, concentration and tissue (Miyazono, Kamiya, and Morikawa 2010; Schmierer and Hill 2007).

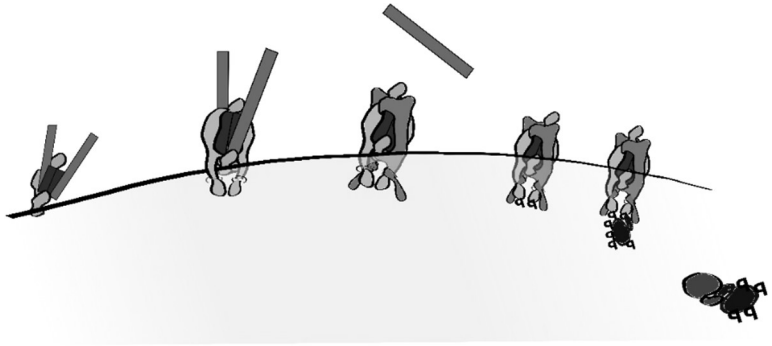

Figure 4. High-affinity BMP9 receptor complex of endothelial cells. Left-to-right: Endoglin binds the ligand, followed by ALK1. BMPR-II or ActR-II joins the complex, displacing the prodomains. ALK1 phosphorylates the cytoplasmic tail of the type-II receptor, and the activated complex phosphorylates R-SMADs. The activated R-SMADs complex with the co-SMAD and translocate into the nucleus. Based on Tillet and Bailly (2015).

Conclusive evidence shows BMP9 and BMP10 primarily act through the ALK1/[BMPR-II/ActR-II]/endoglin complex:

- BMP9 and BMP10 have the closest amino-acid sequence homology of any two BMPs, but are most divergent from other BMPs and well conserved across vertebrates (Ducy 2000)
- Both have high affinity for ALK1 in cell-free assays (Brown et al. 2005; Townson et al. 2012)
- Both bind ALK1, ActR-II and endoglin tightly in crystal structures (Brown et al. 2005; Saito et al. 2017; Townson et al. 2012)

- Both have activity at pg/ml levels on endothelial cells (David et al. 2007; Baeyens et al. 2016)
- BMP9 activity is reduced when each of these receptors are silenced (David et al. 2007; Upton et al. 2009; Lawera et al. 2019)
- BMP9 activity can be mimicked by overexpressing endoglin and ALK1 (David et al. 2007)
- Radiolabelled BMP9 is co-immunoprecipitated with BMPR-II, ActR-II, ALK1 and endoglin from endothelial cells (Scharpfenecker et al. 2007)

Conversely, conclusive evidence shows BMP9 and BMP10 are the preeminent ligands for the ALK1/[BMPR-II/ActR-II]/endoglin complex:

- BMP9 and BMP10 are at active concentrations in blood (David et al. 2008; Jiang et al. 2016)
- Soluble ALK1 and endoglin can neutralise serum activity whereas ALK2,3,4,5,7, BMPR-1B,1A, and ActR-1B cannot (David et al. 2008; Brown et al. 2005; Nikolic et al. 2019)
- Anti-BMP9 can neutralise serum activity, whereas anti-BMP2,4,7, anti-TGFβ and noggin (an inhibitor of BMP2,4,5,6,7,13,14) cannot (David et al. 2008; Lux, Attisano, and Marchuk 1999). In contrast, Herrera and Inman (2009) show anti-BMP4 and 6 can neutralise a minor proportion of serum activity compared to anti-BMP9, but they used a 16-hour time-course which may result in cells being stimulated by any BMP4 and 6 they produced themselves.
- TGFβ1 and TGFβ3 can signal through ALK1, but unlike BMP9 and BMP10, only in the presence of ALK5 (Goumans et al. 2002)
- BMP9 exerts a strong effect on the transcriptome of pulmonary artery endothelial cells and blood outgrowth endothelial cells, whilst BMP2,4,6 have negligible effects (Long et al. 2015)
- BMP9 induces stable SMAD1/5 phosphorylation in endothelial cells over time, whilst other members of the TGFβ superfamily do not (David et al. 2007; Goumans et al. 2002)
- BMP9 and BMP10 can directly bind endoglin in cell-free assays, but neither BMP2,2/7,3, 3b,4,4/7,5,6,7,8b,15, GDF3,5,6,8,9b,11,15, TFGβ1,β3,β4, MIS, nodal, activin-A,B,C,AC,AB, artemin, neurturin, persephin, glial cell-derived neurotrophic factor, nor brain-derived neurotrophic factor can (Castonguay et al. 2011)
- Other members of the TGFβ superfamily adopt different conformations and have different receptor binding residues to BMP9 and BMP10 (Brown et al. 2005; Townson et al. 2012).

1.3.2. Biases in receptor activation

It is not straightforward to elucidate exactly what effects ALK1/BMPR-II signalling has on endothelial cells. This is because cells also express other type-I and type-II receptors, which signal through overlapping downstream pathways. ALK1 is the receptor with highest affinity

for BMP9 and is the most highly expressed type-I receptor on endothelial cells. Nonetheless, many experiments use supraphysiological doses of BMP9 which may activate other type-I receptors, or supraphysiological doses of other BMPs which may activate ALK1.

Secondly, a proportion of BMP9/ALK1 complexes recruit an alternative type-II receptor, activin type-II receptor (ActR-II), instead of BMPR-II (Townson et al. 2012; Upton et al. 2009; Kienast et al. 2016). ALK1/BMPR-II and ALK1/ActR-II signalling induce many overlapping effects to different extents, and this is hypothesised to be why ALK1 and BMP9 deficiency can lead to both HHT and PAH, whilst BMPR-II deficiency only leads to PAH (Upton et al. 2009).

Brown *et al.* (2005) measured the adsorbance of BMP9 onto BIAcore chips coated with different type-I and type-II receptors using surface plasmon resonance. They found BMP9 had highest affinity for ALK1-Fc followed by BMPR-II-Fc. BMPR-II's affinity for BMP9 was 3.5 fold higher than ActR-IIa-Fc, and 13 fold higher than ActR-IIb-Fc. However, Townson *et al.* (2012) used very similar reagents and reported ActR-IIb's affinity for BMP9 was ~30 fold higher than BMPR-II and ~300 fold higher than ActR-IIa, whereas BMP10 had similar affinity for all three receptor complexes. Mi *et al.* (2015) used an ELISA-based method to show BMP9 does not discriminate between BMPR-II and ActR-IIb, but has ten-fold lower affinity for ActR-IIa. However, in the presence of its prodomains, Pro:BMP9 has a ten-fold higher affinity for ActR-IIb than BMPR-II, and does not bind ActR-IIa (Mi et al. 2015). Both BMP9 and BMP10 bind to endoglin with similarly high affinity in BIAcore experiments (Blanco et al. 2005).

Therefore, BMP9 and BMP10 could have different activities depending on features of the receptor complex. For example, BMP10 may signal in the heart differently to BMP9 (see 1.5.5), and BMP9 inhibits myeloma proliferation with high affinity whereas BMP10 cannot (Olsen et al. 2014). Nonetheless, many different endothelial cell types appear to respond to BMP9 in a similar way, BMP9 and BMP10 growth-factor domains have extremely similar structures, are believed to interact with receptor complexes in the same way, and endothelial cells treated with BMP9 and BMP10 have very similar responses (Li *et al* unpublished).

In summary, the BMP9/ALK1/BMPR-II signalling axis is active on endothelial cells, especially pulmonary artery endothelial cells. Loss of components of this axis is expected to impair the protective functions of this signalling. There is potentially some redundancy between ligands, receptors and intermediates, although there are biases in the responses of each. Signal duration and intensity faithfully determines nuclear SMAD activity, so it is difficult to predict exactly how each ligand will affect different cell-types and influence disease (Schmierer and Hill 2007).

1.3.3. Flow & BMP9 signalling

Both blood flow and BMP9 can stimulate endothelial quiescence, vasodilation and reduced proliferation (Baeyens et al. 2016; Laux et al. 2013). This is partly mediated via ALK1 signalling:

- ALK1 loss induces similar transcriptional changes to loss of flow (Laux et al. 2013)
- Knocking out flow responsive genes mimics the phenotype of ALK1 deficiency, including formation of arterio-venous malformations (Laux et al. 2013; Baeyens et al. 2016)
- Flow does not stimulate quiescence if BMP9 is completely absent (Baeyens et al. 2016)
- High shear-stress upregulates ALK1 (Seki, Yun, and Oh 2003)
- Flow sensitises cells to BMP9 (Zhou et al. 2012; Baeyens et al. 2016)
- *Smad* deficiency disrupts artery size only after the heart begins beating (Poduri et al. 2017)
- ALK1 or *Smad* deficiency leads to dysfunctional migration of endothelial cells with respect to direction of flow (Rochon, Menon, and Roman 2016; Poduri et al. 2017)
- Fish without a heart-beat have reduced ALK1 signalling (Laux et al. 2013)

In cell free assays, the EC_{50} of ALK1 for BMP9 is ~50 pg/ml, which is close to the EC_{50} of endothelial cells (40-60 pg/ml) *in vitro* (Kienast et al. 2016; Vion et al. 2018). Under flow, cells' sensitivity seems to increase to 3.5-10 pg/ml at high flow, and just ~1.3 pg/ml in gentle flow (Baeyens et al. 2016; Vion et al. 2018). Laux *et al.* hypothesised that endothelial cells sense flow via rate of BMP10 delivery—in fish without heartbeats, injecting BMP10 can restore ALK1 signalling at the site of injection. However, flow may also cause the rearrangement of cell-surface receptors, changing their signalling dynamics, which endothelial cells may use to sense flow (Franco and Gerhardt 2016). Interestingly, flow increases the physical association of ALK1 with endoglin, and endoglin is required for the potentiation of BMP9 signalling by flow (Baeyens et al. 2016).

In endothelial cells, ALK1 and SMADs localise to the base of the primary cilium, a mechano-chemo sensory organelle which protrudes into the vessel lumen (Goetz and Anderson 2010; Vion et al. 2018). Endothelial cells unable to form primary cilia do not show greater sensitivity for BMP9 under gentle-flow compared to high-flow (Vion et al. 2018). Conversely, normal endothelial cells show reduced migration compared to cells lacking primary cilia only in the presence of BMP9. In combination, these effects mean loss of the primary cilium primarily disrupts angiogenesis in regions of low-flow *in vivo*, possibly because cells here are less responsive to BMP9 than normal (Vion et al. 2018).

In summary, endothelial cells seem to respond to flow partly by determining the strength of ALK1 signalling. Similarly, the potency of circulating BMP9 or BMP10 is partly determined by flow. This modulates the effects of BMP9 and BMP10 *in vivo*.

1.4. Physiology of BMP9 & BMP10

1.4.1 Sources of BMP9 & BMP10

BMP9 is most highly expressed in the livers of zebrafish, mice and humans. However, no two reports agree on a particular secretory cell-type (figure 5; table 4). Miller *et al.* isolated liver sinusoidal cells, hepatic stellate cells, liver endothelial cells, Kupffer cells and hepatocytes, and maintained them in culture. They looked for *Gdf2* mRNA in these cultures with ribonuclease protection assays, and BMP9 protein by Western blotting. The results from cultured cells should be treated with scepticism, since hepatic cell cultures are notoriously difficult to purify and often represent incorrect cell-types (Elvevold, Smedsrød, and Martinez 2008). Moreover, cultured cells often have a different transcriptional profile to cells *in vivo.*

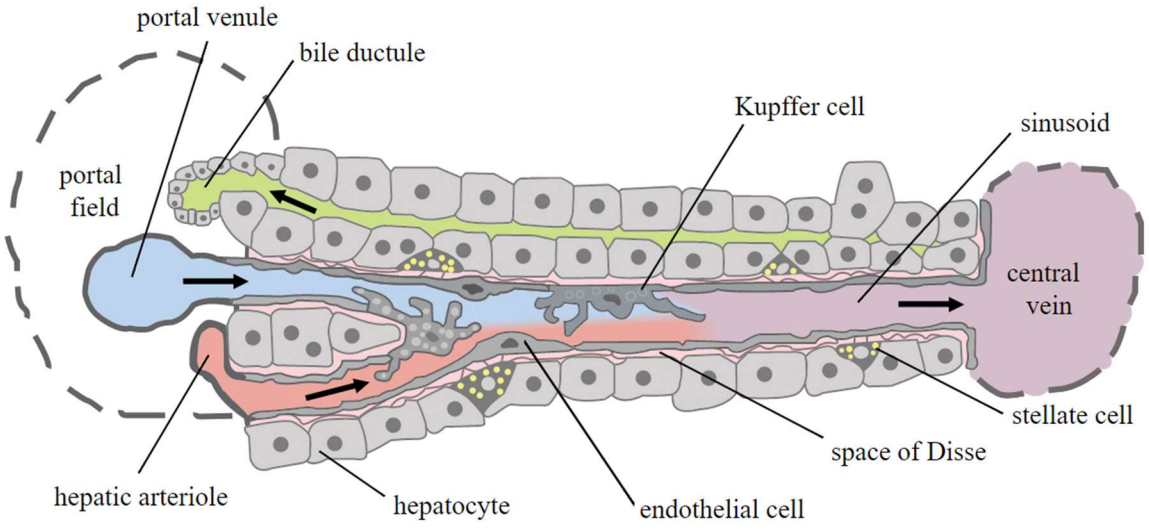

Figure 5. Hepatic cell-types. Modified from Frevert *et al.* (2005).

Bidart *et al.* bought RNA from specific hepatic cell-types, assessed *GDF2* mRNA levels by qPCR and validated the qPCR results by immunostaining human and mouse tissue sections. Cells which stain strongly for BMP9 are not necessarily the cells which secrete it, since it is a diffusible ligand, and has been shown to bind various hepatic cell-types (Miller et al. 2000; Truksa et al. 2006). Breitkopf-Heinlein *et al.* isolated hepatocytes, liver sinusoidal endothelial cells, Kupffer cells and hepatic stellate cells from mice, and bought human hepatic stellate cells. They assessed *Gdf2* expression by qPCR. They showed that hepatic stellate cells in culture maintain *GDF2* expression over-time and demonstrated they secrete BMP9 by ELISA.

Finally, Tillet *et al.* used RNA-*in situ* hybridisation, to show *Gdf2* expression in mouse livers. Whilst *in situs* are the best way to identify which cell-types express BMP9 *in vivo*, Tillet *et al.* did not use any counter stains, so relied entirely on cell-shape to define all Gdf2 positive cells as hepatic stellate cells.

	Miller *et al.* (2000)	Breitkopf-Heinlein *et al.* (2017)		Bidart *et al.* (2012)		Tillet *et al.* (2018)
	Rat	Mouse	Human	Mouse	Human	Mouse
Hepatic stellate cells	+++	+++	++	Cannot asses	Negligible	++
Sinusoidal endothelial cells	Not tested	+	Possibly	Cannot asses	Negligible	—
Liver endothelial cells	+	Not tested	Possibly	Cannot asses	Not tested	Cannot asses
Kupffer cells	+	+	Not tested	Cannot asses	Not tested	—
Hepatocytes	—	Negligible	Negligible	+	+	—
Intrahepatic biliary epithelial cells	Not tested	Not tested	—	+	+++	Cannot asses
Non-parenchymal cells	++	Not tested	Not tested	Cannot asses	Not tested	Cannot asses

Table 4. *GDF2* expressing cell-types identified in different publications. + indicates cell-type expresses *GDF2,* with more +s indicating higher expression. — indicates cell-type does not express *GDF2.*

Miller *et al.* also assessed whole rat tissues and found *Gdf2* expression in liver, but not bone, skin cartilage, intestine, lung, skeletal muscle, spleen, pancreas, brain, kidney, heart nor stomach. Bidart *et al.* assessed twelve types of frozen human tissue by qPCR and found high expression in the liver, but also much lower expression in lung, and even lower expression in brain and skeletal muscle. Li *et al.* (2018) and Chen *et al.* (2013) also report *GDF2* expression in lung, at lower levels than liver, in mouse and humans. Inconsistency in organs identified compared to Miller *et al.* could be species specific, or because qPCR is more sensitive.

BMP10 is expressed in myocardiocytes forming ventricular trabeculae in embryonic hearts (Neuhaus, Rosen, and Thies 1999). As development continues, expression is mostly restricted to the right-atrium, although there is some expression in the left atrium (Neuhaus, Rosen, and Thies 1999; Jiang et al. 2016). *BMP10* expression, as measured by qPCR, is much higher in the liver of adult mice than all other organs, except the right atrium where

expression is much higher still (Tillet et al. 2018). Tillet *et al.* used RNA-*in situ* hybridisation to identify hepatic stellate cells as a source of BMP10, with the same caveats as before.

In summary, BMP9 is secreted from the liver. The strongest evidence suggests that hepatic stellate cells produce BMP9, but it is very possible other cell-types do also. BMP10 is secreted from the right atrium. However, we cannot know whether all circulating BMP9 and BMP10 is secreted from the liver and right atrium respectively without generating organ-specific knockouts. It seems likely that some BMP9 is produced in the lungs and may act as a paracrine here. Some BMP10 seems to be produced by the liver. Expression localisation could be important for how BMP9 and BMP10 ligands reach the pulmonary vascular endothelium.

1.4.2. BMP9 & BMP10 secretion and processing

BMP9 and BMP10 are translated as 429 and 424 amino-acid *PreProProteins*, respectively, with their N-terminal signal peptide directing them into the secretory pathway (figure 6)(Chen et al. 2003). The signal peptide is cleaved to leave a *ProBMP*. The endoplasmic reticulum is oxidising and contains enzymes catalysing the formation of four disulphide bonds in the C-terminal growth-factor domain (Wei et al. 2014). One of these forms between cysteine-393 of two BMP9 molecules, or 388 of two BMP10 molecules, to produce a *ProBMP* dimer (Schlunegger and Grütter 1992). This species is latent, since the prodomains prevent signalling activity. BMP9 is also predicted to be glycosylated at residues N71 and N176, and BMP10 at N67 and N131, as they pass through the secretory pathway. These glycosyl groups improve the efficiency of furin processing (Susan-Resiga et al. 2011).

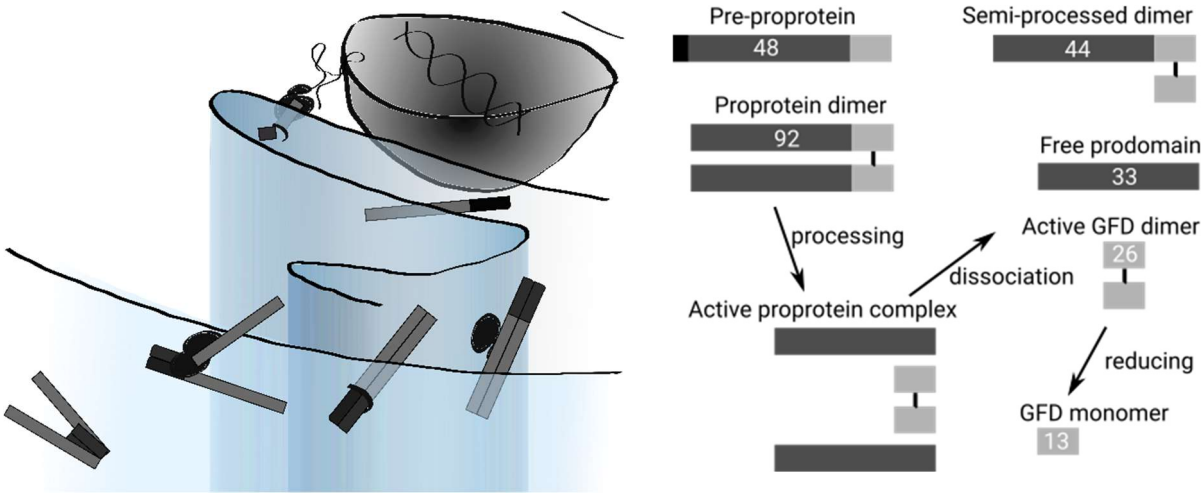

Figure 6. BMP9 and BMP10 production and processing. **Left**: cartoon of BMP9 transcription, translation, translocation, glycosylation, secretion and processing. **Right:** Schematic representation of different BMP9 species. Numbers = predicted molecular weight kDa.

ProBMP9 can be activated by cleaving the prodomains at RRKR^{319}↓, and *ProBMP10* at RIRR^{316}↓, to release a growth-factor domain dimer (Mi et al. 2015; Susan-Resiga et al. 2011). These are canonical furin recognition sequences, so a furin-like protease is hypothesised to be responsible for processing. Furin is widely expressed, enriched in the trans golgi apparatus, and belongs to the subtilisin-like prohormone convertase family (Thomas 2002).

BMP9 is believed to be constitutively activated—serum and plasma from many species contains BMP activity which can be neutralised with anti-BMP9 antibodies, and BMP9 is secreted predominately in its processed form when overexpressed *in vitro* (Herrera and Inman 2009; Bidart et al. 2012; Wei et al. 2014; Wooderchak-Donahue et al. 2013; David et al. 2008). Moreover, David *et al.* (2008) and Nikolic *et al.* (2019) were able to purify active BMP9 in a ~12 kDa fraction from human serum.

One report estimated ~40% of circulating BMP9 is unprocessed (Bidart et al. 2012). This is because furin treating EDTA-plasma increased its activity. The experiment was conducted at pH 9 in the presence of EDTA, which is unphysiological for furin which prefers neutral-acidic conditions and is strictly calcium dependant (Thomas 2002). They showed the activity of BMP9 containing plasma size-fractions increased after furin treatment, and this could be completely neutralised by anti-BMP9 antibodies (Bidart et al. 2012). Nonetheless, their measured activity was very low, suggesting the sensitivity of this assay was poor. If much endogenous activity is not being measured, we cannot tell if BMP9 really constitutes the bulk of it. This means the furin treatment could be activating other ligands, including *ProBMP10.*

Caperuto *et al.* (2008) used Western blotting to show the presence of both unprocessed and active BMP9 in rat liver extracts, and the ratio could be changed by fasting and other stimuli. However, their blots were heavily cropped and had neither molecular weight markers nor positive controls, so the bands could be non-specific. Moreover, the unprocessed bands could be intracellular protein.

ProBMP10 processing appears to be less efficient than *ProBMP9* processing in overexpression systems (David et al. 2007; Wei Li unpublished). Nonetheless, *ProBMP10* can be processed by furin during overexpression *in vitro* (Jiang et al. 2016; Susan-Resiga et al. 2011). Susan-Resiga *et al.* also showed prohormone convertases PC5/6 and paired basic amino-acid-cleaving enzyme 4 can process *ProBMP10 in vitro*. Using enzyme overexpression/inhibition assays, they found intracellular furin was the most important processing factor *in vitro*, although this depends on the cell-type. Neither furin nor PC5/6 knockout mice are viable, so their role in processing cannot be studied *in vivo*. Therefore, we do not know for certain which enzyme(s) processes endogenous BMP9 and BMP10.

Circulating BMP10 was assumed to be processed because ALK1-Fc treatment can neutralise more plasma activity than anti-BMP9 antibodies alone (Jiang et al. 2016). Chen *et al.* (2013) also report that anti-BMP10 antibodies can neutralise some serum activity, although not as much as anti-BMP9 antibodies. However, Jiang *et al.* were unable to show this for plasma using the same antibody. Moreover, anti-BMP9 neutralises 80-100% of human serum activity, and *Gdf2* knockout mice have very little residual plasma BMP activity (Ricard et al. 2012; Nikolic et al. 2019; Jiang et al. 2016). Mouse right atria extracts contain processed BMP10 and can secrete active BMP10 *ex vivo* (Jiang et al. 2016; Susan-Resiga et al. 2011). Whether right atria also secrete unprocessed *ProBMP10* has never been assessed.

In summary, there is good evidence that active BMP9 circulates, but only mixed evidence that *ProBMP9* circulates. There is mixed evidence that active BMP10 circulates. The presence or absence of latent ligands is interesting, because they may be activated in specific circumstances, or at specific sites.

1.4.3. Circulating BMP9 & BMP10

After processing, the prodomains remain tightly associated with the growth-factor domain dimer *in vitro*, forming a non-covalent complex, Pro:BMP9 / Pro:BMP10 (Brown et al. 2005; Jiang et al. 2016). The predominant circulating forms of BMP9 and BMP10 are prodomain bound—after affinity purification and size-exclusion chromatography, endogenous BMP9 and BMP10 have a similar molecular size to Pro:BMP (Bidart et al. 2012; Jiang et al. 2016). An ELISA using a capture antibody against BMP9 growth-factor domains, and a detection antibody against BMP9 prodomains, detects reactivity in this fraction (Bidart et al. 2012). These size-exclusion chromatography experiments were carried out with samples pre-purified on affinity columns then eluted, so any higher-order circulating complexes could be disrupted and not measured. A small proportion of circulating BMP may have its prodomains displaced by circulating endoglin, which could impact its activity in some contexts (Lawera et al. 2019).

The prodomains may solubilise and stabilise the hydrophobic growth-factor domain (Brown et al. 2005). Hydrophobic residues on the surface of the prodomains are important for the correct dimerisation and folding of other TGFβ family members (Gray and Mason 1990; Walton et al. 2009). The prodomains also extend the half-life of TGFβ and activin-A *in vivo*, and the prodomain bound form of activin-A is active, so this is not due to blocking receptor binding (Johnson et al. 2016; Wakefield et al. 1990). The prodomains of several BMPs bind to the extracellular matrix and other TGFβ binding proteins. This includes BMP10 which has a fibrillin binding site in its prodomain (Sengle et al. 2011).

The prodomains could limit growth-factor domain availability to some receptors, especially type-II receptors (Mi et al. 2015). However, they have no effect on high-affinity ALK1 binding, and do not inhibit BMP9 or BMP10 activity on known cells except when at huge molar excess (Jiang et al. 2016; Bidart et al. 2012; Brown et al. 2005; Mi et al. 2015). This is likely because the mature complex adopts an open 'butterfly' conformation, exposing ALK1 and endoglin binding sites (Mi et al. 2015). One report suggested crossveinless-2, which is secreted by endothelial cells, can bind and inhibit BMP9 (Yao et al. 2012). However, this result could not be replicated by our group (Wood et al. 2019). Thus, no BMP9 or BMP10 inhibitors are known.

Notably, the intermolecular disulphide bond between BMP9 monomers is susceptible to reduction in physiological conditions, whereas other BMPs are not. However, the non-covalent dimer retains its overall structure and activity (Wei et al. 2014). The reduced form may only sustain signalling for a shorter time and is more susceptible to degradation in serum (Wei et al. 2014). It is not known if any endogenous BMP9 is reduced.

A recent report claimed the predominant circulating form of BMP9 and BMP10 was a BMP9/10 heterodimer (Tillet et al. 2018). They showed BMP9/10 heterodimers are produced by cells transfected with both. Additionally, ELISAs comprised of capture antibodies against BMP9 and detection antibodies against BMP10 give immunoreactivity to human and mouse plasma. Finally, they showed that BMP9 from human plasma was captured on affinity columns against BMP10. Notably, Dr. Paul Upton showed a striking correlation between circulating levels of BMP9 and BMP10 in human plasma (Hodgson et al. 2019).

However, aspects of Tillet *et al.*'s report are inconclusive. Firstly, the hetero-ELISA results could not be replicated in our lab (Upton unpublished). Secondly, Tillet *et al.* show only modest reductions in circulating BMP9 in *Bmp10* knockout mice and *vice versa*. They previously reported BMP10 levels are unchanged in *Gdf2* knockout mice (Ricard et al. 2012). Numerous reports show *Gdf2* knockout and *Bmp10* knockout mice have different phenotypes (see 1.5.3). Moreover, these results are consistent with BMP9 and BMP10 being in another kind of complex. Dr. Paul Upton finds the circulating level of pBMP10 is 10-fold greater than BMP9, which suggests the majority cannot be in dimeric complexes. Although Tillet *et al.* showed both *Gdf2* and *Bmp10* are transcribed in hepatic stellate cells, they did not show they were transcribed within the same cells by using multi-colour *in situs*. Indeed, the transcriptional level of *Bmp10* was much lower than *Gdf2* and fewer cells were Bmp10 positive.

In summary, the prodomains of Pro:BMP9 and Pro:BMP10 may modulate their function, and this should be considered when recombinant BMP9 or BMP10 is used. The ligands can exist in different forms and could be in complexes which may affect measurements and regulate their activity.

1.4.4. Levels of circulating BMP9 & BMP10

There is no consensus in the literature regarding the circulating concentration of BMP9 or BMP10 (table 5). Reports based on activity assume there is no inhibition or enhancement of BMP9 activity by other factors in serum. High intra- and inter-report variation in measured levels suggests ELISA protocols are ineffective. Moreover, the ELISAs have not been validated.

Report	Substrate	Method	Levels (pg/ml)
Herrera and Inman (2009)	Foetal calf serum	activity on cells, before and after neutralisation	2700-6100
	Human serum		400-1200
Bidart et al. (2012)	Human plasma		13
	Foetal mice plasma		6000
	Adult mouse plasma		2000
David et al. (2008)	Human plasma & serum		2000-12000
Bidart et al. (2012)	Human plasma	ELISA of plasma size fraction	37
Ricard et al. (2012)	Adult mouse plasma	ELISA	200-300
Tillet et al. (2018)			400-1600
Ntumba et al. (2016)			75-125
Ouarné et al. (2018)			500-600
Larriveé et al. (2012)			100
Larriveé et al. (2012)	Foetal mouse plasma		1500
van Baardewijk et al. (2013)	Diluted human plasmas		72-2496
Wang et al. (2019)	Human serum		8-1000
Li et al. (2018)			0-50
Ricard et al. (2012)	Foetal mouse plasma		20 000
	Adult mouse plasma		5000
Tillet *et al.* (2018)			25-175
Ouarné *et al.* (2018)			25-200
Chen *et al.* (2013)	Adult mouse serum		500-2000
	Human serum		1000-3000

Table 5. Levels of circulating BMP9 (top) and BMP10 (bottom) measured *in vivo*.

Nikolic *et al.* and Dr. Paul Upton undertook to optimise and validate a sandwich ELISA comprised of capture and detection antibodies against the BMP9 growth-factor domain. Some plasmas give aberrantly high immunoreactivities due to endogenous antibodies crosslinking ELISA detection and capture antibodies (Tate and Ward 2004). This was overcome by supplementing samples with goat serum. Samples were mixed with Triton-X100 and diluted 1 in 4 to minimise interference from other plasma proteins. This ELISA gives

~85% recovery of Pro:BMP9 from EDTA-plasma. Approximately 150-300 pg/ml of BMP9 is found in control plasmas using this protocol (Nikolic et al. 2019; Hodgson et al. 2019). Interestingly, there is significantly more BMP9 circulating in human females than males, so the sex of animal and human samples should be considered (Hodgson et al. 2019). Dr. Paul Upton optimised and validated a sandwich ELISA comprised of capture antibodies against the growth-factor domain, and detection antibodies against the prodomain, of pBMP10 in a similar way to the BMP9 ELISA. Circulating levels of pBMP10 were about 4000-7000 pg/ml in males and 5000-8000 pg/ml in females (Hodgson et al. 2019).

In summary, the circulating level of BMP9 is ~300 pg/ml, and pBMP10 ~5000 pg/ml when using a validated ELISA in large cohorts of people. Many reports generate spurious results. There seems to be a discrepancy between the amount of BMP9 and BMP10 activity measured in cell-based assays versus ELISAs. However, we do not know whether the ELISAs detect latent and/or active BMPs, and the cell-based assays assume serum factors do not enhance or inhibit BMP9 signalling.

1.5. Function of BMP9 & BMP10

1.5.1. BMP9 in PAH

BMP9 was indirectly implicated in PAH because it was the first high-affinity ligand for ALK1 discovered, can stimulate BMPR-II and circulates at active levels in adults. *In vitro*, BMP9 appears to inhibit cellular phenotypes associated with PAH. BMP9 treatment also partially rescues the apoptotic and leaky monolayer phenotypes of blood outgrowth endothelial cells taken from PAH patients carrying *BMPR2* mutations (Long et al. 2015). Secondly, BMP9 treatment upregulates the expression of BMPR-II; partly a direct effect of SMAD activity on the *BMPR2* promoter (Long et al. 2015; Upton et al. 2009).

Therefore, the Morrell group used intraperitoneal injections of Pro:BMP9 to prevent and reverse PAH-like disease in mice and rats. BMP9 reduced pulmonary vascular leak, partially restored haemodynamics, and rescued BMPR-II expression and signalling (Long et al. 2015). However, this study does not necessarily demonstrate a role for endogenous BMP9 in human PAH, since treatment was administered at supraphysiological doses, through an unphysiological route, and induced disease may not reflect spontaneous human disease.

Tu *et al.* (2019) report *Gdf2* knockout and anti-BMP9 treated mice have less severe pulmonary hypertension and pulmonary vascular remodelling in chronic hypoxia. However, *Gdf2* knockout mice had less muscularised pulmonary arteries at baseline, reminiscent of HHT, and anti-BMP9 treatment appeared to alter the haemodynamics of control mice. Hence

vessels may develop and respond to hypoxia abnormally in this model (Morrell et al. 2019). Nikolic *et al.* (2018) show ALK1-Fc treatment of adult mice in hypoxia exacerbates PAH. Moreover, human genetic data increasingly shows *GDF2* deficiency contributes to PAH.

A five-year-old who developed severe PAH with a dilated right-ventricle, without evidence of HHT or cardiac defects, was discovered to carry a homozygous truncating mutation in *GDF2,* BMP9-Q26X (Wang et al. 2016). The heterozygous parents showed no evidence of disease. Wang *et al.* found this mutation by targeted sequencing *BMPR2, ACVRL1, ENG, SMAD4, SMAD9, CAV1, KCNK3, KCNA5, EIF2AK4, TOPBP1, NOTCH1, NOTCH3* (all of which were mutation-free) and *GDF2*. This child should not produce BMP9, but plasma samples were not analysed so we cannot be sure there is no escape or compensation.

Recently, the Morrell group published a rare variant analysis showing *GDF2* mutations predicted to be deleterious were over-represented in PAH patients compared to controls with genome-wide significance (see 3.1)(Gräf et al. 2018). *GDF2* mutation carriers in this cohort did not have significantly worse haemodynamics, age of diagnosis or prognosis than IPAH patients, and so had milder disease than *BMPR2* mutation carriers (Hodgson et al. 2019). These genetic and phenotypic findings were replicated by whole-exome sequencing Chinese PAH and control cohorts (Wang et al. 2019). Both studies found that putatively pathogenic variants in *GDF2* were predominately heterozygous missense, which makes their effects hard to predict *in silico*. Therefore, I undertook to assess the secretion, activity and circulating levels of BMP9 variants discovered in the Morrell study, and Wang *et al.* reported a similar analysis in their study.

Wang *et al.* found missense BMP9 variants were poorly secreted *in vitro.* This was mirrored within human carriers which had reduced circulating levels of BMP9 (12 pg/ml) compared to healthy controls (36 pg/ml) and other PAH patients (22 pg/ml). However, these BMP9 levels are well below those recorded in previous reports, and the ELISA protocol was not validated (see 1.4.3). Additionally, information about the sex and age of control samples was not recorded. The Chinese cohort exhibits high rates of pathogenic *GDF2* mutations (6.7% versus 0.8% of UK cases), and was generally young and with severe disease, compared to the British cohort. Patients with liver disease were stringently excluded from the British cohort because they can exhibit low plasma BMP9 levels (Nikolic et al. 2019; Upton unpublished). Moreover, the Chinese cohort only included 331 patients.

A targeted analysis of *BMPR2, TBX4, EIF2AK4, CAV1, KCNK3, SMAD9, ACVRL1, ENG, BMP10* and *GDF2* in a European cohort of 181 IPAH patients was published simultaneously (Eyries et al. 2019). They found two *GDF2* truncating mutations and a missense variant

predicted to be deleterious *in silico.* Finally, a rare-variant analysis of 2572 exome-sequences from an American cohort implicates *GDF2* as causal in PAH (Zhu et al. 2019).

Dr. Paul Upton measured circulating BMP9 levels in 260 PAH patients and 120 controls (Hodgson et al. 2019). There was no significant difference in average circulating BMP9 levels between controls and PAH patients. This suggests low BMP9 levels are not generally involved in PAH, in contrast to the claims of Wang *et al.* (2019). Nikolic *et al.* (2018) also find normal BMP9 levels in PAH patients, and rodents with PH, unless they have liver disease. However, a disproportionate number (~10%) of PAH patients not carrying *GDF2* mutations had circulating levels of BMP9 below the lowest control sample, suggesting BMP9 deficiency may contribute to some PAH cases (Hodgson et al. 2019). Dr. Emilia Swietlik assessed the phenotype of PAH patients with low levels of BMP9 and found no impact on age of diagnosis, prognosis or haemodynamics (Hodgson et al. 2019).

In summary, multiple cohorts cross-validate a role for *GDF2* mutations in PAH. Analysis of these variants demonstrates BMP9 deficiency contributes to PAH risk. BMPR-II/ALK1 signalling is deficient in PAH and BMP9 can restore this, making BMP9-like molecules promising treatments for PAH (Ormiston, Upton, et al. 2015). Further study is needed to define how each missense mutation disrupts BMP9.

1.5.2. BMP10 in PAH

The role of BMP10 in PAH and HHT has not attracted as much attention as BMP9—it was identified as a circulating ALK1/BMPR-II ligand later and is generally less well understood. Therefore, neither Wang *et al.* (2019) nor Nikolic *et al.* (2019) measured BMP10 levels in PAH patients compared to controls.

Moreover, *BMP10* mutations have not been statistically associated with human disease in British, American or Chinese cohorts (Gräf et al. 2018; Zhu et al. 2019; Wang et al. 2019). Interestingly, Eyries *et al.* (2019) report a truncating mutation (BMP10-R124X), and a missense mutation predicted to be deleterious (BMP10-R353C), in their cohort. The British study re-sequenced and confirmed the patient carrying BMP10-R353C and discovered a PAH patient carrying BMP10-A361E (Hodgson et al. 2019). These variants are expected to profoundly disrupt the growth-factor domain of BMP10. Unfortunately, *in vitro* expression of Pro:BMP10 is relatively variable which makes analysis difficult and plasmas were not available from these patients. Their age and haemodynamics were not notable (Hodgson et al. 2019).

Dr. Paul Upton found circulating pBMP10 levels were significantly lower in females with PAH, but not males, compared to controls (Hodgson et al. 2019). Additionally, ~12% of PAH patients had circulating levels of pBMP10 below the lowest healthy control. Hence, BMP10 deficiency might contribute to some PAH cases. Circulating pBMP10 levels were not correlated with age at diagnosis, haemodynamics or prognosis (Hodgson et al. 2019).

According to the genome aggregation database, *BMP10* is more intolerant of loss-of-function mutations (observed/expected ratio = 0.03 to 0.39) than *GDF2* (observed/expected ratio = 0.27 to 0.98), which may explain why few pathogenic mutations have been found in *BMP10*. The BMP9 and BMP10 growth-factor domains have extremely similar structures and activity on endothelial cells. Therefore, it is conceivable that BMP10 activity protects against PAH or compensates for BMP9 deficiency. Hence, levels and activity of both ligands should be considered within patients.

1.5.3. BMP9 & BMP10 in vascular development

The ALK1 signalling complex regulates endothelial cells. In turn, endothelial cells regulate blood vessel development, vascular tone, and movement of cells and substances across vessel walls. Vasculogenesis is the first stage of vascular development, when endothelial cells form uniform tubes under the influence of TGFβ (Li et al. 1999). During angiogenesis, endothelial cells take on distinct identities and remodel vessels to give the vasculature appropriate architecture (Li et al. 1999). Neither *Eng* nor *Acvrl1* knockout embryos are viable because they have profoundly disturbed angiogenesis, including hyperdilation of larger vessels, formation of shunts between arteries and veins due to loss of arterial/venous identity, and failure to recruit vascular smooth muscle (Li et al. 1999; Urness, Sorensen, and Li 2000; Oh et al. 2000; Larrivée et al. 2012; Lamouille et al. 2002; Rochon, Menon, and Roman 2016).

[BMP9/BMP10]/ALK1 signalling cross-talks with Notch signalling and other regulators of endothelial development (Larrivée et al. 2012; Ricard et al. 2012). Thus, when neonatal mice are given ALK1-Fc, or DAPT to inhibit Notch signalling, their developing retinas and ears hypervascularise due to increased endothelial cell sprouting (Larrivée et al. 2012). BMP9 administration can rescue the effect of DAPT by directly inducing the expression of Notch target genes such as *HEY1* and *HEY2* (Larrivée et al. 2012; Ricard et al. 2012).

Bmp10 knockout embryos show defective blood-vessel development (Chen et al. 2013). In contrast, *Gdf2* knockout mice are viable and do not show an obvious blood-vessel phenotype (Hao Chen et al. 2013; Ricard et al. 2012). In mice, BMP10 and ALK1 expression

begins at embryonic day 8.5, whereas BMP9 is not produced until embryonic day 9.75 (Chen et al. 2013; Seki, Yun, and Oh 2003). In mice with the coding sequence of *Bmp10* replaced with that of *Gdf2*, blood vessel development is normal (Chen et al. 2013). This suggests the presence of either ligand is sufficient during early vessel development.

Later, neonatal mice given anti-BMP10 do not show any blood-vessel phenotypes (Chen et al. 2013). However, *Gdf2* heterozygous and knockout mice given anti-BMP10, and wild-type mice given ALK1-Fc or both anti-BMP9 and anti-BMP10, show hypervascularisation, dilation, haemorrhaging and impaired vessel muscularisation (Chen et al. 2013; Ricard et al. 2012; Baeyens et al. 2016). This indicates redundancy between the ALK1 ligands in neonatal mice. Notably, anti-BMP9 alone had a similar effect to ALK1-Fc in wildtype mice, suggesting that it disrupts BMP10 signalling (possible if they are in complex) or chronic germline loss of BMP9 leads to better compensation by BMP10 (Ricard et al. 2012). Combined depletion of BMP9 and BMP10 is lethal after ~6 days, similar to ALK1 depletion (Levet et al. 2015).

A consistent result was reported for embryonic zebrafish. BMP9 deficient embryos do not have an early vascular phenotype, but later fish develop a venous remodelling defect in the tail (Laux et al. 2013). In contrast, BMP10 deficient embryos have an early arterial phenotype reminiscent of ALK1 deficiency and lose early endothelial SMAD signalling (Laux et al. 2013).

In adulthood, BMP9 is reported to either promote vascularisation or inhibit it. In a mouse model of macular degeneration, adenovirus expressing BMP9, which leads to increased circulating BMP9, reduces the formation of invasive vessels, whereas ALK1-Fc expression increases it (Ntumba et al. 2016). In mice given ischemic hind-limb injuries, injection of BMP9 enhances vascularisation (Kim et al. 2015). However, this effect was only seen in the presence of exogenous foetal endothelial progenitor cells. ALK1 blockade has been investigated extensively as a tumour vascularisation inhibitor. Conflicting reports show *Gdf2*, but not *Bmp10*, knockout mice have more neovascularisation and faster growth of spontaneous tumours (Ouarné et al. 2018; de Vinuesa et al. 2016).

BMP9 and BMP10 seem to cooperate during ductus arteriosus closure and remodelling. The ductus arteriosus closes normally at birth in *Gdf2* knockout mice, but tends to re-open again after 4 days because intimal and medial remodelling is reduced (Levet et al. 2015). Anti-BMP10 antibodies exacerbate this (Levet et al. 2015). In humans, *BMP10* deletions have been associated with having a patent ductus arteriosus (Levet et al. 2015).

Lymphatic vessels develop after embryonic day 10 in mice, when either ligand could have a role. Mice treated with ALK1-Fc, inducible *Acvrl1* knockout, and *Gdf2* knockout mice given anti-BMP10, have improperly developed lymphatic systems (Niessen et al. 2010; Chen

et al. 2013; Yoshimatsu et al. 2013). However, later reports also argue *Gdf2* knockout alone leads to the development of dysfunctional lymphatic vessels and a loss of lymphatic valves (Levet et al. 2013; Yoshimatsu et al. 2013; Derynck and Akhurst 2013).

In summary, BMP9 and BMP10 are semi-redundant in angiogenesis in adults. There is some evidence that BMP9 deficiency can induce subtle phenotypes alone, but also some evidence chronic deficiency is compensated by BMP10. BMP9 deficiency seems to promote vascularisation in some situations and inhibit it in others. This may reflect the nuanced purpose of angiogenesis, which is to prune some vessels, enlarge others, maintain some redundancy but increase the efficiency of perfusion. These features are consistent with BMP9 or BMP10 deficiency being a rare, poorly penetrant trigger for PAH.

1.5.4. BMP9 & BMP10 in vascular quiescence

ALK1 signalling is necessary for blood vessel homeostasis in adulthood, since inducible *Acvrl1* knockout mice develop arterio-venous malformations, and die of internal haemorrhaging (Park et al. 2009; 2008). BMP9 signalling elicits many effects on adult endothelial cells, but is generally a quiescence factor (David et al. 2008). It alters the secretion of various chemokines and selectins from endothelial cells, some with auto/paracrine roles stabilising the endothelium and recruiting accessory cells, but others that may promote vascular tone and angiogenesis (Young et al. 2012; Upton et al. 2009). This is likely context dependent *in vivo.* Endothelial cells stimulated with BMP9 are less apoptotic, proliferative and migratory, form tighter cell-junctions, and have a different metabolic profile (Bidart et al. 2012; David et al. 2008; Suzuki et al. 2010; Long et al. 2015; Burton et al. 2011; Lamouille et al. 2002; Akla et al. 2018). ALK1 mediates endothelial transcytosis of low-density lipoproteins, but this is not associated with SMAD signalling (Kraehling et al. 2016).

The mechanism leading to quiescence has not been thoroughly explored. SMAD-regulated genes include inhibitor of DNA-binding proteins *ID1* and *ID2* (Miyazono, Kamiya, and Morikawa 2010; Upton et al. 2009; Long et al. 2015). As in development, BMP9 and Notch signalling are synergistic for quiescence, and there is some evidence BMP9 is upregulated to compensate loss of Notch activity *in vivo* (Rostama et al. 2015). BMP9 also upregulates components of its own signalling pathway, including BMPR-II, endoglin and SMAD9 which further stabilises and quiesces the endothelium, even in *BMPR2* deficient cells (Long et al. 2015; Young et al. 2012).

In summary, BMP9 is a quiescence factor in many settings. Sustained signalling is needed for endothelial cells to maintain proper vessel architecture through adulthood. BMP9

promotes normal migration, proliferation, apoptosis and chemokine secretion, and upregulates its own signalling. These features are consistent with BMP9 deficiency contributing to PAH.

1.5.5 BMP10 in the heart

Bmp10 knockout mice are not viable since cardiomyocyte numbers are dramatically reduced (Chen et al. 2004; 2009). Interestingly, a heterozygous, very rare missense-variant, BMP10-V407I, was found in a mother and daughter suffering from left-ventricular non-compaction (Hirono et al. 2019). This variant is predicted to be highly deleterious *in silico*, and was less able to bind BMPR-II *in vitro* (Hirono et al. 2019).

Replacing the coding sequence of *Bmp10* with that of *Gdf2* leads to profound cardiac defects, which indicates BMP10 may signal differently to BMP9 in the heart (Chen et al. 2013). Chen *et al.* checked BMP9 was expressed in place of BMP10 in this model, but it is possible there are nuanced regulatory functions contained within the coding sequences that could be influencing this result. These embryos were not compared side-by-side with *Bmp10* knockouts to see if BMP9 compensated for BMP10 loss to any extent.

One report suggests circulating BMP9 levels are inversely correlated with coronary heart disease and systemic essential hypertension (Liu et al. 2019). However, these data were generated using an ELISA protocol which is unsuitable in our hands. Circulating pBMP10 levels are significantly inversely associated with systemic hypertension in the cohort of PAH patients measured by us (Hodgson et al. 2019). BMP9 levels are not significantly associated with hypertension in this cohort, but a correlation is evident, and BMP9 is very tightly correlated with pBMP10 suggesting both ligands are associated.

1.5.6. BMP9 in the liver

The first investigations into BMP9 identified it as a hepatic paracrine, where it binds specific, high-affinity receptors (Song et al. 1995; Miller et al. 2000). Liver tissue expresses ALK1, ALK2, BMPR-II, ActR-II, and endoglin, with ALK1 the main receptor on hepatic stellate, Kupffer and bile-duct endothelial cells (Bi and Ge 2014). BMP9 treatment leads to SMAD signalling and *ID1* induction in many hepatic cell-types *in vitro*, although it is not completely clear which cell-types are able to respond to BMP9, or at what concentrations.

The first functional study of *GDF2* explored glucose homeostasis (Chen et al. 2003). Of all secreted factors except insulin, BMP9 was found to be the most potent driver of insulin-like effects on hepatoma, myoblast and adipocyte cell lines. Secondly, exogenous BMP9 was

found to be a potent anti-glycaemic in mice (Chen et al. 2003). However, the EC_{50} of cells was supraphysiological (~50 ng/ml), and high BMP9 doses (5 mg/kg) were administered which may have caused severe morbidity.

Circulating BMP9 levels are negatively correlated with insulin resistance in type-II diabetes (Luo et al. 2017). Feeding or injecting glucose leads to *GDF2* upregulation in rat livers, whilst anti-BMP9 injection leads to glucose intolerance (Caperuto et al. 2008). BMP9 overexpression inhibits glucogenesis and lipogenesis in mice and improves insulin resistance (Yang et al. 2019). Circulating pBMP10 levels are significantly inversely associated with type-II diabetes in the cohort of PAH patients we measured (Hodgson et al. 2019). BMP9 levels were not significantly associated with diabetes, but a correlation is evident and BMP9 is tightly correlated with pBMP10 suggesting both ligands are associated. BMP9 mRNA and protein may be decreased in livers of type-II diabetes patients (Yang et al. 2019). BMP9 upregulates the expression of browning genes in mouse fat-tissue and human adipose stem cells (Kuo et al. 2014). This reduces weight gain in mice treated with exogenous BMP9 (Kuo et al. 2014).

Evidence also supports a role for BMP9 in hepatic non-glucose metabolism. BMP9 appears to be a constitutive quiescence factor of hepatocytes, facilitating the expression of metabolic enzymes such as cytochrome P450 and hepcidin (Truksa et al. 2006; Breitkopf-Heinlein et al. 2017). Additionally, BMP9 may have a developmental role in the liver—*Gdf2* knockout mice have sinusoidal endothelial cells which fail to differentiate fully, leading to improper fenestrations and perivascular fibrosis (Desroches-Castan et al. 2019). *Gdf2* knockout livers also have an increased mesenchymal component, which could reflect destabilisation of epithelial hepatocytes (Breitkopf-Heinlein et al. 2017; Addante et al. 2018).

Numerous reports demonstrate *Gdf2* expression is immediately and transiently downregulated upon liver injury, including after lipopolysaccharide, carbon tetrachloride, bile-duct ligation and cholestatic injury (Li et al. 2018; Breitkopf-Heinlein et al. 2017; Addante et al. 2018; Nikolic et al. 2018). *Gdf2* knockout, ALK1-Fc or anti-BMP9 treated mice suffer less liver damage, and show better liver regeneration after such injuries, suggesting this fall in BMP9 levels is adaptive (Breitkopf-Heinlein et al. 2017; Li et al. 2018; Wiercinska et al. 2006; Addante et al. 2018). Conversely, forced *GDF2* overexpression, or BMP9 administration, leads to impaired proliferation, increased apoptosis and reduced regeneration of hepatocytes *in vivo* and *in vitro* (Li et al. 2018; Breitkopf-Heinlein et al. 2017).

Excess BMP9 activity is accompanied by increased liver fibrosis because endoglin/ALK1/SMAD/ID1 signalling drives hepatic stellate cells to transdifferentiate into fibroblasts; drives *SNAIL* expression in hepatocytes which triggers epithelial to mesenchymal

transition; and drives the expression of components of the extracellular matrix (Li et al. 2018; Meurer et al. 2013; Wiercinska et al. 2006; Li et al. 2013; Addante et al. 2018). Anti-BMP9 treatment has even been used to partially reverse liver fibrosis in animals (Li et al. 2018).

Importantly, BMP9 may also have protective effects in the liver. For example, in sinusoidal endothelial cells, *ID1* expression drives the secretion of paracrines which are pro-regenerative, and anti-fibrotic for the liver (Ding et al. 2014). Hence, in the absence of insults, *Gdf2* deficiency may increase fibrosis (Addante et al. 2018; Desroches-Castan et al. 2019). Secondly, although BMP9 deficient livers are less damaged by insults, they may become more inflamed, and secrete inflammatory cytokines (Desroches-Castan et al. 2019). This could precipitate liver dysfunction or induce problems in other organs.

Notably, these animal models of liver damage are severe. In patients with hepatitis B, *GDF2* expression was not correlated with fibrosis (Breitkopf-Heinlein et al. 2017). Similarly, in people with different stages of liver disease, only the most severe cases have reduced circulating levels of BMP9 (Upton unpublished). Circulating BMP9 levels are markedly reduced in patients with portopulmonary hypertension, which likely have cirrhosis, compared to pulmonary hypertension without liver involvement (Nikolic et al. 2019).

In contrast, another report suggested circulating BMP9 levels are increased in fibrotic patients, although they measured serum by an ELISA protocol that is not suitable in our hands (Li et al. 2018). A brief analysis of publicly available datasets from various liver diseases showed that *GDF2, ACVRL1, ACVR2B* and *BMP10* mRNA is upregulated in some cirrhotic cohorts, and downregulated in others (John et al. 2018). However, mRNA level may not correlate well with secretion level in senescent cells.

In summary, BMP9 is likely to have important roles in liver development and quiescence. BMP9 may also have short-term metabolic regulatory roles. There has not been a comprehensive assessment of the baseline phenotype of BMP9 deficient livers. Therefore, metabolic markers and enzyme expression should be assessed as comprehensively as possible in BMP9 deficient animals to give an unbiased view of the roles of BMP9 in the liver.

1.5.7. BMP9 in osteogenesis

BMP2,4,6,7 and 9 are known to be potent osteogenic factors (Luu et al. 2007; Cheng et al. 2003; Peng et al. 2003, 2004). *In vitro*, BMP9 can drive the expression of alkaline phosphatase, an early marker of osteogenesis, in myoblasts, stromal marrow stem cells and mesenchymal stem cells (Luu et al. 2007; Wang et al. 2017; Zhu et al. 2018; Fujioka-

Kobayashi et al. 2017; Luo et al. 2010; Li et al. 2016). Prolonged BMP9 treatment stimulates matrix mineralisation, a late marker of osteogenesis.

Osteogenic effects seem to require ~10 ng/ml of BMP9, a supraphysiological dose (Fujioka-Kobayashi et al. 2017; Morrell unpublished). BMP9 mediated osteogenesis is dependant non-redundantly on both ALK1 and ALK2 in complex with BMPR-II and ActR-II (Luo et al. 2010; Wu et al. 2010). The EC_{50} of ALK2 for BMP9 is about 50 ng/ml. Hence, these studies suggest the osteogenic effects of endogenous BMP9 are limited to special circumstances where concentrations are elevated.

Mice and rats injected with cells transfected with adenoviral vectors expressing BMP9 show enhanced bone formation compared to other BMPs (Luo et al. 2010; Luu et al. 2007; Kang et al. 2004). These animal models use exogenous cells, an unknown dose of BMP9, and are likely to be inflammatory, so it is unclear if they reflect a normal role of BMP9. Notably, *Gdf2* knockout mice do not show any osteogenesis defects (Ricard et al. 2012; Yoshimatsu et al. 2013). Humans with delayed fracture healing do not have lower circulating BMP9 levels (van Baardewijk et al. 2013). Nevertheless, several studies have assessed using BMP9 to aid bone growth and healing (Fu et al. 2019; Nie et al. 2017; Fujioka-Kobayashi et al. 2017).

In adenoviral models, BMP10 did not appear to have osteogenic activity (Luu et al. 2007; Cheng et al. 2003). However, it is unclear how much processed or unprocessed BMP10 the virus produced: it would be useful to reassess this *in vitro* and *in vivo* with purified BMP10 where the dose can be controlled.

1.6. Hypotheses & approaches

1.6.1. Rare *GDF2* variants associated with PAH

Gräf *et al.* (2017) identified several rare missense-variants in *GDF2* which were associated with PAH. These variants are predicted to damage the protein stucture *in silico*. The variants are spread across the prodomain and growth-factor domains of BMP9, so they could disrupt BMP9 function in several ways. We hypothesised they reduce protein secretion, processing or stability, which are known to depend on the prodomain. Additionally, they could lead to missfolding, and reduce receptor binding and activity on endothelial cells, or bias signalling.

To assess this, we over-expressed BMP9 variants *in vitro.* I assessed their secretion level in conditioned media by ELISA and processing defects by Western blotting. Secondly, I assessed the ability of BMP9 variants to activate ALK1 signalling in a heterologous cell-system.

Finally, I judged the function of BMP9 variants on endothelial cells by measuring the transcription of BMP9 signalling target genes and anti-apoptotic activity.

We hypothesised patients carrying PAH-associated BMP9 variants have reduced circulating BMP9 activity and levels. To assess this, I incubated endothelial cells with patient plasmas to measure transcriptional acitivty, and measured circulating BMP9 levels by ELISA. There are mixed reports over whether BMP9 levels are generally low in PAH patients, so I included samples from PAH patients carrying *GDF2* variants shown to be both loss-of-function and benign *in vitro*, as well as age and sex matched healthy controls. We hypothesised that chronic BMP9 deficiency in these patients is compensated by BMP10. To assess this, I measured pBMP10 levels in these samples by ELISA.

The homozygous variant BMP9-Q26X has been found in pediatric PAH (Wang et al. 2016). We hypothesised that this variant is partially rescued by re-initiation of translation at Met^{57}. I expressed this variant *in vitro* to assess expression and secretion by ELISA and Western blotting. Additionally, the homozygous variant BMP9-D179X has been found in a pedriatric case of HHT. Samples from the patients and parents were available, so I measured activity on endothelial cells and circulating levels by ELISA to confirm the *in vitro* findings.

1.6.2. Circulating species of BMP9 & BMP10

There is mixed evidence over the amount of BMP9 and BMP10 circulating in their active versus latent forms. There seems to be a discrepancy between the amount of circulating BMP10 recoverable by ELISA, and the amount of circulating activity attributable to it. Therefore, we hypotheised that more circulating BMP10 is unprocessed than BMP9.

To assess this, I investigated the immunoreactivity of processed and unprocessed species in growth-factor domain only and prodomain/growth-factor domain ELISAs for BMP9 and BMP10. I then investigated the immunoreactivity of human plasmas with the same ELISAs. I assessed the residual activity of serum which had been cleared of BMP9 and/or BMP10 on endothelial cells. Secondly, I incubated serum with furin and a flourometric positive control, to measure whether circulating BMP9 or BMP10 can be processed. Finally, I assessed circulating BMP by Western blotting.

Circulating BMP9 and BMP10 levels are tightly correlated, and there is some evidence that they are in complex. Therefore, I hypothesised that immunopreciptating BMP9 from plasma reduced recovery of BMP10 by ELISA, and *vice versa*. I also analysed plasma and serum by size-exclusion chromotography to assess the size of circulating BMP9 and BMP10.

1.6.3. Pharmacokinetics of BMP9

Intraperitoneal injections of BMP9 have been used in various studies to induce long-lasting changes. However, Dr. Claudia-Gabriela Mitrofan was able to recover excess BMP9 from plasma 1 hour after administration, but not at later time-points (unpublished). Therefore, we hypothesised that the circulating half-life of BMP9 is short, and it may be sequestered to the pulmonary endothelium which highly expresses high-affinity receptors.

To assess this, we administered Pro:BMP9 intravenously to knockout and wildtype mice, and withdrew samples at different times for up to an hour. I measured plasma BMP9 levels by ELISA and activity assays, lung and liver levels by ELISA and transcriptional activity by qPCR. To assess whether endogenous BMP9 and BMP10 behaved similarly, I measured levels by ELISA and activity assays in human plasmas from the superior vena cava, pulmonary artery and brachial artery, to look for trans-vascular gradients.

1.6.4. Phenotype of *Gdf2* knockout mice

BMP9 and BMP10 deficient people are predisposed to PAH, and there is limited evidence they are metabolically dysfunctional. In animals, BMP9 has a potent effect on liver metabolism.

Therefore, we hypothesised that *Gdf2* knockout mice would have disrupted levels of fat and glucose metabolism markers in their serum and elevated levels of markers of liver damage. We hypothesised that *Gdf2* knockout liver transcriptomes would have significantly disrupted expression of metabolic enzymes and proliferation markers.

Materials & Methods

2.1 Production of conditioned media containing BMP9

2.1.1 Site-directed mutagenesis of the BMP9 expression vector

Dr. Rick Salmon prepared the BMP9 missense variant overexpression plasmids, with my assistance in some cases. The template plasmid comprised wildtype *GDF2* cDNA cloned into a pCEP4 plasmid (Wei et al. 2014). Mutagenesis was carried out with a QuickChange kit (Agilent technologies 600250) using primers designed with Amplifx (https://inp.univ-amu.fr/en/amplifx-manage-test-and-design-your-primers-for-pcr)(table 6).

The PCR reaction mix comprised 1 µl *Pfu* turbo polymerase, 35 µl ddH_2O, 5 µl 10% (v/v) DMSO, 5 µl turbo buffer, 1 µl dNTPs (100 mM stock) and 1 µl each of forward and reverse mutagenesis primers (5 µM stocks). A range of 50-125 ng of template plasmid was

included, which was varied until mutagenesis was successful. The PCR mix was incubated in a thermocycler at 95 °C for 45 seconds, followed by 18 cycles of 95 °C for 45 seconds, 50 °C for 1 minute, and 60 °C for 15 minutes, and a final annealing step of 74 °C for 10 minutes. The PCR products were digested with Dpn1 (NEB R0176) to remove template DNA which is methylated: 25 µl of the products were mixed with 5 µl cut smart buffer, 19 µl ddH_2O, and 1 µl enzyme and incubated at 37 °C for 3 hours, then denatured by 15 minutes at 85 °C.

Mutation	Primer Sequences	
p.Gly18Val	For:	5'-CTGCTGGCTgtcTCCCTACAGGGGAAG-3'
	Rev:	5'-CCCTGTAGGGAgacAGCCAGCAGGGAC-3'
p.Gly74Glu	For:	5'-AGCCTTAACCTGAGTgagGTCCCTTCGCA-3'
	Rev:	5'-TGCGAAGGGACctcACTCAGGTTAAGGC-3'
p.Met89Val	For:	5'-CCGCCGCAGTACgtgATTGACCTGTACAAC-3'
	Rev:	5'-GTACAGGTCAATcacGTACTGCGGCGGCT-3'
p.Prol104Leu	For:	5'-AAGTCGACTACGctaGCGTCCAACATTGTG-3'
	Rev:	5'-GCACAATGTTGGACGCtagCGTAGTCGACTTA-3'
p.Arg110Trp	For:	5'-CGTCCAACATTGTGtggAGCTTCAGCAT-3'
	Rev:	5'-ATGCTGAAGCTccaCACAATGTTGGAC-3'
p.Ile118Phe	For:	5'-TGGAAGATGCCttcTCCATAACTGCCACA-3'
	Rev:	5'-GCAGTTATGGAgaaGGCATCTTCCATGCT-3'
p.Glu143Lys	For:	5'-CCATTCCTAGGCATaagCAGATCACCAGA-3'
	Rev:	5'-GCTCTGGTGATCTGcttATGCCTAGGAATG-3'
p.Val154Ile	For:	5'-TGAGCTCCGACTCTATatcTCCTGTCAAAATCACG-3'
	Rev:	5'-TTTTGACAGGAgatATAGAGTCGGAGCTCAG-3'
p.Asp218Asn	For:	5'-GGGTCCGGTCCaacTCCACCAAGAGCA-3'
	Rev:	5'-TTTGCTCTTGGTGGAgttGGACCGGACCC-3'
p.Glu297Lys	For:	5'-TCCACAGAGGCAGGTaagAGCAGTCACGA-3'
	Rev:	5'-CTCGTGACTGCTcttACCTGCCTCTGTGGA-3'
p.Glu302Val	For:	5'-GAGCAGTCACGAGgtgGACACGGATGGC-3'
	Rev:	5'-CCATCCGTGTCcacCTCGTGACTGCTCT-3'
p.Ser320Cys	For:	5'-GGAAAAGGtgcGCCGGGGCTGGCAGCCACT-3'
	Rev:	5'-TGCCAGCCCCGGCgcaCCTTTTCCGCCT-3'
p.Ala347Val	For:	5'-AGCTGGATCATTgtaCCCAAGGAGTATGAA-3'
	Rev:	5'- GCTTCATACTCCTTGGGtacAATGATCCAG-3'
p.Tyr351His	For:	5'-ATTGCACCCAAGGAGcatGAAGCCTACGAGT-3'
	Rev:	5'-CTCGTAGGCTTCatgCTCCTTGGGTGCAAT-3'
p.Lys397Arg	For:	5'-CTGTGTGCCCACCagaCTGAGCCCCAT-3'
	Rev:	5'-AGATGGGGCTCAGtctGGTGGGCACACA-3'
p.Thr413Asn	For:	5'-ATGGGGGTGCCCaacCTCAAGTACCATTA-3'
	Rev:	5'-TGGTACTTGAGgttGGGCACCCCCATGTC-3'

Table 6. Site-directed mutagenesis primers for introducing BMP9 mutations.

The digestion products were amplified in *E. coli*. Fifty µl of DH5-α bacteria (Bioline BIO-85027) were thawed on ice with 5 µl of DNA for 25 minutes, followed by a 45-second heat-shock at 42 °C, then a final 2-minute incubation on ice. Transformed bacteria were transferred into 900 µl of SOC outgrowth medium (CIMR) and incubated for 1 hour at 37 °C with shaking. Bacteria were pelleted by centrifugation, resuspended in 200 µl of SOC medium

and spread onto lysogeny broth agar plates containing ampicillin (CIMR). Plates were incubated overnight at 37 °C. Individual colonies were transferred into 10 ml of lysogeny broth supplemented with ampicillin (CIMR). These were cultured overnight at 37 °C with shaking. Plasmids were recovered by miniprep (Merck PLN70) according to the manufacturer's protocol. The concentration of DNA was measured by NanoDrop (Thermo ND-LITE). Sanger sequencing (Source Bioscience) was used to check to plasmids were correct.

2.1.2 BMP9 over-expression system

Dr. Rick Salmon used the plasmids to produce variant BMP9 protein with my assistance. Human embryonic kidney 293 EBNA (HEK-EBNA) cells constitutively express the Epstein-Barr virus EBNA protein, which stabilises pCEP4 as a nuclear episome. HEK-EBNA cells (American Type Culture Collection) were seeded in 6 cm dishes and grown in Dulbecco's modified Eagle's medium (DMEM)(Gibco 41965) supplemented with 10% (v/v) foetal bovine serum (FBS)(Invitrogen A384000) and antimicrobials (Invitrogen 15420) until confluent.

Two µg of plasmid was mixed with 20 µl of 1mg/ml polyethyleneimine (Polysciences 23966-2), incubated at room-temperature for 2 hours then added to 3 ml of DMEM with 5% (v/v) FBS without antibiotics. Cells were washed twice with PBS, then the transfection mix was added overnight. Transfected cells were washed twice with PBS and placed in 3 ml of chemically defined Chinese hamster ovary cell over-expression medium (Gibco 10743029).

After 6 days, conditioned media were collected and centrifuged at 20 000 g for 30 minutes to remove debris. Clarified conditioned media were aliquoted into PCR tubes and stored at -80 °C. Three independent transfections were carried out on different days for each BMP9 variant and used as biological replicates in subsequent analyses. Each batch of transfections included pCEP4-BMP9-wildtype and pCEP4 without *GDF2* cDNA inserted (empty vector), as positive and negative controls respectively.

2.1.3 Nonsense variant

Dr. Lydia Ruiz Llorente produced expression vectors for wildtype *PreProBMP9*-Q26X and ORF57 variants using pcDNA3.1/V5-His-TOPO/BMP9 (Wooderchak-Donahue et al. 2013) as the template. These were shipped dried on filter paper. Plasmid was reconstituted in 100 µl ddH_2O and the amount of DNA was quantified by NanoDrop. Plasmids were transformed into *E. coli*, purified and sequenced as in section 2.1.1.

pcDNA3 is not stabilised by EBNA, so I transfected it into HEK-293T cells for over-expression. HEK-293T cells were cultured in the same way as HEK-EBNA cells. Fifteen µl of lipofectamine 2000 (Life Technologies) was mixed with 150 µl of optiMEM (Gibco 31985070). Two µg of DNA was mixed with 150 µl of optiMEM, then added to the lipofectamine mix and incubated for 5 minutes at room-temperature. Cells were washed with optiMEM, then placed in 1.7 ml of optiMEM with the transfection mix swirled in gently. After 5 hours, transfected cells were placed in expression media, which were collected after 3 days, as described in section 2.1.2.

2.2 Enzyme-linked immunosorbent assays

2.2.1 BMP9 growth-factor domain in conditioned media

High-binding 96-well ELISA plates (Greiner 655061) were coated with 0.2 µg/well (in 100 µl volume) of monoclonal anti-BMP9 (R&D Systems mAb3209, stock 500 µg/ml in PBS stored at -80 °C) in PBS overnight at 4 °C in a humidified chamber. Unadsorbed antibody was removed by thrice washing with PBS supplemented with 0.05% (v/v) Tween-20 (PBST). The plate was blocked with 150 µl/well of PBS supplemented with 1% (w/v) of bovine serum albumin (BSA)(Fisher BioReagents 12737119) at room-temperature for two hours.

The standard curve comprised recombinant BMP9 (R&D Systems 3209-BP, stock 10 ng/µl in PBS supplemented with 1% (w/v) BSA and 4% (v/v) HCl stored at -80 °C) serially diluted two-fold in PBS supplemented with 1% (w/v) BSA to give concentrations spanning 5000 pg/ml to 4.988 pg/ml). Samples of conditioned media were also serially diluted in PBS supplemented with 1% (w/v) BSA. One hundred µl of each sample/standard was added to duplicate wells and the plate was incubated at room-temperature for two hours.

The plate was thrice washed with PBST and incubated with 4 µg/well (in 100 µl volume) of biotinylated anti-BMP9 (R&D Systems BAF3209, stock 10 ng/µl in PBS supplemented with 1% (w/v) BSA stored at -80 °C) in PBS supplemented with 1% (w/v) BSA for two hours at room-temperature. Unadsorbed detection antibody was removed by thrice washing with PBST, and 100 µl/well of a 1:400 dilution of ExtrAvidin-alkaline phosphatase conjugate (Sigma E2636) in PBS supplemented with 1% (w/v) BSA was added for 30 minutes at room-temperature. For detection, 4-nitrophenylphosphate disodium hexahydrate (Sigma N2640) was dissolved to 1 mg/ml in diethanolamine buffer (1 M diethanolamine, 0.5 mM $MgCl_2$, pH 9.8). The plate was washed thrice with PBST and then ddH_2O, 100 µl/well of detection reagent was added, and the plate was incubated in the dark.

Periodically, the absorbance of each well at 405 nm was measured with a plate reader (BioRad model 680). The mean absorbance of each duplicate standard/sample was calculated. The mean absorbance of the blank (a sample comprised of PBS supplemented with 1% (w/v) BSA alone) was subtracted from each measurement. A standard curve was fitted using four parameter logistic regression and the BMP9 concentration in samples was imputed from this.

2.2.2 BMP9 growth-factor domain ELISA for plasma & serum

Like section 2.2.1, except plates were coated with 5 µg/well of mAb3209 to maximise sensitivity. Additionally, standards and samples were diluted to give final concentrations of 25% (v/v) plasma/serum, 0.2% (v/v) goat serum (Abcam ab7481), 0.5% (v/v) Triton-X100 and 1% (w/v) BSA in PBS. Where indicated, the PBS and BSA in this diluent was replaced with BioRad ELISA diluent (BUF037A). Where indicated, 5 mM EDTA was added. BAF3209 was diluted in PBS supplemented with 1% (w/v) BSA and 0.2% (v/v) goat serum. For quantifying endogenous BMP9 in mouse plasma, recombinant mouse BMP9 (R&D systems 5566-BP) was used in the standard.

2.2.3 BMP9 growth-factor domain ELISA for tissue

Tissue was stored at -80 °C. Eppendorf tubes containing a stainless-steel bead (Qiagen 69989) were weighed then, along with tweezers, razorblades and the benchtop, chilled with dry ice. Pieces of frozen tissue were cut with razorblades and transferred to the tubes, which were re-weighed. Tubes were transferred to chilled TissueLyser II racks (Qiagen) and 25 µl RIPA buffer (50 mM tris-base pH 8, 150 mM NaCl, 1% (v/v) igepal, 0.5% (v/v) deoxycholate, 0.1% (w/v) SDS) per mg of tissue was added. Tissue was homogenised by shaking at 25 Hz in a TissueLyser for ~10 minutes for lung, or ~6 minutes for liver, until there were no visible lumps. Homogenised samples were incubated at 4 °C with rotation for 1 hour, then freeze-thawed. Thawed lysates were sonicated at an amplitude of 10 µm for 10 seconds on ice, then clarified by centrifugation at 21000 g for 10 minutes at 4 °C. The ELISA was carried out as in section 2.2.2 except tissue lysates were diluted to a final concentration of 5% or 25% (v/v) and the standard curve diluent was supplemented with 5% or 25% (v/v) RIPA buffer.

2.2.4 pBMP9 ELISA

Like section 2.2.2 except BAF3209 was replaced by anti-prodomain antibody (BAF3879).

2.2.5 pBMP10 ELISA

Like section 2.2.2, except plasma/serum was diluted to a final concentration of 30% (v/v) and additionally supplemented with 4.5 mM EDTA. The antibodies were different—mAb2926 for

capture and BAF2926 for detection. The standard comprised of Pro:BMP10 purified by Dr. Aleksandra Lawera diluted to give concentrations spanning 100 000 pg/ml to 97 pg/ml.

2.2.6 BMP10 growth-factor domain ELISA

Like section 2.2.5, except the antibodies were from a R&D Systems kit (DY2926). The capture antibody was diluted 1:120 and the detection antibody was diluted 1:60.

2.2.6 Column fractions ELISA

Column fractions were spiked with 5 µl concentrated supplements to give final volumes of 95 µl sample, 0.2% (v/v) goat serum, 0.5% (v/v) triton-x100, and 5 mM EDTA per well. Otherwise, ELISAs were carried out as in section 2.2.2 for BMP9 and 2.2.5 for pBMP10.

2.3 Western blotting

2.3.1 Cell lysate preparation

After media were aspirated, adherent cells were snap-frozen on dry ice. Cells were homogenised in 200 µl SDS lysis buffer (125 mM Tris pH 7.4, 10% glycerol, 2% SDS) supplemented with EDTA-free protease inhibitor cocktail (Roche). Homogenised samples were processed as in section 2.2.3. I used a modified Lowry assay to quantify the amount of protein present in clarified lysates following the manufacturer's instructions (BioRad DC-protein assay 5000111). Since lysates were very concentrated, I diluted them 1 in 10 and assayed this in triplicate. Concentration was determined by colourimetry compared to a standard of bovine serum albumin (BSA) fitted with a four-parameter logistic regression.

2.3.2 Gel electrophoresis and semi-dry transfer

I made SDS-polyacrylamide gels by mixing the resolving gel reagents in table 7 (National Diagnostics Protogel reagents), pouring this mix between glass plates, flattening the top by pipetting on isopropanol and allowing to set for 30 minutes at room-temperature. After pouring off the isopropanol, I added the stacking gel mix, inserted a comb and allowed to set. Figure 11 was produced using WedgeWell gradient gels (Invitrogen XPO0122BOX) to maximise sample volume and resolution of small proteins.

	12 % resolving gel (15 ml)	Stacking gel (7.5 ml)
Protogel	6.0 ml	1.0 ml
Gel buffer	3.9 ml	1.95 ml
dH_2O	4.94 ml	4.47 ml
10% APS	150 µl	75 µl
TEMED	15 µl	8 µl

Table 7. SDS-PAGE gel recipe.

Samples were diluted 4:1 with SDS-loading buffer (312.5 mM Tris-HCl, pH 6.8, 10% (w/v) SDS, 50% (v/v) glycerol and 0.007% (w/v) bromophenol blue). To reduce samples, the SDS-loading buffer additionally contained 12.5% (v/v) β-mercaptoethanol. Samples in buffer were heated at 95 °C for 5 minutes then centrifuged at 3000 g for 1 minute. Gels were submerged in SDS-running buffer (Geneflow EC-870) and denatured samples were loaded into wells. Page-ruler plus (Thermo 26619) was used as a pre-stained ladder and spare wells were filled with diluted loading buffer. A potential difference of 150 V was applied to drive samples into the stacking gel, then proteins were separated by electrophoresis at 180 V.

PVDF membranes with 0.2 µm pores (GE healthcare 162-0177) were activated by submersion in methanol, then equilibrated along with filter paper in transfer buffer (200 ml/l methanol, 15 g/l glycine, 3 g/l Tris-base, 0.02% (w/v) SDS). SDS was not included in the transfer buffer for blots in section 2.3.4 to improve transfer of small proteins. The paper, gel and membrane were layered between electrodes, bubbles were removed with gentle pressure, and 85 mA was applied for ~1.5 hours. Post-transfer, membranes were re-wet with methanol and transfer buffer prior to blocking.

2.3.3 Probing

Membranes were blocked with tris-buffered saline (TBS)(6.05 g/l Tris-base, 8 g/l NaCl, pH 7.4) with the supplements indicated in table 8 for 1 hour at room-temperature with rocking. Blocked membranes were probed as indicated overnight at 4 °C with rocking. Membranes were washed six times over an hour with TBS supplemented with 0.05% (v/v) Tween-20 (TBST). Horseradish-peroxidase (HRP) conjugated antibodies were used to probe blots for 1 hour at room-temperature with rocking.

Antibody	Block	Dilution	Species	Target
mAb3209	TBS with 5% (w/v) BSA	1:1000	Mouse	BMP9 growth-factor domain (non-reduced)
Sc-514211 (SantaCruz)	TBS with 5% (w/v) BSA	1:1000	Mouse	BMP9 growth-factor domain (reduced)
AF3879 (R&D Systems)	TBS with 5% (w/v) Marvel milk	1:2500	Goat	BMP9 prodomain (reduced & non-reduced)
A5441 (Sigma)	TBS with 5% (w/v) Marvel milk	1:5000	Mouse	β-actin
P0447 (Dako)	TBST with 5% (w/v) Marvel milk	1:2000	Goat-HRP	Mouse IgG
ab6742 (AbCam)	TBST with 5% (w/v) Marvel milk	1:2000	Rabbit-HRP	Goat IgG

Table 8. Western blot antibodies & conditions.

Membranes were again washed with TBST, and additionally washed twice with PBS. Membranes were coated in ECL reagent (GE healthcare), sealed in plastic film and exposed

to chemiluminescence film (GE healthcare Amersham hyperfilm) in a dark room. After varying amounts of time, films were developed by an automatic machine. Developed films were scanned into a computer. I used the 'gels' tool of 'FIJI (is just image J)' to measure the intensity of bands, being careful to use films which were not saturated.

2.4 Quantitative real-time PCR

2.4.1 Human aortic endothelial cell culture

Human aortic endothelial cells (AECs)(Lonza) were grown in endothelial growth medium (EGM2)(Lonza CC-1362) supplemented with 5% (v/v) FBS. AECs between passages 5 and 7 were seeded at 150 000 cells/well into 6-well plates and grown to confluence. Prior to treatment, they were washed for 1 hour in endothelial cell basal medium (EBM2)(Lonza CC-3156) supplemented with 0.1% (v/v) FBS, then quiesced in this medium overnight. In the morning, media was refreshed to give 1.5 ml/well. EDTA-plasma samples were thawed on ice, and the indicated volumes were swirled into each well and incubated for 1 hour.

2.4.2 Human pulmonary artery endothelial cell culture

Human pulmonary artery endothelial cells (PAECs)(Lonza) were grown in EGM2. PAECs between passages 4 and 8 were seeded, quiesced and treated as in section 2.4.1.

2.4.3 Human microvascular endothelial cell culture

Human microvascular endothelial cells (HMEC1)(LGC standards)(Ades et al. 1992) were grown in MDCB-131 media (Gibco 10372019) supplemented with 10% (v/v) FBS, 10 mM L-Glutamine (Invitrogen 25030-032), 1 mg/ml hydrocortisone (Sigma HO888), 10 ng/ml endothelial growth factor (Sigma E9644) and antimicrobials. hMECs were seeded, quiesced and treated as in section 2.4.1, except MDCB-131 media was used to quiesce cells.

2.4.4 Blood outgrowth endothelial cell culture

Human blood outgrowth endothelial cells (BOECs) were grown in grown in EGM2 without heparin supplemented with 10% FBS (Ormiston, Toshner, et al. 2015). BOECs were seeded and quiesced as in section 2.4.1. Serial dilutions of HEK-EBNA cell conditioned media were prepared in 1.5 ml of prewarmed EBM2 supplemented with 0.1% (v/v) FBS, and cells were treated with this mix for 4 hours.

2.4.5 RNA extraction & cDNA preparation

After treatment, media were aspirated and cells were lysed with 350 µl RLT buffer supplemented with 1% (v/v) β-mercaptoethanol. RNA was extracted using an RNeasy kit

according to the manufacturer's instructions (Qiagen 74104). An on-column DNA digestion was carried out according to the manufacturer's instructions (Qiagen 79254). The quality and concentration of RNA was assessed by NanoDrop.

For tissues, flushed samples were dissected out of mice and snap frozen. Tissue was stored at -80 °C. Eppendorf tubes containing a stainless-steel bead, tweezers, razorblades and the benchtop were chilled with dry ice. Pieces of frozen tissue (1 lung lobe, or ~2 mm^3 of liver) were cut with razorblades and transferred to the tubes. Tubes were placed in chilled TissueLyser racks and 1 ml of Trizol reagent (Gibco 15596) was added to each. Tissue was homogenised by shaking at 25 Hz for ~10 minutes for lung and ~ 6 minutes for liver until there were no visible lumps. Homogenised samples were freeze-thawed. Lysates were transferred to phase-lock tubes (5prime 2302830) and left to reach room-temperature for 5 minutes. Then 200 µl of chloroform was added to each tube and they were shaken until an emulsion formed. Tubes were centrifuged at 12000 g for 10 minutes at 4 °C and the aqueous layer was transferred to a fresh tube. To precipitate RNA, 500 µl of cold isopropanol was added and tubes were incubated at -70 °C for 30 minutes, followed by centrifugation at 12000 g for 10 minutes at 4 °C. The pellet was washed with 75% (v/v) ethanol in water by vortexing followed by centrifugation at 7500 g for 5 minutes at 4 °C. RNA was dissolved in RNase-free water by trituration and incubation at 65 °C. The concentration and quality of RNA was assessed by NanoDrop: samples were re-extracted if the ratio of absorbances at 260 nm and 280 nm was not ~2. Secondly, RNA was assessed by gel electrophoresis, using 1% (w/v) agarose gels in TBE buffer (BioRad 161-0770) stained with 0.01% (v/v) GelRed. Samples were re-extracted if two clean bands corresponding to rRNA were not visible.

A high capacity reverse-transcriptase kit (Thermo 4368813) was used to produce cDNA with random primers from 1 µg of RNA per sample according to the manufacturer's instructions. Both RNA and cDNA were stored at -80 °C.

2.4.6 qPCR

Quantitative real-time polymerase chain reaction analysis was carried out in 384-well plates (Applied Biosystems). Two µl/well of a 1 in 10 dilution of cDNA was added. Additionally, 0.2 µl ROX reference dye (Invitrogen 12223012), 5 µl SYBR green jumpstart Taq polymerase ready mix (Merck), forward and reverse primers each to a final concentration of 200 nM (table 9), and water to a final volume of 10 µl was mixed into each well.

The cycling profile of the PCR reaction was 95 °C for 2 minutes, followed by 50 cycles of 95 °C for 30 seconds, 55 °C for 30 seconds and 72 °C for 30 seconds. The reaction was

carried out in a QuantStudio6 system (Applied Biosystems) which determined cycle threshold (C_t) values for each well automatically. Each sample was measured in triplicate wells. Any C_t values ≥ those obtained from water in the absence of cDNA were discarded. The mean of triplicate C_t values was calculated. Where multiple housekeeping genes were measured, the geometric mean of all C_t values was used so all had equal weight. Gene expression was normalised to the housekeeping genes and presented as relative fold change compared to a control (as indicated) using the $2^{-\Delta\Delta Ct}$ method (Livak and Schmittgen 2001).

Gene	Primer Sequences	Source
Human *B2M*	Proprietary Cat.№ QT00088935	Qiagen
Human *ID1*	For: 5'- CGAAGTTGGAACCCCGGGG-3' Rev: 5'- CAGGAACGCATGCCGCCTCG-3'	Sigma
Human *ID2*	For: 5'- GACCCGATGAGCCTGCTATAC-3' Rev: 5'- GGTGCTGCAGGATTTCCATCT-3'	Sigma
Human *HEY1*	For: 5'- GGCTCTAGGTTCCATGTCCC-3' Rev: 5'- AGCAGATCCCTGCTTCTCAA-3'	Sigma
Human *HEY2*	For: 5'- GCCATACAGATGCCGACAGA-3' Rev: 5'- CAGTTACCGAGCTGCCTTGA-3'	Sigma
Human *BMPR2*	For: 5'- CAAATCTGTGAGCCCAACAGTCAA-3' Rev: 5'- GAGGAAGAATAATCTGGATAAGGACCAAT-3'	Sigma
Human *SMAD9*	For: 5'- TACTGTCGCGTGTGGCGCTG-3' Rev: 5'- AGCACAGGAGGCAGTACTGGAG-3'	Sigma
Human *SMAD9 vA*	For: 5'- CACCCCTGCCTTATCATGCCAC-3' Rev: 5'- AGTAGGCGACCGAGCACCAGT-3'	Sigma
Mouse *B2M*	For: 5'- GTATACTCACGCCACCCACC-3' Rev: 5'- TGGGGGTGAATTCAGTGTGAG-3'	Sigma
Mouse *Id1*	For: 5'- GCTCACTTTGCGGTTCTGG-3' Rev: 5'- ACGACATGAACGGCTGCTACT-3'	Sigma
Mouse *Id2*	For: 5'- CGATAGTGGGATGCGAGTCC-3' Rev: 5'- CCTGCAGCACGTCATCGAT-3'	Sigma
Mouse *Hprt*	For: 5'- CTTCCTCCTCAGACCGCTTT-3' Rev: 5'- ATCGCTAATCACGACGCTGG-3'	Sigma
Mouse *Actb*	For: 5'- GGGAAATCGTGCGTGACAT-3' Rev: 5'- GTGATGACCTGGCCGTCAG-3'	Sigma
Mouse *Pck1*	For: 5'-TTGAACTGACAGACTCGCCC-3' Rev: 5'- GGCACTTGATGAACTCCCCA-3'	Sigma
Mouse *Fasn*	For: 5'-GGCCCCTCTGTTAATTGGCT-3' Rev: 5'-GGATCTCAGGGTTGGGGTTG-3'	Sigma
Mouse *Srebf1*	For: 5'-CTTTTCCTTAACGTGGGCCT-3' Rev: 5'-TCAAAACCGCTGTGTCCAGT-3'	Sigma
Mouse *Me1*	For: 5'-GGACCCGCATCTCAACAAGG-3' Rev: 5'-CAGGGCGGCAACAATCCAT-3'	Sigma
Mouse *Cola*	For: 5'-CGATGGATTCCCGTTCGAGT-3' Rev: 5'-CATTAGGCGCAGGAAGGTCA-3'	Sigma

Table 9. qPCR primers. Dr Paul Upton designed all primers except mouse *Id1* and *Id2*, and tested all primers except *Pck1, Fasn, Srebp1, Me1* and *Cola,* which I tested. *SMAD9* has two splice variants, with the first primer detecting both, and the second only variant a.

Prior to analysing experimental samples, primers were tested using serially diluted control cDNA. The primer efficiencies were automatically calculated, with 90-110% deemed acceptable. The slopes of amplification curves, and the melt curves were also inspected, with steep curves and a single peak respectively, required.

2.5 Deglycosylation of BMP9

To deglycosylate BMP9 I mixed 1 µl of PNGase F (New England biolabs p0704), a volume HEK-EBNA cell conditioned media containing 15 ng of BMP9 according to ELISA, 2 µl glycobuffer-2, and water to a total volume of 20 µl. This was incubated for 4 hours at 37 °C. I denatured a second set of samples by mixing them with glyco-denaturing buffer and heating at 100 °C for 10 minutes. These were deglycosylated as before, except 2 µl of 10% (v/v) NP-40 was present in the mix, and the reaction only took 1 hour.

2.6 Luciferase-based ALK1 signalling assay

Variations of this assay are published (Wooderchak-Donahue et al. 2013; Wei et al. 2014).

2.6.1 Plasmids

Plasmid containing a palindromic SMAD1/5 binding element that drives firefly luciferase expression (pBRE:Luciferase) was courtesy of Prof. Peter ten Dijke (pGL3-(BRE)2-luciferase from Korchynskyi and ten Dijke 2002). Plasmid constitutively expressing human ALK1 (pcDNA3-ALK1) was courtesy of Prof. Richard Trembath. Plasmid containing thymidine kinase promoter driven sea pansy luciferase (pTK:*Renilla*) was from Promega (E2241). Plasmids were expanded in bacteria as in section 2.1.1. I used a Hi-Pure maxiprep kit to purify plasmid, using high-speed centrifugation, according to the manufacturer's instructions (Invitrogen K210006). I checked the quality and concentration of DNA by NanoDrop.

2.6.2 Cell culture

Mouse myoblast C2C12 cells were grown in DMEM supplemented with 10% (v/v) FBS and antimicrobials. To prevent differentiation, cells were passaged before reaching confluence. Cells were seeded at 30 000 cells/well in 24-well plates and grown overnight. Transfections were performed as in section 2.1.3 using 400 ng of pTK:Renilla, 400 ng of pBRE:Luciferase, and 400 ng of pcDNA3-ALK1. Cells were returned to growth medium overnight. Transfected cells were washed in serum-free DMEM for 1 hour, then incubated in fresh DMEM overnight. Quiescent cells were treated with a 500 µl mix of DMEM and HEK-EBNA cell conditioned

media for six hours. Each treatment was performed in triplicate (in addition to three biological repeats performed on separate days).

2.6.3 Luciferase activity measurement

I measured luciferase activity using a modified version of Promega's DualGlo system (E2920). Treatment solutions were replaced with 150 µl/well of a 1:1 mix of luciferase reagent and DMEM. After 10 minutes, this was transferred to a white 96-well white plate and firefly luciferase activity was measured in a luminometer (Promega GloMax multi+) with a 10 second integration time. To measure *Renilla* luciferase, 75 µl/well of Stop&Glo reagent was added and luminescence was remeasured. Firefly luciferase activity was normalised by *Renilla* luciferase. The mean of each triplicate was calculated. Normalised means were linearly transformed so, for each plate, 100 pg/ml of wildtype Pro:BMP9 had 100% activity and DMEM had 0% activity.

2.7 Caspase 3/7 Glo apoptosis assay

PAECs were grown as in section 2.4.2 and seeded at 30 000 cells/well into 48-well plates. Once confluent, cells were washed with EBM2 supplemented with 0.1% (v/v) FBS, and quiesced in 200 µl/well of this overnight. Treatment wells were additionally supplemented with HEK-EBNA cell conditioned media. The following morning, CaspaseGlo reagent (Promega G8901) was equilibrated to room-temperature, then 100 µl was spiked into each well. The plate was incubated for 10 minutes at room-temperature with shaking, then the contents were transferred to a white 96-well plate and measured in a luminometer with a 0.5 second integration time. Luminescence was brightest ~30 minutes after lysis.

2.8 Annexin-V flow cytometry

2.8.1 Apoptosis induction

BOECs were seeded and grown as in section 2.4.4. Once confluent, they were quiesced in 2 ml of EBM2 supplemented with 2% (v/v) FBS overnight. Additionally, treatment wells were supplemented with HEK-EBNA cell conditioned media. The next morning, cycloheximide (Sigma C7698-1G) was dissolved to 5 mg/ml in EBM2 by vortexing, and tumour necrosis factor (TNFα)(R&D systems 210-TA) was thawed on ice. Concentrated mixes of both were prepared, and wells of cells were spiked with 200 µl so they were exposed to a final concentration of 50 µg/ml cycloheximide and 3 ng/ml TNFα.

2.8.2 Staining & measurement

After ~3.5 hours, when cell morphology began changing but they were still adherent, cells were briefly washed with PBS, trypsinised and suspended in ice-cold PBS. Cells were stained with the Annexin-V / propidium iodide (PI) apoptosis detection kit (BD biosciences 556547) according to the manufacturer's instructions. Unstained and singly stained cells were prepared to facilitate compensation against overlap in the emissions of each dye. Staining of at least 15000 cells/treatment was measured with an accuri flow-cytometer (BD biosciences) using filter 1 to measure PI and filter 3 to measure FITC.

2.8.3 Data analysis

Data were exported to FlowJo (version 10) and channels were compensated using the wizard tool. Samples were gated based on forward and side-scatter such that debris were excluded, but both healthy and apoptotic cells were captured. I applied the same gate to all samples and checked it was appropriate for each. Staining intensity plots were gated such that no unstained cells, and very few cells not exposed to TNFα, were annexin V or PI positive. I applied the same gate to all samples and noted the proportion of cells in each quadrant.

2.9 *BRE*-HMEC activity measurements

Dr. Paul Upton generated a HMEC1 line stably expressing the BRE:luciferase vector by transfecting cells with linearized pGL3-(BRE)2-luciferase and pSelect-puro (Invivogen) followed by selection with puromycin for 10 days. Transduced cells were grown as in section 2.4.3. These were seeded into 96-well plates at 15000 cells/well and grown until confluent. Cells were quiesced in MCDB-131 medium overnight. In the morning, cells were placed in 100 µl/well fresh MCDB-131. This was supplemented with plasma or other treatments where indicated. After 6 hours, 100 µl/well ONE-Glo was added (Promega E6120). Well contents were transferred to a white 96-well white plate and luminescence was measured with a 0.5 second integration time.

2.10 Immunoprecipitations

2.10.1 Immunoprecipitation with anti-BMP9 for Western blotting

Protein-G conjugated sepharose beads (Sigma P3296) were washed thrice by resuspending in PBS supplemented with 1% (w/v) BSA and centrifugation at 12000 g for 3 minutes, using wide-bore pipette tips to reduce loss. One ml plasma samples were precleared of endogenous antibodies by incubating them with 50 µl of washed beads for 1 hour at 4 °C with rotation.

Two µg of either human ALK1-Fc conjugate, mAb3209 or AF3879 were incubated with 50 µl of washed beads for 1 hour at 4 °C with rotation. Coated beads were again washed thrice. Samples were cleared by centrifugation at 12000 g for 5 min and transferred to the coated beads. This mix was incubated overnight at 4 °C with rotation. Beads were pelleted and washed thrice with ice-cold PBS. Beads were heated at 98 °C in reducing SDS-loading buffer for 10 minutes to elute BMP9.

2.10.2 Immunoprecipitation with anti-BMP9/10 for ELISA & activity

Fifteen µl of protein-G conjugated metal beads (Thermo 10004D) were washed thrice by resuspending in PBS followed by magnetic separation. Beads were incubated with 7.5 µg of mAb3209 (anti-BMP9), 15 µg Ab108-C (non-specific IgG), 15 µg mAb2926 (anti-BMP10) or AF3956 (anti-BMP10-prodomain) for 30 minutes at room-temperature with rotation. Beads were again washed thrice and added to 200 µl plasma samples. Samples were incubated for 20 minutes (BMP9) or overnight (BMP10) at room-temperature with rotating, then samples were cleared by magnetic separation.

2.10.4 Immunoprecipitation with ALK1-Fc

Like section 2.10.2, except mAb3209 was replaced with 3 µg ALK1-Fc (R&D systems 370-AL). For Western blotting, amounts were scaled up to use 1 ml of plasma and protein was eluted from the beads as in section 2.10.1. To covalently link ALK1-Fc to beads, they were incubated with 5 mM or 1 mM of BS^3 reagent (Thermo 21580) for 30 minutes at room-temperature, then the reaction was quenched with 0.05 M tris-HCl (Sigma T2663), and beads were washed thrice. For Coomassie staining gels washed thrice in water, incubated with 20 ml SimplyBlue (Invitrogen LC6060) for 1 hour at room-temperature with rocking, then 100 ml water for 1 hour, then 20% (w/v) NaCl in water overnight. Gels were briefly washed in water, sandwiched in plastic and scanned.

2.11 Size exclusion chromatography

2.11.1 Evans blue

For determining whether Evans blue was bound to albumin, 1 g of sephadex G-25 powder (Sigma) was added to 20 ml of boiling water and left to cool overnight. The beads were poured into a 20 cm column (GE healthcare C 10/20) and left to settle under gravity. Evans blue treatment solutions were prepared as in section 2.16.1, and 50 µl was added to the top of the gel bed. Sequentially, 500 µl volumes of PBS were added to the top of the column, and

500 µl fractions were collected from the bottom, as it flowed through under gravity. The absorbance of 100 µl aliquots of each fraction was measured at 595 nm in a plate reader.

2.11.2 Plasma & serum

Sephacryl S-200 gel beads in 20% ethanol (GE healthcare 17-0584-01) were sedimented by gravity and the liquid was poured off. The beads were resuspended in two volumes of water supplemented with 0.05% (v/v) tween-20. This was repeated to produce a final volume of beads plus 0.05% tween that was approximately twice the volume of settled beads. This was gently stirred to produce a homogenous slurry, which was poured into a 70 cm column (GE healthcare C 16/70) that was fitted with a packing reservoir (GE healthcare 19-5110-01) at the top. A plumb line was used to ensure the column was vertical.

A peristaltic pump (Gilson miniplus 3) was attached and ~2 ml/min (speed 4.7) water supplemented with 0.05% (v/v) tween-20 was pumped through the column until the gel bed stabilised. The packing reservoir was removed, and the column was equilibrated with 280 ml of running buffer at 0.8 ml/min (speed 1.8). Running buffer comprised PBS without calcium or magnesium supplemented with 5 mM EDTA, or PBS with 0.9 mM calcium and 0.1 mM magnesium (Sigma D8662) as indicated. When not in use, the column was stored in 20% (v/v) ethanol. Every five uses, the column was washed with 280 ml of 0.2 M NaOH.

Samples were prepared by mixing 1.4 ml of EDTA-plasma, serum or running buffer with coloured markers—50 µl dextran blue (stock 30 mg/ml), 30 µl equine myoglobin (stock 30 mg/ml), 30 µl vitamin B12 (stock 7.5 mg/ml) and 3 µl phenol red (stock 20 mg/ml)—and recombinant BMP9 (100 ng) and Pro:BMP10 (100 ng) as indicated. Samples were centrifuged at 21000 g for 10 minutes at 4 °C to sediment particles. Samples were taken into a 2 ml syringe fitted with column tubing. The pump was disconnected and the syringe tubing was threaded through the column lid so sample could be gently expelled under the running buffer at the surface of the gel bed. The pump was then reconnected and running buffer was applied at ~0.5 ml/minute (speed 1.16).

When the blue dye front reached the end of the column, 55-drop (~2.5 ml) fractions were collected by an automated collector (BioRad model 2110). At this time during the first run, the positions of all the markers was labelled on the column, so fraction collecting could begin at a similar point in subsequent runs. The intensity of marker in each fraction was gauged by eye, and they were stored at -80 °C.

2.12 Furin treatment of serum

Serum was incubated overnight at 30 °C with 10 U/ml furin (NEB P8077). The reaction was quenched by adding EDTA to a final concentration of 5 mM. As a negative control, serum supplemented with 5 mM EDTA was incubated in parallel. Samples were stored at -80 °C. For a positive control, fluorometric furin substrate (Calbiochem 344935) was reconstituted to 10 mg/ml in water. Serum samples prepared as previously were supplemented with 50 µM substrate and protected from light during incubation. Periodically, 20 µl samples, were withdrawn, diluted to 200 µl with water, put in a 96-well black plate and fluorescence was measured with a plate reader (PerkinElmer victor^3) using 355 nm excitation and 460 nm emission wavelength filters.

2.13 *Ex vivo* culture of mouse organs

C57/BL6 mice were killed by CO_2 inhalation. Organs were dissected, chopped into ~1 mm^2 pieces and placed in ice-cold PBS. These were transferred into 24-well plates with 500 µl/well DMEM supplemented with antimicrobials. Additionally, this was supplemented with 5 ng/ml recombinant BMP9, 10% (v/v) FBS or 1 µg/ml LPS (Enzo ALX-581-013) as indicated. Plates were incubated in a cell culture incubator. Periodically, 50 µl samples of conditioned media were taken, centrifuged at 21000 g for 10 minutes at 4 °C to clear debris, and stored at -80 °C.

2.14 *Gdf2* knockout mouse phenotyping

Gdf2 knockout mice were c-terminal deletants on a C57/BL6/J background, courtesy of Prof. Se-Jin Lee (unpublished). Mice had access to food and water *ad libertum*. I genotyped mice using a protocol from Dr. Claudia Mitrofan. I confirmed genotyping via ELISA measurement of plasma BMP9 levels or qPCR of hepatic *Gdf2* transcripts. *Gdf2* knockout, heterozygous and wildtype littermates of both sexes aged 3-6 months are being collected. Blood from live mice was placed in EDTA-tubes as in section 2.14.2. Blood cell counts and morphology was measured using a Wooley ABC (mouse) analyser. Mice were killed by injecting sodium pentobarbital and exsanguinated via the inferior vena cava. To collect serum, blood was placed in Eppendorf tubes, clotted for 20 minutes at room-temperature and centrifuged at 3000 g. Serum was analysed by Adenbrooke's Core Biochemical Assay Laboratory.

2.15 Pharmacokinetic studies

2.15.1 Pro:BMP9 administration

Wildtypes were male C57/BL6 mice purchased from Charles River and used at ~6 weeks old. *Gdf2* knockout mice were males aged ~6 weeks. Mice were weighed at the start of the experiment. To make intravenous injection and saphenous vein bleeding easier, mice were warmed in a 40 °C chamber for 10 minutes prior to either.

Dr. Aleksandra Lawera purified human Pro:BMP9 at a total protein concentration of 100 ng/µl. One µl aliquots were placed into siliconized Eppendorf tubes (Fisher 1199695). Separate aliquots of vehicle—PBS supplemented with 0.1% (w/v) mouse serum albumin (Sigma A3139) filtered through a 0.2 µm filter—were prepared and both were stored at -80 °C. On the day of administration, I thawed each on ice and added 199 µl vehicle to the Pro:BMP9. For *Gdf2* knockout mice, Pro:BMP9 was administered at this concentration (0.5 ng/µl), but for wildtype mice, I transferred this solution serially through 4 more tubes to reach a concentration of 2.5 ng/µl. I drew 5 µl of these solutions per gram of bodyweight into a 1 ml syringe and Stephen Moore administered them by tail-vein injection.

2.15.2 Tissue collection

Dr. Alexi Crosby withdrew 150 µl of blood by pricking the saphenous vein and collected it into EDTA-tubes (Microvette CB 300 K2E). Mice were killed by pentobarbitone injection, and Stephen Moore collected blood into EDTA-tubes by cardiac puncture. I centrifuged EDTA-tubes at 3000 g for 10 minutes at 4 °C, aliquoted plasma and stored it at -80°C. I exposed and snipped the inferior vena cava, and flushed the circulation by injecting ~5 ml of 20 U/ml heparin in PBS through the right ventricle. I dissected organs, snap froze them and stored at -80 °C. For *Gdf2* knockout mice, I left the right lung in place and tied of the right trachea. I then inflated the left lung to twice its collapsed size with 10% formalin (Cellstore pot BAF-5000-08A) by intratracheal injection, tied it to maintain its volume, and placed it in 10% formalin for 48 hours. I transferred fixed lung to 70% (v/v) ethanol in water and sent them for processing into paraffin blocks (Pathology department, Addenbrooke's Hospital).

2.16 Evans blue

2.16.1 Preparation of Evans blue & LPS solutions

Several serotypes of LPS were trialled: *E. coli* O111:B4 (B4)(Sigma L5293), *E. coli* O55:B5 (B5) (Enzo ALX-581-013) and *E. coli* O127:B8 (B8)(Sigma L3129). These were diluted to 1 mg/ml. Doses, timings and routes of administration are indicated. For intranasal administration,

Stephen Moore and I lightly anesthetised mice with isoflurane, held them upright and put LPS solution on their nostrils with a pipette. PBS (Sigma D8537) was supplemented with 1% or 0.5% (w/v) Evans blue dye (Sigma E2129) with or without 4% (w/v) low-endotoxin bovine serum albumin (Sigma A4919) as indicated. The solution was passed through a 0.2 μm filter and stored at -25 °C. Stephen Moore administered 4 μl of Evans blue solution per gram of mouse bodyweight (~20 mg/kg) intravenously or intraperitoneally as indicated.

2.16.2 Extraction & quantification of Evans blue

One hour after Evans blue administration, mice were killed by sodium pentobarbital injection. The inferior vena cava was snipped and ~5 ml of heparinised saline was flushed via the right ventricle. Tissues were dissected and snap frozen. Pieces of lungs were weighed, finely diced with a razor blade and added to 10 μl formamide (Sigma 47670) per milligram of tissue. This was incubated overnight at 37 °C with shaking. Samples were centrifuged at 21000 g for 10 minutes to clarify the supernatant, and 200 μl was transferred to a clear 96-well plate. Absorbance was measured in a plate reader at the indicated absorbance (due to equipment breakdowns, different readers and absorbance wavelengths were used between experiments as indicated).

2.17 Ethics & human samples

All animal studies followed University of Cambridge guidelines and the Animal Scientific Procedures Act as amended 2013. All regulated procedures were approved under project licences 80/2460 and 70/8850. Human patient plasma samples were from the National Cohort of Idiopathic and Heritable PAH (NCT01907295) approved by the ethics review committee (13/EE/0203). Control comparisons for these are previously published (Rhodes et al. 2017). Vascular gradient samples were collected for the Royal Papworth Hospital Tissue Bank. Plasma and serum for characterising ELISAs and circulating species of BMP9 and BMP10 were from volunteers in the Morrell group.

2.17 Statistics

Except where indicated, statistical analyses were carried out using GraphPad Prism 5. Experiments comprising multiple groups were analysed with one-way ANOVAs. Dose responses of ≤ 3 doses, or experiments comprising multiple variables e.g. sex and genotype, were analysed with two-way ANOVAs. Where only two factors were compared (indicated in the text), Student's t-tests were used. Where dose responses of >3 doses were carried out e.g.

ELISA recovery testing, EC50s were calculated using Prism's normalised log(dose)-response function. Matched analyses were used for assays performed in batches e.g. comparison of BMP9 variants generated *in vitro*, or when samples from the same source were exposed to treatments e.g. plasmas treated with IgG versus anti-BMP9. Unmatched analyses were used for assays performed on samples from different sources and measured simultaneously e.g. control versus patient ELISAs. Significant differences between columns, as indicated in figures, were calculated by post-hoc testing. For two-way ANOVAs, Bonferroni testing was used. For one-way ANOVAs, comparisons to a control column (e.g. variant BMP9 versus wildtype BMP9) were made with Dunnett's tests, whilst comparisons between other columns were made with Bonferroni tests.

There were insufficient data to assess for normality. Nonetheless, in the first instance data were analysed with the tests described above, since these are relatively robust against deviations from normality and maximise statistical power. Non-parametric tests are less robust to deviations from unideal distributions and give lower power. However, to affirm conclusions drawn in section 3 and 5.6, one-way matched analyses were repeated with Friedman tests followed by Dunn's post-hoc analyses. On the advice of Dr. James Liley, two-way analyses were repeated using stratified Van Elteren tests using R. Secondly, the results were confirmed by simulation using R. Briefly, data from each experiment were randomly redistributed between conditions multiple times. The rate at which the data produced differences as extreme as those observed was calculated. Each of these tests gave results consistent with the parametric tests at a significance level of 0.05. Reanalyses were not undertaken for other sections, since either there were sufficient data to suggest data were not highly non-normal by eye, or data were used for optimisations and observational discussion where statistical inferences did not determine conclusions.

Results

3. The impact of *GDF2* mutations on BMP9 proteins

3.1. Introduction

A large majority of heritable PAH and a minority of idiopathic PAH is associated with mutations in genes encoding components of the BMPR-II signalling complex (Ma and Chung 2017; Miyazono, Kamiya, and Morikawa 2010; Machado et al. 2009). Excepting *BMPR2*, these genes are also associated with HHT (Vorselaars et al. 2015; Faughnan, Granton, and Young 2009). The known cognate ligands for this receptor complex are BMP9 and BMP10.

The National Institutes of Health Research bio-resource for rare-diseases (NIHR-BRIDGE) study, a pilot study for Genomics England, recruited patients diagnosed with several rare diseases, including PAH, for whole-genome sequencing. Stefan Gräf's group was responsible for genetic analysis of these patients, as briefly described here. After quality control, 1048 whole genome sequences from unrelated people diagnosed with type 1.1 PAH were compared to 7979 from unrelated control patients with other rare diseases. Since this is a relatively small sample, a rare-variant analysis was undertaken to find highly deleterious causal variants associated with PAH (Gräf et al. 2018). Qualifying variants were in protein coding sequences, had a minor allele frequency of <1 in 10 000, a combined annotation dependent depletion (CADD)(Rentzsch et al. 2019) score > 15, and were predicted to be deleterious/damaging by either SIFT (Vaser et al. 2016) or PolyPhen (Adzhubei et al. 2010).

Several versions of burden analysis show that *GDF2* is associated with PAH with genome-wide significance. Unusually, most of the PAH associated variants in *GDF2* are missense-mutations, and so their functional effect is difficult to predict without further analyses (table 10). Moreover, SIFT and PolyPhen predictions do not take context into account, and CADD scores depend on the quality of annotation, so these *in silico* predictors of deleteriousness require validation. Therefore, we undertook to express and analyse some of the BMP9 missense variants found in people *in vitro.*

The Morrell group has an expression vector for *PreProBMP9* in HEK-EBNA cells, which uses genes from the Epstein-Barr virus to stabilise the vector as an episome in the nucleus and a cytomegalovirus promoter to drive transcription. This produces conditioned media rich in Pro:BMP9. HEK-EBNA cells can be grown in chemically defined media without serum which makes the conditioned media amenable to downstream analysis. Dr. Rick Salmon helped me carry out site-directed mutagenesis of the *PreProBMP9* expression vector, transfect mutagenized vectors into HEK-EBNA cells, and collect conditioned media. Sixteen expression vectors were created in total—a mix of *PreProBMP9* variant proteins expected to be pathogenic and benign (table 10 top).

Putatively pathogenic variants were classified as such by the rare-variant analysis described above, except for BMP9-Y351H. This variant, was sufficiently rare and predicted to disrupt protein structure by CADD, SIFT and PolyPhen scores, but a single allele was found in a paediatric case of primary immune deficiency which prevented statistical association with PAH. Nonetheless, residue 351 is found within the core of the growth factor domain interacting with distant residues, so Dr. Wei Li predicted the substitution would prevent proper folding. Moreover, the patient harbouring this variant had a family history of PAH

suggesting a genetic cause. Therefore, BMP9-Y351H was reclassified as putatively pathogenic. Putatively benign variants include some which were common in the population, not associated with PAH, and/or not predicted to disrupt protein structure.

Each vector was transfected into three independent batches of HEK-EBNA cells, so all the following data is based on three separate measurements. Figure 7 shows the species of BMP9 that can result from expression of *PreProBMP9*.

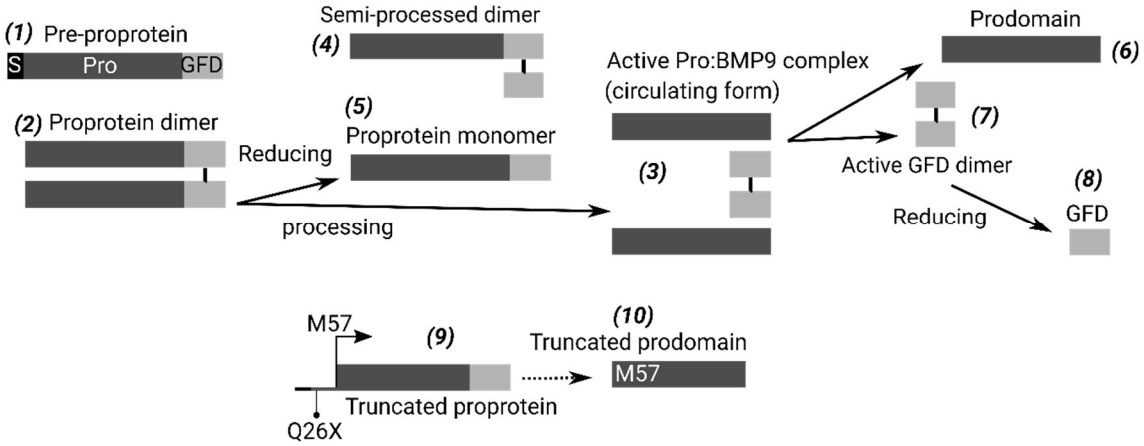

Figure 7. Schematic of BMP9 species. *PreProBMP9* missense variants were expressed *in vitro*. BMP9 dimerises and is processed during secretion, forming a non-covalent prodomain:growth-factor domain complex. This may be dissociated during Western blotting, or spontaneously dissociate when disrupted by deleterious variants. Reduction of the inter-chain disulphide bond can occur spontaneously but the complex remains associated (Wei et al. 2014). The numbers are used to label bands on subsequent Western blots. Species (9) and (10) refer to BMP9-Q26X expressed in section 3.6.

Table 10 (overleaf). Protein coding *GDF2* variants found in the NIHR-BRIDGE study at a minor allele frequency <1/250. Top: variants assessed *in vitro* or measured in patient plasma samples. Bottom: other variants analysed *in silico*. HGVSc = human genome variation society sequence change; csq = consequence type; HGVSp = protein change (bold = acronym used herein); Freq = frequency in exome aggregation consortium database; CADD = combined annotation dependent depletion (includes sequence conservation, *in silico* predictions of disrupted protein structure, sequence DNAse hypersensitivity, transcription factor binding etc. Higher score = more deleterious); SIFT = sorting intolerant from tolerant (a score of deleteriousness based on empirical measurements of how well generic proteins tolerate one amino-acid being substituted for another); PolyPhen = polymorphism phenotyping version 2 (similar to SIFT); Disease found in = which cohort of the NIHR-BRIDGE study the variants were found in (PAH = pulmonary arterial hypertension, a = Specialist pathology: evaluating exomes in diagnostics, b = Genomics England 100,000 genomes pilot study, c = primary immune disorders, d = bleeding and platelet disorders, e = hypertrophic cardiomyopathy, f = paediatric neurodevelopmental disorders, g = multiple primary malignant tumours, h = steroid resistant nephrotic syndrome, i = intrahepatic choliosis of pregnancy, j = stem cell and myeloid disorders, k = cerebral small vessel disease); Other genes = mutations in other genes which could be relevant in PAH that were found alongside the *GDF2* variant reported in the PAH patient. The NIHR-BRIDGE study comprised of 1048 PAH patients, and 7979 genomes from other groups. Shading: lightest = lowest value, darkest = highest value. Note that classifications of benign and pathogenic are made with regard to PAH specifically.

	HGVSc	csq	HGVSp		Plasma sample	Studied *in vitro*	ExAC	cadd	SIFT	PolyPhen	Disease found in (allele count) PAH	a	b	c	d	e	f	g	h	i	j	k	Other mutation
benign *in silico*	c.244A>G	missense	p.Arg82Gly	R82G	+		9.07E-05	24.2	deleterious	PossDam	2	0	0	3	0	0	0	0	0	0	0	0	
	c.871G>A	missense	p.Gly291Ser	G291S	+		3.30E-05	0	tolerated	Benign	1	0	2	0	0	1	0	0	0	0	0	0	
	c.911C>T	missense	p.Thr304Met	T304M	+		1.61E-03	0.01	tolerated	Benign	1	3	2	0	2	0	3	1	2	0	0	0	
	c.997C>T	missense	p.Arg333Trp	R333W	+		1.65E-05	6.43	tolerated	Benign	1	0	0	2	0	0	0	0	0	0	0	0	
	c.53G>T	missense	p.Gly18Val	G18V	+	+	0	18.5	tolerated	Benign	1	0	0	0	0	0	0	0	0	0	0	0	
	c.221G>A	missense	p.Gly74Glu	G74E	+	+	2.72E-04	15.9	deleterious	Benign	1	0	3	0	1	0	0	0	0	0	1	1	
	c.311C>T	missense	p.Pro104Leu	P104L	+	+	3.35E-05	28.8	deleterious	Damaging	1	1	0	0	0	0	0	0	0	0	0	0	
	c.352A>T	missense	p.Ile118Phe	I118F	+	+	1.06E-03	0.01	tolerated	Benign	2	0	0	0	0	0	0	0	1	1	0	0	
	c.460G>A	missense	p.Val154Ile	V154I	+	+	0	8.37	tolerated	Benign	1	0	0	0	0	0	0	0	0	0	0	0	
	c.652G>A	missense	p.Asp218Asn	D218N	+	+	3.18E-03	24.4	deleterious	Damaging	3	7	8	0	4	0	0	0	2	4	7	2	
	c.889G>A	missense	p.Glu297Lys	E297K	+	+	0	5.91	tolerated	Benign	1	0	0	0	0	0	0	0	0	0	0	0	
	c.905A>T	missense	p.Glu302Val	E302V		+	0	5.97	tolerated	PossDam	2	0	0	0	0	0	0	0	0	0	0	0	
	c.1190A>G	missense	p.Lys397Arg	K397R		+	3.01E-04	25.8	deleterious	Damaging	0	0	1	0	0	0	0	0	0	0	0	0	
Pathogenic *in silico*	c.265A>G	missense	p.Met89Val	M89V	+	+	0	24.8	deleterious	Damaging	1	0	0	0	0	0	0	0	0	0	0	0	*KLF2*
	c.328C>T	missense	p.Arg110Trp	R110W		+	0	35	deleterious	Damaging	1	0	0	0	0	0	0	0	0	0	0	0	
	c.427G>A	missense	p.Glu143Lys	E143K		+	0	28	deleterious	Damaging	1	0	0	0	0	0	0	0	0	0	0	0	
	c.958A>T	missense	p.Ser320Cys	S320C		+	0	23.3	deleterious	Damaging	1	0	0	0	0	0	0	0	0	0	0	0	
	c.1040C>T	missense	p.Ala347Val	A347V	+	+	8.25E-06	23.9	deleterious	Damaging	1	0	0	0	0	0	0	0	0	0	0	0	
	c.1051T>C	missense	p.Tyr351His	Y351H	+	+	0	23.8	deleterious	Damaging	2	0	0	1	0	0	0	0	0	0	0	0	*BMPR1a*
	c.1238C>A	missense	p.Thr413Asn	T413N	+	+	1.98E-05	26.3	deleterious	Damaging	1	0	0	0	0	0	0	0	0	0	0	0	
	c.347-1G>A	Splice acceptor/truncating			+			23.6	NA	NA	1	0	0	0	0	0	0	0	0	0	0	0	*BMPR2*
	Large deletion of chromosome segment				+						2		4			1							

	HGVSc	csq	HGVSp	ExAC	cadd	SIFT	PolyPhen	PAH	a	b	c	d	e	f	g	h	i	j	k	
Pathogenic *in silico*	c.137_150delGTGGGCTGCCTGAG	Frameshift	p.Gly46AlafsTer21	0	NA	NA	NA	1	0	0	0	0	0	0	0	0	0	0	0	*SMAD9*
	c.347A>T	Missense & splice region	p.Asp116Val	0	24.4	deleterious	PossDam	1	0	0	0	0	0	0	0	0	0	0	0	
Benign *in silico*	c.40_48dupTCCCTGCTG	Inframe insertion	p.Ser14_Leu16dup	1.87E-04	NA	NA	NA	0	2	0	0	0	0	0	0	0	0	0	0	
	c.52G>C	missense	p.Gly18Arg	0	13.9	tolerated	PossDam	0	0	0	0	1	0	0	0	0	0	0	0	
	c.69G>T	missense	p.Lys23Asn	2.01E-04	27.8	deleterious	Damaging	0	1	0	0	0	0	0	0	0	0	0	0	
	c.89G>C	missense	p.Arg30Pro	9.12E-06	11.5	deleterious	PossDam	0	0	2	0	0	0	0	0	0	0	0	0	
	c.89G>A	missense	p.Arg30Gln	4.56E-05	2.88	tolerated	Benign	0	0	1	0	0	0	0	0	0	0	0	0	
	c.314C>T	missense	p.Ala105Val	2.52E-05	20.3	tolerated	PossDam	0	0	1	0	0	0	0	0	0	0	0	0	
	c.338G>A	missense	p.Ser113Asn	3.51E-05	14.8	tolerated	Benign	0	1	0	0	0	0	0	0	0	0	0	0	
	c.378C>A	missense	p.Phe126Leu	5.19E-04	0.73	tolerated	Benign	0	1	0	0	0	0	0	0	1	0	0	0	
	c.432G>T	missense	p.Gln144His	0	9.93	tolerated	Benign	0	0	0	1	0	0	0	0	0	0	0	0	
	c.463T>A	missense	p.Ser155Thr	0	21.7	tolerated	PossDam	0	0	0	1	0	0	0	0	0	0	0	0	
	c.508G>A	missense	p.Val170Met	3.30E-05	2.41	tolerated	Benign	1	0	0	0	0	0	0	0	1	0	0	0	
	c.548A>G	missense	p.Asp183Gly	0	11.2	tolerated	PossDam	0	0	0	0	1	0	0	0	0	0	0	0	
	c.619G>T	missense	p.Val207Leu	4.95E-05	23.5	tolerated	Damaging	0	2	1	0	0	0	0	0	0	0	0	0	
	c.712G>A	missense	p.Asp238Asn	5.77E-05	11.4	tolerated	Damaging	0	2	0	0	0	0	0	0	0	0	0	0	
	c.740G>T	missense	p.Gly247Val	0	17.8	tolerated	PossDam	0	0	1	0	1	0	0	0	0	0	0	0	
	c.776A>G	missense	p.Asn259Ser	3.71E-04	23.8	deleterious	Damaging	0	0	4	0	0	0	0	2	0	0	0	0	
	c.806G>A	missense	p.Arg269Lys	8.24E-06	7.58	tolerated	Benign	0	0	1	0	0	0	0	0	0	0	0	0	
	c.833A>G	missense	p.His278Arg	0	13.7	deleterious	Benign	0	1	0	0	0	0	0	0	0	0	0	0	
	c.835G>T	Nonsense	p.Glu279Ter	0	37	NA	NA	0	0	0	0	0	0	0	0	0	0	1	0	
	c.847G>A	missense	p.Val283Met	5.77E-05	1.39	tolerated	Benign	0	1	2	0	1	0	0	0	0	0	0	0	
	c.884C>A	missense	p.Ala295Glu	0	0	tolerated	Benign	0	1	0	0	0	0	0	0	0	0	0	0	
	c.883G>T	missense	p.Ala295Ser	0	0.22	tolerated	Benign	0	1	0	0	0	0	0	0	0	0	0	0	
	c.917G>A	missense	p.Gly306Asp	9.08E-05	0.01	tolerated	Benign	0	1	0	0	0	0	0	0	0	0	0	0	
	c.950G>A	missense	p.Arg317Gln	4.95E-05	3.61	tolerated	Benign	0	0	1	0	2	0	0	0	0	0	0	0	
	c.961G>A	missense	p.Ala321Thr	9.08E-05	0.02	tolerated	Benign	0	0	2	0	2	1	0	0	0	0	0	0	
	c.1084T>C	missense	p.Phe362Leu	8.25E-06	22.7	deleterious	Damaging	0	0	0	0	1	0	0	0	0	0	0	0	
	c.1139T>C	missense	p.Val380Ala	1.49E-04	20.1	tolerated	Benign	0	2	0	0	0	0	0	0	0	0	0	0	

3.2. Secretion defects of disease associated BMP9 variants

Firstly, I measured the concentration of secreted BMP9 in conditioned media with an anti-growth factor domain sandwich ELISA. The amount of secreted growth factor domain from putatively pathogenic variants was significantly lower than from putatively benign variants (figure 8). A reduction of ELISA immunoreactivity could result from reduced expression, secretion, stability or detection efficiency of BMP9-variants compared to BMP9-WT. To address the latter, I measured different dilutions of conditioned media, and plotted the absorbance of these against their imputed concentrations to generate detection efficiency curves. This showed all detectable variants were recovered with equal efficiency (figure 9a).

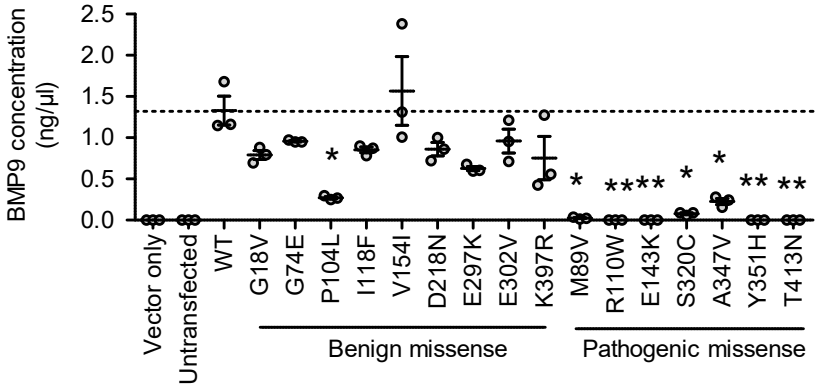

Figure 8. ELISA measurement of secreted BMP9 growth-factor domain in conditioned media. HEK-EBNA cells were transfected with expression vectors for *PreProBMP9*-WT or variants, and placed in serum-free, chemically defined media. Six days post transfection, conditioned media was collected. This was serially diluted in PBS and BMP9 concentration in dilutions was measured by ELISA. Dilutions which gave absorbances in the linear part of the standard curve were used to calculate BMP9 concentration in the media. Three independent batches of HEK-EBNA cell media were assayed independently. Mean ± SEM, n = 3, one-way matched ANOVA/Dunnett's testing of variants compared to WT * p<0.05, ** p<0.01, *** p<0.001.

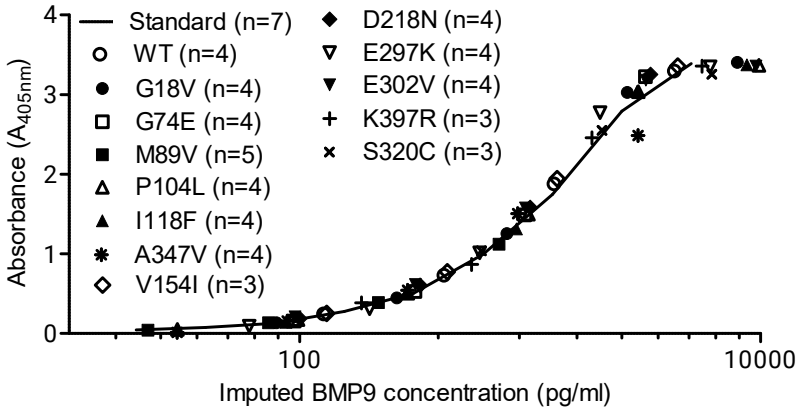

Figure 9a. Efficiency curves for ELISA measurements of BMP9-vairants. After the concentration of BMP9 in conditioned media was calculated using dilutions in the linear part of the standard curve, concentration of BMP9 in all other dilutions was imputed from this and plotted against absorbance, compared to a recombinant BMP9 standard. This showed BMP9 was equally efficiently recovered from all dilutions of media for all variants. n = number of points for variant before absorbance became too low to quantify.

Secreted BMP9 could not be detected by the ELISA in conditioned media from HEK-EBNA cells transfected with *PreProBMP9*-R110W, E143K, Y351H and T413N. I transfected expression vectors for these variants and a wildtype control into fresh cells, and analysed lysates by western blotting. Within cells transfected with wildtype vector, there were appreciable quantities of unprocessed *ProBMP9* (figure 9b). There was also some processed BMP9 dimer within cells, which could indicate intracellular cleavage or retention of cleaved BMP9 at the cell surface. However, the same anti-BMP9 used in the ELISA could not detect the variant proteins. This could either be because they were misfolded or poorly expressed.

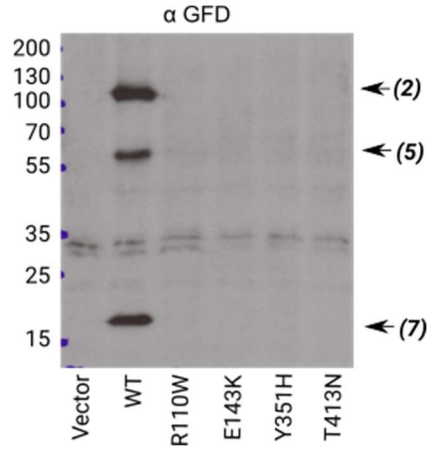

Figure 9b. Western blotting of cell lysates for BMP9 growth-factor domain (non-reducing) of transfected cells. Three independent batches were assayed. One representative blot shown. № = molecular weight (kDa), *(№)* = species identification from figure 7.

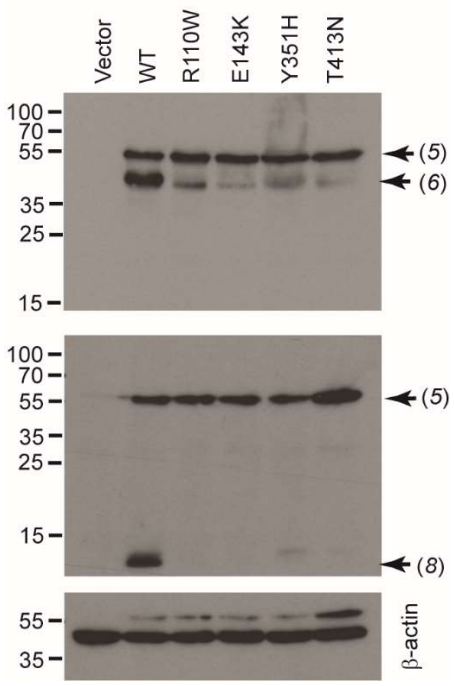

Figure 10. Western blotting of cell lysates for BMP9 prodomain (top) and growth-factor domain (bottom, reducing) of transfected cells. Three independent batches were assayed. One representative blot shown. № = molecular weight (kDa), *(№)* = species identification from figure 7.

An alternative anti-BMP9 growth-factor domain antibody, which only works in reducing conditions, revealed equal expression of unprocessed *ProBMP9*-WT and *ProBMP9*-R100W, E143K, Y351H and T413N within cells (figure 10 bottom). However, there was evidence these variants were otherwise defective, since there was no detectable processed BMP9 in cell lysates. Results obtained with an anti-BMP9 prodomain antibody reinforced these findings: there were high levels of unprocessed *ProBMP9* in lysates but, the levels of processed prodomain were reduced in cells transfected with *PreProBMP9*-R110W, E143K, Y351H and T413N compared to *PreProBMP9*-WT (figure 10 top).

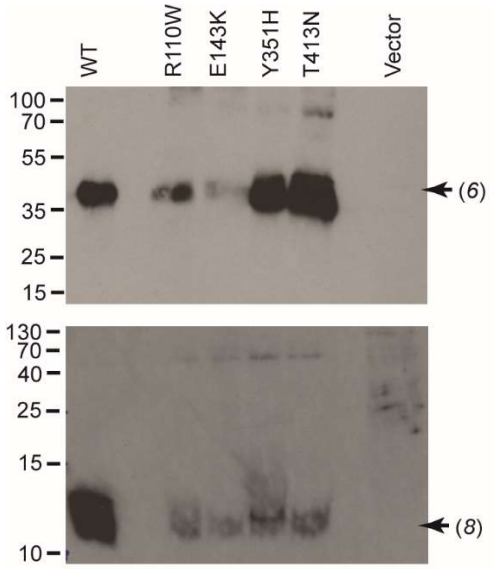

Figure 11. Western blotting of conditioned media for BMP9 prodomain (top, non-reducing) and growth-factor domain (bottom, reducing) from transfected cells. Three independent batches were assayed. One representative blot shown. № = molecular weight (kDa), *(№)* = species identification from figure 7.

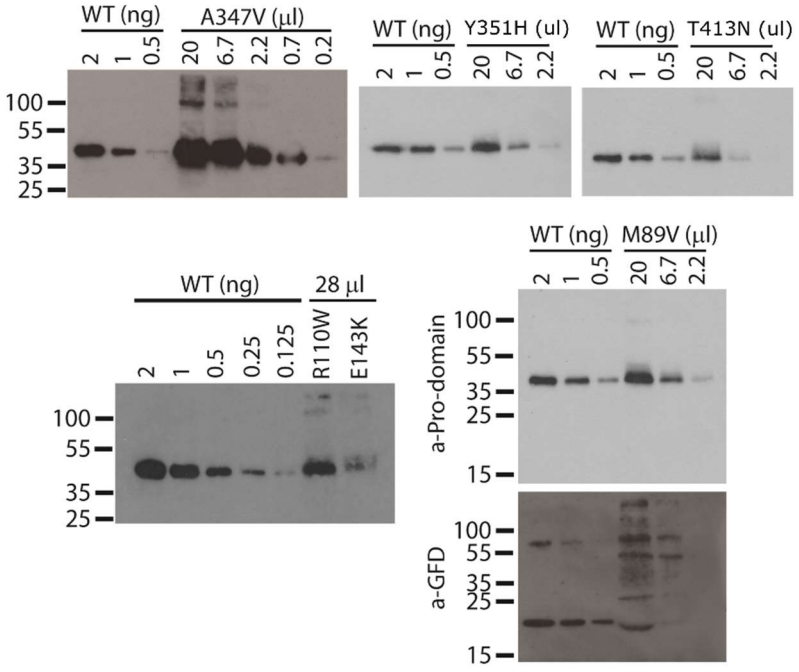

Figure 12 (overleaf). Western blotting of conditioned media for BMP9 prodomain, variants titrated against wildtype. Indicated amounts of BMP9-WT were loaded, calculated based on ELISA quantification of BMP9-WT concentration. Indicated volumes of conditioned media were loaded for BMP9 variants. Additionally, this process was repeated with an antibody against the growth-factor domain for BMP9-M89V. Three independent batches were assayed. One representative blot shown. № = molecular weight (kDa).

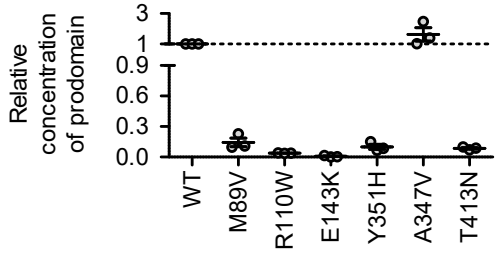

Figure 13. Relative amount of BMP9 prodomain in conditioned media. The relative signal intensity of variant prodomain compared to WT prodomain in Western blots from figure 12. This can be used to calculate the concentration of BMP9 in these samples based on ELISA quantification of the BMP9-WT samples. Three independent batches were assayed. Mean ± SEM.

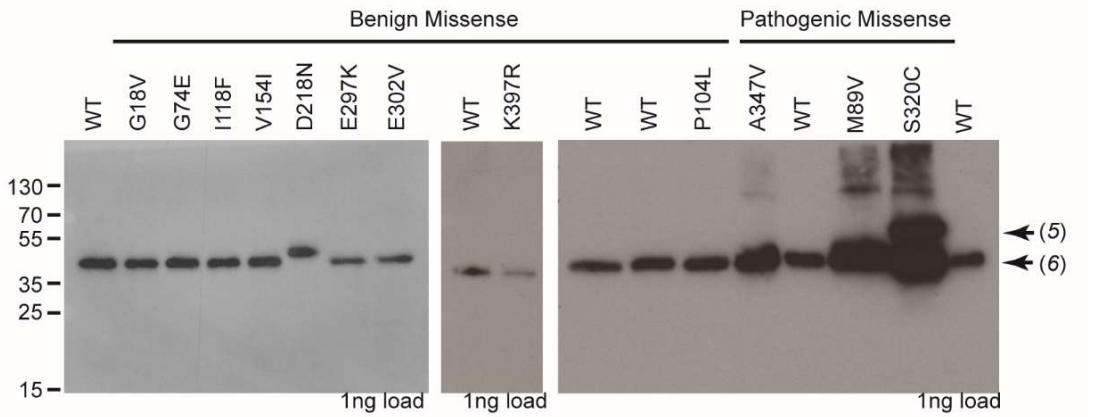

Figure 14. Western blotting of conditioned media for BMP9 prodomain (non-reducing) from transfected cells. Indicated amounts of BMP9 growth-factor domain equivalent were loaded based on quantifications from figure 8. Three independent batches were assayed. One representative blot shown. № = molecular weight (kDa), *(№)* = species identification from figure 7.

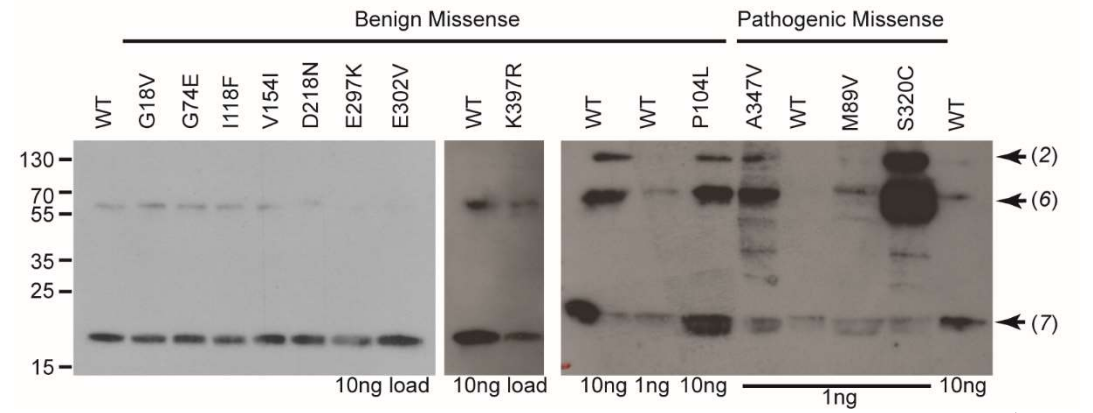

Figure 15. Western blotting of conditioned media for BMP9 growth-factor domain (non-reducing) from transfected cells. Indicated amounts of BMP9 growth-factor domain were loaded based on quantifications from figure 8. Three independent batches were assayed. One representative blot shown. № = molecular weight (kDa), *(№)* = species identification from figure 7.

I used these antibodies to probe western blots of conditioned media. (figure 11). The large majority of secreted BMP9-WT was in its processed, active form. In media, there were vastly reduced amounts of detectable BMP9-R110W, E143K, Y351H and T413N, compared to BMP9-WT. Interestingly, the anti-BMP9 prodomain antibody revealed substantial amounts of free prodomain in conditioned media from cells transfected with these variants, despite the absence of growth-factor domain. I titrated variants with very impaired growth-factor secretion to calculate the concentration of secreted prodomain (figure 12; 13).

I undertook similar western blots of conditioned media for all other ProBMP9 variants (figure 14). Reassuringly, when loading volume was calculated from the ELISA results, the intensity of bands corresponding to the processed growth factor domain dimer was equal across all samples (figure 15). The relative intensity of growth factor domain bands compared to prodomain bands was reduced in media containing putatively pathogenic variants (figure 16). This suggests the Pro:BMP9 complex was destabilised and the growth factor domain was lost. Structural analysis by Dr. Wei Li revealed many of the PAH-associated changes substitute amino-acids at the interface of the growth factor domain and prodomain which may disrupt their association (figure 5b,c in Gräf et al. 2018).

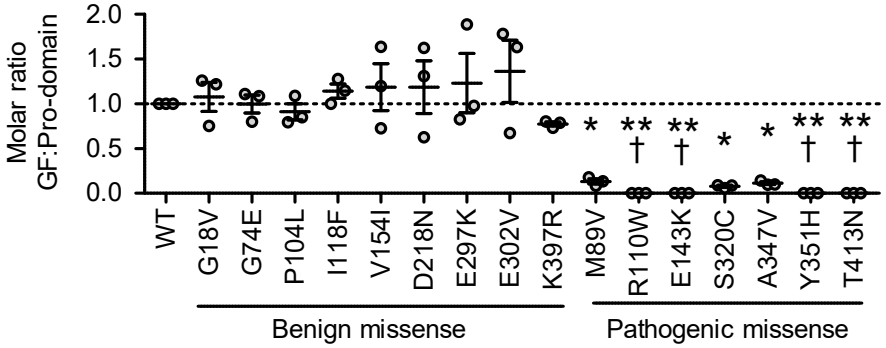

Figure 16. Molar ratios of BMP9 growth factor domain : prodomain in conditioned media calculated by western blotting densitometry. The relative signal intensity of variant growth factor domain compared to wildtype growth factor domain was measured on Western blots. This was repeated for prodomain (example in figure 13). I assumed that there is a 1:1 ratio of growth-factor domain : prodomain in Pro:BMP9-WT, so the relative intensity of the growth-factor domain divided by the relative intensity of the prodomain equals molar ratio. Three independent batches were assayed independently. † indicates that the relative intensity of growth-factor domain was too low to quantify accurately. Mean ± SEM, n = 3, one-way matched ANOVA/Dunnett's testing of variants compared to WT, * p<0.05, ** p<0.01, *** p<0.001.

The growth-factor domains from pathogenic variants could have been degraded within cells or have been secreted then degraded in the media. I undertook a time course of BMP9-M89V signalling on endothelial cells compared to BMP9-WT to assess growth factor domain stability. Importantly, I collected, aliquoted and stored conditioned media at -80 °C

within an hour, minimising prior degradation. There was no significant difference in the activity of BMP9-WT or M89V conditioned media over 4 hours (figure 17).

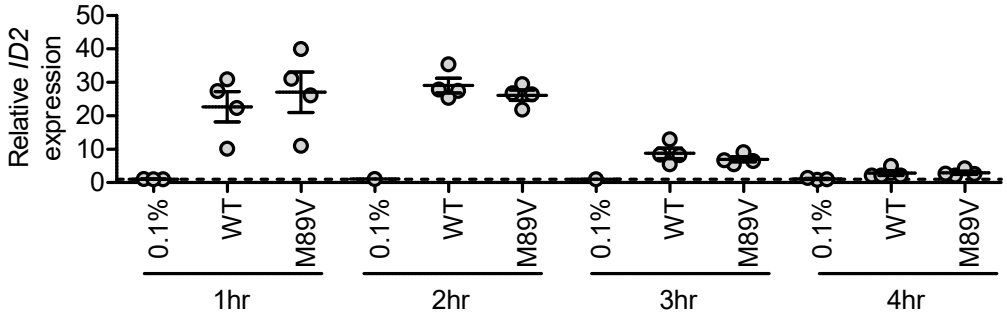

Figure 17. Timecourse of signalling by Pro:BMP9-WT and -M89V. Quiescent human aortic endothelial cells were treated with 50 pg/ml of Pro:BMP9-WT or -M89V for the indicated time. Expression of *ID2* mRNA was measured by qPCR, normalised to the housekeeping gene *B2M*. Mean ± SEM, n = 4.

Western blots showed prodomain-D218N was bigger than prodomain-WT. This missense variant is not associated with PAH, and is fairly common—allele frequency in gnomAD browser = 0.003 (Karczewski et al. 2019). The new asparagine residue could be a substrate for N-linked glycosylation. I treated conditioned media containing Pro:BMP9-WT and Pro:BMP9-D218N with PNGase-F, which cleaves the bond between Asparagine and almost all oligosaccharides, and analysed the products by Western blotting. Deglycosylation restored size-parity between prodomain-WT and -D218N, confirming the difference was due to glycosylation (figure 18). Deglycosylated wildtype prodomains are smaller than native wildtype prodomains since there are two other glycosylation sites. As expected, there was no evidence the growth-factor domain was glycosylated. Notably, Susan-Resiga *et al.* (2011) show a very similar pattern for wildtype Pro:BMP10.

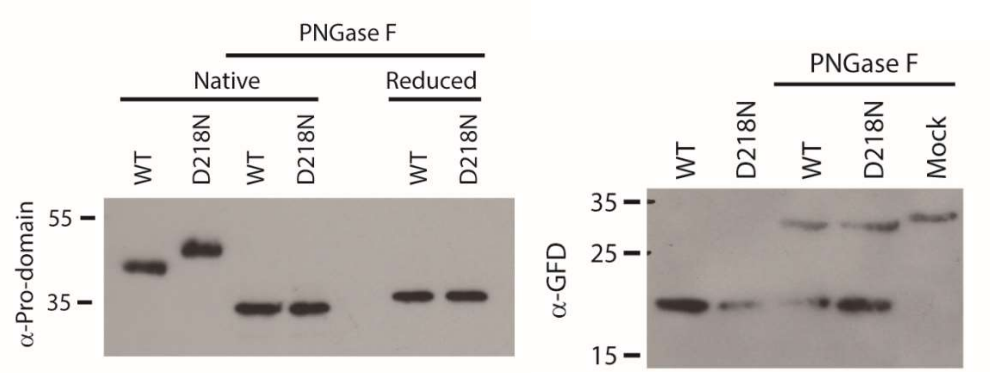

Figure 18. Deglycosylation of conditioned media containing Pro:BMP9-WT and Pro:BMP9-D218N using PNGaseF. One set of samples were denatured and reduced prior to treatment as this improves deglycosylation efficiency for some substrates. **Left:** Western blot probing for prodomain. **Right:** Western blot probing for growth-factor domain. Note that the anti-growth-factor domain antibody used here cannot detect reduced BMP9 and it cross-reacts with a component of the deglycosylation treatment mix, giving a ~30 kDa non-specific band. № = molecular weight (kDa).

Some PAH associated *ProBMP9* variants exhibited a processing defect. Most strikingly, there was a huge excess of uncleaved dimers, uncleaved monomers, and partially cleaved dimers in conditioned media containing ProBMP9-S320C compared to ProBMP9-WT (figure 19; 20). Within cell lysates, there was a similar distribution of WT and S320C species, indicating a processing defect concurrent with secretion. Cleavage usually occurs between amino-acids 319/320 but furin-like proteases are reported to be intolerant of cysteine in this position (Tian 2009)(see 4.7). The novel cysteine may also form inappropriate disulphide bridges. These factors could prevent the engagement of processing enzymes. In the aligned amino acid sequences of BMP9 in every model organism, this residue is a serine (figure 21).

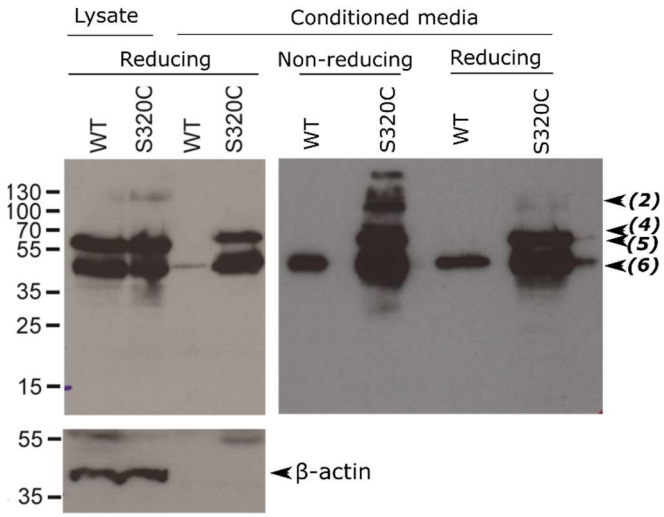

Figure 19. Western blotting for BMP9-WT and BMP9-S320C prodomain. On the left-hand blots 30 µg of total protein, or 1 ng of growth-factor domain equivalent calculated by ELISA quantification of each sample, was loaded per well. On the right-hand blot, different volumes of conditioned media were loaded per well to give a similar band intensity for BMP9-WT and -S320C. Three independent batches were assayed. One representative blot shown. № = molecular weight (kDa), *(№)* = species identification from figure 7.

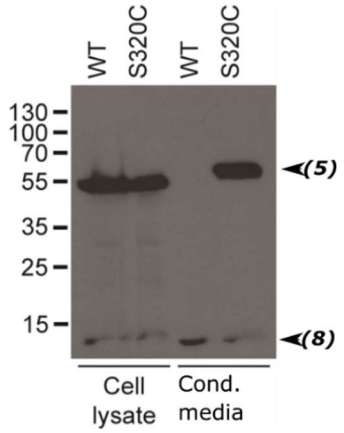

Figure 20. Western blotting for BMP9-WT and BMP9-S320C growth-factor domain. Three independent batches were assayed. One representative blot shown. № = molecular weight (kDa), *(№)* = species identification from figure 7.

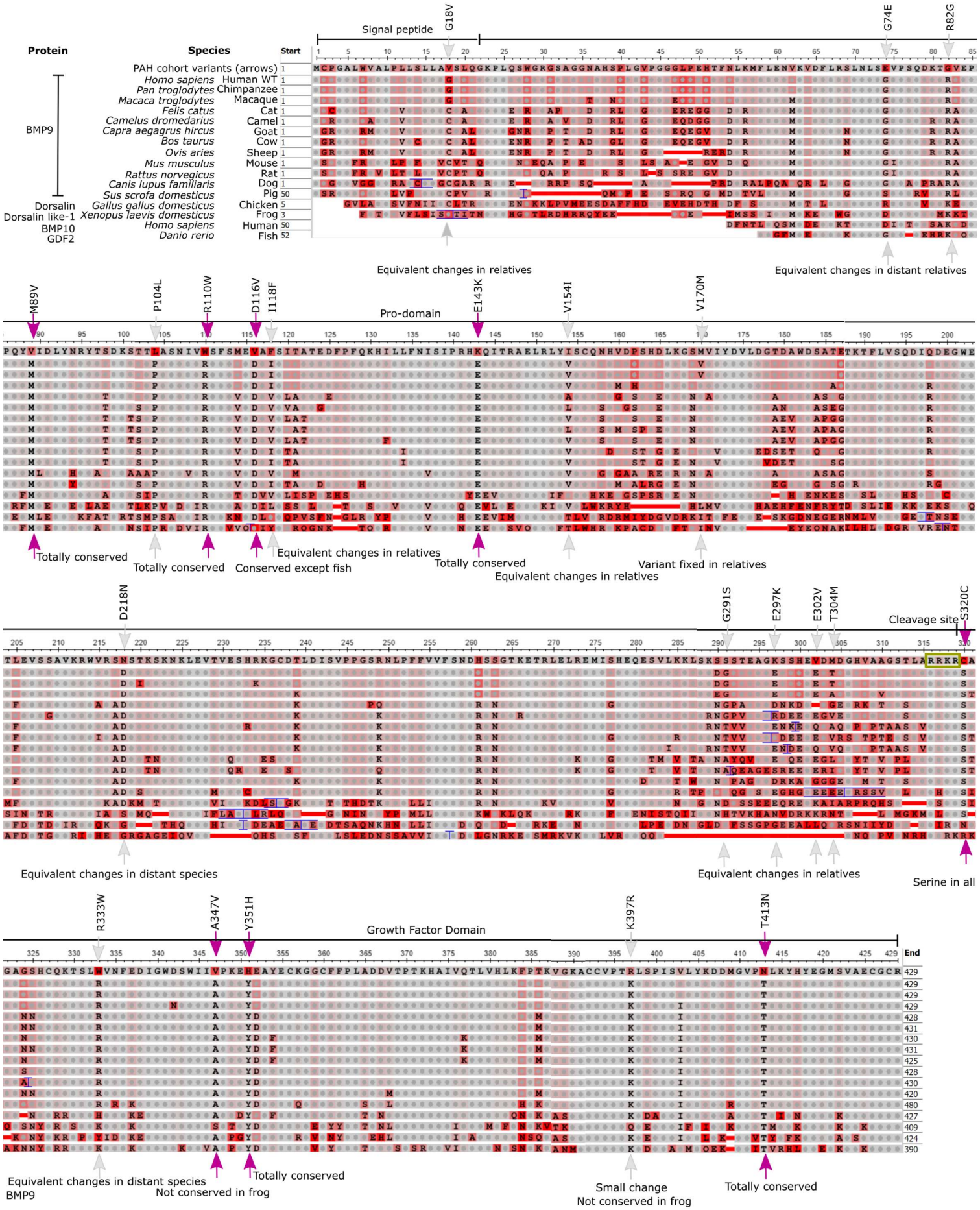
Protein
Species
Start
Signal peptide
G18V
G74E
R82G
PAH cohort variants (arrows)
Homo sapiens Human WT
Pan troglodytes Chimpanzee
Macaca troglodytes Macaque
Felis catus Cat
Camelus dromedarius Camel
Capra aegagrus hircus Goat
Bos taurus Cow
Ovis aries Sheep
Mus musculus Mouse
Rattus norvegicus Rat
Canis lupus familiaris Dog
Sus scrofa domesticus Pig
Gallus gallus domesticus Chicken
Xenopus laevis domesticus Frog
Homo sapiens Human
Danio rerio Fish
BMP9
Dorsalin
Dorsalin like-1
BMP10
GDF2
Equivalent changes in relatives
Equivalent changes in distant relatives
M89V
P104L
R110W
D116V
I118F
Pro-domain
E143K
V154I
V170M
Totally conserved
Totally conserved
Conserved except fish
Equivalent changes in relatives
Totally conserved
Equivalent changes in relatives
Variant fixed in relatives
D218N
G291S
E297K
E302V
T304M
Cleavage site
S320C
Equivalent changes in distant species
Equivalent changes in relatives
Serine in all
R333W
A347V
Y351H
Growth Factor Domain
K397R
T413N
End
Equivalent changes in distant species
BMP9
Not conserved in frog
Totally conserved
Small change
Not conserved in frog
Totally conserved

Figure 21 (overleaf). Amino-acid sequence alignments of BMP9 across vertebrates. I used NCBI's protein basic local alignment sequence tool to search for similar amino acid sequences to human *PreProBMP9* across all life. I selected sequences from common model organisms and used NCBI's constraint based multiple alignment tool to produce the figure. Shading = column quality score (how well the properties of an amino acid agree with the other amino acids of the column). The top row shows variants found in the PAH cohort (table 5) superimposed on the reference sequence of human BMP9. Purple arrows = putatively pathogenic substitutions; grey arrows = putatively benign substitutions. Letters = standard amino acid abbreviation; Circle = amino acid is the same as the top row. Bar = positions not found in the sequence of that species. Box = Furin recognition sequence by furin cleavage site. Numbers = sequence position for that species at which alignment starts and ends.

3.3. Activity defects of disease associated BMP9 variants

A luciferase-based cell signalling assay has been developed to assess the ability of BMP9 to bind and activate ALK1 receptor complexes (figure 22)(Wei et al. 2014; Wooderchak-Donahue et al. 2013). Mouse myoblast C2C12 cells do not ordinarily expresses high-affinity receptors for BMP9. However, I transfected them with vectors containing genes for hALK1 and BMP signalling dependent firefly luciferase. Activity can be normalised to account for transfection efficiency and cell number. I trialled normalisation plasmids encoding sea-pansy (*Renilla*) luciferase driven by the promoter of the housekeeping gene thymidine kinase (TK) or cytomegalovirus (CMV). The best sensitivity and least variability was obtained when cells were transfected with 400 ng of hALK1-plasmid and the luminescence produced by firefly luciferase was normalised to the luminescence produced by *TK*:Renilla luciferase (figure 23). Nonetheless, there was some variability between experiments, so I linearly transformed data such that transfected myoblasts in serum free media without BMP9 had a relative luciferase activity of 0%, and cells exposed to 100 pg/ml of Pro:BMP9-WT had a relative luciferase activity of 100%. Transfected cells had a high-affinity BMP9 response that was strictly dependent on ALK1 signalling in the physiological range of 0-100 pg/ml (figure 24).

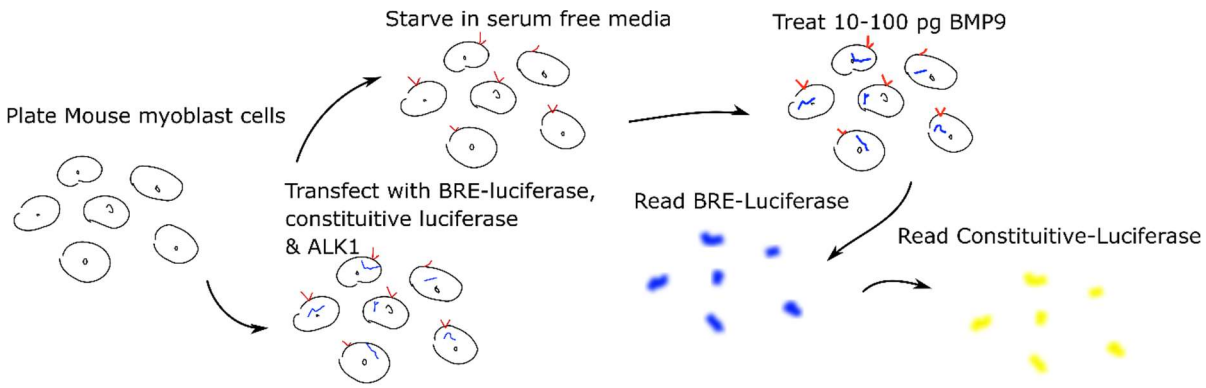

Figure 22. Schematic of ALK1 signalling luciferase assay.

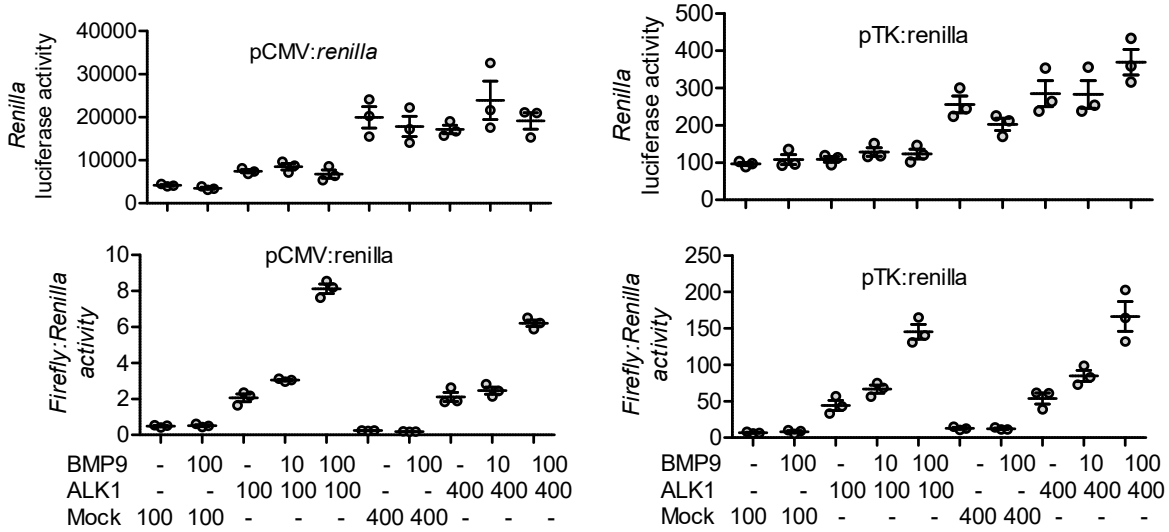

Figure 23. Optimisation of the Dual-Glo ALK1 signalling assay. C2C12 mouse myoblast cells were transfected with *BRE:luciferase(firefly)*. Simultaneously, cells were transfected with 100-400 ng/well of plasmid expressing human-ALK1, or 100-400 ng/well of empty expression plasmid. Additionally, cells were transfected with plasmids expressing *Renilla* luciferase under the constitutively active promoters for Thymidine kinase (TK) or cytomegalovirus (CMV). Transfected cells were treated with 10-100 pg/ml of BMP9 and firefly and *Renilla* luciferase activity were measured. Mean ± SEM, n = 3. Data show that neither *CMV* nor *TK* promoter activity was specifically enhanced in the presence of ALK1 and BMP9. The best sensitivity to 10 pg/ml of BMP9 was obtained by measuring the firefly luciferase activity of cells transfected with 400 ng/well of hALK1, normalised with *TK:Renilla(luciferase)*.

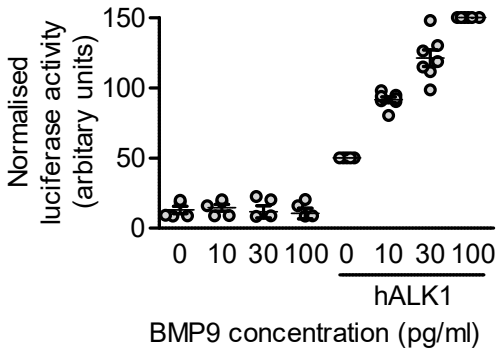

Figure 24. Dose response of the Dual-Glo ALK1 signalling assay. Quiescent transfected cells were treated with 10-100 pg/ml of BMP9 and normalised luciferase activity was measured. Mean ± SEM, n = 6. Data show that these cells have no high-affinity response to BMP9 in the absence of exogenous hALK1.

I assessed the BMP9 activity of conditioned media from HEK-EBNA cells transfected with variant *PreProBMP9* vectors. I treated cells with equal concentrations of processed growth factor domain to compare ligand activity independently of secretion or processing defects. This was based on ELISA quantifications of the amount of growth-factor domain in each sample. For variants which did not produce detectable amounts of processed growth-factor domain, I based dilutions on the concentration of prodomain (figure 12). I ruled out

non-specific activity by treating some cells with large volumes of conditioned media from HEK-EBNA cells transfected with empty vectors.

Interestingly, all variants detectable by ELISA had ALK1 signalling potency equivalent BMP9-WT (figure 25 top). I quantified the concentration of Pro:BMP9-WT and -M89V by either ELISA for the growth factor domain or western blotting for the prodomain. This showed Pro:BMP9-M89V growth-factor domain is fully active but is present at a lower level than the prodomain quantification would suggest. Similarly, there was almost no activity of BMP9-R110W, E143K, Y351H and T413N in conditioned media, confirming an absence of growth factor domain (figure 25 bottom).

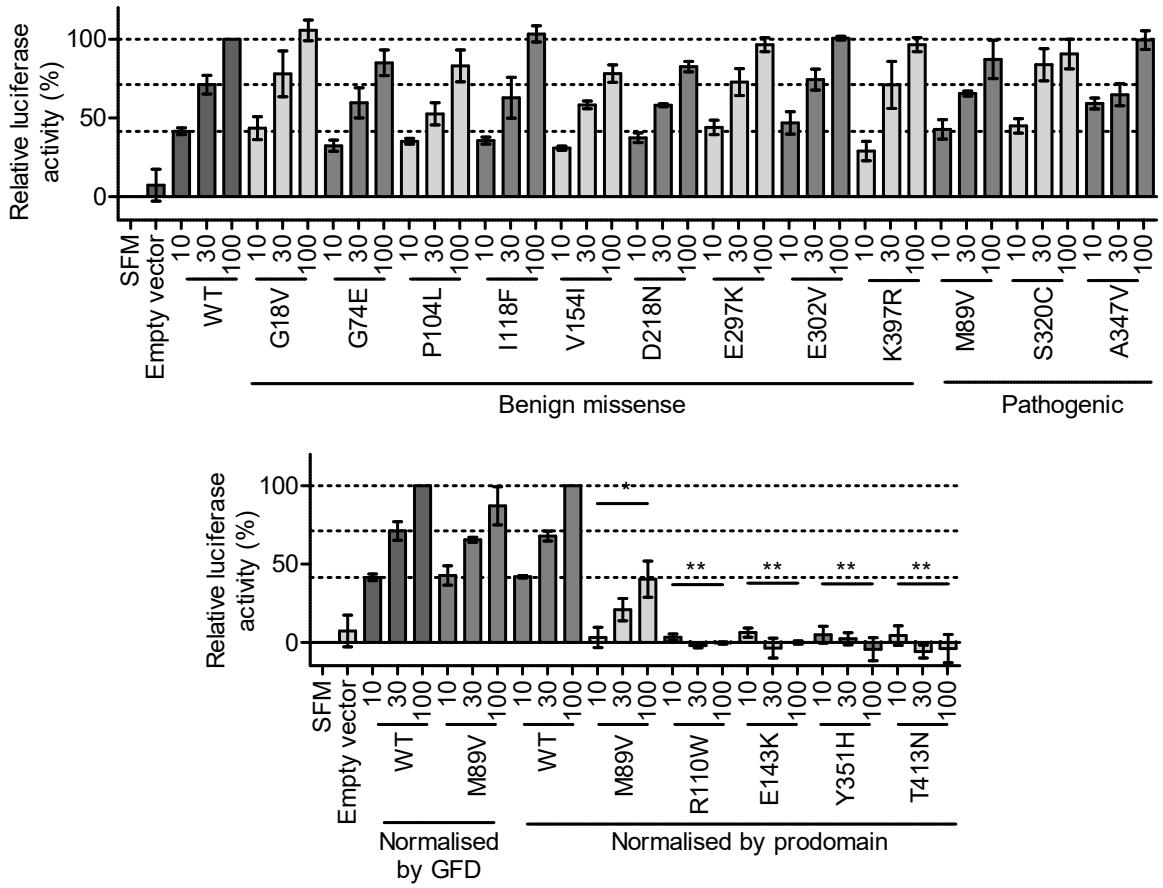

Figure 25. ALK1 signalling of BMP9 variants. Quiescent transfected cells were treated with conditioned media containing 10-100 pg/ml of BMP9-WT or variants. The relative activity of 100 pg/ml of BMP9-WT was set at 100%, and serum-free media at 0%. **Top:** BMP9 dose was calculated based on the amount of growth-factor domain (GFD) measured by ELISA. **Bottom:** BMP9 dose was calculated by Western blotting densitometry of prodomains. Mean ± IQR, n = 3, van Elteren test, ** $p < 0.01$, *$p < 0.05$. A two-way ANOVA/Bonferroni testing of variants compared to WT showed the same groups had significantly lower activity at $p < 0.001$. For pathogenic variants with no activity, EC_{50} could not be determined, whilst for all other variants, EC_{50} was not significantly different from BMP9-WT after adjusting for multiple testing.

I assessed whether BMP9 variants were able to promote pulmonary artery endothelial cell (PAEC) survival as this is a crucial protective effect of BMP9 (Teichert-Kuliszewska et al. 2006; Long et al. 2015). Therefore, I established a protocol for measuring the anti-apoptotic effect of BMP9 on serum starved PAECs using Caspase-GLO reagent. Overnight incubation in basal media with 0.1% FBS significantly increased apoptosis, whilst 500-5000 pg/ml of BMP9 was sufficient to partially rescue the PAECs (figure 26).

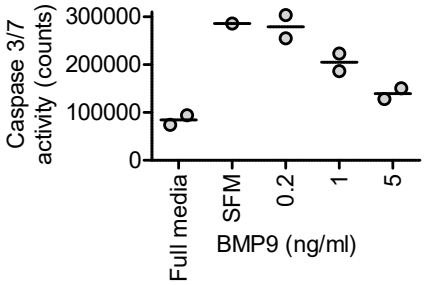

Figure 26. Dose response of BMP9 anti-apoptotic activity. Pulmonary arterial endothelial cells incubated in full media or starved in serum-free basal media supplemented with 0-5 ng/ml of BMP9 overnight. Caspase activity was measured in cell lysates with a luminescent substrate. Mean ± SEM, n = 2.

Mock conditioned media from HEK-EBNA cells could exacerbate PAEC apoptosis when present at >2% v/v, overwhelming the protection offered by of BMP9 (figure 27). Therefore, I prepared subsequent experiments using mixes of conditioned media from HEK-EBNA cells transfected with variant BMP9 expression vectors and empty vectors: all PAECs were exposed to 500 pg/ml of BMP9 in a total of 1% v/v conditioned media, or 1000 pg/ml of BMP9 in a total of 2% v/v conditioned media.

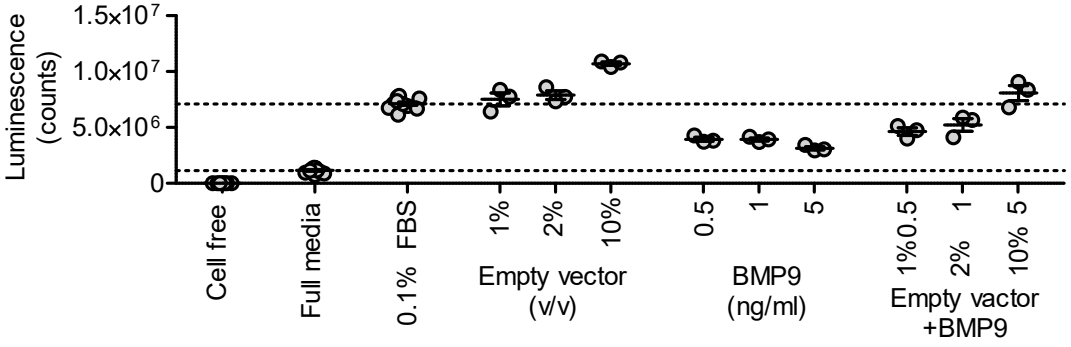

Figure 27. Dose response of BMP9 anti-apoptotic activity on cells supplemented with HEK-EBNA cell conditioned media. **Cell free:** media+Caspase-Glo reagent in a well without cells. **Full media:** pulmonary arterial endothelial cells left in full growth media. **0.1% FBS:** apoptosis induced by overnight incubation in basal media supplemented with 0.1% (v/v) FBS. **Empty vector:** apoptosis induced by overnight incubation in basal media supplemented with 0.1% (v/v) FBS and 1-10% (v/v) conditioned media from HEK-EBNA cells transfected with an empty vector. **BMP9:** apoptosis could be rescued by adding 0.5-5 ng/ml of Pro:BMP9. **Empty vector + BMP9:** apoptosis could no longer be rescued when conditioned media from HEK-EBNA cells transfected with the empty expression vector was added to a final concentration of 10% (v/v). Mean ± SEM, n = 3.

The anti-apoptotic activity of variant BMP9 proteins on PAECs closely mirrored signalling activity through ALK1. Variants which were detectable by ELISA were able to inhibit apoptosis robustly, whereas variants which destabilised the growth factor domain had little anti-apoptotic activity (figure 28). Again, Pro:BMP9-M89V was quantified by either its growth factor domain or prodomain. Assaying potency relative to each confirmed a loss of activity due to loss of the growth factor domain.

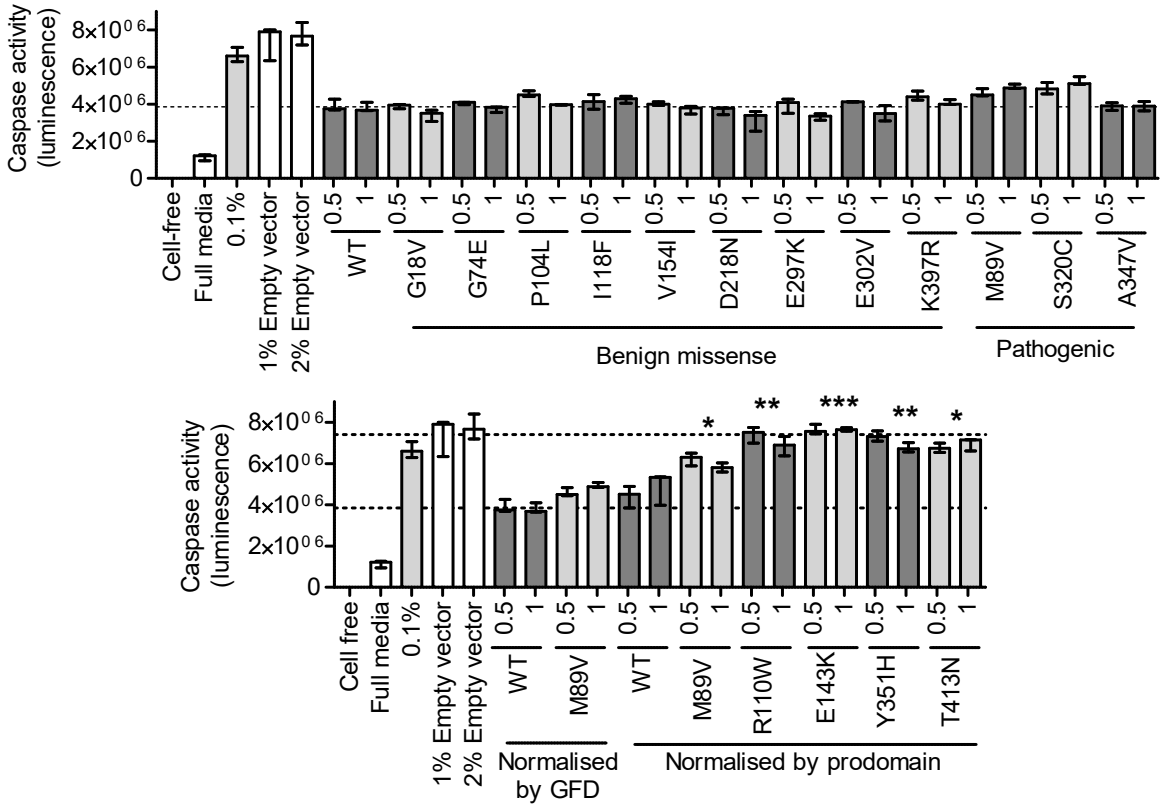

Figure 28. Anti-apoptotic activity of BMP9 variants. Apoptosis was induced in human pulmonary arterial endothelial cells by overnight incubation in basal media supplemented with 0.1% (v/v) FBS and conditioned media from HEK-EBNA cells containing Pro:BMP9-WT or variants. The treatments were also supplemented with conditioned media from HEK-EBNA cells transfected with an empty expression vector such that wells contained 1% (v/v) conditioned media + 0.5 ng/ml of BMP9, or 2% (v/v) conditioned media + 1 ng/ml of BMP9. **Top:** BMP9 dose was calculated based on the amount of growth-factor domain (GFD) measured by ELISA. **Bottom:** BMP9 dose was calculated by Western blotting densitometry. Mean ± IQR, n = 3, van Elteren test, ***p < 0.001, **p < 0.01, * p < 0.05. A two-way ANOVA/Bonferroni testing of variants compared to WT showed the same groups had significantly lower activity at p < 0.001.

To validate the Caspase-Glo assays, I used flow cytometry. Phosphatidylserine is presented on the outer leaflet of plasma membranes to opsonise cells during the early stages of apoptosis (Verhoven, Schlegel, and Williamson 1995). This can be visualised by staining with FITC-conjugated annexin-V. Annexin-V could stain phosphatidylserine on the inner leaflet if membrane integrity is lost due to damage, necrosis or later in apoptosis. Therefore,

propidium iodide was used as counterstain since it is membrane impermeant. The Morrell group has previously shown BMP9 is able to supress basal apoptosis in quiesced endothelial cells, but the signal is stronger when TNFα is used to induce higher rates of apoptosis via the JNK/SPAK pathway (Long et al. 2015). TNFα can also stimulate a pro-survival transcriptional response, therefore the translation inhibitor cycloheximide is also added to cells (Dhanasekaran and Reddy 2008; Franzoso, Zazzeroni, and Papa 2003). Flowcytometry requires large numbers of cells and PAECs are expensive and cannot be expanded hugely. Therefore, I used blood outgrowth endothelial cells, which have very similar BMP9 responses to PAECs, as a surrogate cell (Ormiston, Toshner, et al. 2015).

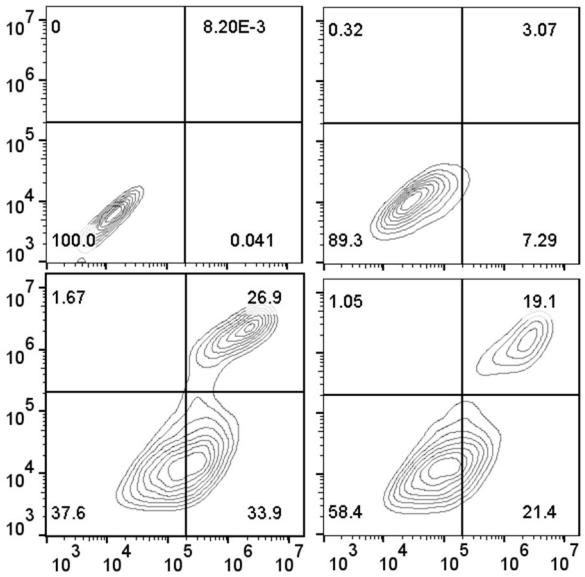

Figure 29. Gating strategy for flow cytometry measurement of blood outgrowth endothelial cell apoptosis. X-axis = Annexin V staining compensated for interference from other signals. Y-axis = propidium iodide staining compensated for interference from other signals. **Top left**: unstained cells. **Top right:** quiescent cells. **Bottom left**: quiescent cells induced with cycloheximide and TNFα. **Bottom right:** quiesced cells treated with 5 ng/ml of BMP9 overnight prior to induction with cycloheximide and TNFα. Cells in the bottom left quadrant are viable, cells in the bottom right quadrant are undergoing early-apoptosis, and cells in the top right quadrant are undergoing late-apoptosis or necrosis.

I quiesced BOECs overnight in basal media supplemented with 2% (v/v) FBS and HEK-EBNA supernatants. The following morning, I spiked in TNFα and cycloheximide. The rate of apoptosis induction seemed dependent on cell passage and confluence, among other things. Therefore, when cell morphology began changing, about 3.5 hours after induction, I trypsinised cells and placed them in ice-cold PBS to prevent further apoptosis whilst they were stained and analysed. Conditioned media from HEK-EBNA cells transfected with empty expression vectors increased the proportion of necrotic or late apoptotic cells, but did not alter the proportion of healthy cells (Annexin-V and propidium iodide negative)(figure 31). Therefore, I only compared the proportion of healthy cells in subsequent experiments.

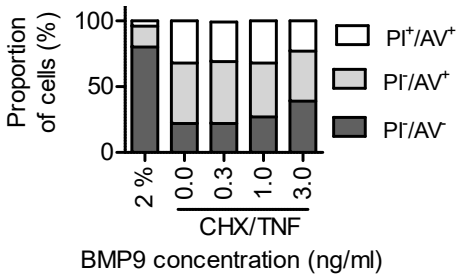

Figure 30. Dose response of BMP9 anti-apoptotic activity. Blood outgrowth endothelial cells were quiesced in 0-3 ng/ml of BMP9 overnight, prior to induction of apoptosis with cycloheximide and TNFα. Apoptosis was measured flow cytometry. PI^-/AV^- cells are viable, PI^-/AV^+ cells are undergoing early apoptosis, and PI^+/AV^+ cells are undergoing late apoptosis or necrosis.

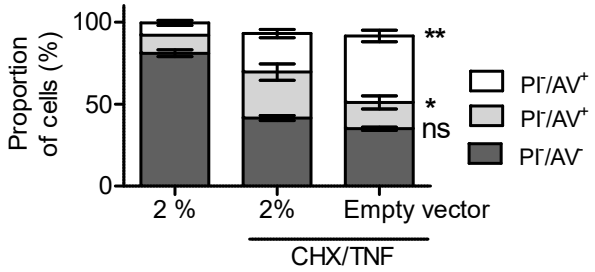

Figure 31. Effect of HEK-EBNA cell conditioned media on apoptosis assessment. Blood outgrowth endothelial cells quiesced in basal media supplemented with 2% (v/v) FBS. 10% (v/v) conditioned media from HEK-EBNA cells transfected with empty vector was also added where indicated. Apoptosis was induced with-cycloheximide and TNFα and apoptosis was measured by flow cytommetry. PI^-/AV^- cells are viable, PI^-/AV^+ cells are undergoing early apoptosis, and PI^+/AV^+ cells are undergoing late apoptosis or necrosis. Mean ± SEM, n = 4, paired two-tailed Student's t-test between cells with and without conditioned media, * $p < 0.05$, ** $p < 0.01$.

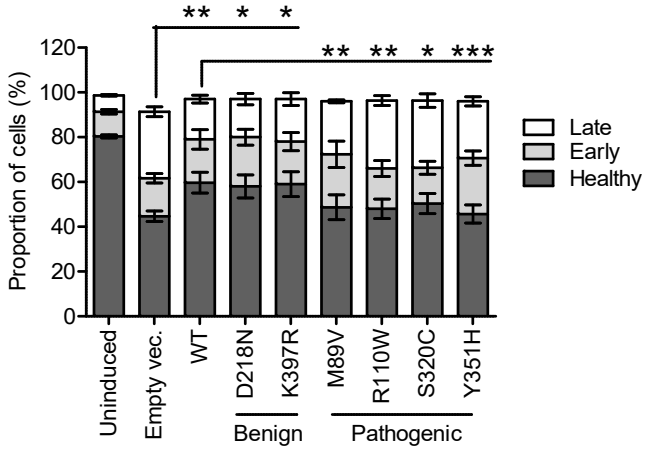

Figure 32. Anti-apoptotic activity of BMP9 variants. Blood outgrowth endothelial cells were quiesced in 3 ng/ml of BMP9 overnight as calculated by western blotting of the prodomain, prior to induction of apoptosis with-cycloheximide and TNFα. Apoptosis was measured flow cytometry. PI^-/AV^- cells are viable, PI^-/AV^+ cells are undergoing early apoptosis, and PI^+/AV^+ cells are undergoing late apoptosis or necrosis. PI^-/AV^- cells are viable, PI^-/AV^+ cells are undergoing early apoptosis, and PI^+/AV^+ cells are undergoing late apoptosis or necrosis. Mean ± SEM, n = 3, one-way matched ANOVA/Dunnett's test of variants compared to WT using proportion of PI^-/AV^- cells, * $p < 0.05$, ** $p < 0.01$, *** $p < 0.001$. A non-parametric Friedmann test gave similar results.

I chose to measure PAH-associated Pro:BMP9-M89V, -R110W, and -Y351H as they demonstrated instability due to mutations in either the prodomain or growth factor domain. Additionally, *ProBMP9*-S320C possessed a processing defect, whilst Pro:BMP9-D218N was not expected to be pathogenic but did exhibit a glycosylation defect. The mutation BMP9-K397R is common and not associated with PAH, so I included this variant as a control. Supernatants from HEK-EBNA cells transfected with an empty vector were used to rule out responses due to non-specific factors. Treatment with Pro:BMP9-WT, D218N and R397K significantly increased the number of healthy cells (figure 32). As expected, Pro:BMP9-M89V, R110W and Y351H were significantly less functional than Pro:BMP9-WT. Interestingly, Pro:BMP9-S320C also had slightly less anti-apoptotic effect than Pro:BMP9-WT, which could indicate some dysfunction.

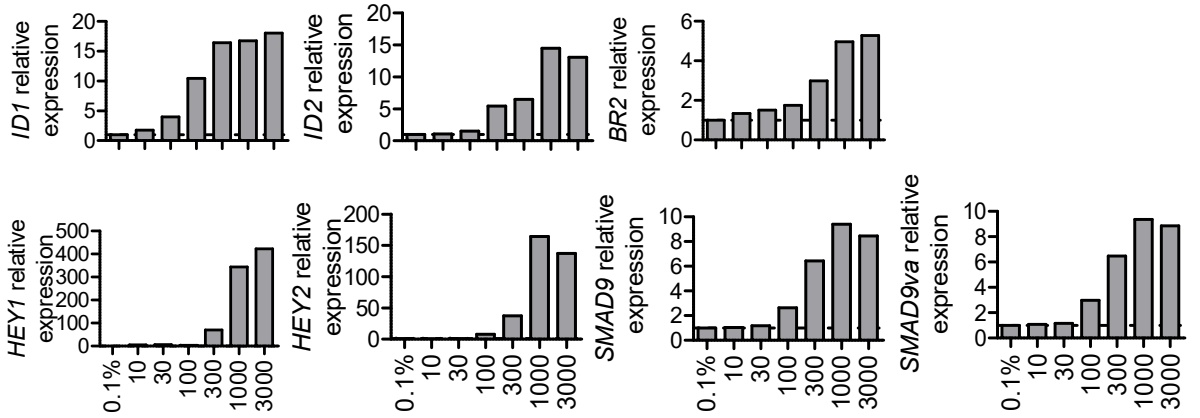

Figure 33. Transcriptional response of endothelial cells to BMP9. Quiescent blood outgrowth endothelial cells were treated with the indicated dose of recombinant BMP9 (pg/ml). mRNA from the indicated genes was measured by qPCR relative to the housekeeping gene *B2M*. *SMAD9* produces two splice variants, a and b; *SMAD9* relative expression includes both, whilst *SMAD9va* is specific for variant a. n = 1.

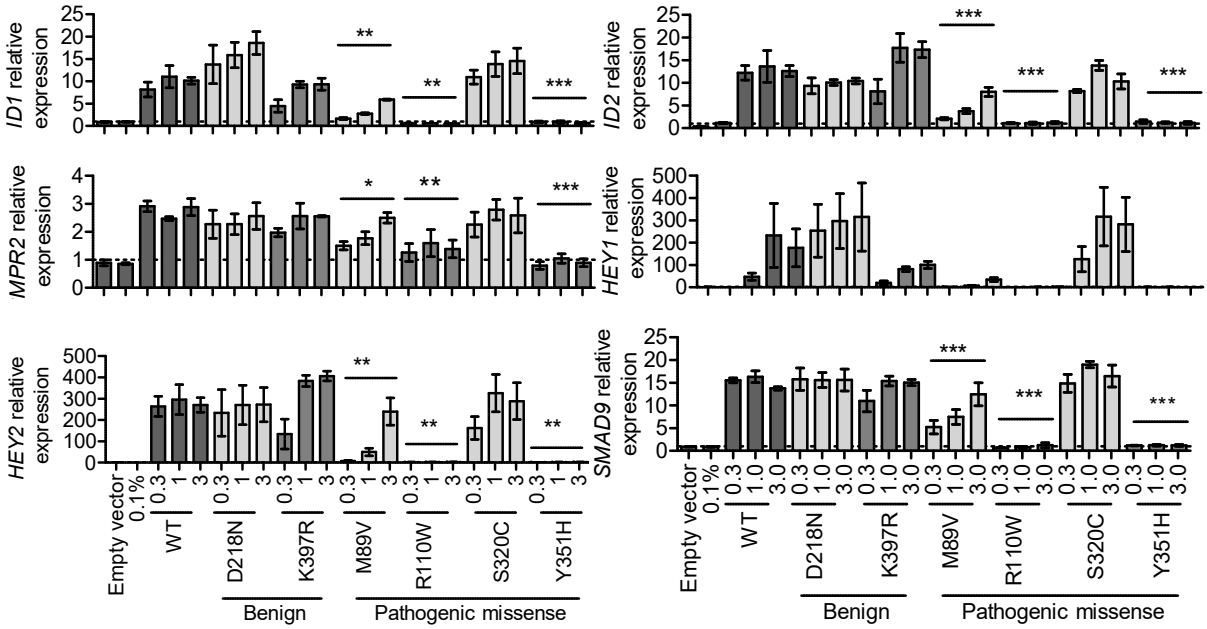

Figure 34 (overleaf). Transcriptional response of endothelial cells to BMP9 variants. Quiescent blood outgrowth endothelial cells were treated with 0.3-3 ng/ml of BMP9 as measured by Western blotting densitometry of the prodomain. mRNA from the indicated genes was measured by qPCR relative to the housekeeping gene *B2M*. *SMAD9* produces two splice variants, a and b; *SMAD9* relative expression includes both, whilst *SMAD9va* is specific for variant a. Mean ± SEM, n = 3, Two-way ANOVA/Bonferroni comparison of variants vs WT, * $p < 0.05$, ** $p < 0.01$, *** $p < 0.001$. A stratified van Elteren test showed the same groups had significantly lower activity at $p < 0.05$.

Finally, I assessed transcriptional responses of quiescent BOECs to BMP9 variants. PAECs were able to discriminate between doses of BMP9 ranging from 10-3000 pg/ml, with 300 pg/ml at the limit of sensitivity depending on the gene (figure 33). Hence, I measured the transcriptional responses of BOECs to 300, 1000 and 3000 pg/ml of BMP9 variants in conditioned media (figure 34). As expected, Pro:BMP9-D218N, S320C and -K397R had normal stimulatory effects on BOECs. At doses calculated by Western blotting densitometry of the prodomain, Pro:BMP9-M89V, -R110W and Y351H had reduced stimulatory effect on BOECs. This confirms loss of active growth-factor domain in these variants.

3.4. BMP9 & pBMP10 levels & activity in *GDF2* mutation carriers

The PAH patients carrying pathogenic *GDF2* mutations were heterozygotes. It is possible that dimerisation causes these mutations to act as dominant negatives, or wildtype alleles could compensate the mutated alleles. Many patients enrolled into the NIHR-BRIDGE study were also enrolled into the National Cohort of Idiopathic and Heritable PAH, which collected samples from patients. Therefore, we sought plasma samples from PAH patients carrying pathogenic and benign mutations in *GDF2* to validate my *in vitro* results. I measured circulating levels of BMP9 with an ELISA protocol validated by Dr. Paul Upton (see 1.4.4).

We had samples from eleven PAH patients carrying putatively benign *GDF2* missense variants, although I had not assessed all of these *in vitro*. A previous publication confirmed that BMP9-R333W is benign and it has a gnomAD frequency of 0.0004 (Wooderchak-Donahue et al. 2013; Karczewski et al. 2019). We had samples from four patients carrying putatively pathogenic missense variants. Additionally, two samples were from *GDF2* deletion carriers with a deletion encompassing many flanking genes. These patients had no evidence of comorbidities, and the flanking genes are only associated with recessive conditions. One sample was from a patient carrying a splice acceptor region mutation expected to cause a truncation. All the patient samples came from *GDF2* heterozygous (or hemizygous) females, so we included samples from eight age-matched healthy females as controls.

PAH patients carrying putatively pathogenic *GDF2* missense variants had levels of plasma BMP9 significantly reduced to ~50% of healthy controls or benign variant carrying

patients (figure 35). Reduction in plasma BMP9 was due to the presence of pathogenic alleles, rather than as a consequence of PAH. The *GDF2* deletion/truncation carriers had plasma BMP9 levels comparable to deleterious missense carriers. This could indicate missense variant proteins do not act as dominant negatives, so patients suffer haploinsufficiency.

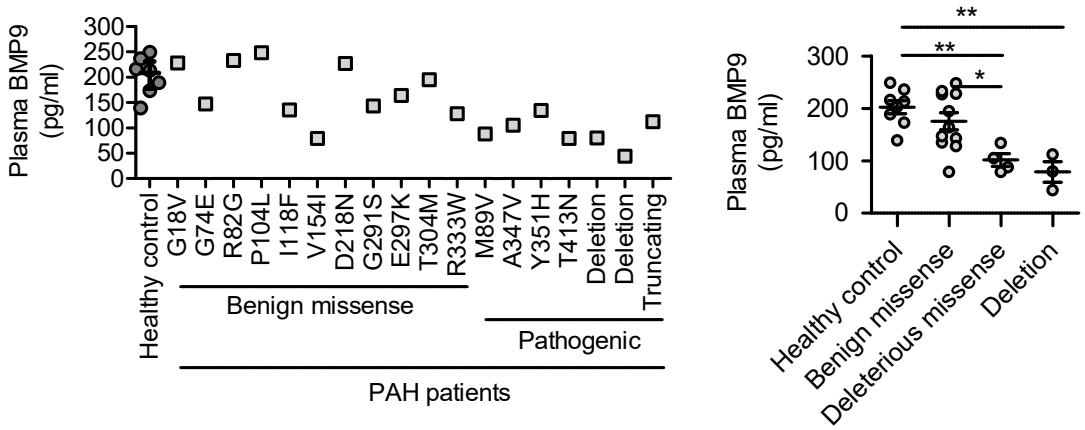

Figure 35. Plasma levels of BMP9 in PAH patients harbouring *GDF2* mutations. ELISA against the BMP9 growth-factor domain. Plasma from female, age-matched, healthy controls, and female PAH patients harbouring heterozygous mutations in *GDF2*. Left: samples were assayed in duplicate, and the mean is shown. Right: data grouped according the classification of the *GDF2* mutation. Mean ± SEM, one-way ANOVA with Bonferroni post hoc testing, * p<0.05, ** p<0.01.

To validate the ELISA results, I undertook to measure plasma activity on quiescent aortic endothelial cells. The peptide GPRP can bind fibrin and prevent clotting so I trialled using this with high plasma concentrations to boost signal. However, GPRP inhibited the transcriptional response to BMP9 (not shown). Therefore, I diluted plasma to 1% (v/v) in media to prevent clotting. I assessed induction of *ID1,2* and *HEY1* since these were the strongest responders to recombinant BMP9. However, there were no significant differences in plasma activity of pathogenic *GDF2* variant carriers versus other groups (figure 36).

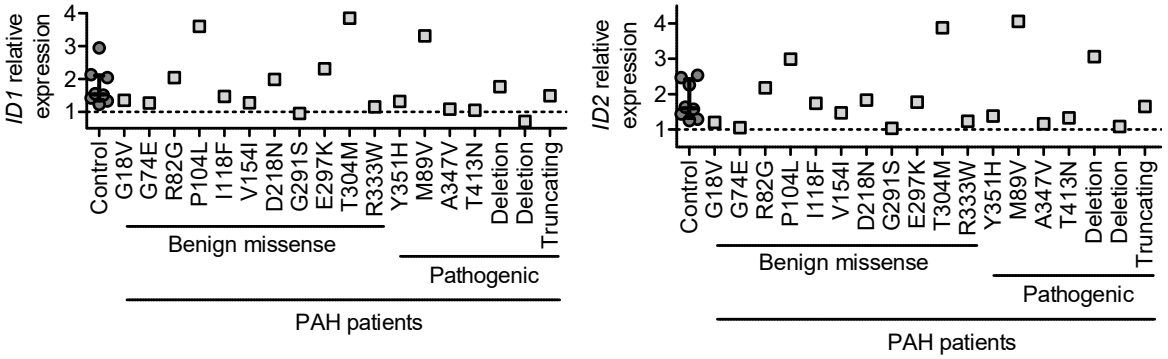

Figure 36. Plasma activity of PAH patients harbouring *GDF2* mutations. Quiescent human aortic endothelial cells treated with 1% (v/v) plasma. *ID1*, *ID2* and *HEY1* mRNA was measured by qPCR relative to the housekeeper *B2M*. Plasma from female, age-matched, healthy controls, and female PAH patients harbouring heterozygous mutations in *GDF2* was assayed. Samples were assayed in singlet.

There was a promising trend in these data, so I treated cells with 3% plasma, which led to some clotting, but boosted the transcriptional response (figure 37). Plasma from PAH patients carrying pathogenic *GDF2* alleles had reduced activity, which almost reached significance. This difference in activity was likely due to a reduction in BMP9 levels, since plasma cleared of BMP9 by immunoprecipitation was less able to stimulate a response.

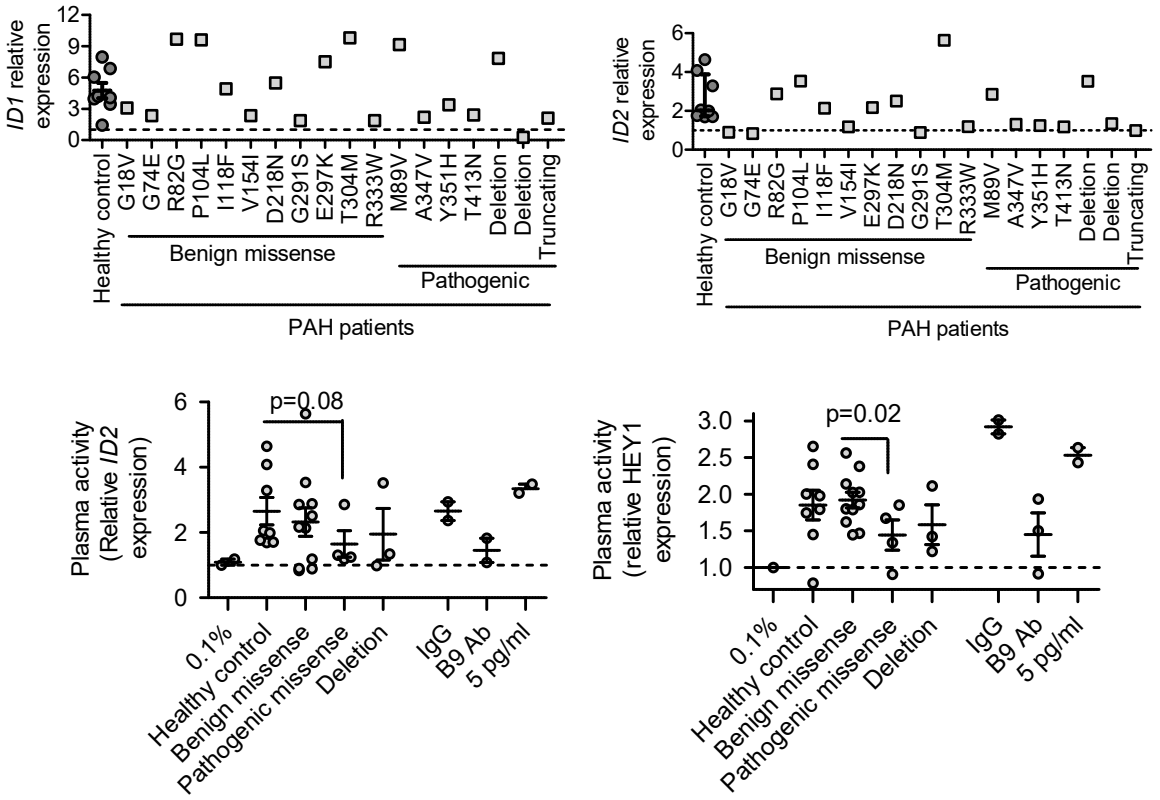

Figure 37. Plasma activity of PAH patients harbouring *GDF2* mutations. Quiescent human aortic endothelial cells treated with with 3% (v/v) plasma. *ID1*, *ID2* and *HEY1* mRNA was measured by qPCR relative to the housekeeper *B2M*. Plasma from female, age-matched, healthy controls, and female PAH patients harbouring heterozygous mutations in *GDF2* was assayed. Samples were assayed in singlet. **Bottom:** data grouped according the classification of the *GDF2* mutation. Mean ± SEM, unpaired, one-tailed Student's t-test of controls compared to pathogenic missense carriers. Control plasma from four healthy controls underwent a mock immunoprecipitation with non-specific IgG or anti-BMP9, before activity was assessed. A positive control consisting of 5 pg/ml of recombinant BMP9 is shown.

Dr. Paul Upton generated a stable endothelial reporter cell line by transducing human microvascular endothelial cells with a BMP signalling driven *luciferase* gene (Korchynskyi and ten Dijke 2002; Ades et al. 1992). I confirmed these *BRE*-HMECs had a high affinity response to BMP9 and responded to plasma (figure 38). Supplementation with GPRP and EDTA to inhibit clotting supressed the BMP9 response (not shown). Supplementing plasma with $CaCl_2$, to stimulate clotting to generate serum prior to treatment, did not work. I treated *BRE*-HMECs with 1%, 2% or 5% (v/v) patient plasma, all of which gave a similar pattern. At 5%

(v/v) plasma, some clotting occurred, but I added lysis reagent directly to the media so there was no risk of aspirating cells with the clot, and clotting did not reduce the BMP9 response. The activity of plasma mirrored the levels of BMP9 detectable by ELISA, with patients carrying pathogenic *GDF2* variants having ~50% the circulating activity of controls (figure 39).

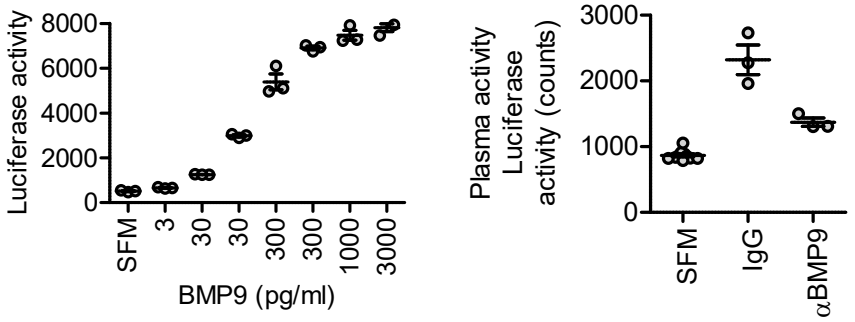

Figure 38. *BRE*-HMECs have a high affinity response to BMP9. **Left:** cells were treated with the indicated dose of recombinant BMP9. **Right:** cells were treated with 5% (v/v) plasma from four healthy volunteers. Plasma either underwent a mock immunoprecipitation, or immunoprecipitation with anti-BMP9. Mean ± SEM, n = 4.

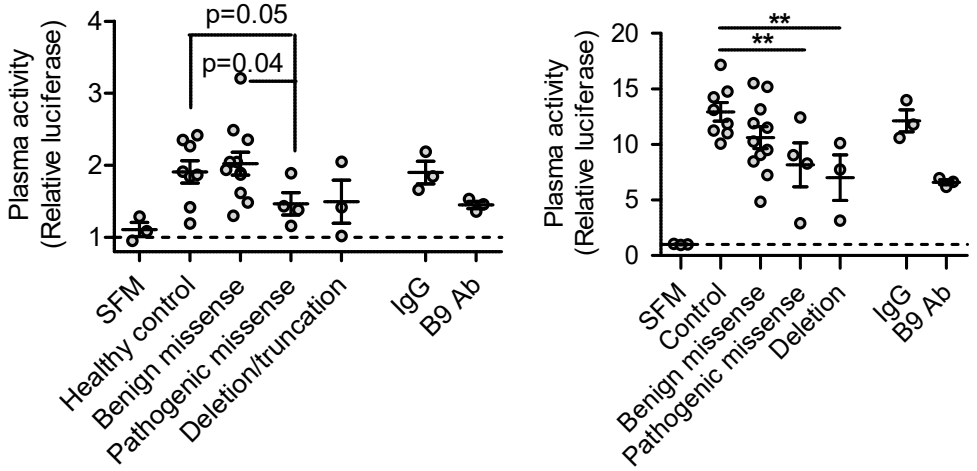

Figure 39. Plasma activity of PAH patients harbouring *GDF2* mutations. *BRE*-HMECs were supplemented with **left** 2% (v/v) or **right** 5% (v/v) of plasma. Plasma from female, age-matched, healthy controls, and female PAH patients harbouring heterozygous mutations in *GDF2* was assayed. Samples were assayed in triplet with mean plotted. Healthy control plasma underwent immunoprecipitation with non-specific IgG (mock) or anti-BMP9. Mean ± SEM, unpaired, one-tailed Student's t-test of controls compared to pathogenic missense carriers, **p<0.01.

It is possible BMP9 deficiency is compensated for by increased BMP10 expression. This did not appear to be the case in activity measurements of plasma from *GDF2* deficient patients. Nevertheless, I assessed pBMP10 levels in these plasmas using an ELISA developed by Dr. Paul Upton (see 1.4.4). Surprisingly, patients carrying pathogenic *GDF2* variants had greatly reduced levels of circulating pBMP10 (figure 40). There was a striking correlation

between circulating BMP9 and pBMP10 levels, suggesting both a lack of compensation and a degree of co-regulation (figure 41). Since the genetic mutation of *GDF2* preceded a reduction in plasma pBMP10, there could be some dependency of BMP10 on BMP9.

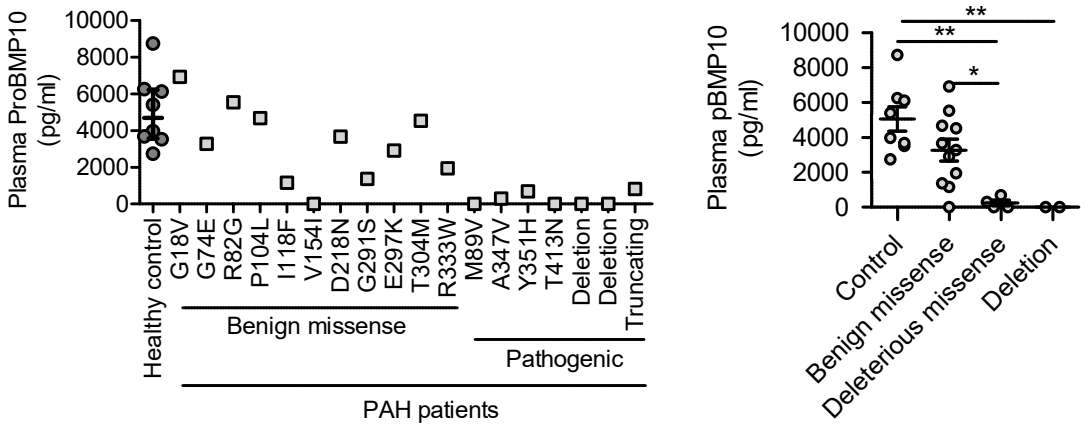

Figure 40. Plasma levels of pBMP10 in PAH patients harbouring *GDF2* mutations. An ELISA using a capture antibody against the BMP10 growth-factor domain and a detection antibody against the BMP10 prodomain. Plasma from female, age-matched, healthy controls, and female PAH patients harbouring heterozygous mutations in *GDF2* was measured. **Left:** samples were assayed in duplicate, and the mean is shown. **Right:** data grouped according the classification of the *GDF2* mutation. Mean ± SEM, one-way ANOVA with Bonferroni post hoc testing, * p<0.05, ** p<0.01.

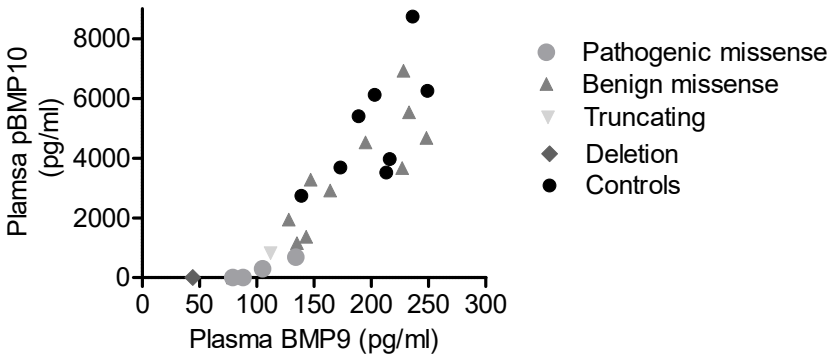

Figure 41. Plasma levels of BMP9 and pBMP10 is correlated in PAH patients harbouring *GDF2* mutations and in healthy controls. Data from figures 35 and 40 were compared.

3.5. BMP9 levels & activity in patients not carrying *GDF2* mutations

Dr. Paul Upton measured plasma BMP9 and pBMP10 levels in 254 PAH patients and 120 age/sex-matched healthy controls (Hodgson et al. 2019). These data confirmed that in general PAH is not associated with reduced BMP9 levels. Again, levels of BMP9 and pBMP10 were very tightly correlated in controls and patients. However, there was an over-representation of patients which had very low or undetectable BMP9 levels, in addition to

those that carried *GDF2* mutations. I re-measured samples from these patients with ELISA and activity assays. Both assays confirmed a loss of circulating ligands in a subset of PAH patients unexplained by *GDF2* mutations (figure 42).

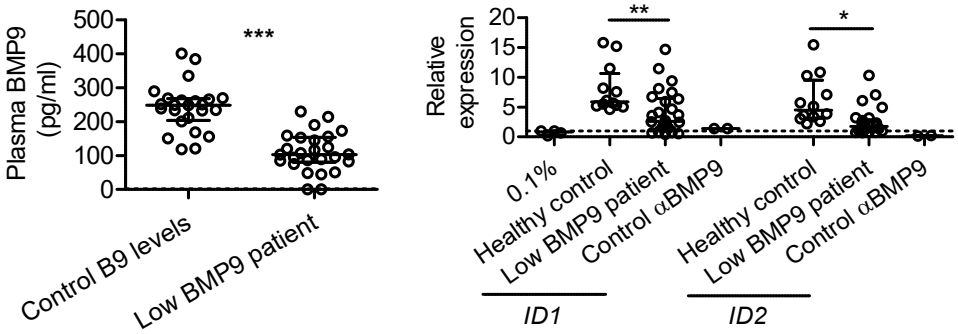

Figure 42. Plasma levels of BMP9 and plasma activity was re-measured in a subset of PAH patients which had low levels of BMP9. Left: plasma BMP9 levels were measured in duplicate by ELISA. **Right**: activity was measured by treating quiesced aortic endothelial cells with 3% (v/v) plasma. *ID1* & *ID2* mRNA levels were measured by qPCR, relative to the housekeeping gene *B2M.* Age and sex matched healthy control plasmas were included as a control. n = 26 patients, 24 controls, Mean ± IQR, unpaired, one-tailed Student's t-test of controls compared to low BMP9 patients, * $p < 0.05$, ** $p < 0.01$, ***$p < 0.001$.

3.6. Homozygous truncating mutations in paediatric HHT & PAH

Wang *et al.* (2016) reported a 5-yearold with PAH carrying a homozygous nonsense mutation, BMP9 -Q26X. Collaborators in Utah and Spain, to whom this patient was referred aged 10, hypothesised this mutation could be rescued by initiation of translation from Met57, resulting in a short N-terminal truncation of the prodomain. They provided me with expression vectors for *PreProBMP9*-WT, Q26X and a version with the first 56 amino acids deleted (ORF57). I validated that the expression vector sequences introduced the correct mutations. I transfected HEK-293T cells with the wildtype vector and optimised transfection conditions and timepoints (not shown). The BMP9 from this vector had identical activity to recombinant purified BMP9 (not shown).

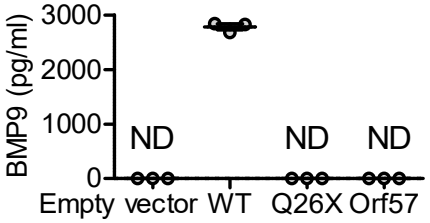

Figure 43. ELISA measurement of secreted BMP9 growth-factor domain in conditioned media. HEK-293T cells were transfected with expression vectors for myc/His tagged *PreProBMP9*-WT or variants, and placed in serum-free, chemically defined media. Three days post transfection, conditioned media was collected. This was serially diluted and BMP9

concentration in dilutions was measured by ELISA. Dilutions which gave absorbances in the linear part of the standard curve were used to calculate BMP9 concentration in the media. Three independent batches of HEK-293T cells were transfected and assayed independently. Mean ± SEM, n = 3, ND = not detectable.

There was no detectable secretion of Pro:BMP9-Q26X or ORF57 into conditioned media as measured by ELISA (figure 43) or Western blotting (figure 44). Within cell lysates, there was good expression of unprocessed, but truncated, *ProBMP9* (figure 45). Despite this, there was no evidence of processed free prodomain or growth factor domain from the variant proteins. This contrasts wildtype BMP9, which exhibited bands corresponding to the unprocessed and mature forms as expected. These data suggest ribosomes can spontaneously initiate translation at Met57. This produces *ProBMP9* without a secretion signal peptide, so it may not enter the secretory and processing pathway. Alternatively, truncating the prodomain could simply disrupt folding which is essential to proper processing and secretion.

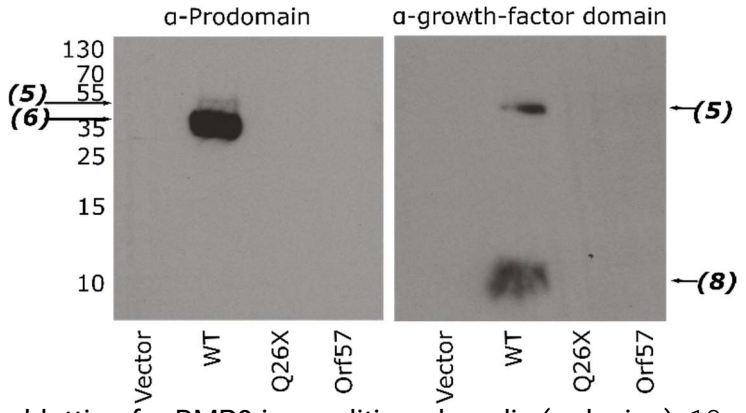

Figure 44. Western blotting for BMP9 in conditioned media (reducing). 10 µl of WT conditioned media, or 50 µl of variants, were loaded per lane. Three independent batches were assayed. One representative blot shown. Nº = molecular weight (kDa), *(Nº)* = species identification from figure 7.

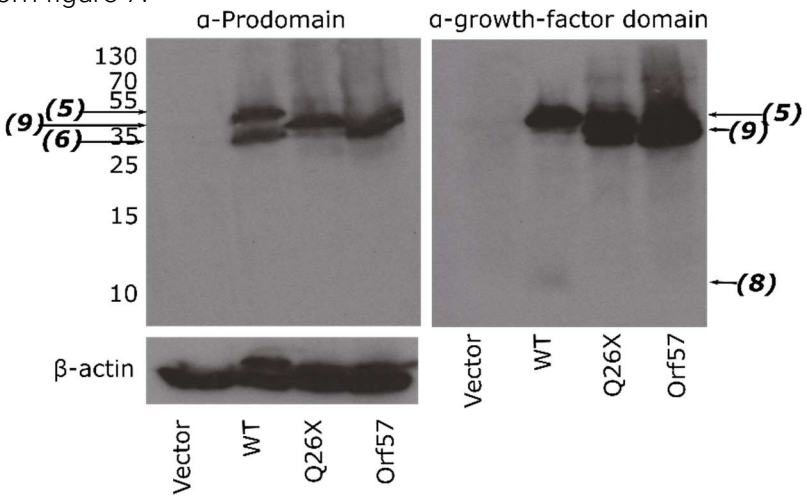

Figure 45. Western blotting for BMP9 in cell lysates (reducing). Three independent batches were assayed. One representative blot shown. Nº = molecular weight (kDa), *(Nº)* = species identification from figure 7.

A child with HHT, but no evidence of PAH, has been found with a second homozygous truncating variant BMP9-E179X. Samples from this child's mother and father were available. Therefore, I measured plasma BMP9 levels in the children, parents and control samples. As expected, plasma from the homozygous truncation carriers contained no detectable BMP9 (figure 46). To try and confirm this, I used 50 µl of plasma and an alternative buffer in the ELISA to maximise sensitivity to low levels of BMP9 (figure 47)(see 4.3). Notably, plasma levels of BMP9 in the heterozygous parents were reduced compared to controls, although they do not appear to be diseased.

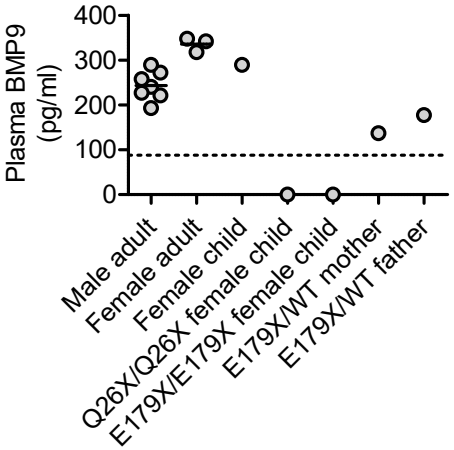

Figure 46. Plasma levels of BMP9 in paediatric PAH & HHT patients harbouring *GDF2* mutations. Plasma from four healthy adult males, three healthy adult females, a healthy female child, a female child with PAH harbouring a homozygous nonsense mutation BMP9-Q26X, a female child with HHT harbouring a homozygous nonsense mutation BMP9-E179X, and the healthy parents each carrying BMP9-E179X heterozygously, were measured in duplicate and the mean is shown.

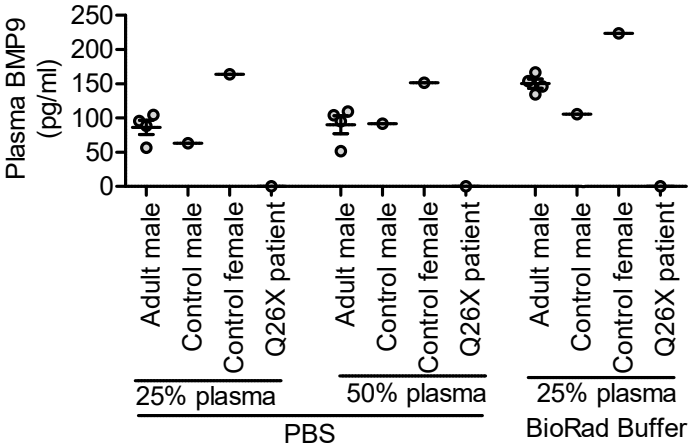

Figure 47. Plasma levels of BMP9 in a PAH patient harbouring *GDF2* mutations. Plasma from four healthy adult males, a healthy male child, a healthy female child and a female child with PAH harbouring a homozygous nonsense mutation were measured. The usual ELISA conditions were used (25% (v/v) plasma, 1% (w/v) BSA, 0.5% (v/v) triton-x100, 0.2% (v/v) goat serum in PBS) but 50% (v/v) plasma, and replacing PBS with BioRad plasma ELISA buffer was also tested. Samples were measured in duplicate and the mean is shown.

Secondly, I measured plasma levels of pBMP10 in these samples (figure 48). They demonstrated the same pattern seen in the previous data-sets, with *GDF2* deficiency leading to reduced circulating pBMP10. Similarly, I measured the activity of 10% (v/v) serum from these people on BRE-HMECs (figure 49). These data show truncating variants in *GDF2* lead to a reduction in circulating BMP activity

.

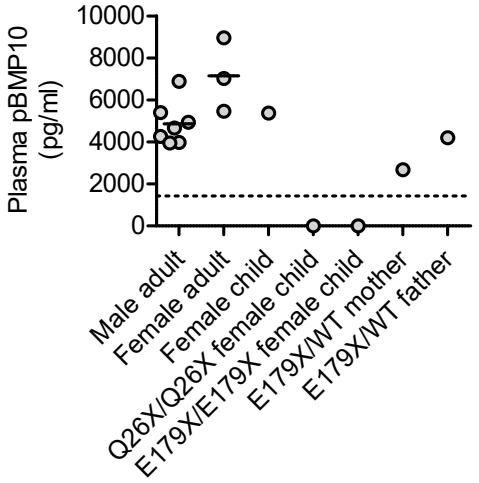

Figure 48. Plasma levels of pBMP10 in paediatric PAH & HHT patients harbouring *GDF2* mutations. Plasma from four healthy adult males, three healthy adult females, a healthy female child, a female child with PAH harbouring a homozygous nonsense mutation BMP9-Q26X, a female child with HHT harbouring a homozygous nonsense mutation BMP9-E179X and the healthy parents carrying heterozygous BMP9-E179X mutations were measured in duplicate and the mean is shown.

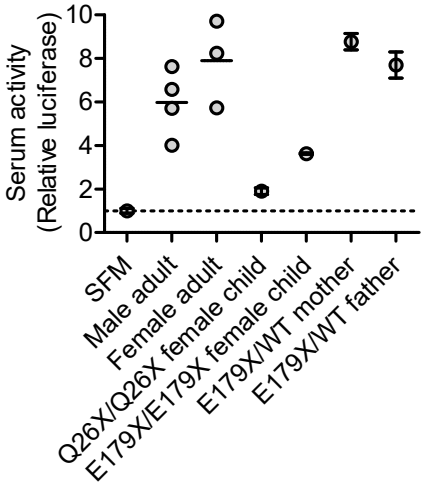

Figure 49. Serum activity of paediatric PAH & HHT patients harbouring *GDF2* mutations. Quiescent *BRE*-HMECs were supplemented with 10% (v/v) of serum from four healthy adult males, three healthy adult females, a healthy female child, a female child with PAH harbouring a homozygous nonsense mutation BMP9-Q26X, a female child with HHT harbouring a homozygous nonsense mutation BMP9-E179X, and the healthy parents each carrying heterozygous BMP9-E179X mutations. Samples were measured in triplicate and the mean is shown ± SEM.

3.7. Discussion

Robustly demonstrating BMP9 or BMP10 deficiency causes human disease increases confidence in potential therapies based on them. Additionally, most PAH cases are currently unexplained so it may aid clinicians and patients if some of their disease can be linked to BMP9 or BMP10. Dr. Paul Upton undertook to measure plasma levels of BMP9 and BMP10 in a large cohort of PAH patients and healthy controls to see if levels are repressed in PAH. Another approach is to link mutations in *GDF2* or *BMP10* to disease.

Gräf *et al.* (2018) carried out a rare variant analysis with conservative parameters: only very rare variants which were predicted to be highly damaging and associated with PAH were classified as pathogenic. Missense mutations in *GDF2* were significantly associated with PAH on a genome wide basis. We wanted to explore the mechanism by which these missense mutations lead to disease. Additionally, *in silico* predictions of deleteriousness are based on empirical analysis of many proteins, so it was important to validate the pathogenicity of the PAH associated variants. Therefore, we selected a range of variants for analysis, including both those predicted to be pathogenic and benign.

An overexpression system was used to generate missense variants. This system revealed that the preeminent defect of putatively pathogenic pBMP9 variants was improper processing and secretion of the mature growth-factor domain. Variant pro-proteins were expressed at similar levels within cell lysates, but active growth-factor domain dimers were found at heavily reduced concentrations in the conditioned media. Structural analysis revealed that many of the putatively pathogenic mutations altered residues at the prodomain / growth-factor domain interface. These two observations led us to hypothesise the active Pro:BMP9 complex of pathogenic variants is unstable, which leads to the loss of the growth-factor.

Over-expression systems can introduce artefacts, since they saturate the cellular translation, folding and secretion machinery (Jones et al. 1994; Israel et al. 1992). For example, pule-chase experiments involving cells transfected with BMP2 reveal the majority of protein is degraded before secretion (Israel et al. 1992). Nevertheless, there were highly reproducible results across three transfections. Moreover, *in silico* predictions of deleteriousness were consistent with the *in vitro* results.

The only exception is that BMP9-P104L was inefficiently secreted despite being assigned as benign. Unlike pathogenic variants, BMP9-P104L exhibited normal molar ratios of growth-factor domain to prodomain, and the patient plasma sample contained high levels of

BMP9 and activity. Structural analysis by Wei Li indicated that residue 104 is located on a loop domain of the prodomain which does not contact other parts of BMP9.

PAH patients harbouring pathogenic *GDF2* mutations had reduced plasma BMP9 levels and activity on endothelial cells. A previous report shows transfecting cells with a mix of variant and wildtype BMP6 to causes dominant-negative deficiency via dimerisation (Daher et al. 2016). However, this does not necessarily reflect how cells express endogenous BMP9 from different alleles (Elowitz et al. 2002). Our patients carrying pathogenic missense variants were heterozygous, and their circulating BMP9 levels were about 50% lower than controls, supporting *in vitro* evidence of a stability defect and a haploinsufficiency model. Based on these results, figure 50 shows how either deficiency in receptor levels or ligand levels can contribute to PAH, and how this may be rectified with exogenous BMP9. It is not known if BMP9 levels in plasma are a good predictor of BMP9 activity on the pulmonary vasculature, since there could be local sources or buffers. Similarly, the prodomains could stabilise and target the growth-factor domain *in vivo*, so patients carrying missense variants might have dysfunctional signalling beyond reduced circulating levels.

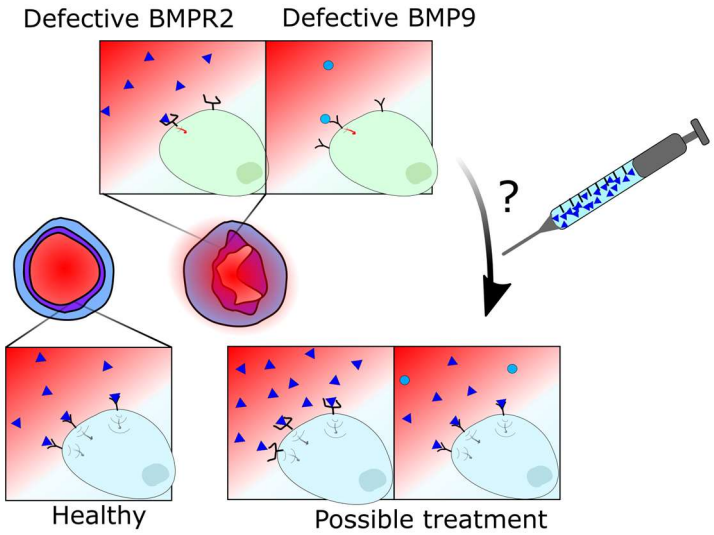

Figure 50. In healthy people, BMP9 circulates at active levels, and contributes to endothelial cell quiescence. Insufficient BMPR2 signalling, including *BMPR2* mutations, is a well-established contributor to PAH. The Morrell group has shown that administering exogenous BMP9 is able to reverse disease in animal models with defective BMPR2 signalling. Here, I present evidence showing a subset of patients carry deleterious BMP9 variants or have insufficient circulating levels of BMP9. These patients may also be amenable to treatment with exogenous BMP9.

Pathogenic mutations in *GDF2* led to a striking reduction in plasma pBMP10 levels. *BMP10* expression could be induced by BMP9, or plasma BMP10 could be sequestered to vacant BMP9 binding sites. Alternatively, Tillet *et al.* (2018) suggest BMP9 and BMP10 are

heterodimeric. *GDF2* mutations actually led to a greater loss of pBMP10 than BMP9; further evidence that any physical association between them is not 1:1. It is possible that *GDF2* mutations contribute to PAH via their effect on *BMP10,* or this could be an unrelated effect.

During the course of this project, another group carried out a similar analyses of pathogenic BMP9 proteins discovered in a Chinese PAH cohort (Wang et al. 2019). They reproduced several findings, including reduced secretion but normal ALK1 signalling of variant BMP9 proteins *in vitro* and a processing defect of *ProBMP9*-S320C. However, in their hands, pathogenic BMP9 variants exhibited no anti-apoptotic activity on PAECs in a caspase-GLO assay. This could be because they did not treat cells with normalised amounts of conditioned media—I showed conditioned media itself stimulates apoptosis. Although Wang *et al.* report reduced plasma BMP9 levels in PAH patients carrying pathogenic *GDF2* variants, they also observe a general reduction in PAH patients, and report mean healthy plasma BMP9 levels of just ~30 pg/ml. This is likely because they are not using an ELISA protocol suitable for measuring BMP9 levels in plasma (see 1.4.4).

A European group used a targeted gene panel to find two truncating mutations in *GDF2* and rediscovered Pro:BMP9-E143K (Eyries et al. 2019). Similarly, Pro:BMP9-R110W and R333W missense mutations were re-discovered in an American cohort (Zhu et al. 2019). Neither group carried out *in vitro* analyses. A previous group reported a mutation, BMP9-R317Q, in the furin recognition sequence associated with HHT (Hernandez et al. 2015). However, Tillet *et al.* (2019) expressed this variant *in vitro* and observed no processing defect. Notably, residue 317 is unspecified in canonical furin recognition sequences, whereas furin is intolerant of cysteines in the motif region (Tian 2009). This highlights the importance of *in vitro* analysis to uncover structural defects. Nonetheless, although Pro:BMP9-D218N is aberrantly glycosylated, it is fully functional, showing the importance of *in silico* analysis.

Missense variants predicted to benign *in silico* did not show significantly reduced levels or activity *in vitro* or *in vivo.* However, there was a tendency for them to be secreted less efficiently than Pro:BMP9-WT *in vitro*, mirrored by a tendency for carriers to have slightly reduced circulating levels and activity of BMP9 and BMP10. *GDF2* is exceptionally well conserved across species, which indicates powerful purifying selection, so it is likely that all these rare/very-rare variants are deleterious to an extent.

HHT and PAH are known to have overlapping genetics. Interestingly, I analysed two children with severe manifestations of each disease. Both children were homozygous carriers of completely non-functional alleles. The heterozygous parents were haploinsufficient but showed no disease. This hints that complete *GDF2* deficiency may be more severe than

haploinsufficiency or acquired loss of circulating BMP9. It is unclear what triggers some patients develop HHT without PAH or vice versa. It seems likely that mutations in HHT are more penetrant, although symptoms might not manifest until old-age, after some patients have died from PAH (Girerd et al. 2010). Therefore, these children and their haploinsufficient parents should be monitored overtime to assess whether they begin to manifest HHT or PAH.

4. Characterising circulating BMP9 & BMP10

4.1. Introduction

Scientific consensus suggests BMP9 is produced and cleaved within the liver, then circulates in complex with its prodomains until it binds a target receptor (Bidart et al. 2012). Some reports find active Pro:BMP10 in the blood, which is thought to be secreted from the right atrium (Jiang et al. 2016). Plasma and serum have complex compositions and plasma requires agents to prevent clotting. This interferes with many antibodies, enzymes and cell-based assays. BMP9 and BMP10 have similar properties so it can be difficult to know which is being assessed in activity assays. Few ELISA protocols for measuring BMP9 and BMP10 in plasma or serum have been validated, so we do not know their recovery efficiency or what species of BMP9 and BMP10 they detect. The following properties of circulating BMP9 and BMP10 are ambiguous in the current literature: whether the liver and the right atria are the only source of circulating BMP9 and BMP10 respectively; the proportion of circulating pBMP9 and pBMP10 which is processed and active versus unprocessed; the concentration of BMP9 and BMP10 in plasma and serum; and whether BMP9 and BMP10 bind to carrier proteins in blood (see 1.4).

Figure 51. Schematic of species detected by different ELISAs. The pBMP10 ELISA is able to detected both processed and unprocessed BMP10, whilst the BMP9 and BMP10 growth factor domain ELISAs are only able to detect processed species. The ProBMP9 detects an unprocessed form of ProBMP9 of uncertain identity. See following sections for how this was determined. See figure 7 for a schematic of how BMP9 and BMP10 are processed.

Several sandwich ELISAs are available for measuring human BMP9 and BMP10 (figure 51). Different capture and detection antibodies are targeted against their prodomains or growth-factor domains, so could be used in combination to detect processed and/or

unprocessed species. Activity neutralisation and immunoprecipitation protocols have also been published. Therefore, I used these to assay circulating BMP9 and BMP10. Secondly, I investigated the potential existence of circulating BMP9 and BMP10 binding proteins.

4.2. Minimal circulating processed Pro:BMP10 is detectable by ELISA

The pBMP10 ELISA we use comprises capture antibody specific for the growth-factor domain and detection antibody specific for the pro-domain. A second ELISA using both capture and detection antibodies against the BMP10 growth-factor domain is commercially available. It was unclear whether each ELISA measures both processed and unprocessed forms of pBMP10. Therefore, I tested both the pBMP10 and BMP10 growth-factor domain ELISAs with standards of either processed Pro:BMP10 or unprocessed *ProBMP10.* The latter was generated by Jingxu Guo by introducing a BMP10-R313A mutation in the furin recognition sequence (see figure 78)(Susan-Resiga et al. 2011). The BMP10 growth-factor domain ELISA was able to detect processed Pro:BMP10 and recombinant BMP10 growth-factor equally efficiently, but not unprocessed *ProBMP10*-R313A—log(EC_{50}) = 3.8 ± 0.02, 4.1 ± 0.04 and ~10 respectively (figure 52). The pBMP10 ELISA was equally efficient at detecting Pro:BMP10 and *ProBMP10*-R313A—log(EC_{50}) = 4.5 ± 0.04 and 4.7 ± 0.02 respectively . In combination, these ELISAs could be used to distinguish processed and unprocessed BMP10.

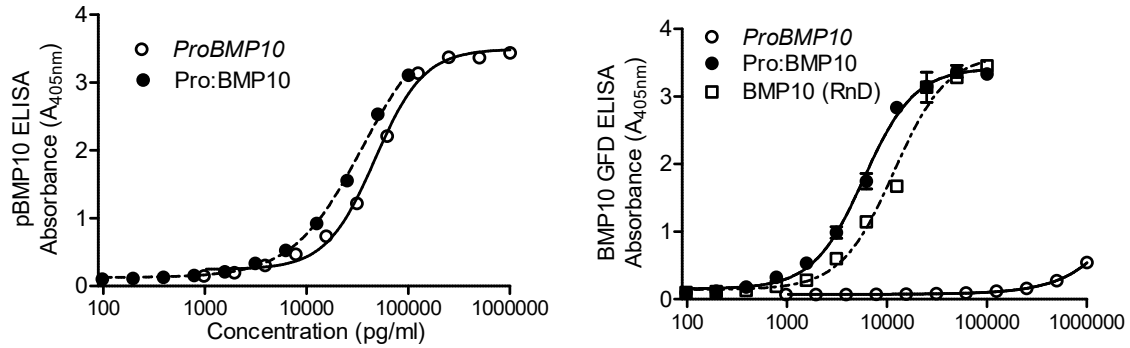

Figure 52. The pBMP10 ELISA detects dimeric Pro:BMP10 or *ProBMP10*, whilst the BMP10 growth-factor domain ELISA detects Pro:BMP10. Purified Pro:BMP10 was produced by He Jiang, whilst unprocessed *ProBMP10*-R313A was purified by Jingxu Guo. Immunoreactivity in the pBMP10 (**left**) and BMP10-growth factor domain (**right**) ELISAs was measured. Mean ± SEM of duplicates, curves = four parameter logistic regression, n = 3 with one representative experiment shown.

Dr. Paul Upton optimised the pBMP10 ELISA. I optimised the BMP10 growth-factor domain ELISA for use with plasma based on the same additives and dilutions. The BMP10 growth-factor domain ELISA was not very efficient at recovering exogenous BMP10 spiked into plasma (figure 53). Unspiked plasmas gave readings below the blanks, indicating plasma introduced non-specific inhibition, perhaps due to the high protein concentration of plasma.

I replaced 1% (w/v) BSA in PBS as the diluent base with BioRad ELISA diluent which contains high levels of goat serum proteins. This resulted in efficient recovery of Pro:BMP10 (figure 54).

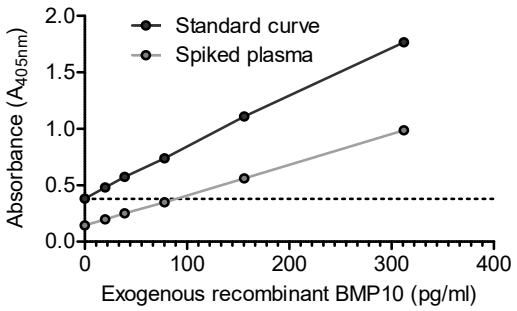

Figure 53. Recovery efficiency of the BMP10 growth factor domain ELISA from plasma. Recombinant BMP10 was serially diluted in plasma or 1% (w/v) BSA in PBS. Thirty µl samples were diluted with 70 µl 1% (w/v) BSA in PBS supplemented with 0.5% (v/v) Triton-X100, 0.2% (v/v) goat serum and 5 mM EDTA. Immunoreactivity was measured in the BMP10 growth-factor domain ELISA by colourimetry. Mean ± SEM of duplicates, n = 1. Dashed line = absorbance of blank.

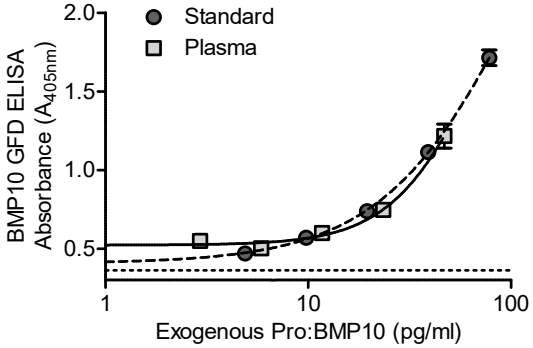

Figure 54. BioRad diluent results in high recovery efficiency from plasma in the BMP10 growth-factor domain ELISA. Pro:BMP10 was serially diluted in plasma or BioRad ELISA buffer (standard). Thirty µl samples were diluted with 70 µl of BioRad ELISA buffer supplemented with 0.5% (v/v) Triton-X100, 0.2% (v/v) goat serum and 5 mM EDTA. Immunoreactivity was measured in the BMP10 growth-factor domain ELISA by colourimetry. Curves = four parameter logistic regression, dashed line = absorbance of blank. Mean ± SEM of duplicates, n = 3, one representative experiment shown.

Surprisingly, the growth-factor domain ELISA only detected 0-45 pg/ml of endogenous Pro:BMP10 in plasma. These values are below the reliable quantification limit of this ELISA—replicates fell anywhere in this range (not shown). Similar data were generated by Dr. Paul Yu's group using the same ELISA (personal communication). The pBMP10 ELISA detected ~5 ng/ml of endogenous pBMP10. The discrepancy between ELISAs was either because endogenous BMP10 primarily consists of unprocessed *ProBMP10,* or endogenous Pro:BMP10 is somehow masked from the growth-factor domain ELISA.

As expected, immunoprecipitation of plasma with hALK1-Fc cleared all endogenous BMP10. I tried numerous conditions to immunoprecipitate purified Pro:BMP10 from PBS or plasma using several anti-BMP10 antibodies. Unfortunately, they could not clear BMP10 (not

shown). This is consistent with findings that anti-BMP10 antibodies also fail to neutralise any plasma activity (Jiang et al. 2016). The anti-BMP10 antibody mAb2926 worked in ELISAs, so can bind natively folded BMP10 within plasma. To trouble-shoot the immunoprecipitation, I confirmed antibody was binding to the protein G beads by eluting them followed by SDS-PAGE and Coomassie staining (figure 55). Next, I supplemented samples with EDTA and detergents to mimic the ELISA conditions. Unfortunately, EDTA had no beneficial effect, whilst detergents were incompatible with cell-based assays (not shown). Finally, I extended the incubation time of sample with antibody-beads from 10 minutes to over-night at room temperature. This facilitated successful clearance of Pro:BMP10 from the samples.

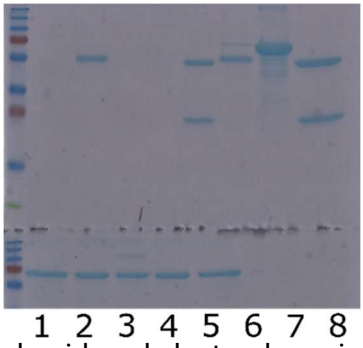

Figure 55. Reducing SDS polyacrylamide gel electrophoresis & Coomassie staining of immunoprecipitations. Top: Eluates Bottom: Analytes. 1 = protein G conjugated metal beads with Pro:BMP10 alone, 2 = beads with ALK1-Fc and Pro:BMP10, 3 = beads covalently linked to ALK1-Fc with 5 mM BS^3 with Pro:BMP10, 4 = beads covalently linked to ALK1-Fc with 1 mM BS^3 in PBS with Pro:BMP10, 5 = beads and anti-BMP10 (mAb2926) with Pro:BMP10, 6 = ALK1-Fc positive control, 7 = Pro:BMP10 positive control, 8 = anti-BMP10 positive control.

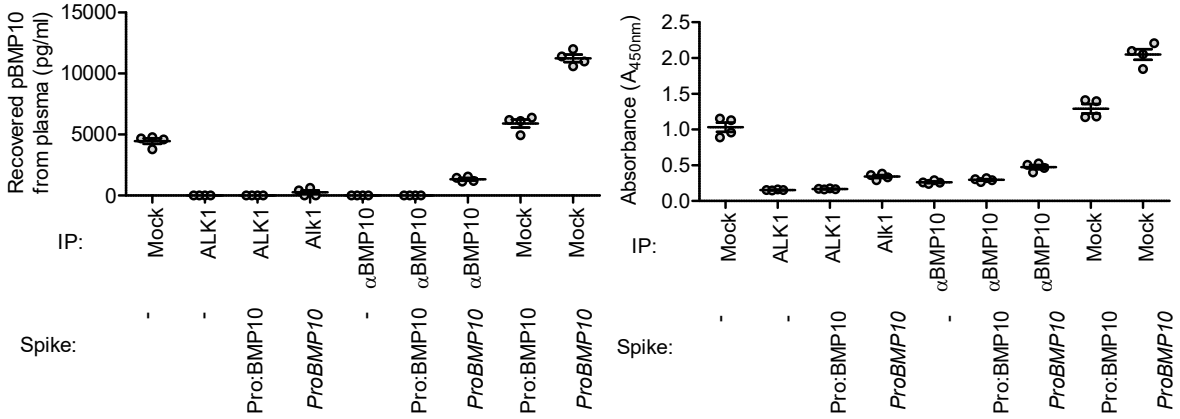

Figure 56. Endogenous BMP10 behaves like *ProBMP10* or Pro:BMP10 in immunoprecipitations and the pBMP10 ELISA. Left: EDTA-plasma from four healthy males. Plasmas were spiked with 2.5 ng/ml of Pro:BMP10 or 5 ng/ml of *ProBMP10*-R313A where indicated. Samples were immunoprecipitated with non-specific IgG (mock), hALK1-Fc, or anti-BMP10. Immunoreactivity was measured in the pBMP10 ELISA. Right: The raw absorbance of the same ELISA. Mean of duplicates plotted. Mean ± SEM, n = 4. Dashed line = absorbance of blank.

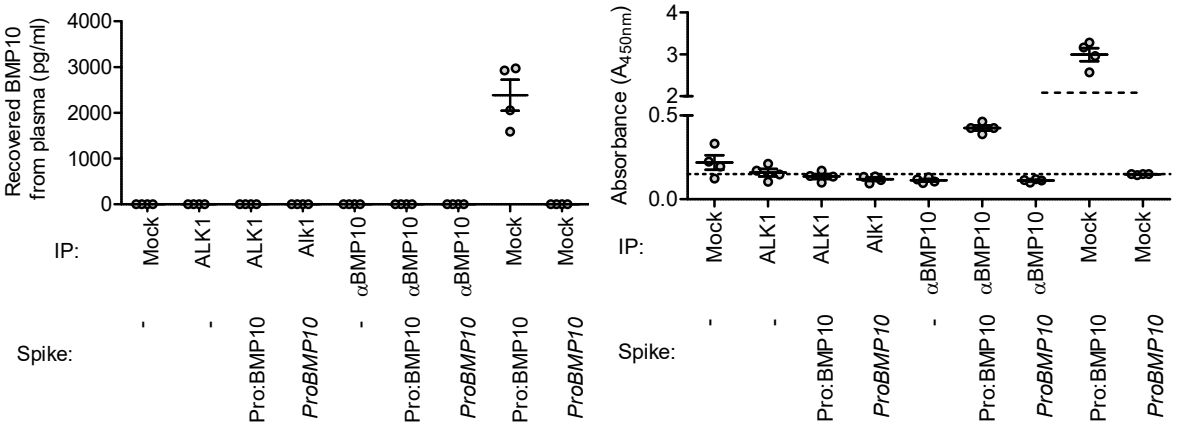

Figure 57. Endogenous BMP10 does not cross-react to any great extent in the BMP10 growth-factor domain ELISA. **Left:** EDTA-plasma from four healthy males. Plasmas were spiked with 2.5 ng/ml of Pro:BMP10 or 5 ng/ml of *ProBMP10*-R313A where indicated. Samples were immunoprecipitated with non-specific IgG (mock), hALK1-Fc, or anti-BMP10. Immunoreactivity was measured in the BMP10 growth-factor domain. **Right:** The raw absorbance of the same ELISA. Mean of duplicates plotted. Mean ± SEM, n = 4. Dashed line = absorbance of blank.

I was then able to show endogenous pBMP10, and both exogenous *ProBMP10* and Pro:BMP10, could be immunoprecipitated from plasma using ALK1-Fc and anti-BMP10 (figure 56; 57). Immunoprecipitation led to a large decrease in endogenous immunoreactivity in the pBMP10 ELISA. Immunoprecipitation caused very little change in endogenous immunoreactivity in the growth-factor domain ELISA. This further showed endogenous pBMP10 has almost no immunoreactivity in the growth-factor domain ELISA (otherwise absorbance would decline below the blank samples after immunoprecipitation). Therefore, we conclude unprocessed *ProBMP10* is the major circulating species.

4.3. Active levels of circulating Pro:BMP9 are detectable by ELISA

We refined a commercially available ELISA for measuring BMP9 growth-factor domain to maximise accuracy of plasma measurements. Most of the optimisation was undertaken by Drs. Paul Upton, Paul Yu, and Ivana Nikolic who established dilution factors and additives (see 1.4.4). I validated that diluting 25 ul of plasma from four healthy males in 75 ul of buffer containing 0.2% (v/v) goat serum and 0.5% (v/v) triton x-100 gave the most reproducible results and most efficient recovery of endogenous BMP9 (figure 58).

BMP9 was undetectable in serum using this ELISA. Additionally, Drs. Paul Upton and Claudia Mitrofan found BMP9 was measurable in sodium-citrate plasma, but not heparinised plasma. The most obvious technical difference between measurable and unmeasurable substrates is the presence of chelating agent. Accordingly, I showed equally efficient recovery

of BMP9 from EDTA-plasma and serum supplemented with 5 mM EDTA (figure 58). Dr. Paul Upton then showed BMP9 was recoverable in heparinised plasma supplemented with EDTA. Hence, chelating agent should be present in all samples used in this ELISA.

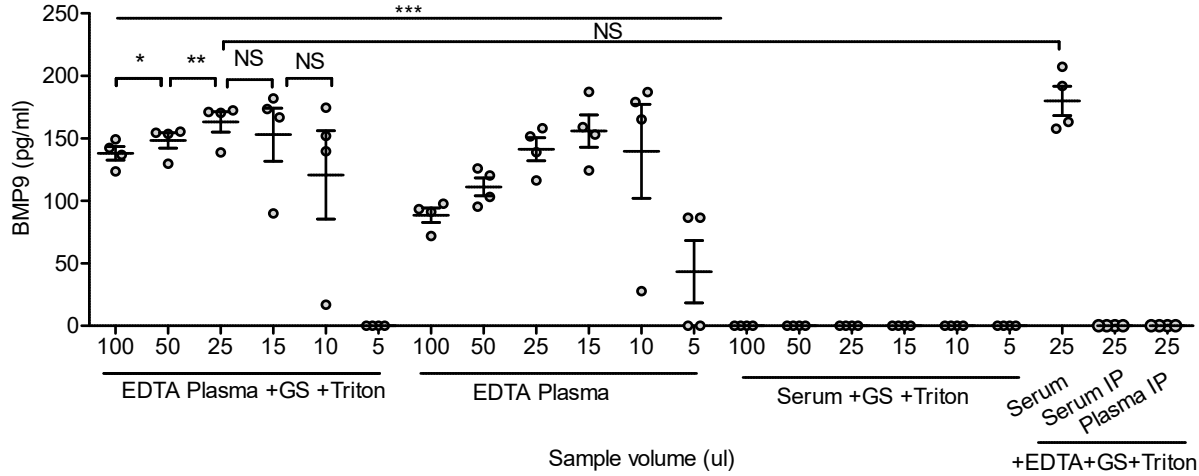

Figure 58. Validation of BMP9 growth factor domain ELISA. EDTA-plasma and serum were prepared from the same 4 healthy male volunteers. The indicated volumes of sample were diluted with 1% (v/v) BSA in PBS to give a total volume of 100 ul. Final concentrations of 0.2% (v/v) goat serum (GS), 0.5% (v/v) triton x-100 and 5 mM EDTA were added to diluted samples where indicated. For the 100 ul sample volumes, the additives were added directly to neat plasma or serum, to give a final volume of 105 ul. Endogenous BMP9 was precleared from the serum IP and plasma IP samples. Immunoreactivity was measured in the BMP9 growth-factor domain ELISA. Mean of duplicates plotted. Comparison between individual conditions = paired, two-tailed Student's t-tests. Comparison of the effect of additives on plasma = matched two-way ANOVA. Mean ± SEM, n = 4, * $p<0.05$, ** $p<0.01$, *** $p<0.001$, NS = not significant.

The BMP9 growth-factor domain ELISA could plausibly cross-react with unprocessed *ProBMP9* and processed Pro:BMP9. Nikolic *et al.* (2019) immunoprecipitated endogenous BMP9 from human serum using the capture antibody and analysed it by Western blotting using the detection antibody as a probe. They only found cross-reactivity with a ~12 kDa band, so concluded the ELISA only detects processed growth-factor domain. However, the antibodies may have different sensitivity to processed and unprocessed species in an ELISA format or healthy serum may only contain processed BMP9.

I confirmed this ELISA only detected processed BMP9 in chapter 3.2. Densitometry of Western blots suggested there was a ~35 fold excess of unprocessed monomeric and dimeric *ProBMP9*-S320C in conditioned media compared to processed growth-factor domain (figure 19; 59). Unprocessed species did not interfere with the ELISA—doses of BMP9-S320C and BMP9-WT calculated from ELISA results had equal activity on cells and equal intensity of processed growth-factor domain on Western blots (figure 15; 24).

As expected, immunoprecipitation using either anti-BMP9 or hALK1-Fc completely cleared plasma of detectable endogenous BMP9 (figure 60). Samples immunoprecipitated with hALK1-Fc had slightly lower absorbances than samples immunoprecipitated with anti-BMP9, which could indicate hALK1-Fc is more efficient at clearing BMP9.

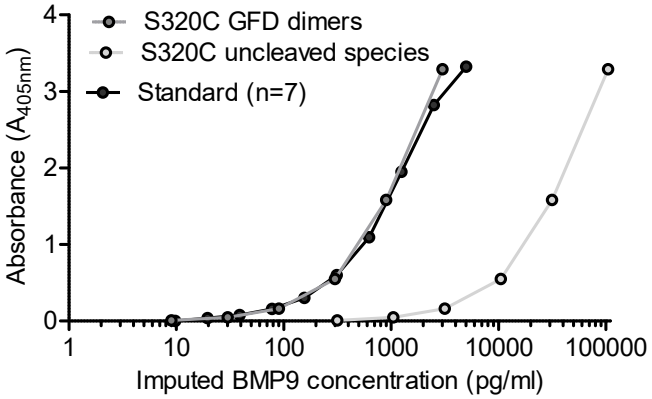

Figure 59. The BMP9 ELISA only detected processed dimers. Immunoreactivity of recombinant BMP9 (standard, seven dilutions) and processed or unprocessed *PreProBMP9*-S320C (as determined by western blotting, figure 19) in the BMP9 growth-factor domain ELISA. Mean ± SEM of duplicates, n = 3 with one representative result shown.

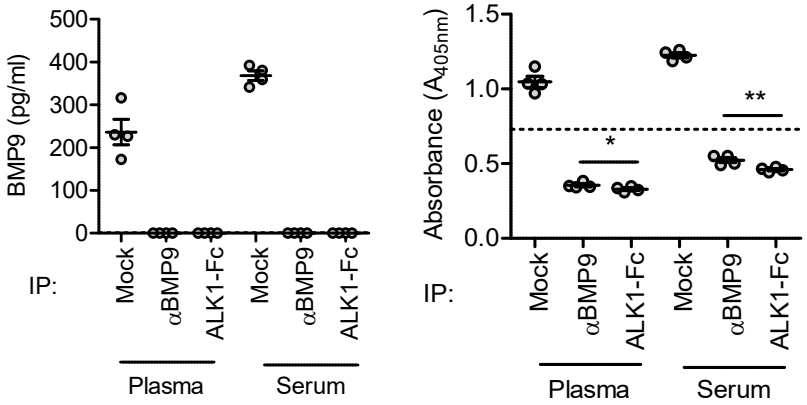

Figure 60. Plasma and serum immunoreactivity in the BMP9 ELISA could be cleared by immunoprecipitation with anti-BMP9 or ALK1-Fc. Plasma and serum were collected from four healthy males. Samples were immunoprecipitated with non-specific IgG (mock), anti-BMP9 or hALK1-Fc. Immunoreactivity was assessed in the BMP9 ELISA. **Right:** raw-absorbance data. Mean of duplicates plotted. Mean ± SEM, n = 4, matched two-tailed Student's t-testing, * $p<0.05$, ** $p<0.01$. Dashed line = absorbance of blank (diluent alone).

The immunoreactivity of plasma and serum cleared of BMP9 was below that of blanks, indicating plasma and serum introduced non-specific inhibition. Again, BioRad ELISA diluent reduced the immunoreactivity of the standard curve so cleared samples gave similar absorbances to blanks (figure 61). Hence, BioRad ELISA diluent could be used in place of 1% BSA in PBS to maximise recovery from plasma.

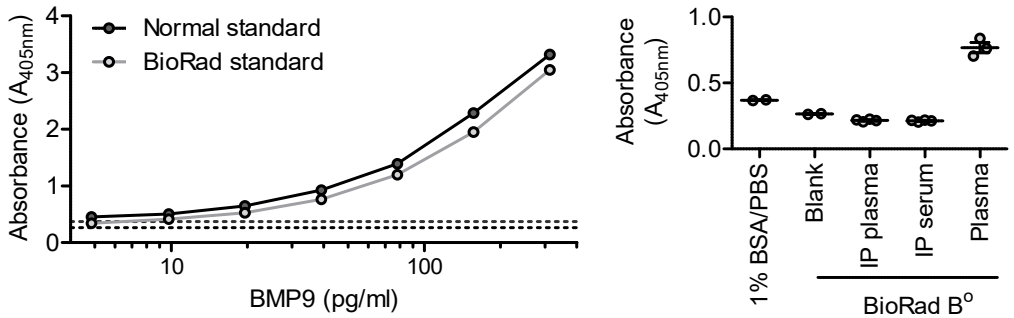

Figure 61. BioRad buffer mimicked the non-specific inhibition of immunoreactivity of plasma & serum, improving BMP9 ELISA sensitivity. Left: standard curves were prepared by serially diluting recombinant BMP9 in 1% (w/v) BSA in PBS, or BioRad ELISA buffer and immunoreactivity was measured in the BMP9 ELISA. The upper dashed line is the blank in 1% (w/v) BSA, whilst the lower dashed line is the blank immunoreactivity of BioRad ELISA buffer. Mean ± SEM of duplicates, n = 1. **Right:** Plasma and serum from four healthy males were cleared of BMP9 by immunoprecipitation using anti-BMP9. Mean ± SEM, n = 4.

4.4. No circulating unprocessed *ProBMP9* is detectable

Based on the results of the BMP10 ELISAs, we trialled a pBMP9 ELISA which uses a capture antibody against the growth-factor domain and a detection antibody against the prodomain. The pBMP9 ELISA did not react potently with purified cleaved Pro:BMP9, but was sensitive to conditioned media containing *ProBMP9*-S320C. This suggested the pBMP9 ELISA primarily detects unprocessed *ProBMP9*, and I will refer to it as the *ProBMP9* ELISA. The *ProBMP9*-S320C media appeared to contain a mix of unprocessed and semi-processed covalent and non-covalent dimers on immunoblots, so it is unclear which the *ProBMP9* ELISA detects (figure 19). Additionally, the extra cysteine may cause misfolding of this protein which could influence its immunoreactivity.

I validated the *ProBMP9* ELISA for measuring unprocessed *ProBMP9* in plasma and serum. The recovery efficiency of *ProBMP9*-S320C from plasma was ~50% (figure 62). Low recovery could have been due to non-specific interference—absorbances from unspiked plasmas were below the blanks. Therefore, I tested the BioRad buffer, and this improved the sensitivity of the *ProBMP9* ELISA. Immunoreactivities were still below the blanks suggesting this ELISA protocol is not well suited to plasma (figure 63). Since the concentration of endogenous unprocessed *ProBMP9* could not be precisely quantified due to non-specific inhibition, I measured the relative absorbance of samples after immunoprecipitation to establish whether any unprocessed *ProBMP9* was present. Immunoprecipitation with anti-BMP9 did not change the endogenous immunoreactivity of plasma in the *ProBMP9* ELISA. This suggested there is no circulating unprocessed *ProBMP9* (figure 65).

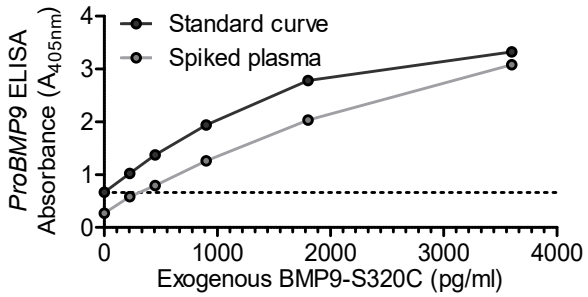

Figure 62. Recovery efficiency of the *ProBMP9* ELISA was low in plasma. *ProBMP9*-S320C was serially diluted in plasma or 1% (w/v) BSA in PBS. Immunoreactivity was measured in the *ProBMP9* ELISA. Mean of duplicates plotted. Dashed line = absorbance of blank. n = 1.

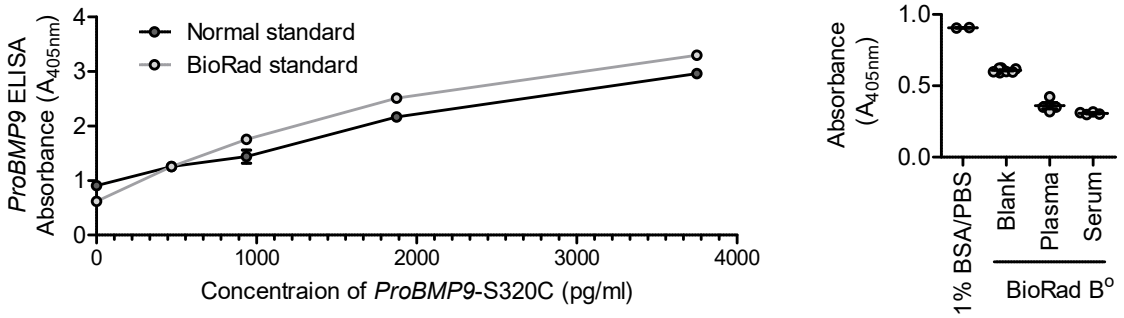

Figure 63. BioRad ELISA buffer improved the sensitivity of the *ProBMP9* ELISA. Left: *ProBMP9*-S320C was serially diluted in plasma or BioRad diluent. Immunoreactivity was measured in the *ProBMP9* ELISA. Mean ± SEM of duplicates n = 1. **Right:** Plasma and serum from four healthy males was measured in the *ProBMP9* ELISA by colourimetry. Mean of duplicates plotted. Mean ± SEM, n = 4.

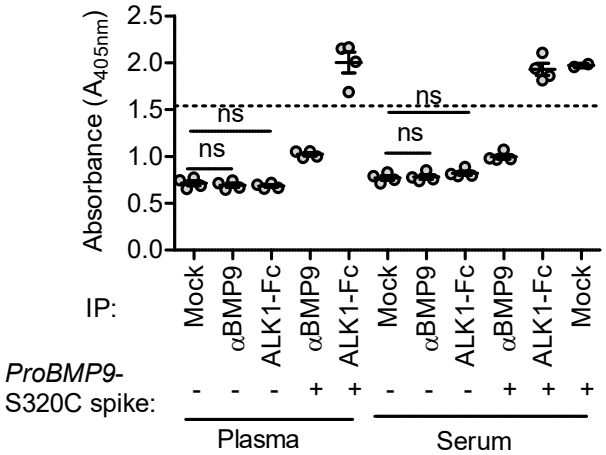

Figure 64. Plasma and serum immunoreactivity in the *ProBMP9* ELISA were unchanged by immunoprecipitation with anti-BMP9 or ALK1-Fc. Plasma and serum from four healthy males were spiked with *ProBMP9*-S320C where indicated, then immunoprecipitated with IgG (mock), anti-BMP9 or hALK1-Fc. Immunoreactivity was assessed in the *ProBMP9* ELISA. Mean of duplicates plotted. Mean ± SEM, n = 4, matched two-tailed Student's t-testing, ns = not significant. Dashed line = absorbance of blank.

As controls, I spiked samples with ~100 pg/ml of *ProBMP9*-S320C before immunoprecipitation which confirmed anti-BMP9 successfully cleared unprocessed *ProBMP9*. In contrast, ALK1-Fc was incapable of clearing any immunoreactivity from samples spiked

with *ProBMP9*-S320C (figure 64). ALK1-Fc was able to immunoprecipitate *ProBMP10*-R313A, which suggests either *ProBMP9* behaves differently, or the *ProBMP9* ELISA detects monomeric or misfolded *ProBMP9*-S320C. Hence, I can conclude the BMP9 growth-factor domain ELISA used in many reports only detects active BMP9, but not whether unprocessed BMP9 circulates.

4.5. Western blotting circulating BMP9 & BMP10

A complementary approach to investigate whether circulating BMP is processed is by Western blotting. Plasma and serum cannot be denatured without clotting, so I attempted to immunoprecipitate BMP9 and BMP10. Nikolic *et al.* (2019) used immunoprecipitation followed by Western blotting with two anti-BMP9 growth-factor domain antibodies to show only processed BMP9 was present in pooled serum. However, they did not demonstrate both antibodies are able to bind epitopes of unprocessed BMP9. In contrast, I have selected antibodies that are able to detect both processed and unprocessed BMP on Western blots.

I tested the capacity of anti-prodomain, anti-growth-factor domain and ALK1-Fc to immunoprecipitate Pro:BMP9 from conditioned media. I probed blots with anti-prodomain, since this antibody had highest sensitivity. Only anti-prodomain could immunoprecipitate Prodomain (figure 65). The recovery efficiency of this protocol was good at physiological concentrations of Pro:BMP9 (figure 66). I included controls spiked with Pro:BMP9-D218N because this should give a shifted band and we were curious if this variant is hyper-glycosylated in human carriers. Unfortunately, when using plasma, the lanes were smeared due to carry-over of non-specific proteins (figure 67). In future, I could use metal, rather than sepharose, protein-G beads and include a larger amount of detergent in wash steps.

For blotting endogenous BMP10, I found ALK1-Fc was more efficient at immunoprecipitating BMP10 from plasma than anti-BMP10 antibodies (see 4.2). ALK1-Fc dimers are a similar weight to *ProBMP10* dimers and ALK1-Fc cross reacted with anti-goat and anti-mouse detection antibodies to a small extent, despite having a human Fc domain (not shown). CleanBlot (Thermo 21230) is a reagent designed not to cross-react with denatured Fc domains, but in my hands, it resulted in poor specific signal and high non-specific signal (not shown). Therefore, I covalently linked ALK1-Fc to protein G beads using BS^3 reagent. Coomassie staining showed BS^3 prevented elution of ALK1-Fc when used at both 5 mM and 1 mM (figure 55). However, BS^3 reagent also inhibited immunoprecipitation.

I carried out Western blots of non-BS^3 ALK1-Fc immunoprecipitates using Pro:BMP10 spiked plasma as a positive control and ALK1-Fc alone as a negative control. Although the controls worked, the pattern of bands potentially representing endogenous pBMP10 was

variable between blots (not shown). In future, I could spike samples with physiological concentrations of Pro:BMP10 and *ProBMP10*-R313A as positive controls.

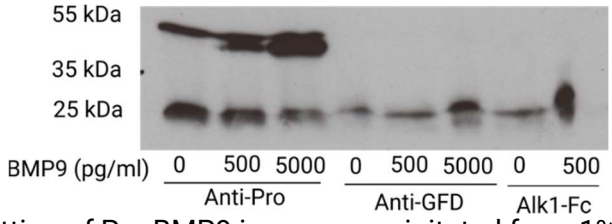

Figure 65. Western blotting of Pro:BMP9 immunoprecipitated from 1% BSA in PBS. *PreProBMP9* was diluted in 1% (w/v) BSA in PBS to a final volume of 2 ml at the indicated final concentrations and immunoprecipitated with anti-prodomain, anti-growth-factor domain or ALK1-Fc. Precipitate was analysed by Western blotting. Probe = anti-BMP9 prodomain. N = 3, one representative blot shown.

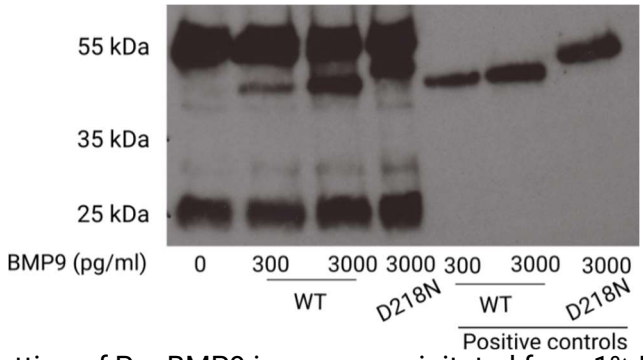

Figure 66. Western blotting of Pro:BMP9 immunoprecipitated from 1% BSA in PBS. *PreProBMP9*-WT and D218N was diluted in 1% (w/v) BSA in PBS to a final volume of 1.5 ml at the indicated final concentrations. These samples were immunoprecipitated with anti-prodomain and precipitates were analysed by Western blotting. Probe = anti-BMP9 prodomain. n =1.

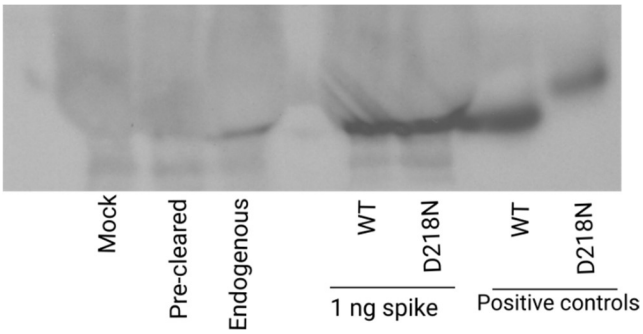

Figure 67. Western blotting of Pro:BMP9 immunoprecipitated from Plasma. Pro:BMP9 was spiked into plasma where indicated and immunoprecipitated with non-specific IgG (mock) or anti-prodomain. Additionally, a sample of plasma immunoprecipitated with anti-prodomain was put back through the protocol with anti-prodomain as a negative control (pre-cleared). Precipitate was analysed by Western blotting. Probe = anti-BMP9 prodomain. n =3, one representative blot shown.

4.6. BMP10 constitutes a minor proportion of circulating activity

Dr. Claudia Mitrofan generated data showing serum, EDTA-, citrate- and heparin-plasma possess BMP9 or BMP10 activity. Similarly to BMP9, I was able to show pBMP10 was detectable in serum by ELISA if EDTA is added (figure 68)(see 4.3). Recovery of pBMP10 from serum+EDTA was ~20% lower than for EDTA-plasma. I undertook to analyse plasma and serum BMP9 and BMP10 activity on endothelial cells. I reproduced published results showing a large majority of plasma BMP activity can be neutralised by anti-BMP9 (figure 37; 43). These data were produced by treating quiescent human aortic endothelial cells with 3% (v/v) of plasma, plasma which had been immunoprecipitated with anti-BMP9, or recombinant BMP9, for 1 hour followed by measurement of transcriptional responses. I generated similar results treating four pulmonary artery endothelial cell lines (not shown). Similarly, *Gdf2* knockout mice had no circulating BMP activity (figure 90). The reduction in activity caused by anti-BMP9 immunoprecipitation compared to the activity of recombinant BMP9 suggested plasma had approximately 200 pg/ml of activity, which is consistent with ELISA measurements.

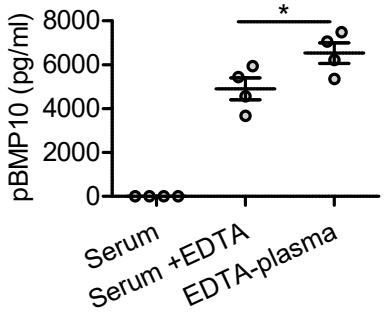

Figure 68. The pBMP10 ELISA recovers pBMP10 from plasma or serum supplemented with EDTA. EDTA-plasma, serum and serum spiked with EDTA from four healthy males was measured in the pBMP10 ELISA. Mean of duplicates plotted. Mean ± SEM, n = 4, matched two-tailed Student's t-test, *p < 0.05.

Serum and EDTA-plasma possessed equal BMP9 activity on HMEC1 cells when *ID1* and *ID2* induction was measured after one hour (figure 69). Serum perhaps had slightly higher activity than plasma when luciferase induction in *BRE*-HMECs treated for six hours was measured (figure 70). It is not clear why the transduced cells respond differently to serum and plasma. It could reflect the longer time they have to respond to serum factors in a 6-hour luciferase protocol versus 1-hour qPCR protocol.

In further contrast to qPCR activity measurements, luciferase induction was only reduced by ~50% after sera and plasmas were cleared of BMP9 by immunoprecipitation (figure 40; 71). Therefore, I cleared samples of BMP10 using anti-BMP10 antibodies. Serum gave more robust and reliable results than plasma because cells could be treated with higher

concentrations of serum without clotting. I found ~50% of circulating BMP activity was neutralised by anti-BMP10 treatment. ALK1-Fc or a combination of both anti-BMP9 and anti-BMP10 was able to neutralise ~100 and 90% of circulating BMP activity respectively.

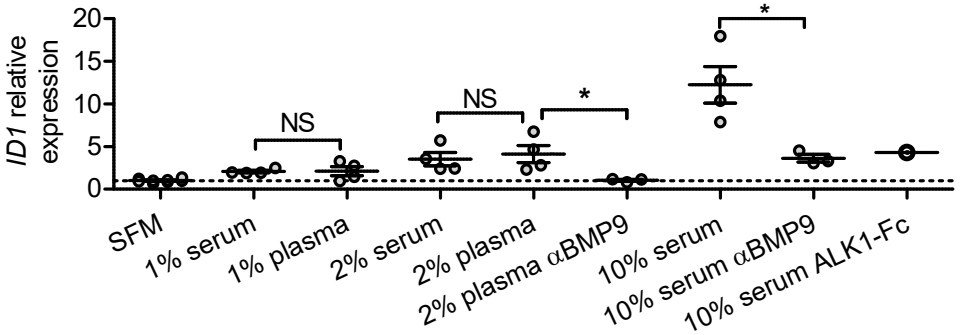

Figure 69. BMP9 activity of plasma and serum measured by qPCR. Quiescent HMEC1 cells were treated with the indicated amounts of plasma or serum from four healthy individuals. Levels of *ID1* mRNA were assessed by qPCR relative to the housekeeping gene *B2M*. Plasmas/sera were immunoprecipitated with anti-BMP9 or ALK1-Fc where indicated. Mean ± SEM, n = 4, matched two-tailed Student's t-testing, *p < 0.05, NS = not significant. Dashed line = expression level of untreated quiescent cells (SFM).

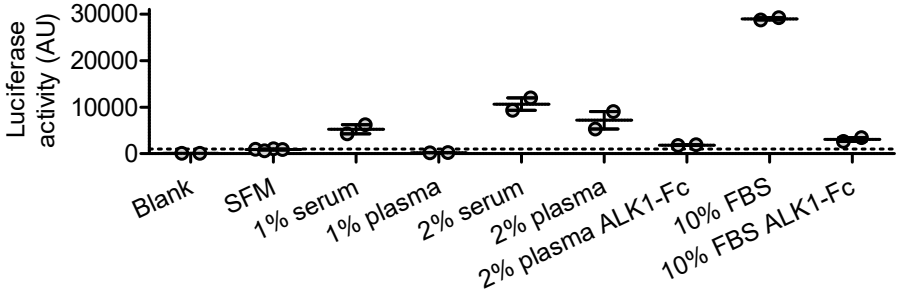

Figure 70. BMP9 activity of plasma and serum. Quiescent *BRE*-HMEC1 cells were treated with the indicated amounts of plasma or serum from two individuals. Plasmas/sera were immunoprecipitated with ALK1-Fc where indicated. FBS = foetal bovine serum. Mean ± SEM, n = 2, mean of duplicates plotted. Dashed line = luciferase activity of untreated cells (SFM).

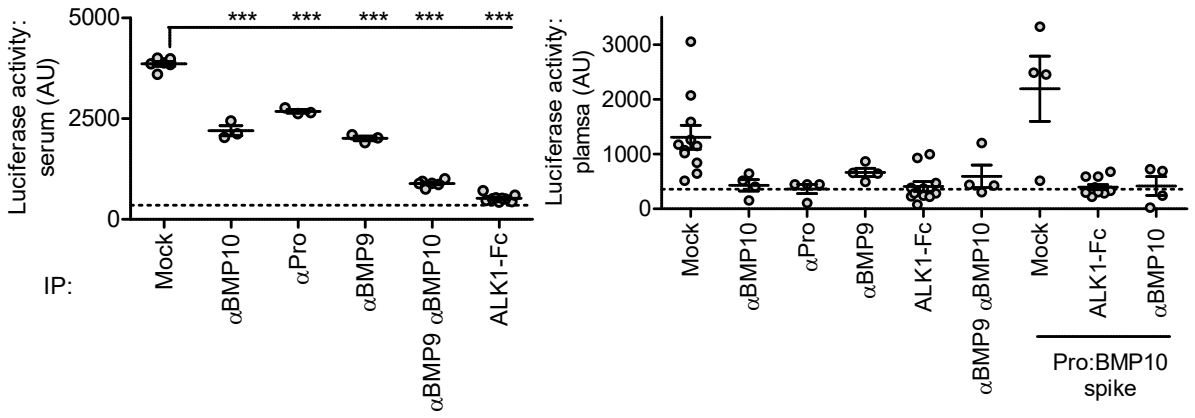

Figure 71. Circulating BMP9 and BMP10 activity measured by luciferase induction. Plasma and serum from four healthy males were immunoprecipitated with non-specific IgG (mock), anti-BMP9, anti-BMP10, anti-BMP10 prodomain (Pro), or ALK1-Fc, and/or 5 ng/ml of Pro:BMP10 where indicated. Quiescent *BRE*-HMEC1 cells were treated with 10% (v/v) of serum (**left**) or 3% (v/v) or plasma (**right**). One-way matched ANOVA/Dunnett's test of

immunoprecipitated samples compared to mock treatment, mean ± SEM, n = 4, mean of triplicates plotted. For plasma, extra samples prepared from the same individuals were available. Dashed line = luciferase activity of untreated quiescent cells.

These luciferase induction data are still consistent with most endogenous BMP9 being active, and most endogenous BMP10 being inactive, since there is vastly more circulating pBMP10 than BMP9. As expected, Pro:BMP10 induced a strong response in *BRE*-HMECs, whilst *ProBMP10*-R313A did not possess high-affinity activity (figure 72). This could indicate most circulating BMP10 is unprocessed.

To quantify the amount of circulating BMP activity, I spiked Pro:BMP10 back into serum which had been cleared with ALK1-Fc. Surprisingly, ~16 ng/ml of Pro:BMP10 was needed to reconstitute the activity of cleared serum (figure 73). This is much greater than the combined circulating amount of BMP9 and pBMP10 measured by ELISA. Serum spiked with Pro:BMP10 had depressed activity compared to serum-free media spiked with Pro:BMP10, which suggested serum contains factors which inhibit BMP signalling. These results could be explained if ALK1-Fc cleared serum of circulating BMPs, other than BMP9 and BMP10, which usually add to their effects, or if some ALK1-Fc remained within serum after beads were removed, neutralising exogenous Pro:BMP10. Samples could be incubated with excess protein G beads to remove unconjugated ALK1-Fc.

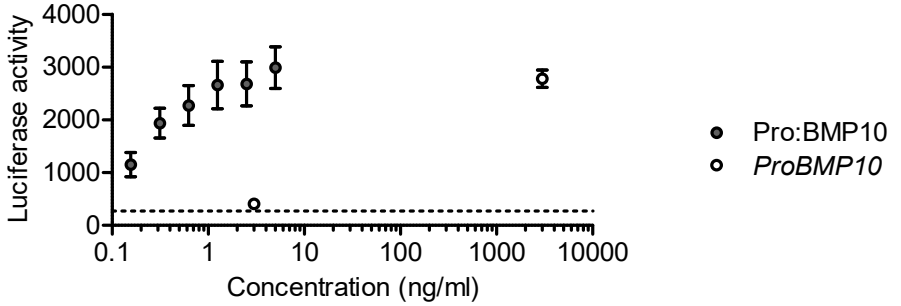

Figure 72. Activity of Pro:BMP10 and *ProBMP10*. *BRE*-HMECs treated with *ProBMP10*-R313A or Pro:BMP10. Mean ± SEM, mean of duplicates plotted. n = 3 with one representative experiment shown. Dashed line = luciferase activity of untreated quiescent cells (SFM).

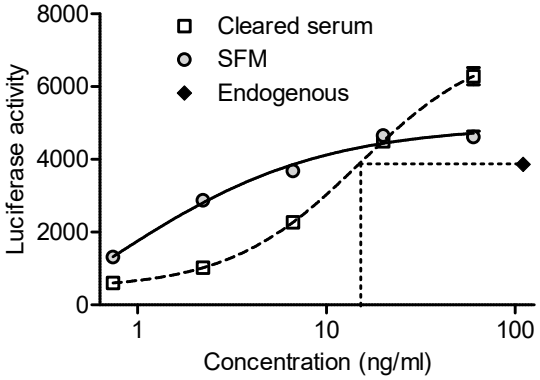

Figure 73. Reconstituting signalling activity of serum cleared with ALK1-Fc. Serial dilutions of Pro:BMP10 were prepared in serum-free media or serum precleared with ALK1-Fc. 10% (v/v)

of these samples, or uncleared serum (endogenous) were incubated with *BRE*-HMECs. Curves = four parameter logistic regressions. Mean ± SEM, n = 3.

4.7. Furin treatment of serum

I found endogenous BMP10 may be predominantly unprocessed. *ProBMP10* contains a furin recognition sequence and serum contains adequate free calcium to activate furin. Hence, I treated neat serum with furin and quenched the reaction with 5 mM EDTA. Furin treatment did not increase immunoreactivity of serum in the BMP10 growth-factor domain ELISA, which suggests furin did not cleave endogenous *ProBMP10* (figure 74). Furin treatment did not increase the activity of serum on cells, reinforcing this result (figure 75). Furin treatment did not lead to an increase in processed Pro:BMP9 as measured by the BMP9 growth-factor domain ELISA (figure 76). Instead, there was a modest reduction in BMP9 levels, possibly because overnight incubation without EDTA lead to degradation by endogenous proteases.

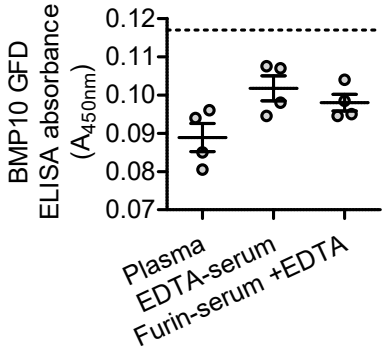

Figure 74. Serum Pro:BMP10 levels are not increased by furin treatment. Serum from four healthy males was incubated with furin or EDTA, then the reaction was quenched with EDTA. Immunoreactivity was measured in the BMP10 growth-factor domain ELISA. Mean of duplicates plotted. Mean ± SEM, n = 4, dashed line = absorbance of blank.

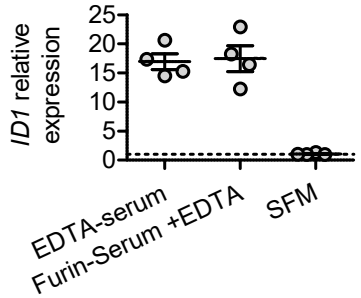

Figure 75. Serum activity is not increased by Furin treatment. Cells were incubated with 5% (v/v) of serum and the level of *ID1*mRNA was measured by qPCR relative to the housekeeper *B2M*. Mean ± SEM, n = 4, dashed line = expression in untreated quiescent cells (SFM).

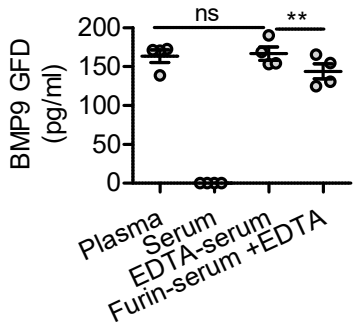

Figure 76. Serum Pro:BMP9 levels are not increased by serum treatment. BMP9 levels were measured in the growth-factor domain ELISA. Mean of duplicates plotted. Mean ± SEM, n = 4, matched two-tailed Student's t-test, **p < 0.01, NS = not significant.

I needed a positive control to demonstrate furin was active under these conditions. Fluorometric readouts of furin activity comprise the furin recognition peptide quenching the fluorophore AMC (Pyr-Arg-Thr-Lys-Arg-AMC). I added it to serum in identical conditions to those used above. Furin treatment significantly enhanced fluorescence, showing furin was active (figure 77). However, there was significant cleavage in serum without furin or with EDTA. This indicated serum contains calcium-independent proteases which were able to cleave this peptide, despite the protective pyroglutamyl residue on this molecule.

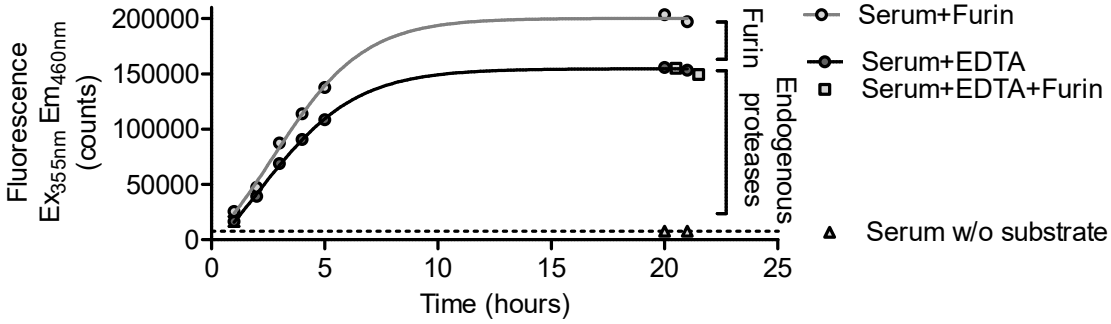

Figure 77. Furin is active in serum. Serum was incubated with furin, EDTA and/or fluorometric furin substrate. At the times indicated, fluorescence was measured. Mean ± SEM of duplicates. The experiment was performed on three separate occasions and one representative is shown. Dashed line = non-specific fluorescence of serum.

To investigate whether serum *ProBMP10* is likely to be a furin substrate, I analysed the twenty amino-acid furin binding region of *ProBMP9* and *ProBMP10* using the structural and empirical analysis of Tian (2009). As expected, both proteins show characteristics of good furin substrates: *ProBMP10* has an RIRR^{316}↓ motif aligned with RRKR^{319}↓ in *ProBMP9*, both of which correspond to furin's most favoured recognition sequence, RX[K/R]R↓. However, the furin binding region of *ProBMP10* contains several large, inflexible residues in positions where small residues are expected to aid furin binding (figure 78). This could predict that furin processing of *ProBMP10* is less efficient than *ProBMP9* processing.

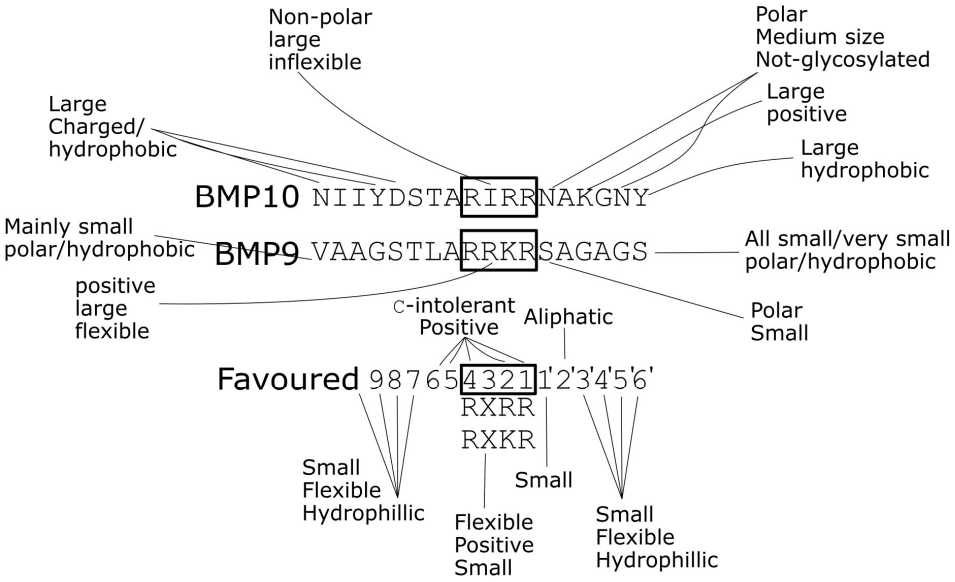

Figure 78. Furin recognition sequences of *ProBMP9* & *ProBMP10*. BMP9: The amino acid sequence of *ProBMP9* from residue 308-325 annotated according to the properties of those amino acids. BMP10: The amino acid sequence of *ProBMP10* from residue 305-322 annotated according to the properties of those amino acids. Favoured: The characteristics of the most efficiently cleaved Furin substrates according to Tian (2009). Cleavage occurs between residue 1 and 1'. The box is the most important furin recognition sequence, whilst the surrounding twenty amino-acid region tends to have particular motifs.

To assess whether *ProBMP10* is processed during secretion *ex vivo,* I took mouse right-atria, left-atria, livers and lungs, and cultured them in serum-free media alone, or media supplemented with foetal bovine serum, BMP9, or lipopolysaccharide. I was able to recover low levels of secreted processed BMP10 in conditioned media from right-atria, but not other organs, using the BMP10 growth-factor domain ELISA (figure 79). Similarly, conditioned media from right-atria, but not other organs, had activity on cells (figure 80). Unfortunately, the pBMP10 ELISA did not cross-react with mouse samples (not shown), and western blots of the atrial conditioned media contained several non-specific bands (not shown). Therefore, I was unable to show what proportion of secreted BMP10 is processed versus unprocessed. These results suggest the correlation in plasma BMP9 and pBMP10 levels is not via BMP9 stimulating atrial BMP10 secretion.

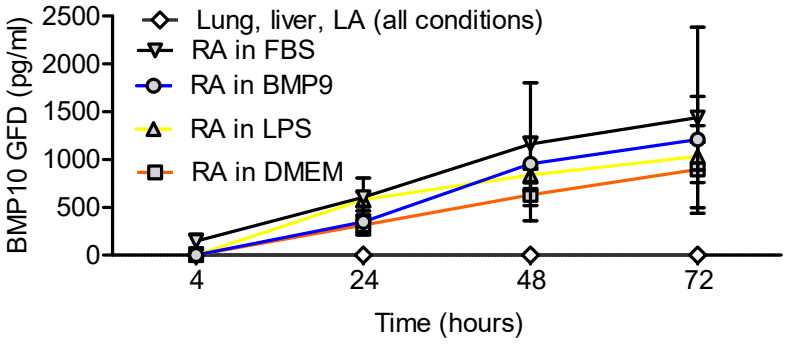

Figure 79 (overleaf). Processed BMP10 is secreted from mouse right atria *ex vivo*. Mouse organs were transferred into DMEM media supplemented with 5 ng/ml BMP9, 1 µg/ml LPS or 10% FBS where indicated. Levels of BMP10 in conditioned media were measured in the BMP10 growth-factor domain ELISA. No BMP10 was detectable in conditioned media from organs other than the right-atria. Mean ± SEM, n=3.

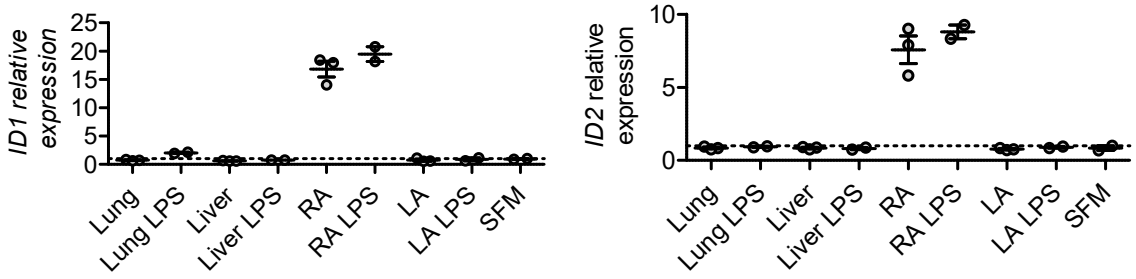

Figure 80. Processed BMP10 is secreted from mouse right atria *ex vivo*. Quiescent HMECs were incubated with 10% (v/v) conditioned media and the level of *ID1*& *ID2* mRNA was measured by qPCR relative to the housekeeper *B2M*. Mean ± SEM, n = 3, dashed line = expression in untreated quiescent cells (SFM).

4.8. Circulating BMP9 & BMP10 may be in complex

We found circulating levels of BMP9 and *ProBMP10* are tightly correlated (figure 42), and Tillet *et al.* (2019) report cross-immunoreactivity of endogenous, but not pure, BMP9 and BMP10 in ELISAs and affinity columns. This suggests these ligands may be in complex, perhaps with other proteins.

Immunoprecipitation with anti-BMP9 antibodies cleared about one-third of the *ProBMP10* from plasma as measured by ELISA (figure 81). Conversely, immunoprecipitation with anti-BMP10 antibodies cleared about one-quarter of the Pro:BMP9 from plasma. This suggested a proportion of the two ligands are physically coupled in plasma. Any physical association between BMP9 and BMP10 appears not to be 1:1 based on the very different circulating concentrations of BMP9 and BMP10, and the fact vastly more BMP10 is cleared by immunoprecipitation than BMP9.

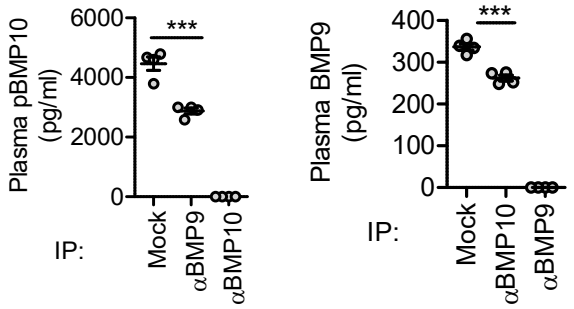

Figure 81. Immunoprecipitating BMP9 from plasma pulls-down some pBMP10 and *vice versa*. I immunoprecipitated plasma from four healthy males with anti-BMP9, anti-BMP10 or non-specific IgG (mock). Immunoreactivity was measured in the pBMP10 (**left**) and BMP9 GFD (**right**) ELISAs. Mean of duplicates plotted. Mean ± SEM, n = 4, matched two-tailed Student's t-test, *** p<0.001.

Neither BMP9 nor BMP10 could be detected by ELISA in serum without the presence of the calcium chelator EDTA. This could be because chelation reduces non-specific inhibition, or there may be a factor that binds and masks BMP9 and BMP10 in a divalent cation dependent way. To investigate the effect, I spiked Pro:BMP9 into human serum with and without 5 mM EDTA and measured its immunoreactivity by ELISA (figure 82). At high concentrations of exogenous BMP9, recovery efficiency was similar with and without EDTA—85-100%. With EDTA, recovery efficiency increased above 100% at low concentrations of exogenous BMP9, as expected when endogenous BMP9 is also being recovered. When the concentration of endogenous BMP9 was subtracted from the concentration of recovered BMP9, recovery of exogenous BMP9 was 85-100% efficient to a limit of ~20 pg/ml. Without EDTA, recovery abruptly dropped to 0% at ~100 pg/ml of exogenous BMP9. Since detection of both endogenous and exogenous BMP9 is inhibited without EDTA, either there is a non-specific cause, or a binding protein is present in excess.

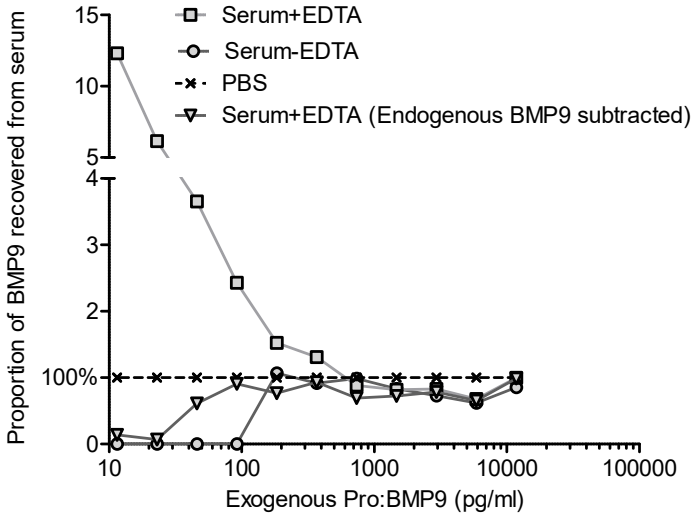

Figure 82. EDTA is needed for the detection of endogenous and exogenous BMP9 in serum. I prepared serial dilutions of Pro:BMP9 in serum, serum supplemented with EDTA, and PBS. Immunoreactivity was measured in the BMP9 growth-factor domain ELISA. BMP9 concentration in each sample was calculated based on a curve fitted with four parameter logistic regression to the PBS samples. I subtracted the concentration of endogenous BMP9 from the total BMP9 concentration recovered from spiked serum to leave the amount of exogenous BMP9 recovered. I then normalised the BMP9 concentration recovered from serum by the BMP9 concentration recovered from PBS to calculate the proportion of exogenous BMP9 recovered. In the presence of EDTA, 20-40 pg/ml of exogenous BMP9 was the minimum amount required for efficient recovery. In the absence of EDTA, 200 pg/ml of exogenous BMP9 was the minimum amount required for efficient recovery. Mean ± SEM of technical duplicates. n = 3, one representative result shown. Similar results were obtained with recombinant BMP9.

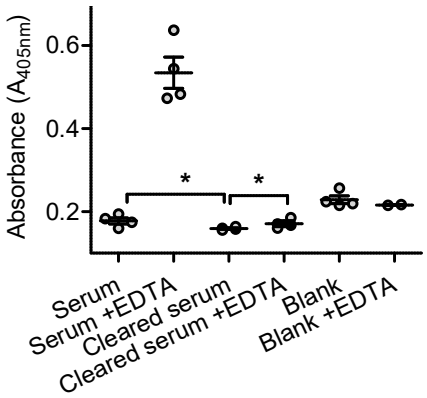

Figure 83. EDTA relieves specific inhibition of BMP9 immunoreactivity in serum. Serum from four healthy males was cleared with anti-BMP9 where indicated. EDTA was added where indicated. Immunoreactivity was measured in the BMP9 GFD ELISA. Mean of duplicates plotted. Mean ± SEM, n = 4, matched two-tailed Student's t-testing, * $p < 0.05$. Blank = diluent alone without serum.

EDTA had no effect on immunoreactivity in blank wells of the ELISA, so EDTA does not have a serum-independent effect (figure 83). Presence versus absence of EDTA barely altered the immunoreactivity of serum cleared of BMP9 by immunoprecipitation—EDTA did not relieve much non-specific inhibition of immunoreactivity. In the absence of EDTA, BMP9-immunoprecipitation barely altered the immunoreactivity of serum—BMP9 had minimal immunoreactivity without EDTA. In the presence of EDTA, BMP9 immunoprecipitation resulted in a profound reduction in immunoreactivity—BMP9 had high immunoreactivity with EDTA. These data indicate the biggest effect of EDTA was to relieve specific inhibition, perhaps a binding protein.

To test whether BMP9 and BMP10 are bound to macromolecules within serum, I undertook column-based size-exclusion chromatography. Firstly, I assessed columns of different lengths, different fraction collection volumes, and different matrices with samples comprising molecular weight markers, Pro:BMP10 and recombinant BMP9. It was particularly important that there were several fractions separating blue-dextran, a marker of void volume (~2 MDa), and Pro:BMP10, since any Pro:BMP complexes would resolve here. Sephacryl S-200 in a 70 cm column gave sufficient resolution.

Firstly, I assayed a ladder comprising coloured size markers, recombinant BMP9 growth-factor domain and Pro:BMP10. Next, I assayed EDTA-plasma supplemented with the same size-markers, but without exogenous BMP9 or Pro:BMP10 (figure 84). For both, the eluent was PBS supplemented with EDTA to prevent plasma clotting. I measured the immunoreactivity of samples in the BMP9 and pBMP10 ELISAs. Most plasma BMP9 and BMP10 eluted in the same volume as Pro:BMP10, although there was some immunoreactivity

in later fractions, perhaps representing BMP9 and BMP10 which bound the matrix or non-specific immunoreactivity. Secondly, there was a peak of immunoreactivity in early fractions, which could have been complexes, aggregates, BMP bound to blue-dextran, or non-specific immunoreactivity.

Next, I assayed serum using PBS containing calcium and magnesium as the eluent, to stabilise any EDTA-sensitive complexes. To measure immunoreactivity in the ELISAs, I supplemented EDTA back into fractions so eluted BMP9 and pBMP10 could be measured. Serum immunoreactivity was confined to fractions eluting with blue-dextran, or late fractions, with no peak eluting in the same volume as Pro:BMP10. Since there was some immunoreactivity in the ladder in early fractions, I re-ran the ladder and serum excluding blue-dextran as a marker. This prevented the elution of exogenous BMP9 or Pro:BMP10 in early fractions of the ladder, showing this was an artefact of BMP binding to blue-dextran. This did not reduce the elution of endogenous immunoreactivity in early fractions of serum, showing this is due to complexes, aggregates or non-specific immunoreactivity (figure 85). I also eluted serum supplemented with EDTA in PBS supplemented with EDTA. This recapitulated the pattern seen with EDTA-plasma, confirming the hypothesis that BMP9 circulates in an EDTA sensitive complex.

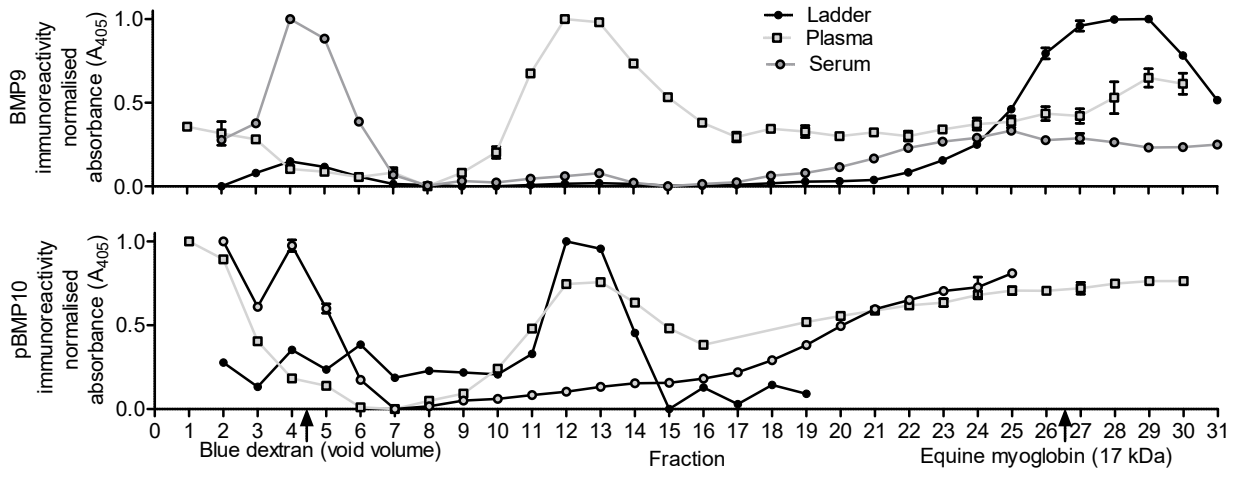

Figure 84. Size exclusion chromatography of BMP9, Pro:BMP10, plasma & serum. Ladder comprised BMP9 GFD and Pro:BMP10. Plasma & ladder were eluted in PBS supplemented with EDTA. Serum was eluted in PBS with calcium & magnesium. The centre of the elution peak for dextran blue and equine myoglobin is indicated. Immunoreactivity was measured in the BMP9 ELISA (top) and pBMP10 ELISA (bottom). Technical duplicates, mean ± SEM, n = 1. Curves have been shifted by up to 1 position to align the ladder between samples. Absorbance is normalised for each sample so the highest absorbance = 1, and lowest = 0.

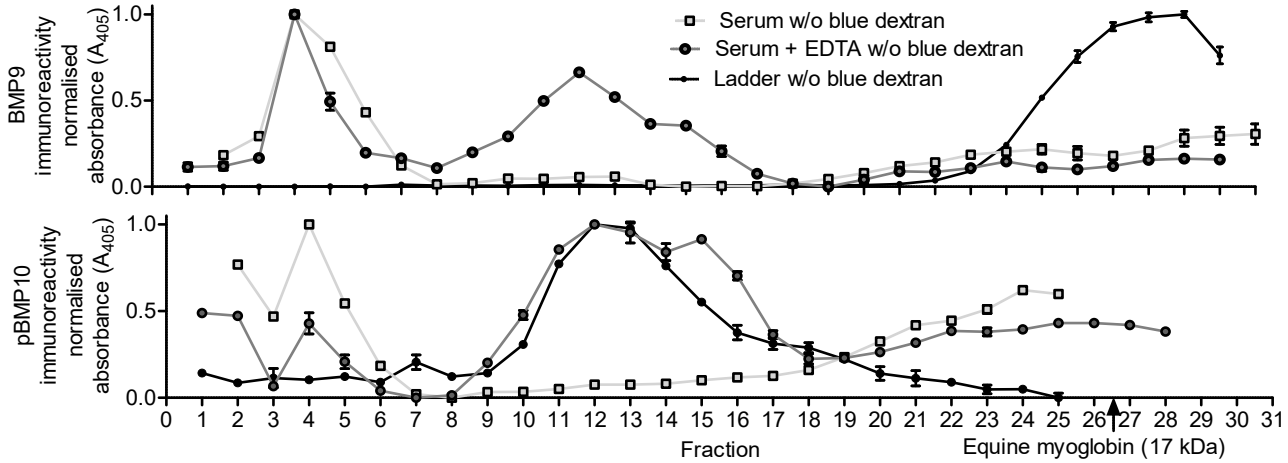

Figure 85. Size exclusion chromatography of BMP9, Pro:BMP10 & serum. Ladder comprised BMP9 GFD and Pro:BMP10. Serum + EDTA was eluted in PBS supplemented with EDTA. Serum and ladder were eluted in PBS with calcium & magnesium. Immunoreactivity was measured in the BMP9 ELISA (**top**) and pBMP10 ELISA (**bottom**). Technical duplicates, mean ± SEM, n = 1. Curves have been shifted by up to 1 position to align the ladder between samples. Absorbance is normalised for each sample so the highest absorbance = 1, and lowest = 0.

To show these peaks are due to specific immunoreactivity, I measured the activity of different fractions on *BRE*-HMECs. Unfortunately, there was insufficient Pro:BMP10 activity in the ladder to stimulate HMECs, and serum contained potentially non-specific activity in a large number of fractions (figure 86). These experiments will be repeated with serum from three individuals to confirm these findings.

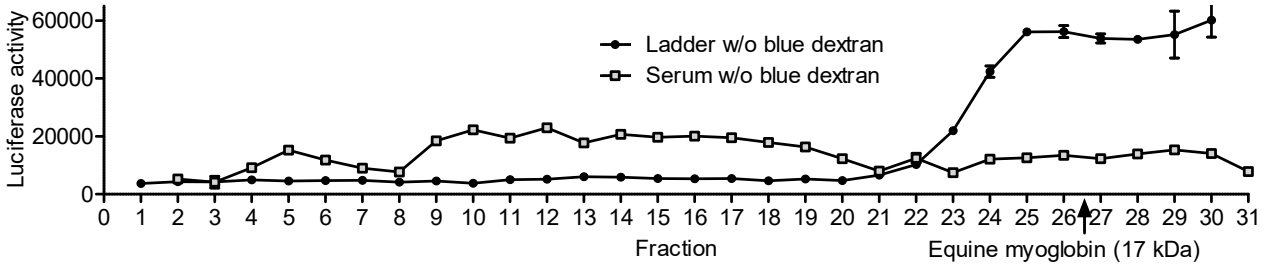

Figure 86. Size exclusion chromatography of BMP9, Pro:BMP10 & serum. Fractions from figure 85. 10% (v/v) of ladder fractions or 25% (v/v) serum fractions were added to quiescent *BRE*-HMECs. Mean of duplicates plotted ± SEM, n = 1. Curves have been shifted by up to 1 position to align the ladder between samples.

4.9. Discussion

I demonstrated the BMP9 growth-factor domain ELISA only detected processed BMP9, supporting the assumption of Nikolic *et al.* (2019). This contrasts Bidart *et al.* (2012) who speculated this antibody pair detects both processed and unprocessed BMP9. Therefore, we conclude Pro:BMP9 circulates at active concentrations in healthy adults, and *GDF2* mutation carriers have reduced circulating levels of active BMP9. Conversely, an ELISA which only detects *ProBMP9*-S320C did not detect any endogenous circulating *ProBMP9.* The *ProBMP9*

ELISA was inefficient in plasma but depleting endogenous BMP9 lead to very little change in immunoreactivity. Therefore, I hypothesised there is very little circulating *ProBMP9.* To test this, recovery efficiency from plasma of a non-processable but otherwise properly folded and secreted variant of *ProBMP9* could be tested.

I demonstrated the BMP10 growth-factor domain ELISA only detects processed BMP10. This ELISA detected low levels of endogenous immunoreactivity, despite high recovery efficiency of exogenous Pro:BMP10 from plasma. Depleting endogenous BMP10 leads to little change in immunoreactivity. Therefore, I hypothesised only low levels of Pro:BMP10 circulate in healthy people. Conversely, the pBMP10 ELISA detected both Pro:BMP10 and *ProBMP10,* and recovered high levels of endogenous immunoreactivity. Therefore, I hypothesised *ProBMP10* is the predominant circulating species.

Unfortunately, I have not been able to Western blot endogenous BMP9 and BMP10 to visualise the circulating species of each. Similarly, I was unable to cleave endogenous *ProBMP10* by furin treating serum. Positive controls comprised of wildtype *ProBMP9* and *ProBMP10*, perhaps produced by overexpression in HEK-EBNA cells treated with prohormone convertase inhibitors, would be ideal. Additionally, plasma/serum size fractions may be more amenable to analysis since they are likely to contain less non-specific immunoreactivity.

I found anti-BMP9 could clear 80-100% of the activity of a 1-hour treatment of 10% serum or 1% plasma on microvascular, aortic and pulmonary artery endothelial cells as measured by *ID* gene expression. But I found anti-BMP9 could only clear ~50% of the activity of a 6-hour treatment of 10% serum or 1% plasma on *BRE*-HMECs. The receptors expressed by HMEC1 and pulmonary artery endothelial cell lines were characterised in Upton *et al.* (2008). They express ALK1,2,3, BMPR2,4 and 6, enabling them to respond to BMP2,4,6,7 and 9. Nonetheless, in developing the *BRE*-HMEC line, Dr. Benjamin Dunmore tested their responses and found minimal responses to 1 ng/ml of BMP2 and 4, a small response to 10 ng/ml of BMP6, but a maximal response to BMP9 at just 0.3 ng/ml. Hence, these cells are unlikely to be responding to other BMPs in plasma or serum. Confirming this, immunoprecipitation with anti-BMP10 and anti-BMP9 together cleared almost all activity.

Complicating assessment of the relative contribution of BMP9 and BMP10 to serum activity, some BMP10 is removed by immunoprecipitating BMP9 and *vice versa*. Unlike immunoprecipitations, BMP9 neutralisations should only alter BMP9 activity. Herrerra and Inman (2009) found anti-BMP9 can neutralise ~50% of the activity of a 16-hour treatment of 10% serum on C2C12 cells transfected with *BRE:LUCIFERASE.* Similarly, Chen *et al.* (2013)

find anti-BMP9 neutralises ~60% of the activity of serum on human umbilical cord endothelial cells as measured by *SMAD6* expression (details not explained).

In contrast, Jiang *et al.* (2016) report anti-BMP9 can clear 80% of the activity of a 1-hour treatment of 1% plasma on pulmonary artery endothelial cells as measured by *ID* gene expression. David *et al.* (2008) and Bidart *et al.* (2012) report anti-BMP9 can neutralise ~100% of the activity of a 15-hour treatment of 1% plasma and serum on NIH-3T3 cells transfected with *ALK1* and *BRE:LUCIFERASE*. Nikolic *et al.* (2019) find anti-BMP9 neutralises 80-100% of the activity of a 30-minute treatment of 8% serum on pulmonary microvascular endothelial cells as measured by nuclear phospho-SMAD staining. Similarly, David *et al.* (2008) report anti-BMP9 can neutralise ~100% of the activity of a 1-hour treatment of 2% serum on microvascular endothelial cells as measured by phospho-SMAD blotting.

There are no obvious patterns in cell-type, treatment length, assay readout or substrate concentration to explain the different degree of residual activity after BMP9 neutralisation. This has implications for whether circulating BMP10 is active—Chen *et al.* claim BMP10 accounts for ~40% of activity and Jiang *et al.* 20%, whilst others conclude all activity is accounted for by BMP9. My data suggests BMP10 accounts for ~50% of circulating activity as measured by *BRE*-luciferase experiments, but <20% as measured by *ID* transcription. I showed *Gdf2* knockout mice and homozygous nonsense children have little-to-no residual circulating BMP9/10 activity, although the latter also have low circulating pBMP10 levels. Ricard *et al.* report *Gdf2* knockout mice have normal BMP10 levels, but no plasma activity on NIH-3T3 cells transfected with *ALK1* and *BRE:LUCIFERASE*. Whatever the nuance, all reports agree circulating BMP9 has more activity than circulating BMP10, suggesting the latter is predominately unprocessed. My ELISA data supports this interpretation.

HEK-EBNA cells overexpressing *ProBMP9* readily process it with endogenous proteases. However, HEK-EBNA cells overexpressing *ProBMP10* must be transfected with additional furin, and processing remains less efficient than for *ProBMP9* (Jiang et al. 2016). Less efficient processing of *ProBMP10* compared to *ProBMP9* was also reported by David *et al.* (2007). These observations lend weight to the idea that circulating *ProBMP10* is unprocessed and resistant to furin cleavage despite the fact that *ProBMP10* can be processed by furin and other prohormone convertases *in vitro* (Susan-Resiga et al. 2011).

Active BMP10 was secreted from mouse right-atria, validating Jiang *et al.* (2016), although it is not clear if any secreted BMP10 is unprocessed. In future, I could develop tissue extract ELISAs and Western blots to look at frozen human atria, which are more tractable with the antibodies we have. Circulating *ProBMP10* may be processed in specific tissues,

whilst circulating Pro:BMP9 is already fully active. This could partly explain the different disease associations, activities, and knockout animal phenotypes of *GDF2* and *BMP10*.

Immunoprecipitations reveal that a minority of plasma BMP9 and BMP10 are in complex with one another. This would seem unlikely to be an artefact of cross-reactivity since similar amounts of antibody were used in ELISAs and Dr. Paul Upton demonstrated Pro:BMP9 and Pro:BMP10 do not cross-react in ELISAs. Nonetheless, samples of Pro:BMP9 or Pro:BMP10 in PBS could be assayed through the same immunoprecipitation protocol to check for non-specific effects. Some of the complexes may represent a heterodimer, as proposed by Tillet *et al.* (2019). However, we have shown the majority of each are not in a dimeric complex. Moreover, EDTA can relieve something which masks the immunoreactivity of endogenous and exogenous BMP9 in serum. Size exclusion chromatography suggests this is likely to be a large macromolecule, since serum BMP9 and BMP10 eluted in the void volume, and the matrix has an upper resolution limit of ~1.5 million Daltons. This changes the interpretation of Tillet *et al.*'s results. The potential existence of BMP9 and BMP10 binding proteins is important because they could alter their stability, activity and bioavailability.

5. Pharmacokinetics of BMP9

5.1. Introduction

The Morrell group is interested in using BMP9 therapeutically and in animal models, so understanding its stability and utilisation in the circulatory system is important. BMP9 is secreted from the liver, and perhaps the lung, and mediates endothelial SMAD signalling (David et al. 2007; Bidart et al. 2012). BMP10 is secreted from the right-atrium, and perhaps the liver, and mediates SMAD signalling proximal to the heart (Tillet et al. 2018; Laux et al. 2013). Endogenous BMP9 and BMP10 need only travel a short distance before reaching the pulmonary vasculature (figure 87). Pulmonary artery endothelial cells highly express high-affinity BMP9 and BMP10 receptors. Therefore, it has been hypothesised there is gradient of BMP9 and BMP10 activity, with the pulmonary vasculature stimulated by the greatest levels (Li et al. 2016). This could partly explain why the pulmonary vasculature is particularly sensitive to loss of BMP9 in PAH.

No one knows whether BMP9 and BMP10 distribute across compartments or are confined to the blood. Their prodomains may mediate binding to extracellular molecules, and they may be sequestered to specific vascular beds. If circulating BMP10 is predominately unprocessed (see 4.2), then specific tissues may process *ProBMP10*. There may be local sources of each ligand,

especially in the lung, which expresses *GDF2* and to a lesser extent, *BMP10.* Circulating binding proteins, suggested to exist in 4.8, may stabilise or modulate the availability of BMP9 and BMP10. In humans, neither the pharmacokinetics of BMP9 nor BMP10 has been explored.

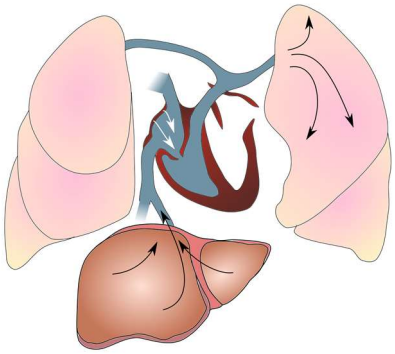

Figure 87. The pulmonary vasculature is the first organ bed endogenous BMP9 and BMP10 travel through. Endogenous BMP9 is primarily expressed in the liver. Hepatic capillary beds drain into the hepatic veins which join the inferior vena cava close to where it empties into the right atrium. BMP10 is primarily expressed in the right atrium and vessels here drain into the right-atrial lumen. From the right atria, blood flows into the right ventricle, and is expelled into the pulmonary arteries.

We wanted to investigate the half-life of circulating BMP9 and where it binds. Therefore, Dr. Paul Upton, Stephen Moore, Dr. Alexi Crosby and I gave wildtype and *Gdf2* knockout mice purified human Pro:BMP9 intravenously and I measured BMP9 levels in different compartments over time. To explore the distribution of endogenous BMP9 in humans, Drs. Emilia Swietlik and Kasia Zalewska collected blood from different blood vessels of the same patients and I measured BMP9 levels in the plasma.

5.2 Administration of Pro:BMP9 to *Gdf2* knockout mice

First, we administered exogenous Pro:BMP9 into *Gdf2* knockout mice by intravenous injection (figure 88). This ensures that a known amount of BMP9 entered the circulation at a known time and that all detectable protein and activity is due to the exogenous dose. We used purified human Pro:BMP9 since the Morrell group routinely produces this and it has almost identical signalling activity and immunoreactivity to mouse BMP9.

We diluted the Pro:BMP9 in PBS supplemented with mouse-serum albumin. This vehicle minimises osmotic shock and reduces adsorption of Pro:BMP9 to syringes *etc.* Concentrated aliquots were stored at -80 °C in siliconized tubes. To reduce variability, we normalised the injection volume by body weight of each mouse. To increase sensitivity, we used a supraphysiological dose of 2.5 µg of Pro:BMP9 per kg of bodyweight, which is equivalent to ~13 ng of recombinant BMP9 per ml of blood.

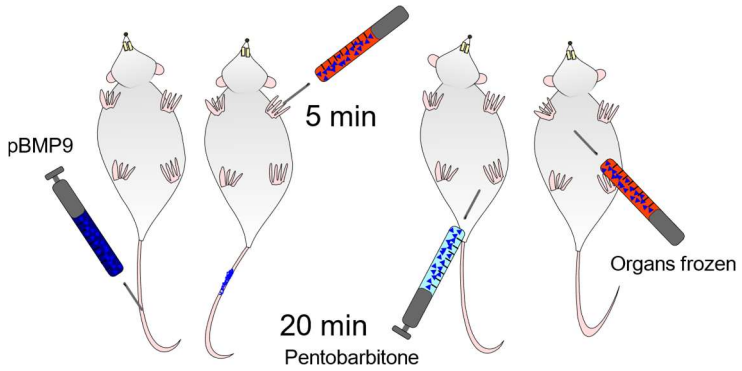

Figure 88. Experimental plan of Pro:BMP9 administration to *Gdf2* knockout mice. Purified human Pro:BMP9 was diluted to 0.5 ng/µl in 1% (w/v) mouse serum albumin in PBS. Five µl/g (~10% blood volume, 2.5 µg/kg) of Pro:BMP9 solution or vehicle was administered by tail vein injection to three mice each. After 5 minutes, blood was withdrawn from the saphenous vein, and after 20 minutes, a lethal dose of pentobarbitone was administered. Mice were exsanguinated by cardiac puncture. Blood was collected into EDTA tubes, and plasma collected by centrifugation. The circulatory system was flushed with heparinised saline and liver and lung were snap frozen. One lung was inflated and fixed with formalin.

I measured plasma levels of BMP9 in blood taken 5 minutes and 20 minutes after injection of Pro:BMP9 or vehicle. Surprisingly, I was unable to detect any BMP9 in any of these plasmas by ELISA (figure 89). Similarly, I was unable to detect any plasma BMP9 activity on endothelial cells (figure 90). Importantly, BMP9 recovery efficiency from the residual fluid in the syringe was close to 100%, indicating successful delivery into the mice.

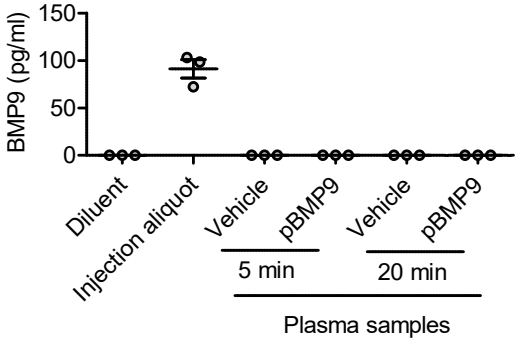

Figure 89. Intravenously administered Pro:BMP9 is undetectable in plasma by ELISA. *Gdf2* knockout mice were given Pro:BMP9. After 5 & 20 minutes, plasma was collected. BMP9 levels were measured in an aliquot of Pro:BMP9 which was passed through a syringe to simulate injection and diluted to bring it into range of the ELISA, and plasmas. Samples were measured in duplicate and the mean is shown. Mean ± SEM, n = 3.

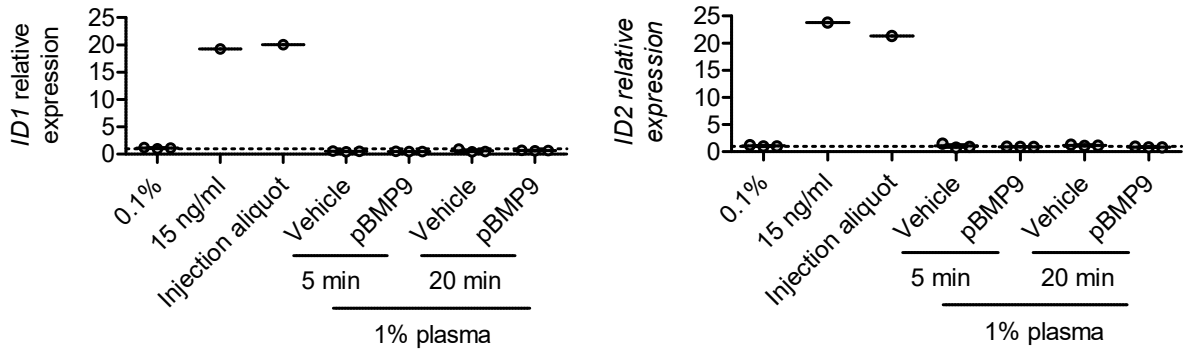

Figure 90 (overleaf). *Gdf2* knockout mice have no plasma BMP9 activity on endothelial cells even after intravenously administering Pro:BMP9. Mice were given Pro:BMP9 or vehicle. After 5 & 20 minutes, plasma was collected. Quiescent aortic endothelial cells were incubated with 1% (v/v) plasma, or diluted Pro:BMP9 solution from the syringe, or with 15 ng/ml of recombinant BMP9. The latter serves as a positive control for the expected plasma activity of mice given Pro:BMP9. mRNA levels of *ID1* and *ID2* were measured by qPCR relative to the housekeeping gene *B2M*. Mean ± SEM, n = 3, dashed line = expression in untreated quiescent cells (0.1%).

Pro:BMP9 spiked into human plasma can be recovered with ~85% efficiency (Hodgson et al. 2019). I spiked Pro:BMP9 into whole human blood in EDTA-tubes, incubated it for 1 hour at 37 °C, centrifuged it, and measured recovery from the plasma fraction (figure 91). Simultaneously, I spiked Pro:BMP9 into pre-prepared EDTA-plasma. Recovery from spiked whole blood-plasma was more efficient than for spiked plasma. This could be explained by Pro:BMP9 being excluded from cells and so concentrated in the smaller plasma compartment: plasma and blood spike-recovery curves overlay if haematocrit is assumed to be ~46%. Recovery from spiked PBS was least efficient, perhaps because of adsorption to pipettes and tubes. These data confirmed that exogenous Pro:BMP9 would be detectable from blood.

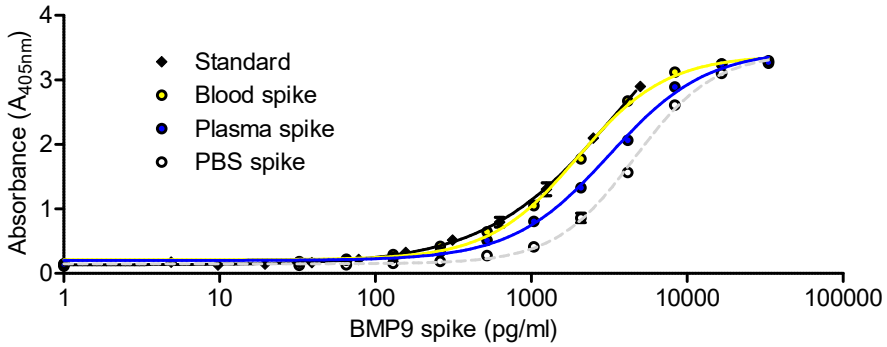

Figure 91. Pro:BMP9 is efficiently recovered from blood. I serially diluted human Pro:BMP9 in whole human blood treated with EDTA to prevent clotting, EDTA-plasma prepared from the same blood and PBS. I incubated samples for 1 hour at 37 °C then centrifuged to collect plasma from the EDTA-blood. I measured BMP9 levels in samples by ELISA using recombinant BMP9 in 1% (w/v) BSA in PBS as the standard. Mean ± SEM of technical duplicates, n = 3 with one representative experiment shown.

Since exogenous BMP9 was not present in the blood of injected mice, I investigated whether it was sequestered into the liver or lungs—two organs which are known to express BMP9 receptors highly. I developed an ELISA protocol to quantify BMP9 levels in frozen tissue extracts. First, I checked whether RIPA tissue lysis buffer was compatible with the ELISA we use for plasma (figure 92). RIPA buffer had no effect on the immunoreactivity of BMP9 standards when ≤ 25 µl was present per 100 µl well. I tested the immunoreactivity of BMP9 standards made up in tissue extracts from *Gdf2* knockout mice versus plain RIPA buffer (figure 93). This showed liver extract inhibited BMP9 detection, but diluting extract to ≤ 5% (v/v)

enabled efficient recovery. In lung extracts, recovery efficiency decreased with increasing BMP9 concentrations, but quantification was more accurate below ~30 pg/ml (figure 94).

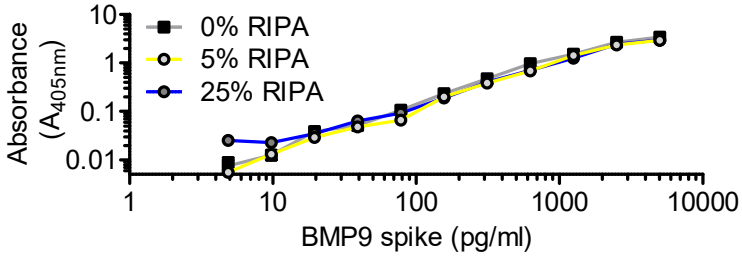

Figure 92. RIPA tissue lysis buffer is compatible with the BMP9 growth-factor domain ELISA. I serially diluted recombinant BMP9 in 0-25% (v/v) RIPA buffer. I measured the immunoreactivity of these samples by ELISA. Mean ± SEM of technical duplicates.

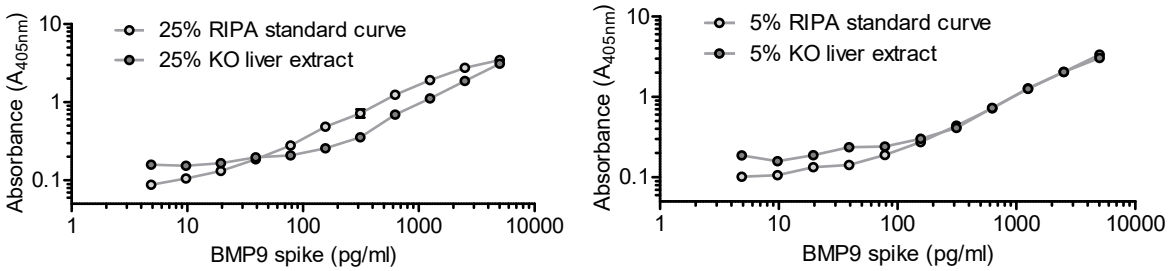

Figure 93. Liver extract may repress BMP9 detection by ELISA unless diluted. I serially diluted recombinant BMP9 in either empty RIPA buffer or liver extract from a *Gdf2* knockout (KO) mouse. I measured the immunoreactivity of these samples by ELISA. Mean ± SEM of technical duplicates.

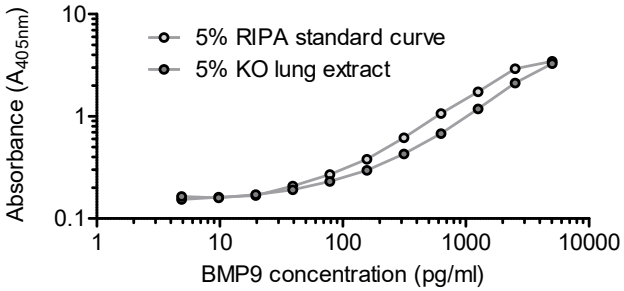

Figure 94. Lung extract may repress detection of high concentrations of BMP9 by ELISA. I serially diluted recombinant BMP9 in either empty RIPA buffer or lung extract from a *Gdf2* knockout (KO) mouse. I measured the immunoreactivity of these samples by ELISA. Mean ± SEM of technical duplicates.

Next, I compared BMP9 levels in livers from wildtype versus *Gdf2* knockout mice, since the former is very likely to contain BMP9, whilst the latter should not. As expected, diluting extracts 1 in 20 lead to highest recovery of BMP9 from wildtype livers (figure 95). Importantly, there was some non-specific signal in *Gdf2* knockout mice which gave an absorbance equivalent to ~20 pg/mg of tissue in liver extracts and ~15 pg/mg in lung extracts.

EDTA was necessary to recover BMP9 from serum. To see if it was necessary for tissue extracts, I measured immunoreactivity of liver samples from wildtype mice with and without

EDTA (figure 96). I also assessed lung extracts of wildtype mice injected with Pro:BMP9, since there was little BMP9 in wildtype lungs at baseline (see 5.4). EDTA did not alter recovery, but I elected to continue including EDTA. Since the ELISA measurements were affected by the concentration of tissue extract, I decided to add exactly 1 ml of RIPA buffer per 40 mg of tissue before homogenising experimental samples. Therefore, although absolute quantifications likely have some small error, the relative absorbances and concentrations of samples can be compared fairly.

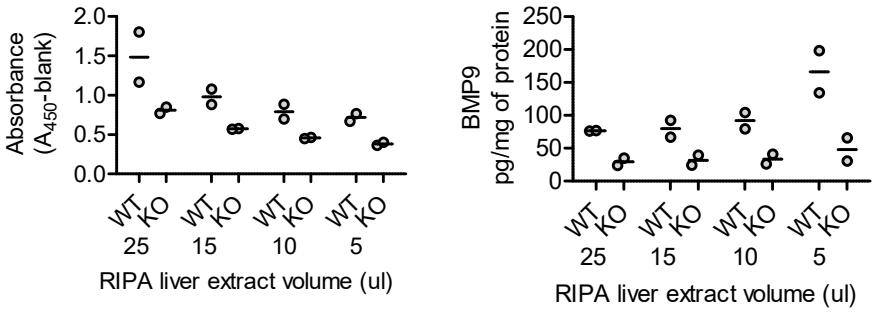

Figure 95. The ELISA can discriminate effectively between positive and negative control tissue. I prepared liver lysates from wildtype (WT) and *Gdf2* knockout (KO) mice. Total protein concentration of lysates was measured by Lowry assay. I diluted 5–25 ul of lysate and measured ELISA immunoreactivity. **Left:** Raw absorbances of samples. **Right:** Concentration of BMP9 in samples. Technical duplicates with mean plotted, n = 2, line = grand mean.

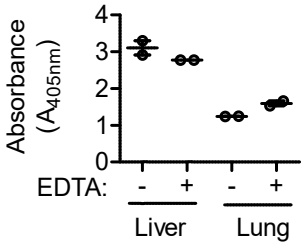

Figure 96. EDTA hardly affects BMP9 measurement in tissue extracts. Liver lysates from wildtype mice, and lung lysates from wildtype mice injected with Pro:BMP9, were prepared ± 5 mM EDTA. I measured immunoreactivity of the samples in the BMP9 ELISA. Technical duplicates with mean plotted, n = 2, line = grand mean.

Having optimised a tissue ELISA protocol, I compared BMP9 levels in the flushed livers of *Gdf2* knockout mice injected with Pro:BMP9 or vehicle (figure 97). There was no significant difference between groups. This could indicate BMP9 is not taken up by the liver to a great extent, in fitting with the idea BMP9 is primarily an autocrine/paracrine in the liver. I confirmed this by looking at *Id1* mRNA levels, since these are expressed by hepatic cells in response to BMP9 signalling (see 1.5.6). There was no difference in levels between mice given Pro:BMP9 or vehicle (figure 98).

I also assessed whether exogenously administered Pro:BMP9 was sequestered to the lung. ELISA revealed lung lysates from mice injected with Pro:BMP9 had significantly higher immunoreactivity than lung lysates from mice given vehicle (figure 99). As mentioned, there

was consistently ~15 pg/ml of non-specific immunoreactivity in lungs of *Gdf2* knockout mice given vehicle, but levels were > 20 pg/mg in mice given Pro:BMP9.

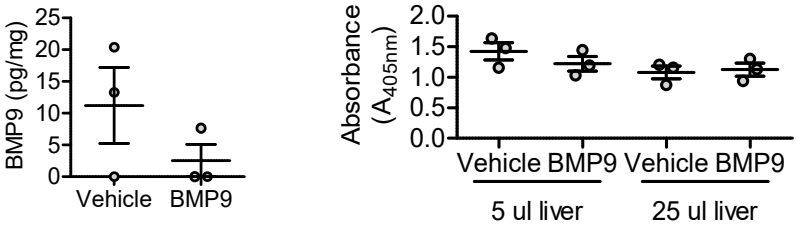

Figure 97. Intravenously administered BMP9 does not accumulate in the liver. *Gdf2* knockout mice were given Pro:BMP9 or vehicle by tail vein injection. After 20 minutes, mice were killed. I measured liver extracts in the BMP9 ELISA. Samples were measured in duplicate and the mean is plotted. **Left:** BMP9 concentration plotted as normalised concentration per mg of tissue. Mean ± SEM, n = 3. All values are within the range of non-specific background for this assay (0-20 pg/mg). **Right:** Immunoreactivity of 5 µl and 25 ul lysates shown to demonstrate the pattern is not an artefact of sample volume.

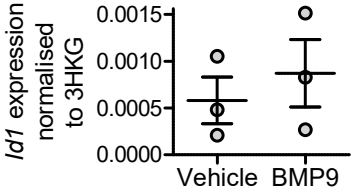

Figure 98. Intravenous administration of BMP9 does not increase in BMP9 signalling in the liver. *Gdf2* knockout mice were given Pro:BMP9 or vehicle. After 20 minutes, mice were killed. Liver RNA was extracted and levels of *Id1* mRNA was measured compared to three house-keeping genes (*B2M, Hprt, bAct*) by qPCR. Mean ± SEM, n = 3.

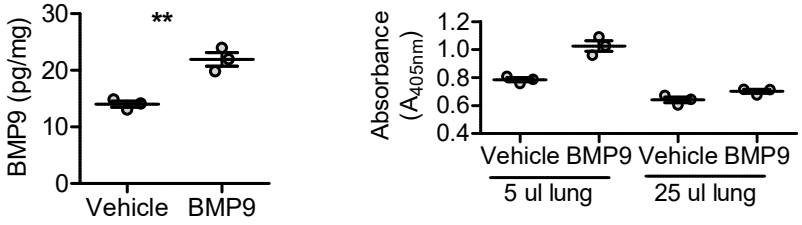

Figure 99. Intravenous administration of BMP9 leads to an increase in BMP9 levels in flushed lungs. *Gdf2* knockout mice were given Pro:BMP9 or vehicle. After 20 minutes, mice were killed. I measured lung extracts in the BMP9 ELISA. Samples were measured in duplicate and the mean is plotted. **Left:** normalised concentration per mg of tissue. Mean ± SEM, n = 3, unmatched two-tailed Student's t-test. **p<0.01. Note ~15 pg/mg non-specific signal. **Right:** Immunoreactivity of 5 µl and 25 ul lysates shown to demonstrate the pattern is not an artefact of sample volume.

To assess whether BMP9 was signalling in the lungs, I measured transcriptional induction of *Id1*. Transcription was trending upwards in the lungs of mice injected with Pro:BMP9 compared to controls (figure 100). This was not significant, but the duration of treatment was brief (20 minutes) and there were only 3 mice in each group. *Id2* expression in the lung was no higher in wildtype mice than *Gdf2* knockout mice, so did not represent a robust readout of BMP9 signalling in this context (not shown).

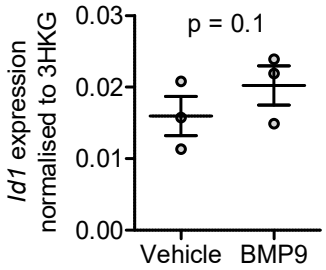

Figure 100. Intravenous administration of BMP9 may lead to a small increase in BMP9 signalling in the lungs. *Gdf2* knockout mice were given Pro:BMP9 or vehicle. After 20 minutes, mice were killed. Lung levels of *Id1* mRNA was measured compared to three house-keeping genes (*B2M, Hprt, bAct*) by qPCR. Mean ± SEM, n = 3, unmatched two-tailed Student's t-test.

5.3 Administration of Pro:BMP9 to wildtype mice

We hypothesised rapid clearance of exogenous Pro:BMP9 from *Gdf2* knockout mice was a consequence of sequestration to a potential abundance of unoccupied receptors. Wildtype mice may have differing levels of BMP9 binding proteins and receptors, depending on feedback mechanisms, and will have endogenous BMP9 occupying some of these sites. We gave wildtype mice a higher dose of Pro:BMP9, equivalent to ~65 ng of recombinant BMP9 per ml of blood, to make it easier to detect and see whether we could saturate animals' buffering capacity. We introduced a second group of mice that were followed for longer and included four mice per group to improve statistical power (figure 101).

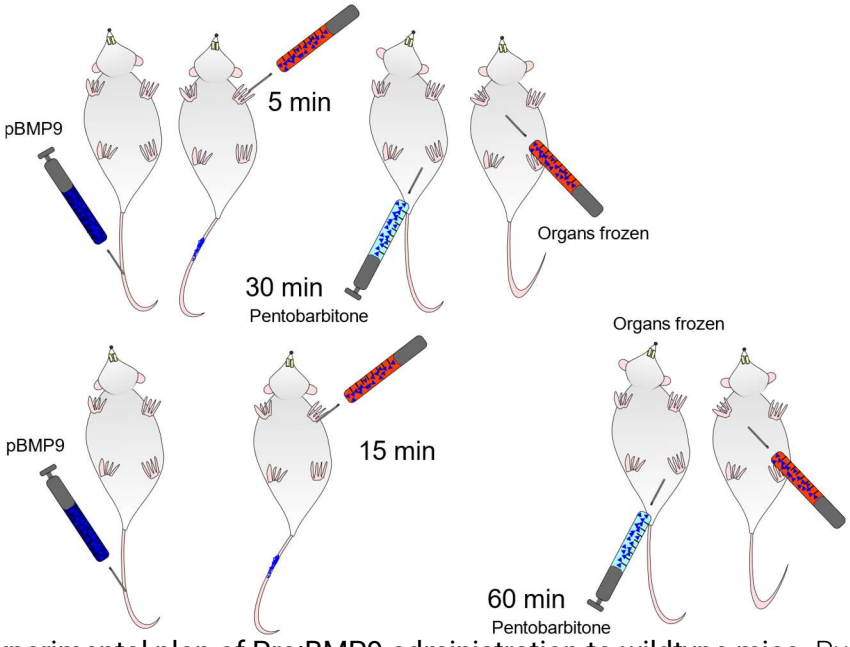

Figure 101. Experimental plan of Pro:BMP9 administration to wildtype mice. Purified human Pro:BMP9 was diluted to 2.5 ng/µl in 1% (w/v) mouse serum albumin in PBS. Five µl/g (~10% blood volume, 12.5 µg/kg) of Pro:BMP9 solution or vehicle was administered by tail vein injection to eight mice respectively. Four vehicle and Pro:BMP9 injected mice had blood taken from the saphenous vein after 5 minutes and a lethal dose of pentobarbitone was administered after 30 minutes. The remaining mice had blood taken from the saphenous vein after 15 minutes and a lethal dose of pentobarbitone was administered after 60 minutes. Mice

were exsanguinated by cardiac puncture. Blood was collected into EDTA tubes, and plasma collected by centrifugation. The circulatory system was flushed with heparinised saline and tissues were collected and snap frozen.

Again, I measured circulating levels of Pro:BMP9 by ELISA (figure 102). There was a small, significant increase in plasma BMP9 levels in mice given exogenous Pro:BMP9 compared to vehicle (two-way unmatched ANOVA, $p = 0.001$). This increase did not account for the vast majority of exogenous Pro:BMP9 we administered. It was hard to see if the magnitude of this increase was stable across the time-course: there was no significant interaction between treatment and time for mice in the 5-30 minute arm ($p = 0.17$), but there was a significant interaction in the 15-60 minute arm ($p = 0.0081$). Therefore, I could not calculate the half-life of exogenous Pro:BMP9. There was a significant decrease in plasma BMP9 levels in mice over time ($p < 0.001$). This could be due to factors such as increased circulatory volume (injection volume ~10% blood volume), stress or heat exposure (used to enable intravenous injections).

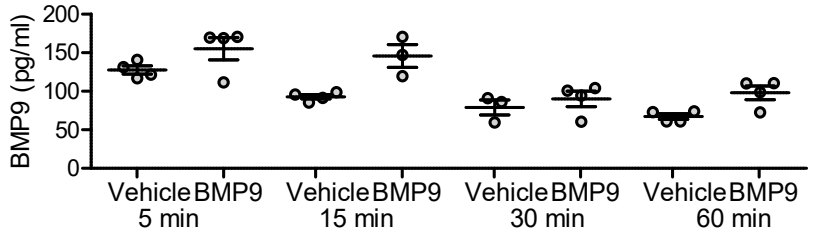

Figure 102. Intravenously administering Pro:BMP9 increases plasma levels. Mice were given Pro:BMP9 or vehicle by tail vein injection. After 5, 15, 30 & 60 minutes, plasma was collected. BMP9 levels were measured plasmas by ELISA. Technical duplicates with mean plotted. Mean ± SEM, n = 4.

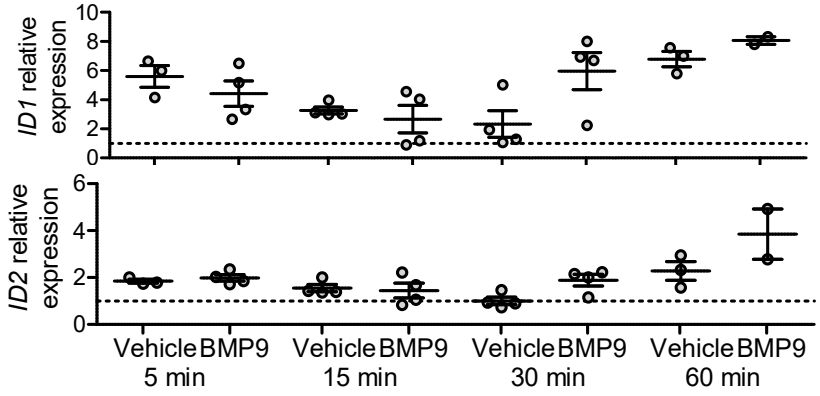

Figure 103. Plasma activity of mice after intravenous administration of Pro:BMP9. Mice were given Pro:BMP9 or vehicle by tail vein injection. After 5, 15, 30 & 60 minutes, plasma was collected. Quiescent aortic endothelial cells were incubated with 1% (v/v) plasma and mRNA levels of *ID1* and *ID2* were measured by qPCR compared to the housekeeping gene *B2M*. Mean ± SEM, n = 4 (except for 60 min samples).

Plasma activity did not show a robust pattern (figure 103). As expected, *ID2* expression in endothelial cells was upregulated after exposure to plasma from mice treated

with Pro:BMP9 compared to vehicle (p = 0.009), but *ID1* expression was not (p = 0.24). Plasma activity increased significantly with time (p = 0.001 and 0.0002 for *ID1* and *ID2* respectively). Discordance between plasma BMP9 levels and activity could be explained because: BMP9 levels only changed subtly; activity assays were relatively noisy; activity assays had lower sample sizes because sufficient plasma was not available from all mice; the activity of circulating BMP9 could be modulated independently of levels; or other factors, such as BMP10, may also respond to Pro:BMP9 treatment. These experiments were undertaken before *BRE*-HMEC cells, which offer a better signal-to-noise ratio, were developed.

In the liver, BMP9 levels measured by ELISA tended to be lower in mice killed 60 minutes after injection versus 30 minutes (p = 0.04), but levels were not different between mice given Pro:BMP9 or vehicle (figure 104). This again suggests circulating BMP9 is not sequestered into the liver. Instead, the liver may have either secreted more endogenous BMP9, or reduced *Gdf2* expression, over time. *Id1* mRNA levels were similar in the livers of all groups (figure 105). I am unsure if *Id1* transcription was a good marker of hepatic BMP9 signalling, since levels were not different between *Gdf2* knockout and wildtype mice. Addante *et al.* (2018) also reported this, but believed it was due to accommodation in chronically BMP9 deficient animals, whereas acute ALK1-Fc administration was able to reduce *Id1* transcription.

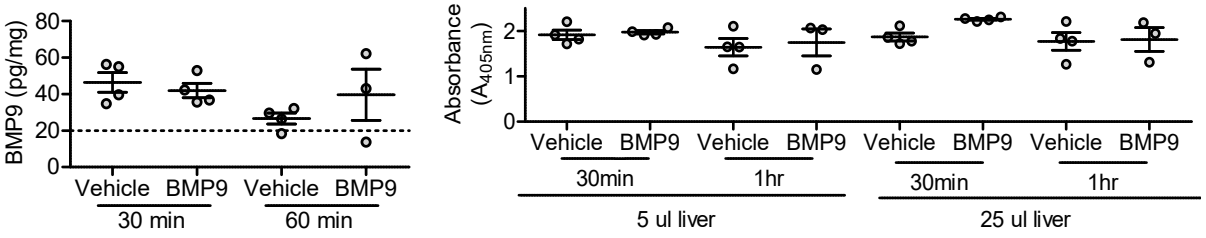

Figure 104. Intravenously administered BMP9 does not accumulate in the liver. Mice were given Pro:BMP9 or vehicle. After 30 or 60 minutes, mice were killed, and I measured immunoreactivity of liver extracts in the BMP9 ELISA. Samples were measured in duplicate and the mean is plotted. **Left:** normalised concentration per mg of tissue. Mean ± SEM, n = 4. Dashed line = non-specific background of this assay. **Right:** Immunoreactivity of 5 µl and 25 ul lysates shown to demonstrate the pattern is not an artefact of sample volume.

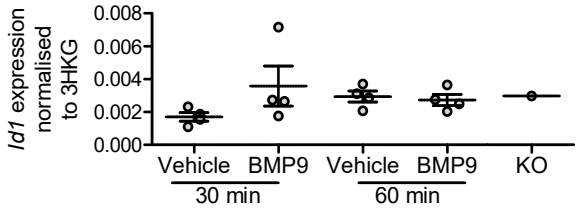

Figure 105. Intravenous administration of BMP9 does not increase BMP9 signalling in the liver. Mice were given Pro:BMP9 by tail vein injection. After 30 or 60 minutes, mice were killed. Liver RNA was extracted and levels of *Id1* mRNA were measured compared to three house-keeping genes (*B2M, Hprt, bAct*) by qPCR. Mean ± SEM, n = 4. KO = sample from *Gdf2* knockout mouse.

In the lung, BMP9 levels were higher in mice given Pro:BMP9 compared to vehicle (figure 106). This increase was greater in those mice killed at 30 minutes than 60 minutes, which suggested exogenous BMP9 was cleared from lungs over this time. These data were mirrored by BMP9 signalling in the lung as measured by *Id1* transcription (figure 107).

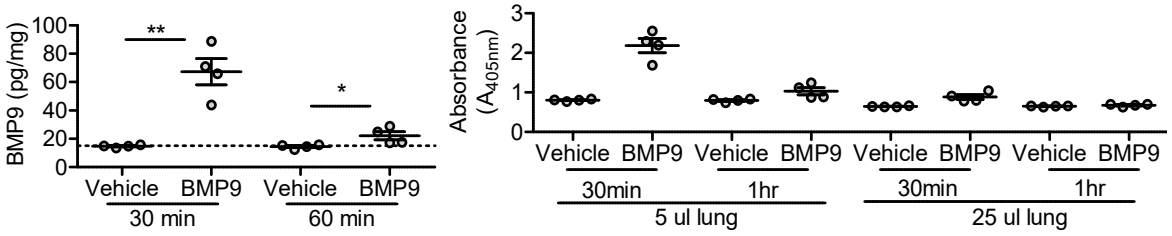

Figure 106. Intravenously administered BMP9 accumulates in flushed lungs. Mice were given Pro:BMP9 or vehicle. After 30 or 60 minutes, mice were killed, and liver extracts were measured in the BMP9 ELISA. Samples were measured in duplicate and the mean is plotted. **Left:** normalised concentration per mg of tissue. Mean ± SEM, unpaired two-tailed Student's t-test, * p<0.05, ** p<0.01, n = 4. Dashed line = non-specific background of this assay. **Right:** Immunoreactivity of 5 µl and 25 ul lysates shown to demonstrate the pattern is not an artefact of sample volume.

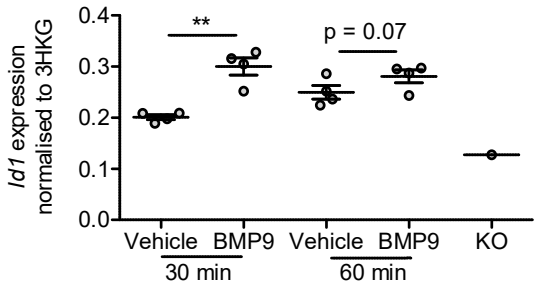

Figure 107. Intravenous administration of BMP9 leads to an increase in BMP9 signalling in the lungs. Mice were given Pro:BMP9 or vehicle. After 30 or 60 minutes, mice were killed, and lung levels of *Id1* mRNA were measured compared to three house-keeping genes (*B2M, Hprt, bAct*) by qPCR. Mean ± SEM, n = 4, unpaired two-tailed Student's t-test ** p<0.01. KO = sample from *Gdf2* knockout mouse.

5.4. Endogenous BMP9 in pharmacokinetic mice

I assessed the expression of endogenous *Gdf2* by qPCR in the livers and lungs of mice given exogenous Pro:BMP9 to explore whether compensation occurs (figure 108). In the liver, *Gdf2* transcripts were more abundant at 60 minutes than 30 minutes post injection (p = 0.0007), and slightly higher in animals given Pro:BMP9 compared to vehicle (p = 0.016). ELISA and qPCR data are consistent with blood volume increasing after injection, followed by secretion of BMP9 protein from the liver, compensated by increased *Gdf2* transcription.

As expected, *Gdf2* expression was much lower in lungs compared to liver. Nonetheless, some BMP9 may be produced endogenously within lungs, since *Gdf2* mRNA was more abundant in lungs from wildtype mice than *Gdf2* knockouts. This confirms previous reports (Bidart et al. 2012; Hao Chen et al. 2013). Importantly, lung *Gdf2* mRNA levels did not change in response to administration of exogenous Pro:BMP9, indicating the increased ELISA immunoreactivity of these lungs was due to them sequestering exogenous Pro:BMP9.

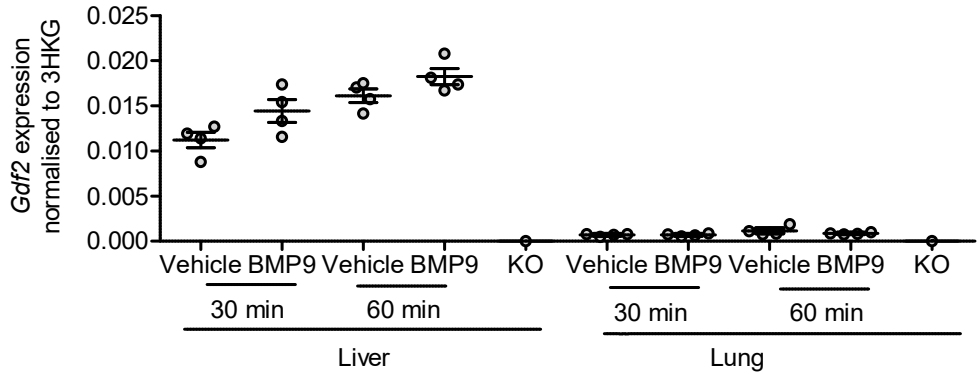

Figure 108. *Gdf2* is expressed in the liver and lungs. Liver expression increased over the time-course of the experiment whereas lung expression was stable. Mice were given Pro:BMP9 or vehicle. After 30 or 60 minutes, mice were killed, and levels of *Gdf2* mRNA were measured compared to three house-keeping genes (*B2M, Gapdh, bAct*) by qPCR. Mean ± SEM, n = 4, KO = sample from *Gdf2* knockout mouse.

I analysed tissue lysates from all the pharmacokinetic mice simultaneously. Therefore, I could compare BMP9 levels in the lungs of wildtype and *Gdf2* knockout mice given vehicle. Interestingly, wildtype lungs did not contain significantly more BMP9 than *Gdf2* knockout lungs (figure 109), despite experiencing more signalling (figure 107). There was a slight tendency for wildtype lungs to have higher immunoreactivity, and there were only three knockout lungs for comparison. Nevertheless, these data suggest endogenous BMP9 protein exists in an equilibrium where it does not accumulate greatly in the lungs. This is consistent with data from figure 106 showing exogenous Pro:BMP9 is rapidly cleared from the lungs.

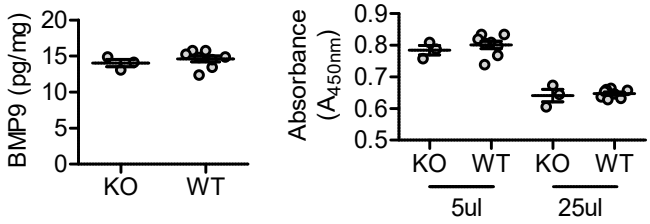

Figure 109. Endogenous BMP9 does not accumulate within the lungs. Samples from mice given vehicle were measured in duplicate in the BMP9 ELISA and the mean is plotted. **Left:** normalised concentration per mg of tissue. Mean ± SEM. Non-specific background of this assay ~ 15 pg/ml. **Right:** Immunoreactivity of 5 µl and 25 ul lysates shown to demonstrate the pattern is not an artefact of sample volume.

5.5. Binding of BMP9 to endothelial cells *in vitro*

Some factors bind matrix secreted by their target cells and local pools stimulate prolonged signalling. It is unknown how long BMP9 remains active once bound to its receptors, or if endothelial cells maintain a reservoir of active BMP9 after exposure. I studied the signalling kinetics of endothelial cells *in vitro* to assess whether exogenous BMP9, which is rapidly cleared from plasma, could be sequestered by endothelial cells and if it could have a prolonged stimulatory effect.

Firstly, I exposed human aortic endothelial cells to physiological doses of BMP9. After 5 minutes, I washed them with fresh media which either also contained BMP9 or did not (figure 110). Cells incubated for 1 hour after a pulse of BMP9 exposure had the same transcriptional response as continuously exposed cells. However, the efficacy of the pulse rapidly tailed off between 1 and 4 hours, indicating cells did not sequester a pool of BMP9 able to maintain signalling. This is consistent with figure 106 and 109.

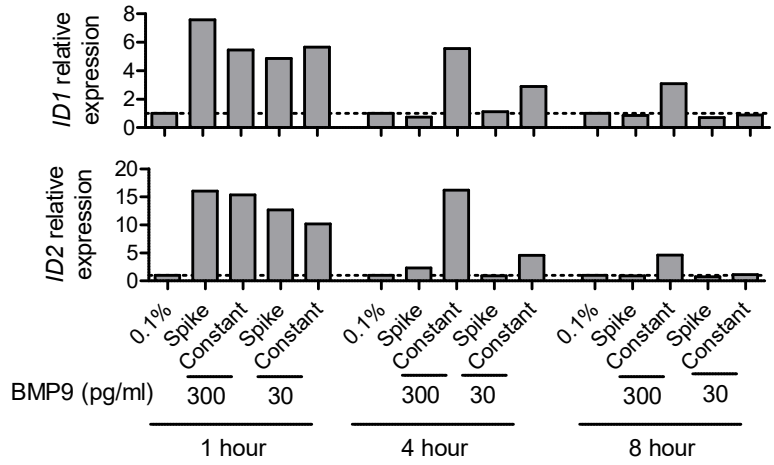

Figure 110. Brief exposure to BMP9 elicits a brief transcriptional response. Human aortic endothelial cells grown to confluence in 6-well plates were quiesced overnight and then media was replaced with fresh 0.1% (v/v) FBS in EBM2 that was supplemented with 0, 30 or 300 pg/ml BMP9. After 5 minutes, this was replaced with fresh 0.1% FBS (v/v) in EBM2 supplemented with 0 (spike), or 30 and 300 (constant) pg/ml BMP9. Cells were incubated for 1, 4 or 8 hours. Levels of *ID1* and *ID2* mRNA were measured by qPCR compared to the housekeeping gene *B2M*. Technical triplicates, mean plotted, n = 1.

Secondly, I treated endothelial cells with physiological concentrations of BMP9 for 30 minutes or 30 hours. I then transferred this media onto fresh cells to measure residual activity (figure 111). This experiment indicated endothelial cells needed longer than 30 minutes to appreciably clear BMP9 activity, but could consume all available BMP9 within 30 hours. I performed a similar experiment and used an ELISA to show that a confluent monolayer of ~1 million endothelial cells could almost completely clear 6 ng of BMP9 within 24 hours (figure

112). Taken together, these data are consistent with endothelial cells consuming BMP9 relatively rapidly during signalling, but not sequestering a pool of BMP9.

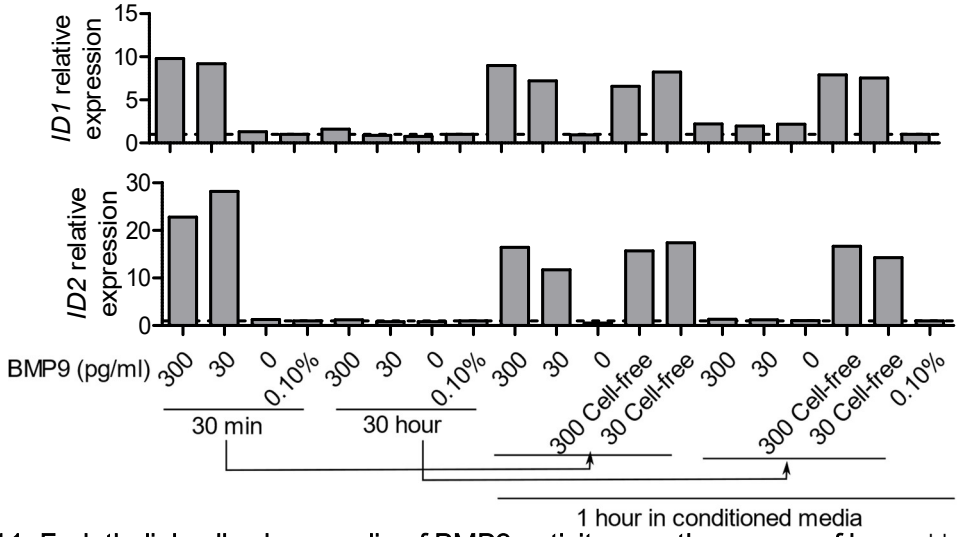

Figure 111. Endothelial cells clear media of BMP9 activity over the course of hours Human aortic endothelial cells grown to confluence in 6-well plates were quiesced overnight in 0.1% (v/v) FBS in EBM2. Cells, or empty wells (cell-free) were then incubated with 0.1% (v/v) FBS in EBM2 containing 0, 30 or 300 pg/ml of BMP9. After 30 minutes, or 30 hours, this media was collected and frozen and cells were lysed. The conditioned media or cell-free control media were then thawed and incubated with fresh quiesced cells for 1 hour before lysis. Levels of *ID1* and *ID2* mRNA were measured by qPCR compared to the housekeeping gene *B2M*. Technical triplicates with mean plotted, n = 1. Conditioned media exposed to cells for 30 minutes remained fully active, whilst conditioned media exposed to cells for 30 hours had no activity. Media not exposed to cells retained full activity.

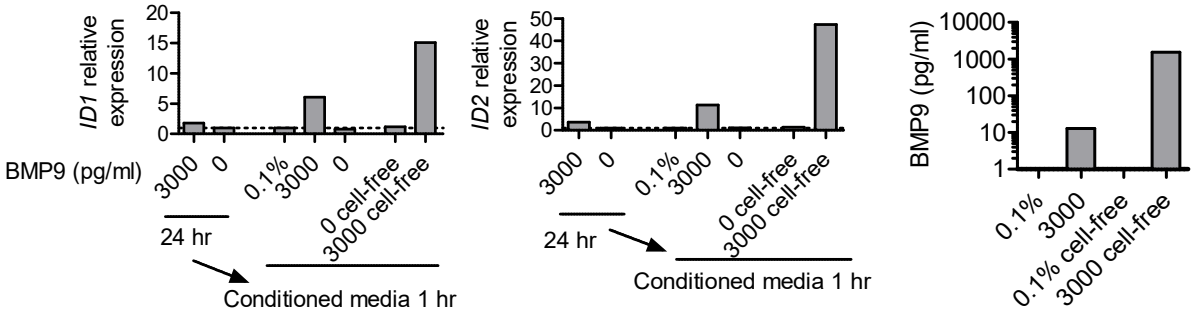

Figure 112. Endothelial cells clear media of BMP9 activity over the course of hours by removing BMP9 protein from the media. Human aortic endothelial cells were grown to confluence in 6-well plates and quiesced overnight. Cells, or empty wells (cell-free) were then incubated with 0.1% FBS (v/v) in EBM2 containing 0 or 3000 pg/ml BMP9 for 24 hours. I collected conditioned media and lysed these cells. I aliquoted conditioned media for measurement in the BMP9 ELISA and incubated the rest with fresh quiescent cells. I lysed the fresh cells after 1 hour. **Left, middle:** levels of *ID1* and *ID2* mRNA were measured by qPCR compared to the housekeeping gene *B2M*. **Right:** BMP9 levels in conditioned media as measured by ELISA. Technical triplicates with mean plotted, n = 1.

5.6. Transvascular gradients of BMP9 & pBMP10 in humans

Intravenously administered exogenous Pro:BMP9 appeared to primarily accumulate in mouse lungs, but not peripheral venous plasma or liver. This led us to hypothesise that in unmanipulated animals and humans, pulmonary arterial blood contains high levels of endogenous BMP9, which is quickly bound by the endothelium of the lung vasculature, so systemic blood has relatively reduced levels of BMP9. Although we suspect circulating BMP10 is mostly unprocessed, we hypothesised the pulmonary vasculature binds and activates it.

To assess these hypotheses, I obtained plasma samples collected from different human vascular beds by clinical researchers at Royal Papworth Hospital. Samples from 15 female and 3 male IPAH patients, aged 23-73, were available. As a comparison group, I selected 8 females and 7 males with a patent foramen ovale (PFO), both to confirm IPAH samples did not have an unusual pattern, and because cardiac defects may be associated with *BMP10* deficiency.

Plasmas were from the superior vena cava (SVC), pulmonary artery (PA) and brachial artery (Art). I measured these in the BMP9 (figure 113) and pBMP10 (figure 114) ELISAs. For each individual, the transpulmonary gradient is PA-Art, whilst the gradient across systemic organs is Art-SVC. The data may not be normally distributed (D'Agostino-Pearson $p < 0.0001$ sexes grouped; too few to assess when split) so I analysed data with Friedman tests. There was no significant difference between IPAH and PFO groups. Males had reduced levels of both BMP9 and pBMP10, as expected, although this did not reach significance. Unexpectedly, BMP9 levels were very slightly lower in pulmonary arteries (273 ± 15 pg/ml) and brachial arteries (273 ± 16 pg/ml) than superior vena cavas (280 ± 17 pg/ml)($p = 0.048$).

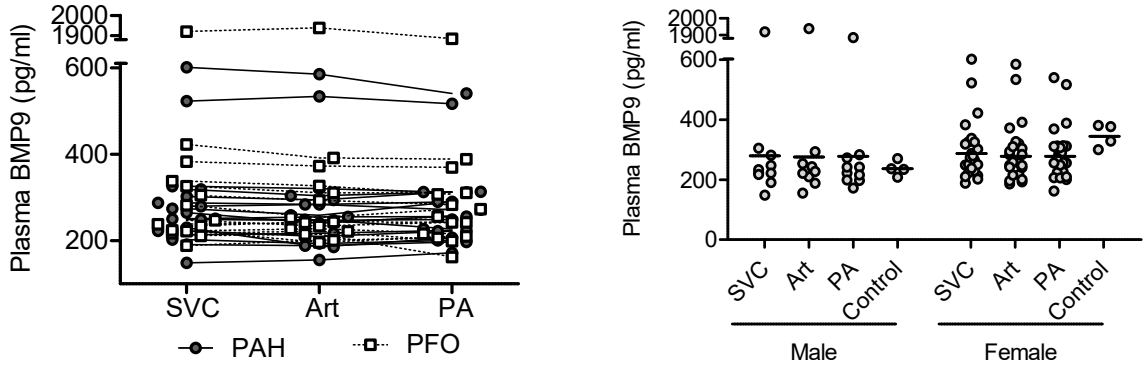

Figure 113. BMP9 growth-factor domain levels measured in plasma from different vessels by ELISA. Plasma from 15 female & 3 male PAH patients, 8 female & 7 male PFO patients, collected from the superior vena cava (SVC), brachial artery (Art) and pulmonary artery (PA). **Left:** data grouped according to disease classification and sampling location. Lines connect samples from the same individual. **Right:** data grouped according to sex and sampling location. Controls = four samples taken from the cephalic vein of healthy adults. Samples were assayed in duplicate with the mean plotted. Bar = grand mean.

Surprisingly, pBMP10 levels followed a different pattern, with levels higher in the pulmonary arteries (6511 ± 540 pg/ml) than brachial arteries (6467 ± 570 pg/ml) than superior vena cava (6246 ± 499 pg/ml), as expected (p = 0.009). I also measured samples from the cephalic vein of four healthy males and females, since this is the location sampled in other cohorts. Levels of BMP9 and pBMP10 in cephalic vein samples showed pronounced sex differences as expected. Unexpectedly, levels were higher in these controls than the great vessels, but they were collected in different circumstances.

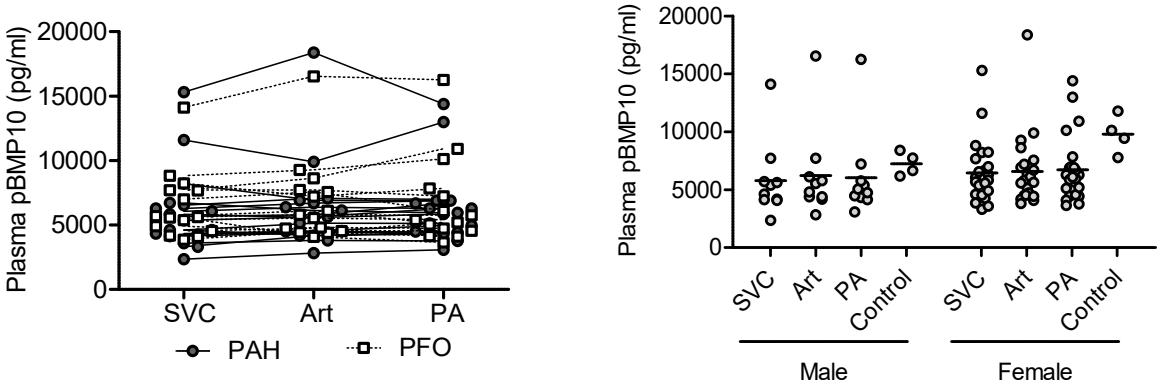

Figure 114. pBMP10 levels measured in plasma from different vessels by ELISA. Plasma from 15 female & 3 male PAH patients, 8 female & 7 male PFO patients, collected from the superior vena cava (SVC), brachial artery (Art) and pulmonary artery (PA). **Left:** data grouped according to disease classification and sampling location. Lines connect samples from the same individual. **Right:** data grouped according to sex and sampling location. Controls = four samples taken from the cephalic vein of healthy adults. Samples were assayed in duplicate with the mean plotted. Bar = grand mean.

I hypothesised the slight fall in total pBMP10 levels across the pulmonary vasculature could represent utilisation of processed Pro:BMP10. Therefore, I measured plasma activity of these samples on *BRE*-HMECs (figure 115). This showed no significant difference between plasmas from different vessels. Notably, PAH patients tended to have lower plasma activity than PFO patients (p = 0.065) driven by plasma from the superior vena cava. *BRE*-HMECs possibly process endogenous *ProBMP10* and serum is a preferable substrate to plasma. (see 4.6). Hence, I directly measured levels of processed BMP10 in these samples by ELISA (figure 116). There was no evidence of a transpulmonary gradient in Pro:BMP10 levels.

As expected from 4.2, most samples contained no detectable processed Pro:BMP10 as measured by the BMP10 growth-factor domain ELISA. However, plasmas from all three vessels within 8/33 patients contained 50-300 pg/ml of Pro:BMP10, suggesting some people have meaningful circulating Pro:BMP10 levels. I investigated correlations between Pro:BMP9, Pro:BMP10 and total pBMP10 levels (figure 117). As expected, there was a tight correlation between BMP9 and pBMP10 levels in all samples. Surprisingly, Pro:BMP10 and pBMP10 levels

were not as robustly correlated. In contrast, processed BMP10 was only detectable in plasma samples with >300 pg/ml of BMP9, and levels were well correlated with BMP9. This could suggest some co-regulation between the amount of circulating BMP9 and processed BMP10.

Notably, one male with a patent foramen ovale had very high levels of both Pro:BMP9 (~1900 pg/ml) and Pro:BMP10 (1500 pg/ml), with levels of BMP9 higher than measured by the Morrell group before (maximum in controls ~700 pg/ml). The plasma activity of this patient was relatively high, although these results may still be due to non-specific immunoreactivity. The levels of pBMP10 in these samples were not notable. Exclusion of this patient does not alter the statistical conclusions drawn previously.

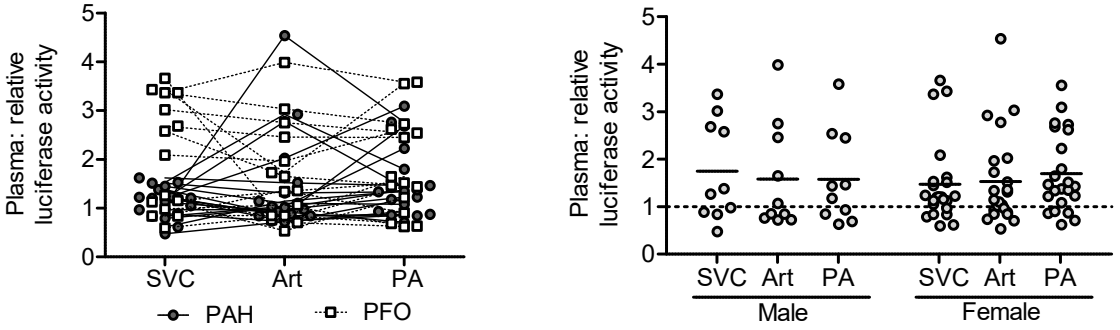

Figure 115. Activity of plasma from different vessels. Quiescent *BRE*-HMECs treated with 1.5% (v/v) plasma from 15 female & 3 male PAH patients, 8 female & 7 male PFO patients, collected from the superior vena cava (SVC), brachial artery (Art) and pulmonary artery (PA). **Left:** data grouped according to disease classification and sampling location. Lines connect samples from the same individual. **Right:** data grouped according to sex and sampling location. Samples were assayed in duplicate with the mean plotted. Bar = grand mean. Dashed line = luciferase activity of untreated quiescent cells.

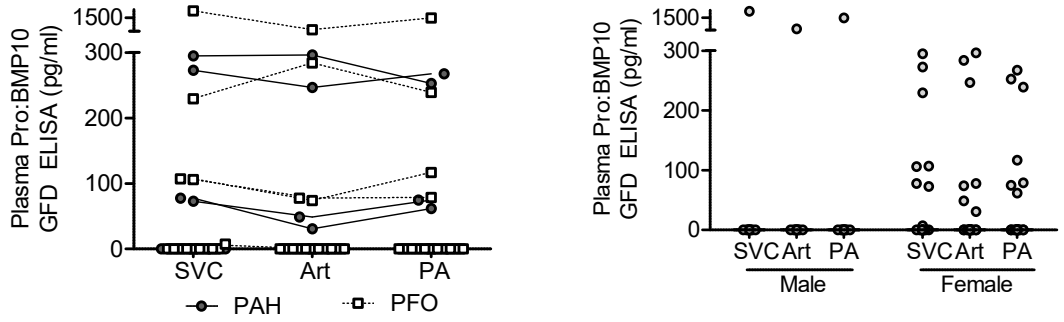

Figure 116. Pro:BMP10 levels measured in plasma from different vessels by BMP10-GFD ELISA. Plasma from 15 female & 3 male PAH patients, 8 female & 7 male PFO patients, collected from the superior vena cava (SVC), brachial artery (Art) and pulmonary artery (PA). **Left:** data grouped according to disease classification and sampling location. Lines connect samples from the same individual. **Right:** data grouped according to sex & sampling location.

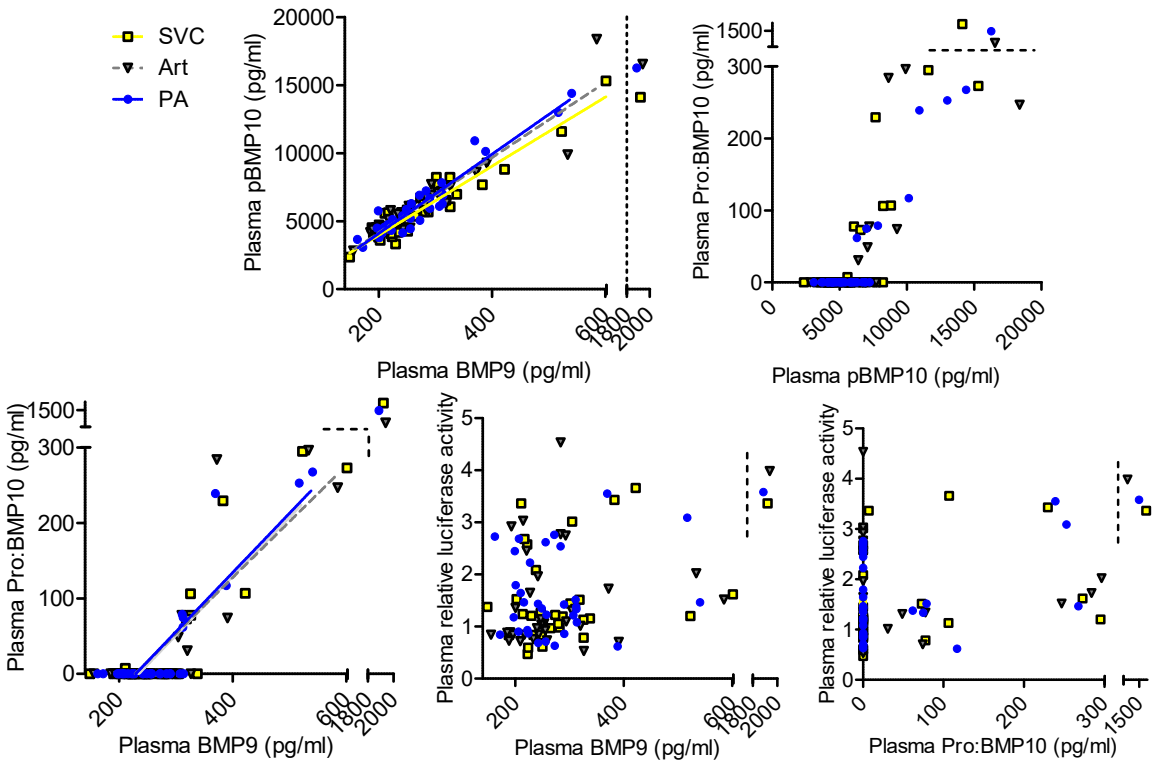

Figure 117. Correlations between data from figures 113-116. Dashed lines = axis breaks. Linear regressions excluding the three outlying samples.

5.7. Discussion

It is important to know if BMP9 and BMP10 are classic endocrines, secreted from the liver and right atrium respectively, binding cells according the expression level of ALK1/endoglin. Or they may also be paracrines/autocrines produced locally, require local processing or have modulating binding partners. This could impact the design of BMP9-based drugs, whether activity on a given vascular bed correlates with plasma levels, and influence which tissues are most vulnerable to *GDF2* deficiency.

We expected circulating BMP9 to have long half-life because it is able to exert protective effects in animals when administered once daily (Long et al. 2015). However, most animal experiments use intraperitoneal injections, so rate of uptake into the circulation is unclear. Previously, Dr. Claudia Mitrofan was unable to recover recombinant BMP9 administered intravenously or intraperitoneally by ELISA but did detect some increased plasma activity after 1 hour and not longer time-points (unpublished). Therefore, we administered high doses of Pro:BMP9 to both wildtype and *Gdf2* knockout mice and took samples 5 minutes to 1 hour after administration. I similarly found plasma levels of BMP9 changed very little after intravenous administration of exogenous Pro:BMP9.

To identify where exogenous BMP9 was being sequestered, I validated a protocol for measuring BMP9 levels in tissue extracts by ELISA. These ELISAs recovered BMP9 efficiently, but they gave some non-specific signal in the absence of BMP9. Despite this, the quantifiability, specificity, sensitivity and dynamic range of the ELISA is greater than alternative techniques. Moreover, the ELISA gave good discrimination between the livers of wildtype and *Gdf2* knockout mice.

Using the ELISA, I found exogenous BMP9 was bound by the lungs. There is a risk this result is due to incomplete flushing of the pulmonary vasculature. However, there was no detectable BMP9 in the blood of *Gdf2* knockout animals and *Id1* transcription was also activated in lungs. I did not find evidence exogenous BMP9 accumulated in the liver by ELISA. I could use some of the BMP9 responsive targets identified in 6.4, or phospho-SMAD stains to confirm a lack of activity in the liver. Labelled-BMP9 could be given to animals to allow rapid assessment of levels in all organs. The technique used should be compatible with whole-body analysis. One possibility could be to use ^{125}I-labelled BMP9, with mice killed, frozen, sectioned and exposed to autoradiograph film immediately after injection (Maguire, Kuc, and Davenport 2012). Labelling might disrupt the physiology of BMP9 so the tissue ELISAs could be used to validate findings with unlabelled Pro:BMP9.

We found BMP9 was completely cleared from the circulation of *Gdf2* knockout mice within 5 minutes of administration. There was only a subtle increase in circulating BMP9 in wildtype mice given Pro:BMP9 apparent between 5 minutes and 1 hour after administration. Blood completes ~three circuits around the vasculature every minute, so these data could be explained by exogenous BMP9 binding vacant sites within its first few circuits. The wildtype mice were given a higher dose of BMP9, and have some endogenous BMP9 and BMP10, which may explain why excess remained in their circulation. Mice could be given escalating doses of Pro:BMP9 to measure when binding capacity is saturated and plasma retention occurs.

Nonetheless, this model does not explain why endogenous BMP9 is constitutively present in plasma when exogenous BMP9 was rapidly cleared from it. Perhaps binding partners of endogenous BMP9 stabilise it in the circulation. Alternatively, endogenous BMP9 may be continuously secreted, so some is always present in the plasma prior to being cleared. Similarly, BMP9 did not accumulate in the lungs of wildtype animals compared to *Gdf2* knockouts, so endogenous BMP9 may normally be degraded or released from the lungs as rapidly as it binds.

I found *Gdf2* mRNA and BMP9 protein was most highly expressed in the liver, although there is transcript in the lungs. Therefore, we hypothesised BMP9 protein is

constitutively secreted from the liver, travels through the right-heart, then binds and activates signalling in the lungs, with residual BMP9 travelling to the systemic circulation. However, there was no evidence of a transpulmonary gradient of BMP9 levels in humans. This suggests either: lung binding sites are relatively saturated; lung binding is relatively slow; plasma BMP9 is masked from lung binding sites, perhaps by circulating binding partners; or lungs secrete as much BMP9 as they bind. The first explanation is inconsistent with the mouse pharmacokinetic data, but the latter are plausible.

In contrast to BMP9, we hypothesised circulating BMP10 is predominately unprocessed (see 4.4). Therefore, it may display different kinetics, only being taken up by those cells able to process it. However, *ProBMP10* was able to bind ALK1, so it may be adsorbed onto endothelial cells similarly to Pro:BMP9. Additionally, circulating Pro:BMP9 and *ProBMP10* appeared to be at least partially in complex (see 4.8), so they may be released into blood and taken up from it simultaneously, or exist in independent equilibriums. Since there are such high levels of circulating BMP10, whether it competes for the same binding sites may strongly impact the pharmacokinetics of BMP9.

Surprisingly, there was a slight drop in pBMP10 levels as plasma traversed the lungs. This could be because the lungs express *GDF2* robustly, but much less *BMP10*, so any BMP10 which binds is not replaced. Alternatively, lungs may preferentially bind BMP10 over BMP9, or it may simply be easier to detect a very small change in pBMP10 levels because they are much higher. Results from the BMP10 growth-factor domain ELISA and activity assay suggest lungs are unlikely to be preferentially binding Pro:BMP10 over *ProBMP10*, but did reveal some people have active levels of circulating Pro:BMP10 which may be co-regulated with Pro:BMP9.

6. Phenotyping of *Gdf2* knockout mice

6.1. Introduction

In mouse lungs, BMP9 promotes endothelial barrier function, and exogenous BMP9 can reverse histological and haemodynamic signs of PAH (Long et al. 2015). In humans, hypomorphic *GDF2* mutations cause PAH and HHT (Gräf et al. 2018; Wooderchak-Donahue et al. 2013). *GDF2* mutations have not been associated with other pathologies and there are not obvious differences between PAH patients carrying them and idiopathic patients. Two patients with early-onset PAH and HHT were found to carry homozygous *GDF2* loss-of-function mutations. In contrast, *Gdf2* knockout mice do not develop disease spontaneously.

In PAH patients, low plasma BMP9 levels were associated with elevated circulating levels of bilirubin. Low plasma pBMP10 levels were associated with significantly reduced circulating levels of albumin and significantly increased levels of alkaline phosphatase (ALP) (Hodgson et al. 2019; Nikolic et al. 2019). These are signs of liver dysfunction, but on average levels were not outside the healthy range, and levels of alanine aminotransferase (ALT) and aspartate aminotransferase (AST), which are enzymes released into the blood after liver damage, were not correlated with BMP9 levels. A recent report measured serum levels of ALT and lactate dehydrogenase in *Gdf2* knockout mice, and found that both were slightly elevated, indicating liver dysfunction (Desroches-Castan et al. 2019). Importantly, this was reported in 129/Ola mice which spontaneously develop severe liver fibrosis, whereas C57/BL6 mice do not.

BMP9 is reported to be insulin sensitising and stabilises expression of metabolic enzymes in the liver (Chen et al. 2003; Breitkopf-Heinlein et al. 2017). In human PAH patients, BMP9 and pBMP10 levels correlated with body mass index and type-II diabetes (Hodgson et al. 2019). This hints BMP9 deficiency may disrupt metabolism. Additionally, BMP9 deficiency may be inflammatory and weakly pro-fibrotic at baseline (Desroches-Castan et al. 2019; Desroches-Castan et al. 2019 b; Addante et al. 2018). Similarly, levels of C-reactive protein were significantly elevated, and above the normal range, in PAH patients with low circulating BMP9 or pBMP10 levels (Hodgson et al. 2019). Finally, in mouse livers, BMP9 prevents proper healing and promotes fibrosis following induced injury, so BMP9 deficiency promotes regeneration.

We have a colony of *Gdf2* knockout mice on a C57BL/6J background, although recent genotyping suggests the presence of some C57BL/6N haplotypes. We undertook to assess whether these mice have exacerbated PAH-like symptoms, metabolic dysfunction, or endothelial dysfunction. Therefore, we exposed *Gdf2* knockout and wildtype mice to sugen-hypoxia to induce PAH and analysed haemodynamic and histological differences. We are prospectively collecting tissues and blood from *Gdf2* heterozygous, knockout and wildtype mice to assess BMP9 levels, liver and lung transcriptomics and histology. Finally, we developed a protocol to assess pulmonary endothelial permeability using Evans blue dye. These data could suggest co-morbidities to assess in patients with BMP9 deficiency and possible effects of BMP9 treatment.

6.2. *Gdf2* deficiency did not exacerbate sugen-hypoxia induced PAH

Dr. Alexi Crosby and Stephen Moore measured haemodynamic parameters in *Gdf2* knockout and wildtype mice given sugen-5416 then placed in hypoxia for 2 weeks. Genotype did not have any significant impact on the development of pulmonary hypertension. Mice were also assessed at baseline (table 11). I measured Fulton index (right ventricular weight normalised by left ventricular and septum combined weight) and this was significantly decreased in *Gdf2* deficient mice (figure 118). Mark Southwood performed a histological analysis of lung samples I prepared and found a tendency for *Gdf2* knockout mice to have less muscularised vessels, consistent with Tu *et al.* (2019) and the Fulton index. This reflects the role of BMP9 in angiogenesis (see 1.5.3) and are reminiscent of the paediatric HHT patient discussed in 3.6.

Parameter	Wildtype	*Gdf2*$^{-/-}$	*Gdf2*$^{+/-}$
Pulmonary acceleration time (ms)	26.7 ± 2	23.8 ± 1	26.6 ± 0.9
Pulmonary ejection time (ms)	72.7 ± 4.2	68.9 ± 2.4	75 ± 1.4
Stroke volume (µl)	52.1 ± 4.2	46.4 ± 3.1	51.8 ± 3
Ejection fraction (%)	58.4 ± 2.4	58.9 ± 2.9	60 ± 2.7
Cardiac output (ml/min)	20 ± 1.9	19.6 ± 1.4	20.6 ± 1
Fulton index	0.29 ± 0.02	0.24 ± 0.01	0.22 ± 0.01
Right ventricular systolic pressure (mmHg)	23.4 ± 0.7	24.1 ± 0.9	22.4 ± 0.6

Table 11. Assessment of right-heart function in *Gdf2* knockout mice. Five wildtype, 10 *Gdf2* heterozygous & 13 knockout mice assed by echocardiography and right-heart catheterisation by Dr. Alexi Crosby and Stephen Moore. Mean ± SEM.

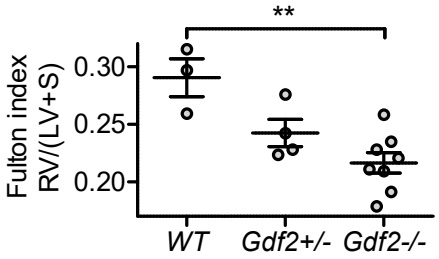

Figure 118. Assessment of Fulton index in *Gdf2* knockout mice. Right-ventricular wall was cut away from the left-ventricle and septum. The two pieces were weighed, and right-ventricle weight was normalised by the rest of the heart. One-way unmatched ANOVA/Bonferroni test, Mean ± SEM.

6.3. Levels of serum factors in *Gdf2* knockout mice

Markers of metabolic and organ health in serum from *Gdf2* knockout and wildtype mice were measured by the Addenbrooke's Core Biochemical Assay Laboratory. Only sera from male mice were included to remove confounding due inter-sex differences. I performed statistical comparisons by t-testing, but after correcting for the number of markers measured, no differences would be significant. I also assessed the correlation of plasma BMP9 levels with serum markers in wildtype mice. No significant correlations were observed (not shown).

Cholesterol and triglycerides are components of cell-membranes and precursors for biosynthetic and metabolic pathways. They are transported in blood as low-density lipoproteins (LDL) and high-density lipoproteins (HDL). Non-esterified fatty-acids (NEFA) are a product of the hydrolysis of triglycerides, and are transported bound to proteins such as albumin. There was no obvious dysfunction in lipid handling in *Gdf2* knockout mice (figure 119). The ratio cholesterol : HDL, which is a risk factor for heart disease in humans, was not different between genotypes (not shown). *Gdf2* knockout mice had lower serum glucose levels than wildtype littermates (figure 120). This was surprising because BMP9 is reported to be an anti-glycaemic and insulin-sensitising factor. The diets of these mice were not restricted, and they were not fasted prior to sample collection, which could contribute to the unexpected result. The ratio glucose : insulin, which is an indicator of dysfunctional blood-glucose regulation, was not different between genotypes.

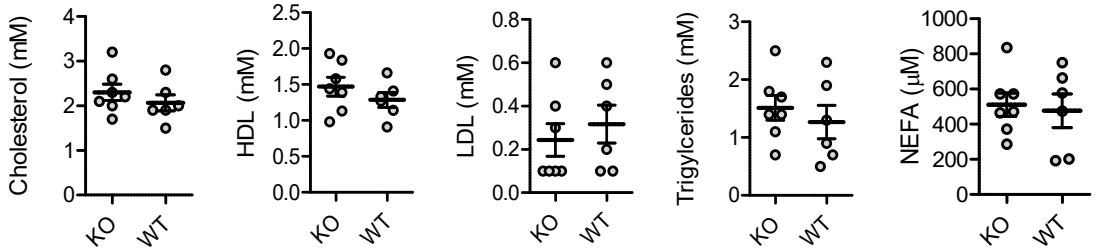

Figure 119. Serum lipid levels in *Gdf2* knockout and wildtype mice. Six wildtype and seven *Gdf2* knockout male mice, aged 4-6 months. Cholesterol, high-density lipoprotein (HDL), low-density lipoprotein (LDL), triglyceride and non-esterified fatty acid (NEFA) levels were measured in sera. Mean ± SEM.

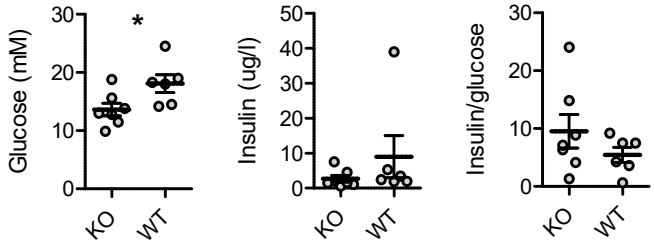

Figure 120. Glucose handling in *Gdf2* knockout and wildtype mice. Six wildtype and seven *Gdf2* knockout male mice, aged 4-6 months. Glucose and insulin levels were measured in sera. Mean ± SEM, unpaired two-tailed Student's t-test, *p < 0.05.

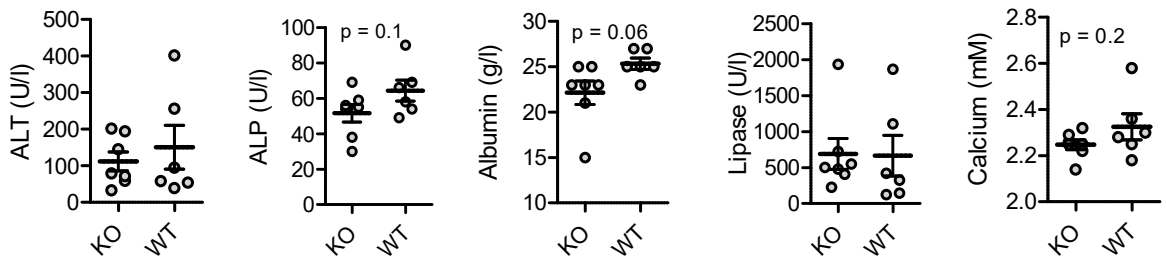

Figure 121. Markers of organ function in *Gdf2* knockout and wildtype mice. Six wildtype and seven *Gdf2* knockout male mice, aged 4-6 months. Alanine amino-transferase (ALT), alkaline phosphatase (ALP), albumin, lipase and calcium levels were measured in sera. Mean ± SEM, unpaired Student's two-tailed t-test.

ALT and ALP are metabolic enzymes, predominantly of the liver, so levels can be elevated after feeding or liver damage. Albumin levels can be depressed after liver damage. *Gdf2* knockout mice had reduced serum albumin levels, but hepatic enzymes were not elevated in serum (figure 121). Lipase can be released into serum after damage to the pancreas and serum calcium levels depend on absorption/secretion from the intestines, bone and kidney. Levels of lipase and calcium were the same in *Gdf2* knockout and wildtype mice.

6.4. Liver transcriptome of *Gdf2* knockout mice

Serum markers provided inconclusive evidence that *Gdf2* knockout mice had dysfunctional livers. Therefore, I measured the level of mRNAs encoding metabolic enzymes in whole-liver extracts from *Gdf2* knockout and wildtype mice by qPCR (figure 122). These genes were found to be regulated by BMP9 *in vitro* by Chen *et al.* (2003). Phosphenolpyruvate carbokykinase 1 (Pck1) catalyses the rate-limiting step of gluconeogenesis. As such, *Pck1* is transcriptionally repressed by insulin, but should be upregulated when blood-glucose levels are low. Despite *Gdf2* knockout mice having lower blood-glucose levels than wildtype littermates, *Pck1* expression was not significantly different between genotypes.

Fatty acid synthase (FASN) catalyses the biosynthesis of aliphatic molecules from acetyl-CoA, so is upregulated after feeding and when glucose levels are high, and ultimately leads to the liver secreting lipids. The expression of *Fasn* was not significantly different between genotypes. Sterol regulatory element binding protein 1 (SREBP1) upregulates the expression of genes required lipogenesis, including *Fasn*. SREBP is primarily regulated by protein cleavage and translocation, but is also transcriptionally activated by insulin. The expression of *Srebp1* was not significantly different between genotypes but the qPCR primers I used were specific to isoforms 1a and 1b. Isoform 1c should be checked since Yang *et al.* (2019) report BMP9 overexpression can regulate it *in vivo* (they did not test a or b).

NADP-dependent malic enzyme (ME) generates NADPH which is the reducing agent required for fatty acid biosynthesis. *Me1* expression can be regulated by diet, thyroid hormones and other factors. Interestingly, *Me1* expression was significantly reduced in *Gdf2* knockout mice compared to wildtype littermates. Importantly, the difference remains significant even after correcting for testing multiple genes. There was also a sex-based trend in *Me1* expression, with female mice having lower levels than males, but this was not statistically significant. Since these metabolic enzymes are regulated by insulin, I tested correlations between their expression level and serum insulin and glucose levels. There were no robust relationships or differences between *Gdf2* knockout and wildtype mice (not shown).

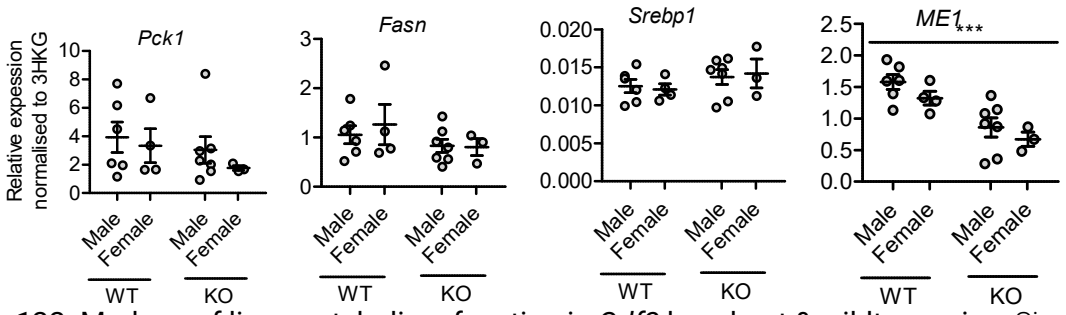

Figure 122. Markers of liver metabolism function in *Gdf2* knockout & wildtype mice. Six male & 4 female wildtype, and 7 male & 3 female *Gdf2* knockout mice, aged 4-6 months. Liver levels of *Pck1, Fasn, Srebp1* & *ME1* liver mRNA were measured compared to three house-keeping genes (*B2M, Hprt, bAct*) by qPCR. Mean ± SEM. Two-way unpaired ANOVA, ***p < 0.001.

To get a comprehensive view of the liver phenotype, I sent whole liver RNA samples to Dr. Mattia Frontini for RNAseq analysis. He returned a list of genes up or downregulated in *Gdf2* knockouts compared to wildtype littermates with a posterior probability of 0.5 (202 genes) or 0.3 (486 genes). I calculated the mean expression level of each gene in each genotype and the relative fold-change in expression between genotypes (figure 123). Reassuringly, there was a high probability of *Gdf2* expression being different between groups. *Me1* expression was also different between groups, which I had already shown by qPCR.

In order to predict the consequences of these transcriptome changes, I carried out pathway analysis. Firstly I analysed the list of genes differently expressed between wildtype and *Gdf2* knockout mice with the Gene Ontology Consortium's GO-term enrichment analysis tool (Ashburner et al. 2000; The Gene Ontology Consortium 2019). Genes involved in lipid metabolism were heavily overrepresented ($p_{adj} < 10^{-9}$) in this list. Fatty-acid metabolism was particularly dysregulated ($p_{adj} < 10^{-9}$), but so were various other lipid handling pathways. Consistent with the data for *ME1*, most of these genes appeared to be downregulated in *Gdf2* knockout mice, suggesting reduced lipid metabolism. Additionally, xenobiotic metabolism or oxidative catabolism pathways were downregulated in *Gdf2* knockout mice ($p_{adj} < 10^{-3}$), including several cytochrome P450s, glutathione S-transferases and genes involved in the peroxisome. Strikingly, factors involved with circadian regulation of gene expression were disrupted ($p_{adj} < 10^{-2}$). Finally, responses to misfolded proteins, vesicle budding, and transport may have been impaired.

Figure 123 (overleaf). Genes dysregulated in *Gdf2* knockout mice. Five wildtype and *Gdf2* knockout male mice, aged 4-6 months analysed by RNAseq. Top: genes with higher expression in wildtype livers. Bottom: genes with lower expression in wildtype livers. X-axis = mean relative fold change in expression between genotypes, y-axis = posterior probability, bubble size = mean expression level in wildtype liver.

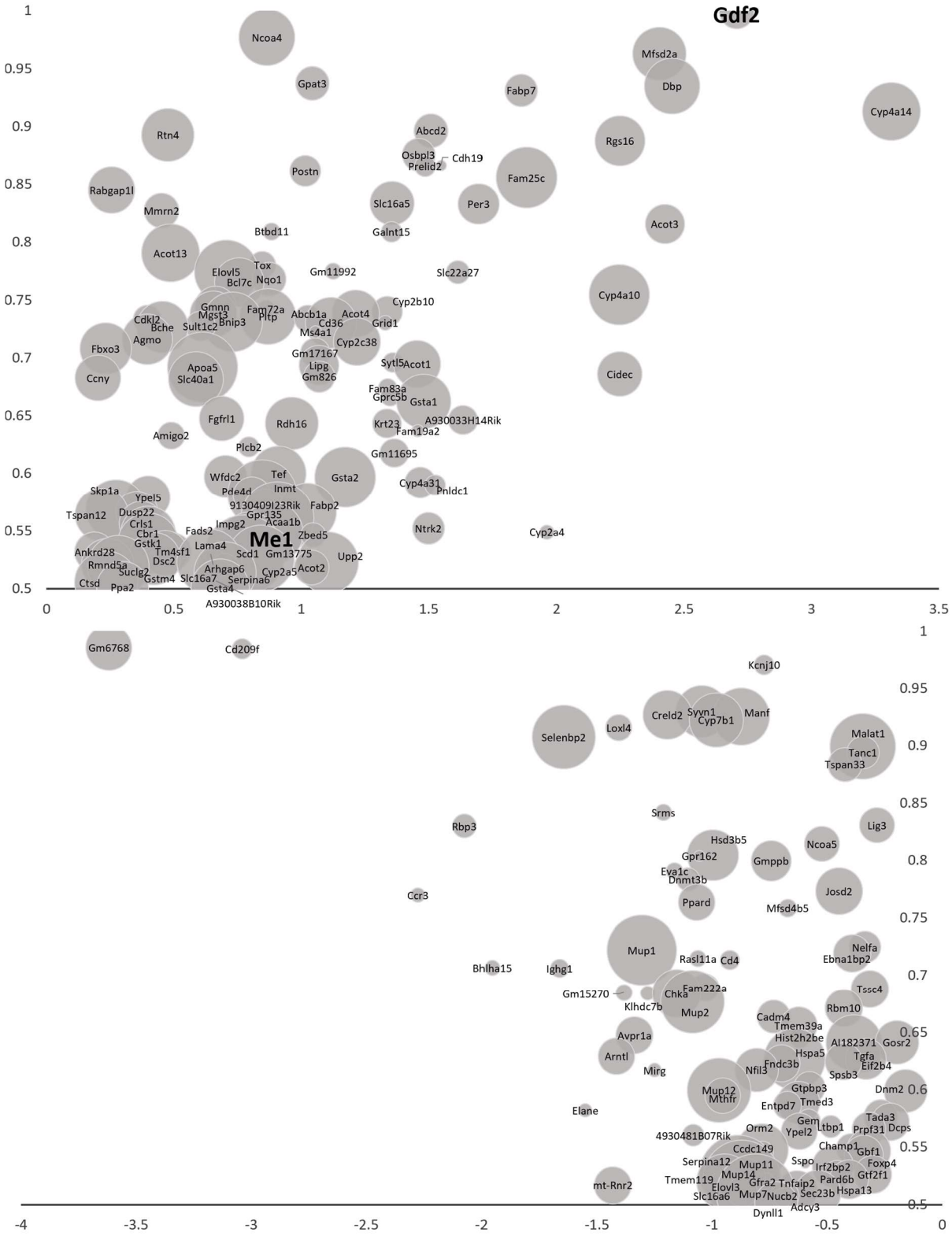

To confirm these results and identify additional pathways, I used network analysis of reported gene interactions using the STRING consortium tool (Szklarczyk et al. 2019). As expected, many genes differently expressed between *Gdf2* knockout and wildtype mice were linked in a cluster responsible for fatty-acid and xenobiotic metabolism (figure 124). The tool

imputed the involvement of genes that were not themselves dysregulated in *Gdf2* knockout mice if they were linked with high confidence to those that were. This produced a cluster involved in circadian rhythms, including *Cry*, *Per* and *Clock* genes. Several genes involved in the endoplasmic reticulum, glycosylation, protein translation and transport *etc.* were also clustered. These results validated the gene ontology analysis. Unexpectedly, many genes encoding components of the spliceosome were implicated by network analysis. Dr. Mattia Frontini is re-analysing the RNAseq data to search for mRNA splice-variants, rather than just transcript counts, to see what affects this might have. Similarly, several core cell-cycle regulators were linked to genes dysregulated in *Gdf2* knockout mice. These included genes encoding Cul, Skp and other ubiquitin ligase proteins, and several DNA replication factors.

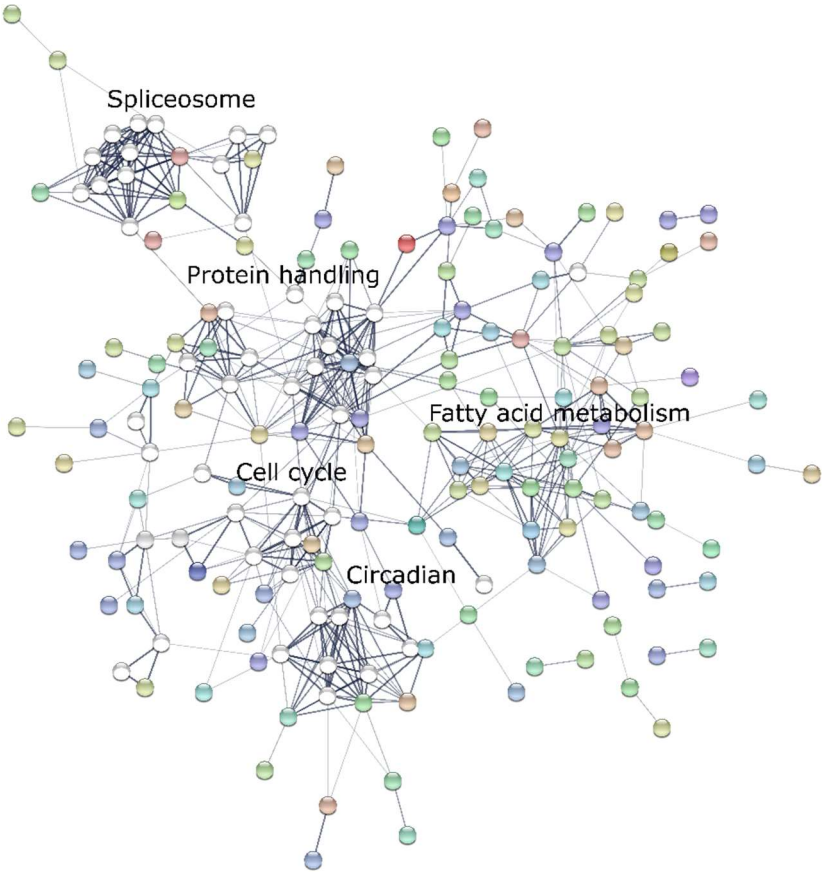

Figure 124. Network analysis of genes dysregulated in *Gdf2* knockout mice. Genes up/down regulated in *Gdf2* knockout mice compared to wildtype littermates with posterior probability > 0.5 were used as query genes (coloured nodes) in the Search Tool for Retrieval of Interacting Genes/Proteins. Other genes (white nodes) in the network were imputed by their relationship to query genes. Thickness of edges = strength of evidence linking nodes. Evidence includes experimentally determined interactions, predicted interactions, text-mining, co-expression and homology. Only genes linked in the network are shown. I manually identified clusters by eye, and by K means clustering with 5 clusters, and assigned processes by reviewing the function of each gene in each cluster.

BMP9 is reported to modulate hepatic inflammation and fibrosis. Inflammation associated genes were not significantly overrepresented among those dysregulated in *Gdf2* knockout mice. However, GO-term enrichment and network analyses did not take many factors, including the direction, degree and confidence of expression change, the organ of interest, or the phenotypes of interest, into account. Therefore, I identified all genes dysregulated in *Gdf2* knockout livers with a posterior probability > 0.3 which were associated with terms related to inflammation and liver disease/regeneration (figure 125).

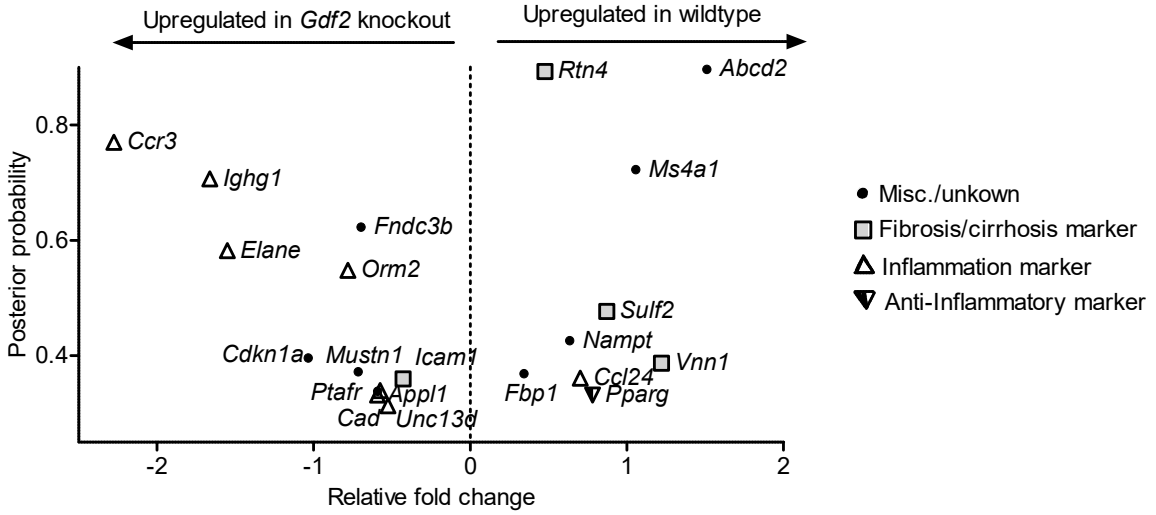

Figure 125. Inflammation & damage associated gene expression in *Gdf2* knockout livers. Genes associated with gene ontology terms related to inflammation and liver disease are shown. I have manually classified these as markers of fibrosis or inflammation. X-axis = mean relative fold change in expression between genotypes.

Several genes upregulated in *Gdf2* knockout mice with high confidence are markers of inflammation. These include: *Ccr3*, encoding a chemokine receptor; *Ighg1*, encoding the constant region of immunoglobulin heavy chain γ; *Elane*, encoding neutrophil elastase; *Orm2*, encoding an acute-phase protein which is reported to be secreted by stressed livers (Porez et al. 2013); *Ptafr*, encoding a platelet activating receptor; *Appl1*, encoding a positive regulator of inflammation and proliferation associated with fatty-liver disease (Barbieri et al. 2013); and *Unc13d*, encoding a protein involved with release of cytolytic granules from immune cells. Similarly, *Pparg* which encodes a receptor involved with triglyceride metabolism, but is known to have anti-inflammatory effects, is downregulated in *Gdf2* knockout livers (Martin 2010).

Three genes downregulated in *Gdf2* knockout livers are markers of fibrosis or cirrhosis. These are: *Rtn4*, which is upregulated in cirrhosis with *Rtn4* knockout mice protected from fibrosis (Gao et al. 2013; D. Zhang et al. 2011); *Sulf2*, which is upregulated in cirrhosis and injury induced regeneration (Singer et al. 2015; Graham, Murphy, and Dhoot

2016); and *Vnn1*, which is upregulated after liver injury with *Vnn1* knockout mice predisposed to liver injury (Chen et al. 2014; Ferreira et al. 2016).

However, *Icam1* was upregulated in *Gdf2* knockout mice, and is a marker of fibrosis, with *Icam1* knockout mice protected from liver disease (Kono et al. 2001; Theruvath et al. 2012). However, ICAM1 also facilitates regeneration and proliferation, so this might be expected (Selzner et al. 2003). Similarly, *Ccl24*, which encodes an inflammatory chemotaxic chemokine, is downregulated in *Gdf2* knockout mice. Notably, *Col1a1*, encoding type-1 collagen, which is a read-out in models of fibrosis, was not differently expressed between wildtype and *Gdf2* knockout mice (figure 126).

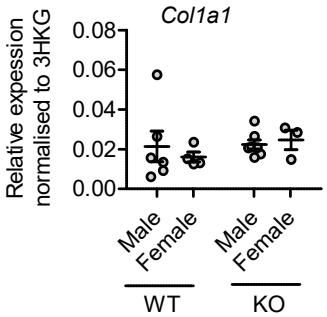

Figure 126. Marker of liver fibrosis in *Gdf2* knockout and wildtype mice. Six male & 4 female wildtype, and 7 male & 3 female *Gdf2* knockout mice, aged 4-6 months. Levels of *Col1a1* mRNA were measured compared to three house-keeping genes (*B2M, Gapdh, bAct*) by qPCR. Mean ± SEM.

6.5. *Gdf2* knockout mice have normal blood cell counts

Some transcriptional markers of inflammation were increased in *Gdf2* knockout mice. Additionally, the Morrell group has found *Bmpr2* deficient mice have different numbers of circulating immune cells than wildtype mice (Crosby et al. 2018). The Morrell group and others found PAH patients have altered white blood cell profiles, and there is evidence that PAH is associated with immunological dysfunction (Ormiston et al. 2012; Holmes et al. 2010). In humans with PAH, those with the lowest plasma BMP9 levels had significantly higher red-cell distribution widths (RDW) and significantly lower platelet counts than patients with normal plasma BMP9 levels (although the averages of both are within the healthy range) (Hodgson et al. 2019). Similarly, patients with the lowest plasma pBMP10 levels have significantly higher RDWs, and higher white blood cell counts (WBC) than patients with normal plasma pBMP10 levels. WBC also trends to be lower in patients with low plasma BMP9 levels ($p = 0.08$)(Hodgson et al. 2019). Therefore, I performed cell counts of EDTA-blood from *Gdf2* knockout, heterozygous and wildtype mice (figure 127). In mice, there were significant differences in blood counts between sexes, but no significant differences or

promising trends between genotypes. Nonetheless the effect sizes in humans for RDW, WBC and platelet count were small (10-20%), which this mouse study was underpowered to detect.

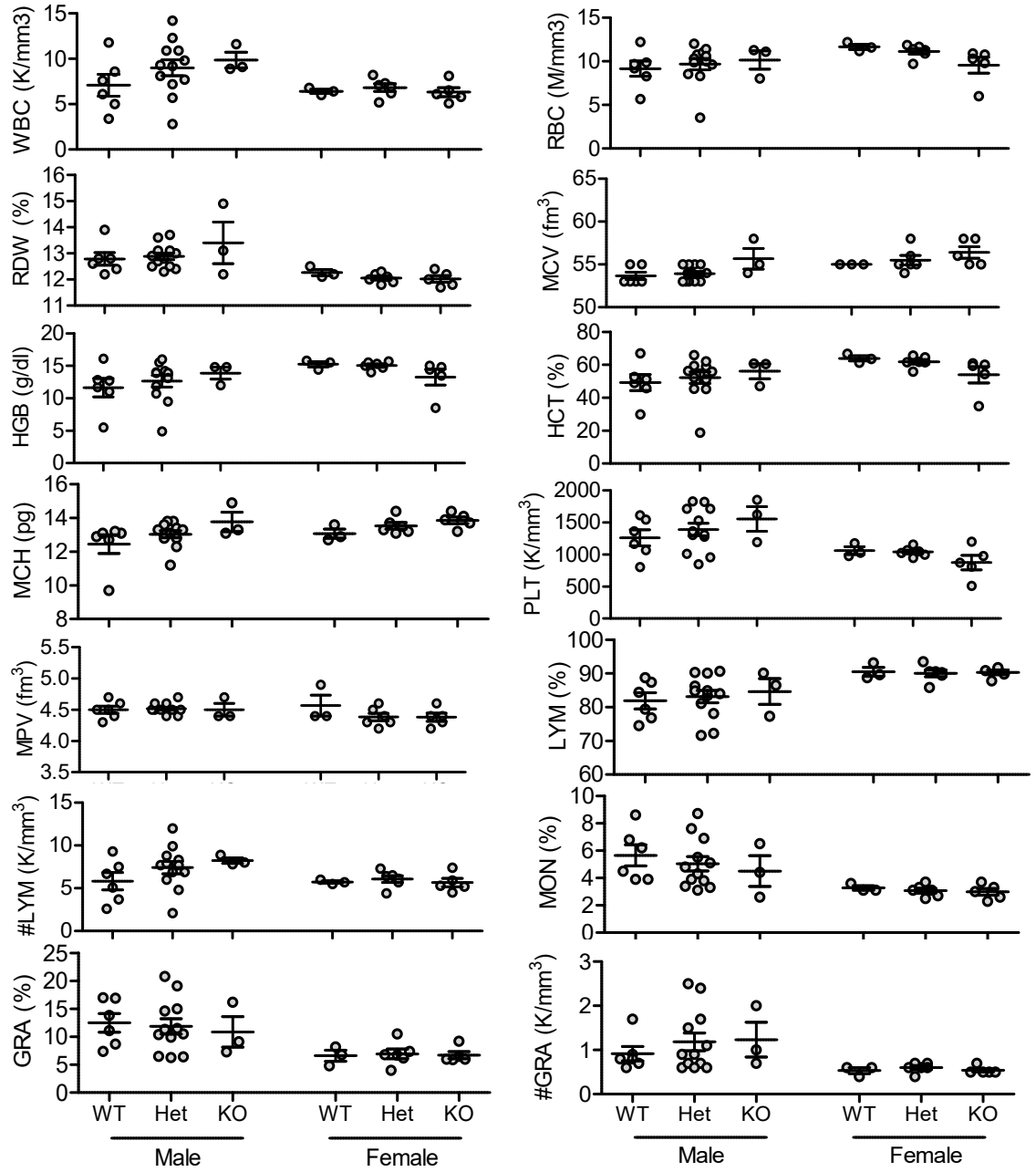

Figure 127. Blood counts of *Gdf2* knockout, heterozygous and wildtype mice. Blood cell properties were analysed by a Wooley ABC cell-counter. WBC = white blood cell count, RBC = red blood cell count, RDW = red blood cell distribution width (MCV deviation / MCV x 100), MCV = mean cell volume, HGB = haemoglobin concentration, HCT = haematocrit, MCH = mean amount of haemoglobin per red blood cell, PLT = platelet count, MPV = mean platelet volume, LYM = lymphocytes, MON = monocytes, GRA = granulocytes. Mean ± SEM

6.6. BMP9 & BMP10 levels in *Gdf2* knockout mice

Bmp10 is primarily expressed in the right atrium, but it may also be expressed in the liver. *Gdf2* is primarily expressed in the liver, but also the lung. In humans we observed

heterozygous *GDF2* mutation carriers had BMP9 levels reduced by about 50%, very low levels of pBMP10, and this predisposed them to disease (see 3.4). We wanted to assess how *Gdf2* mutations alter BMP9 and BMP10 expression and signalling in different tissues, to understand why the pulmonary vasculature is destabilised. I undertook to measure mRNA and protein levels of BMP9 and BMP10 in different organs by qPCR and ELISAs in *Gdf2* knockout, heterozygous and wildtype mice.

Since I already had the samples, I began by measuring mRNA levels in livers. Both *Gdf2* and *Bmp10* were more highly expressed in the livers of females than males (figure 128). Consistent with transcriptomic databases, *Bmp10* expression was much lower than *Gdf2* expression in the liver. In accordance with Tillet *et al.* (2019), liver *Bmp10* expression was not disrupted in *Gdf2* knockout mice. In human plasma, BMP9 and pBMP10 levels are correlated. Therefore, I assessed the correlation of their transcripts in mouse livers. There was a striking correlation between *Gdf2* and *Bmp10* expression in wildtype mice ($p = 0.003$). However, unlike the correlation in plasma levels, this was entirely explained by sex (figure 129).

The expression of *Gdf2* and *Bmp10* in the liver was well correlated due to sex, and both decline after insults such as LPS injection (figure 138). Therefore, both genes may be regulated by the same transcription factors. To investigate this, I interrogated both genes on Genevestigator which ranks the correlation in expression between genes (https://genevestigator.com/gv/). For both mouse and human datasets, of all genes, *GDF2* expression was most correlated with *BMP10* expression. However, I could not assess how comprehensive and reliable the underlying datasets are.

I used ChIP-Atlas to investigate which transcription factors may regulate both *Gdf2* and *Bmp10* (Oki et al. 2018). Both genes bound many factors, with binding sites clustered in certain regions as expected. *Gdf2* appeared to have a fairly canonical architecture, with the greatest number of factors binding immediately upstream of the transcription start site. *Bmp10* was more difficult to analyse since the most active regulatory region appeared to be within the intron, shortly downstream of the transcription start site. Several transcription factors bound to both *Gdf2* and *Bmp10*, including numerous binding sites for sex-hormones (oestrogens, progestrogen, glucocorticoids) which could explain the sex difference in expression. Nonetheless, ChIPseq data is notoriously noisy, and it is difficult to assign functional importance to these binding sites. Moreover, it is difficult to assess whether certain factors bind *Gdf2* and *Bmp10* more than expected compared to other genes, and whether they share a disproportionate number of common factors.

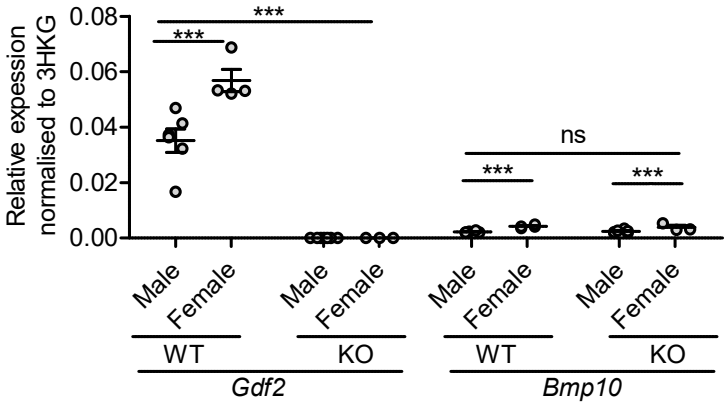

Figure 128. *Gdf2* & *Bmp10* expression in *Gdf2* knockout & wildtype mouse livers. Six male & 4 female wildtype, and 7 male & 3 female *Gdf2* knockout mice, aged 4-6 months. Levels of *Gdf2* and *Bmp10* mRNA were measured compared to three house-keeping genes (*B2M, Gapdh, bAct*) by qPCR. Two-way unmatched ANOVA/Bonferroni test, ***p < 0.001, ns = not significant, mean ± SEM.

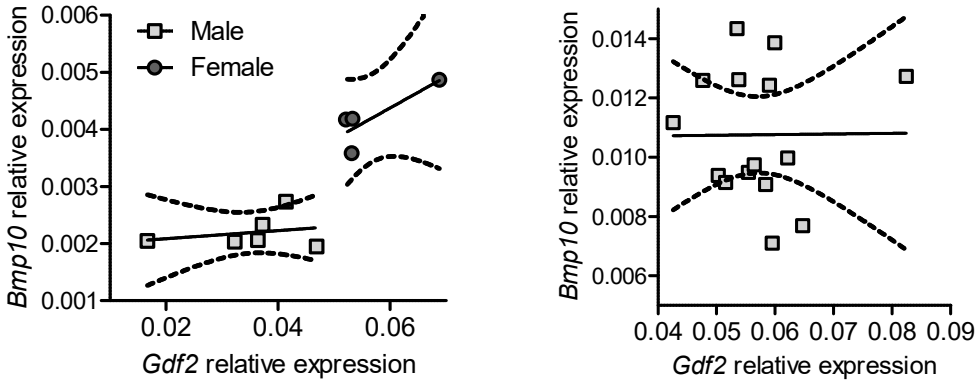

Figure 129. *Gdf2* & *Bmp10* expression in *Gdf2* knockout & wildtype mouse livers. Left: Correlation between data in figure 128. **Right:** left, repeated with 15 males.

6.7. Use of Evans blue to measure pulmonary vascular leak

Evans blue is a dye which can be administered to live animals and binds albumin. The Morrell group reported that pulmonary vascular permeability to macromolecules, as measured by the accumulation of Evans blue in lungs, can be supressed by administering BMP9 to mice (Long et al. 2015). Conversely, anti-BMP9 enhanced pulmonary vascular leak (Li et al. 2018). In these studies, some mice were given LPS by intraperitoneal injection to stimulate vascular leak. Sixteen hours after LPS administration, a solution of Evans blue and bovine serum albumin was given by intraperitoneal injection. After a further hour, mice were killed, and lungs were flushed with heparinised saline to remove Evans blue remaining within blood vessels. The amount of residual Evans blue in lungs was measured.

We assessed the extravasation of Evans blue into lungs of *Gdf2* knockout and heterozygous mice, and *Bmpr2-C118w* and *Bmpr2-R584X* heterozygous mice. We gave Evans blue intravenously, rather than intraperitoneally, to control the concentration of circulating

dye. We did not have many littermates of each genotype, so this study was underpowered. There was no trend for *Gdf2* deficient mice to have increased extravasation of Evans blue into lungs (figure 130). Unlike published results for *Bmpr2-R899X* heterozygous mice, *C118W* and *R584X* mice exhibited no evidence of reduced endothelial integrity (figure 131).

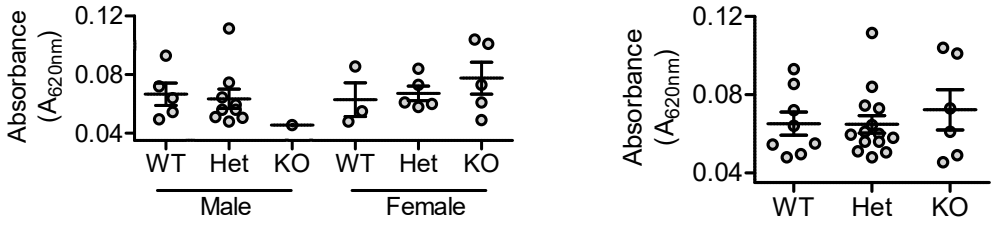

Figure 130. Leak of Evans blue across the pulmonary vasculature of *Gdf2* knockout, heterozygous and wildtype mice. 1 % (w/v) Evans blue dye was dissolved in PBS supplemented with 4% endotoxin free BSA. Mice were given 20 mg/kg of Evans blue intravenously. After 30 minutes, mice were killed and flushed. The amount of residual Evans blue extracted from lungs was measured by colourimetry. Left: Separated by sex Right: Grouped. Mean ± SEM.

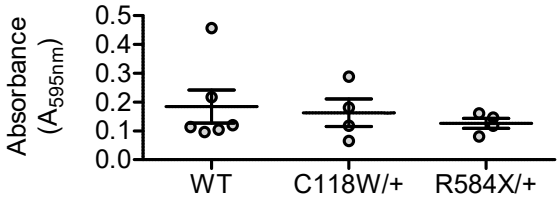

Figure 131. Leak of Evans blue across the pulmonary vasculature of *Bmpr2* heterozygous and wildtype mice. 1 % (w/v) Evans blue dye was dissolved in PBS. Mice were given 20 mg/kg of Evans blue intravenously. After 30 minutes, mice were killed and flushed. The amount of residual Evans blue extracted from lungs was measured by colourimetry. Mean ± SEM.

We were not sure if our Evans blue protocol was working, and if so, we wanted to stress mice to reveal a phenotype. Firstly, we replicated existing results by showing intraperitoneal injections of LPS increased extravasation of intraperitoneally administered Evans blue into lungs by approximately the expected amount (figure 132). However, the intestines of these mice appeared to accumulate Evans blue, and there were large amounts of unabsorbed Evans blue within the abdomen. This protocol used intraperitoneal injection of Evans blue and LPS, which potentially means altered uptake of Evans blue from the abdomen into blood, rather than altered pulmonary vascular leak, determines the absorbance of lung extracts. To investigate this, I measured the wet to dry weight ratio of lungs from the same mice, to assess whether oedema fluid was accumulating in the lungs of LPS treated mice (figure 133). However, lungs must be flushed thoroughly prior to Evans blue extraction, and the high pressures used may also cause oedema.

Intravenous administration of Evans blue is more likely to give an unconfounded measure of pulmonary vascular leak. Some protocols use higher concentrations of Evans blue,

or Evans blue that is not premixed with albumin (Akla et al. 2018; Wick et al. 2018). The optimal time for assessing leak is reported to be one-hour after injection of Evans blue (Moitra, Sammani, and Garcia 2007). The dose, route of administration and duration of LPS treatment varies considerably between published protocols.

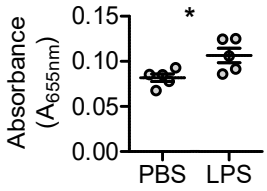

Figure 132. Leak of Evans blue across the pulmonary vasculature of mice given LPS. Male mice were given 1 mg/kg LPS (B5 serotype) or PBS vehicle control intraperitoneally. 1 % (w/v) Evans blue dye was dissolved in PBS supplemented with 4% endotoxin free BSA. After 20 hours, mice were given 40 mg/kg of Evans blue solution intraperitoneally. After 60 minutes, mice were killed and flushed. The amount of residual Evans blue extracted from lungs was measured by colourimetry. Unmatched one-tailed Student's t-test, *p < 0.05, n = 5, mean ± SEM.

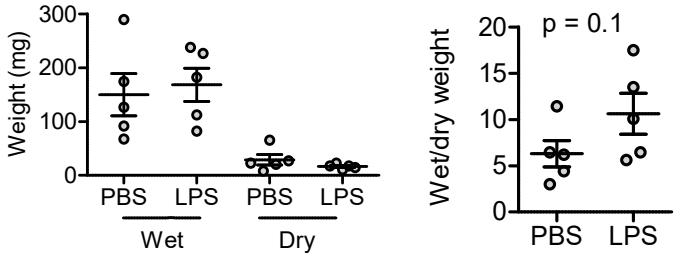

Figure 133. Leak of fluid across the pulmonary vasculature of mice given LPS. Male mice were given 1 mg/kg LPS (B5 serotype) or PBS vehicle control intraperitoneally. After 20 hours, mice were killed. **Left:** lungs were weighed before (wet) and after (dry) a 48-hour incubation at 60 °C in unsealed tubes. **Right:** the ratio of wet weight / dry weight was calculated for each lung. . Unmatched one-tailed Student's t-test, n = 5, mean ± SEM.

To optimise a protocol for studying pulmonary vascular leak, I used column filtration to show the majority of Evans blue in treatment solutions was not bound to albumin (figure 134). This is consistent with early reports of binding kinetics (Freedman and Johnson 1969). Therefore, we used free Evans blue in subsequent protocols as a method to assess the leak of small molecules, rather than a composite of small molecules and macromolecular complexes. Firstly, we administered 1 mg/kg of LPS intraperitoneally. The next morning, we administered 20 mg/kg of free Evans blue intravenously one-hour before mice were killed. The mice became very sick after LPS injection and several had to be euthanised which precluded us from repeating this protocol. Moreover, there was no evidence of increased leak across the pulmonary vasculature of LPS treated mice compared to control mice (figure 135). We tested several different isoforms of LPS, since there are reports they stimulate different responses. Isoform did not appear to make a difference.

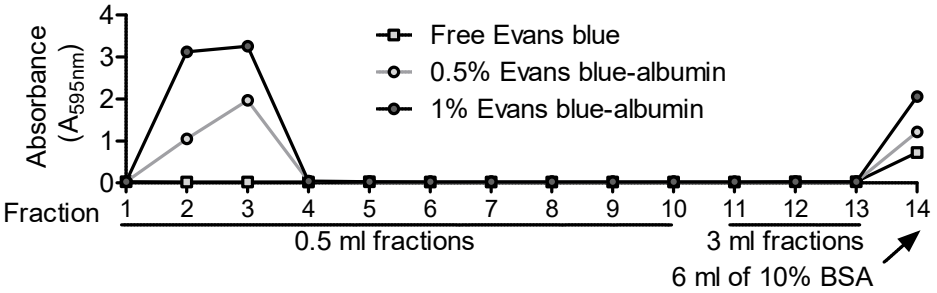

Figure 134. Size exclusion chromatography of Evans blue. Evans blue (1% or 0.5% (w/v)) dissolved in PBS or PBS supplemented with 4 % mouse serum albumin was analysed by size exclusion chromatography. The amount of Evans blue in fractions was assessed by colourimetry.

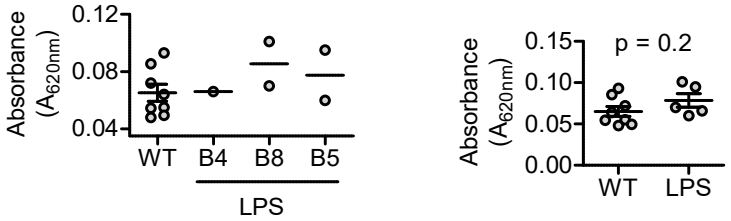

Figure 135. Leak of Evans blue across the pulmonary vasculature of mice given LPS. Male mice were given 2 mg/kg LPS or PBS vehicle control intraperitoneally. 1 % (w/v) Evans blue dye was dissolved in PBS. After 20 hours, mice were given 20 mg/kg of Evans blue solution intravenously. After 60 minutes, mice were killed and flushed. The amount of residual Evans blue extracted from lungs was measured by colourimetry. **Left:** serotypes of LPS shown, **right:** composite of serotypes, unmatched one-tailed Student's t-test, n = 5, mean ± SEM.

Next, we referred to data showing transcriptional markers of inflammation in the liver and lungs respond to lower doses of intraperitoneal LPS if shorter time-points are assessed (Morrell unpublished). We designed a protocol where mice were given 0.1 mg/kg LPS for 3 hours, which does not cause unacceptable sickness, prior to an intravenous injection of Evans blue. Power was calculated based on the variability and effect size reported in Long *et al.* (2015). Again, there was no evidence of increased pulmonary vascular leak caused by LPS (figure 136; 137). To confirm the LPS was active, I assessed the expression of *Gdf2*, which is known to fall in response to LPS, and *Bmp10* in livers of these mice (figure 138).

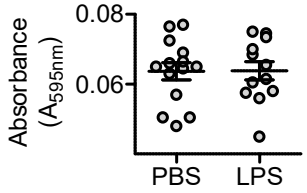

Figure 136. Leak of Evans blue across the pulmonary vasculature of mice given LPS. Male mice were given 0.1 mg/kg LPS (B5 serotype) or PBS vehicle control intraperitoneally. 1 % (w/v) Evans blue dye was dissolved in PBS. After 3 hours, mice were given 40 mg/kg of Evans blue solution intravenously. After 60 minutes, mice were killed and flushed. The amount of residual Evans blue extracted from lungs was measured by colourimetry. Unmatched one-tailed Student's t-test, n = 20, mean ± SEM.

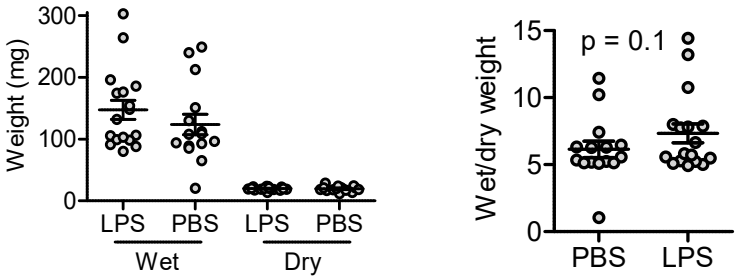

Figure 137. Leak of fluid across the pulmonary vasculature of mice given LPS. Male mice were given 0.1 mg/kg LPS (B5 serotype) or PBS vehicle control intraperitoneally. After 4 hours, mice were killed. **Left:** lungs were weighed before (wet) and after (dry) a 48-hour incubation at 60 °C in unsealed tubes. **Right:** the ratio of wet weight / dry weight was calculated for each lung. Unmatched one-tailed Student's t-test, n = 20, mean ± SEM.

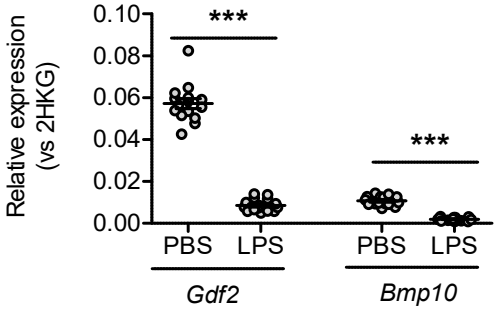

Figure 138. Transcriptional response to intraperitoneal LPS administration. Male mice were given 0.1 mg/kg LPS (B5 serotype) or PBS vehicle control intraperitoneally. After 4 hours, mice were killed. Liver levels of *Gdf2* and *Bmp10* mRNA were measured compared to two housekeeping genes (*B2M, Gapdh*). Unmatched one-tailed Student's t-test, n = 20, mean ± SEM.

We then tried intranasal administration of LPS as this is used in models of acute respiratory distress syndrome. Three hours after LPS inhalation, mice were given Evans blue intravenously and killed after a further hour. I found no evidence of increased pulmonary vascular leak in these mice (figure 139). I assessed whether there was an inflammatory response in the lungs to LPS by qPCR. There was a slight reduction in lung *Smad9* and *Gdf2* relative expression, but LPS treatment increased the expression of housekeeping genes used for normalisation, likely because this model causes neutrophils to accumulate within the lungs (figure 140). Nonetheless, *IL6* expression was strongly upregulated, which would be even more pronounced if housekeepers were stable. Therefore, intranasally administered LPS successfully caused lung inflammation, even though vascular permeability was unchanged.

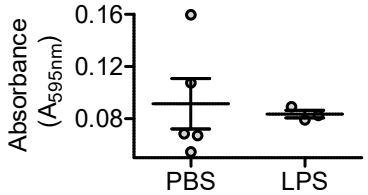

Figure 139. Leak of fluid across the pulmonary vasculature of mice given LPS. Male mice were given 0.1 mg/kg LPS (B5 serotype) or PBS vehicle control intranasally. 1 % (w/v) Evans blue dye was dissolved in PBS. After 3 hours, mice were given 40 mg/kg of Evans blue solution intravenously. After 60 minutes, mice were killed and flushed. The amount of residual Evans blue extracted from lungs was measured by colourimetry. Unmatched one-tailed Student's t-test, n = 5, mean ± SEM.

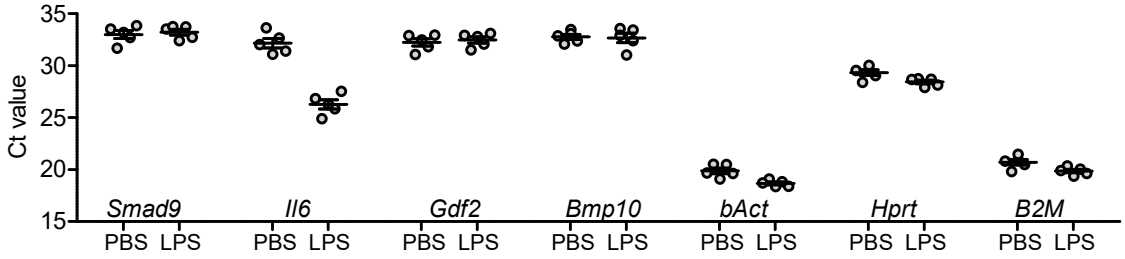

Figure 140. Lung inflammation in mice lungs given LPS. Male mice were given 0.1 mg/kg LPS (B5 serotype) or PBS vehicle control intranasally. 1 % (w/v) Evans blue dye was dissolved in PBS. After 4 hours, mice were killed. Lung expression of *Smad9, Il6, Gdf2, Bmp10* and the housekeepers *bAct, Hprt* and *B2M* was assessed by qPCR. n = 5, mean ± SEM.

Protocols simulating acute respiratory distress syndrome often wait one to three days after LPS exposure before disease reaches its greatest severity (Moitra, Sammani, and Garcia 2007; Schlosser et al. 2018; Honglei Chen et al. 2014; Birukova et al. 2010). Therefore, we repeated the intranasal LPS protocol, but did not administer Evans blue until the following day. These mice showed increased pulmonary vascular leak as measured by Evans blue extravasation, indicating targeted administration of LPS could disrupt the pulmonary endothelium after 24 hours (figure 141).

In summary, I was able to show intravenous injection of 40 mg/kg Evans blue 1 hour prior to sacking is an appropriate way to assess pulmonary vascular leak. As a positive control, or to exacerbate leak phenotypes, LPS could be administered intranasally 24 hours before assessing leak. To reduce batch effects, all mice should be put through the protocol together. Where this is impossible, lungs should be frozen until Evans blue can be extracted simultaneously and control mice should be present in each batch. *Gdf2* deficient mice did not have pulmonary endothelial leak at baseline, when given 20 mg/kg of Evans blue 30 minutes prior to killing. This is in contrast to what Li *et al.* (2018) found with acute BMP9 neutralisation, suggesting chronic loss may be partially accommodated. LPS could be given to reveal any cryptic pulmonary vascular leak phenotype of *Gdf2* knockout mice.

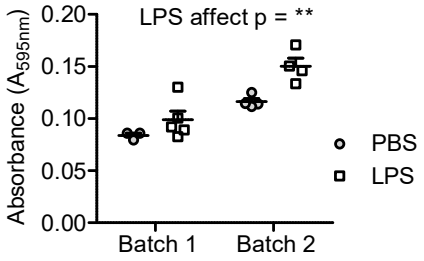

Figure 141. Leak of fluid across the pulmonary vasculature of mice given LPS. Male mice were given 0.1 mg/kg LPS (B5 serotype) or PBS vehicle control intranasally. 1 % (w/v) Evans blue dye was dissolved in PBS. After 15 hours, mice were given 40 mg/kg of Evans blue solution intravenously. After 60 minutes, mice were killed and flushed. The amount of residual Evans blue extracted from lungs was measured by colourimetry. Two batches of mice underwent the protocol on separate days, and results were analysed by unmatched two-way ANOVA, n = 4, mean ± SEM.

6.8. Discussion

BMP9 administration or overexpression has been shown to alter glucose and lipid handing (Chen et al. 2003; Yang et al. 2019). However, this has never been assessed in the more physiological setting of *Gdf2* deficiency. Serum markers provided no evidence of impaired lipid handling although there was a tendency for glucose levels to be altered in *Gdf2* knockout mice. Expression of insulin sensitive enzymes was not changed in the livers of *Gdf2* knockout mice, but more nuanced glucose tolerance tests and assessments of body fat, in mice given more inducive diets, may reveal a phenotype. For example, Yang *et al.* (2019) found *Fasn* expression was only dysregulated in BMP9 over-expressing mice fed a high-fat diet. Besides, for the first time, we undertook an unbiased, comprehensive assessment of gene expression in *Gdf2* knockout mice. Liver transcriptomics revealed they had disrupted fatty acid metabolism and oxidative catabolism.

In the liver, BMP9 signalling inhibits hepatocyte proliferation and predisposes to injury. I saw evidence of this in the liver transcriptome of *Gdf2* knockout mice, with cell-cycle pathways dysregulated, some markers of inflammation upregulated, and some markers of injury downregulated. It would be sensible to measure circulating cytokines in *Gdf2* knockout mice and people with mutations or low BMP9 levels, especially because an inflammatory milieu may predispose to PAH.

Nonetheless, the liver did not appear to be profoundly damaged in *Gdf2* knockout mice, since serum markers such as ALP, ALT and albumin were normal, and liver collagen expression was not elevated. This is not consistent with data in Desroches-Castan *et al.* 2019, however they had ten mice in each group and relatively high variability. Moreover, they recently reported the hepatic inflammatory and fibrotic phenotype of *Gdf2* knockout mice is only seen on the 129/Ola background, not C57/BL6 or BALB/c mice (Desroches-Castan et al. 2019 b). Similarly, BMP9 levels in wildtype mice did not correlate with markers of liver dysfunction and inflammation, although there were some subtle relationships in human serum (Hodgson et al. 2019). Mark Southwood is undertaking a histological analysis of livers I collected from *Gdf2* knockout and wildtype littermates to look for gross abnormalities. Staining for inflammatory cells may be interesting since Desroches-Castan *et al.* report they accumulate within *Gdf2* knockout livers. Overall, the unbiased whole-transcriptome data provides more robust evidence supporting the current literature suggesting *Gdf2* deficiency causes relatively subtle liver dysfunction.

Surprisingly, there was transcriptomic evidence that circadian rhythms, splicing and protein handling were disrupted in the livers of *Gdf2* knockout mice. These are novel findings, which need validating and could have broad implications. For example, we expected BMP9 deficiency to alter cell proliferation, and circadian cycles are often synchronised to cell cycles (Heltberg and Jensen 2019; Droin, Paquet, and Naef 2019). Many metabolic pathways are circadian controlled or regulated by alternative splicing (Reinke and Asher 2016). Therefore, it is unclear exactly which pathways are direct targets of BMP9.

To reproduce these findings, I am collecting tissues from fresh *Gdf2* knockout, heterozygous and wildtype mice. Additionally, I could look at these transcripts in mice given anti-BMP9 or BMP9-AAV, which are models of short-term *Gdf2* deficiency and short-term overexpression respectively, already being prepared. I am preparing lung samples from *Gdf2* knockout mice for RNAseq, and it will be interesting to see if the same pathways are dysregulated here. BMP9 levels could be measured in plasmas collected at different times of day to see if levels oscillate.

Plasma levels of BMP9 and BMP10 are tightly correlated in humans, and they are expressed in the same organs, albeit at different levels. Similarly, there is some evidence *Gdf2* and *BMP10* mRNA levels are correlated. We are collecting samples to assess levels of both factors in different organs (right-atria, liver, lung, kidney, spleen) in *Gdf2* knockout, heterozygous and knockout mice. This may shed light on their co-regulation. Additionally, markers of BMP9/10 signalling will also be assessed in these organs to develop a comprehensive picture of how *Gdf2* deficiency affects them.

Discussion & future directions

Mutations in *BMPR2* cause the majority of heritable PAH, and deficiency of BMPR-II receptor complex signalling has been invoked to explain the majority of PAH. Nonetheless, Gräf *et al.* (2018) were the first to systematically link mutations in the gene encoding the high-affinity ligand for this receptor, *GDF2*, to PAH. More recently, Wang *et al.*, Eyries *et al.*, and Zhu *et al.* (2019) also discovered rare, PAH-associated missense variants in *GDF2* predicted to be deleterious *in silico*. We expressed *GDF2* missense variants found in PAH *in vitro* and showed only those predicted to be pathogenic *in silico* have impaired secretion due to instability of the processed Pro:BMP9 complex. Previous reports showed a secretion defect in some missense variants predicted to be pathogenic, but did not compare them to those predicted to be benign, or attempt to explain the secretion defect (Wang et al. 2019; Wooderchak-Donahue et al. 2013). Notably, no single predictor of deleteriousness was sufficient to define

whether missense variants were pathogenic or benign. For example, Pro:BMP9-D218N contained a novel glycosylation site, but had normal bioactivity. Pro:BMP9-Y351H has severely impaired secretion and activity *in vitro* and *in vivo*, disrupting the core of BMP9, but was not significantly over-represented in PAH in the British cohort.

Surprisingly, measurement of patient samples revealed that *GDF2* mutation carriers have heavily reduced plasma levels of both BMP9 and pBMP10. Therefore, both ligands could be necessary to protect the pulmonary vasculature from PAH. The Morrell group has an inducible *Bmp10* knockout mouse, so the haemodynamics and histology of this animal could be measured in the sugen-hypoxia model of PAH. However, given this approach did not reveal a phenotype in *Gdf2* knockout mice, a negative result should not rule out a role for BMP10 in protecting against PAH. Larger genetic analyses may definitively link loss-of-function *BMP10* mutations in humans to PAH, building on the cases reported by Eyries *et al.* and Gräf *et al.*

Levels of circulating total pBMP10 are ~5 ng/ml in healthy people, but consensus in the literature suggests half to all circulating activity is due to BMP9 (Jiang et al. 2016; Chen et al. 2013; Bidart et al. 2012). Therefore, I compared levels of unprocessed *ProBMP10* and processed Pro:BMP10 by ELISAs, immunoprecipitations and activity assays. These suggested plasma pBMP10 is predominately unprocessed in most people. To confirm this novel hypothesis, Western blots of endogenous pBMP10 could be refined, perhaps by immunoprecipitation of fractions separated by size exclusion chromatography, which may be cleaner than immunoprecipitation of neat plasma/serum. Similarly, furin treatment of these fractions could be attempted, which may work more efficiently than treatment of neat serum. Finally, tissue extracts of human right atria could be probed by ELISA to establish the proportion of processed versus unprocessed pBMP10 within them, and live biopsies could be incubated in media to demonstrate these species are also secreted.

To investigate whether certain cells can process circulating *ProBMP*, wildtype BMP9 and BMP10 could expressed in the presence of protease inhibitors, as in Susan-Resiga *et al.* (2011). Then, different endothelial cell lines could be incubated with *ProBMP10*-WT compared to uncleavable *ProBMP10*-R313A to show whether cells can activate them. Similarly, cells could be stimulated with different factors, such as inflammatory cytokines, to see if this alters their ability to process *ProBMP10*. If *ProBMP10* predominates over Pro:BMP9 and Pro:BMP10 in blood, dynamic regulation of processing could be a major determinant of signalling. Demonstrating whether the pulmonary vasculature is stimulated by BMP10 would

help answer whether the loss of plasma pBMP10 in *GDF2* mutation carriers and a subset of other PAH patients contributes to their disease.

A minority (~25%) of people (only PAH and PFO patients were tested) seemed to have plasma levels of processed Pro:BMP10 similar to levels of Pro:BMP9. Royal Papworth Hospital may hold more information about the clinical phenotype of these patients, which might reveal why a subset have higher levels of detectable Pro:BMP10. These people had unremarkable levels of total pBMP10, but perhaps higher than average levels of Pro:BMP9. This suggests there may be co-regulation between BMP9 and BMP10 processing. Serum from such people would allow us to assess the impact of this on circulating activity. In addition, levels of Pro:BMP9 and total pBMP10 are tightly correlated, and Tillet *et al.* (2019) suggested they may be heterodimers. Since levels of pBMP10 are much higher than BMP9, we instead hypothesised they are in larger complexes.

I found in serum that BMP9 and pBMP10 appeared to circulate in large macromolecular complexes. In EDTA-plasma, the majority appeared to circulate as a simple Pro:BMP complex, and this form was also present in EDTA-serum. Similarly, BMP9 and BMP10 are masked from ELISAs except in the presence of chelating agent. Hence, we hypothesised the current consensus that BMP9 and BMP10 circulate as a simple Pro:BMP complex are a result of only assessing EDTA plasma, and purification steps prior to chromatography. It will be interesting to perform size exclusion chromatography of heparin-plasma, to see whether solely calcium presence determines the size of the complex, or it has something to do with clotting.

Unpublished data from the Morrell group suggests levels of BMP9 are correlated with levels of kallikrein and factor 10, and associated with genes encoding bradykinin and clotting pathways by quantitative trait loci studies. Therefore, co-immunoprecipitations with these factors could be investigated, which may implicate BMP9 and BMP10 in regulating responses to vessel damage. Secondly, a minority of plasma BMP9 could be immunoprecipitated with BMP10 and *vice versa*. The results of such immunoprecipitations may be more striking in serum where a much greater proportion of BMP9 and BMP10 appears to be in large complexes.

We struggled to elucidate the pharmacokinetics of BMP9 because exogenous BMP9 is cleared rapidly from the circulation of mice, which appears to be at least partly due to binding and signalling in the lung, but there were no transpulmonary gradients of BMP9 or BMP10 levels in humans. Preliminary evidence also suggested endogenous BMP9 does not accumulate in the lungs of wildtype mice. If endogenous BMP9 and BMP10 do circulate in

macromolecular complexes, this may stabilise them in the blood by restricting their binding to the pulmonary endothelium. Lungs from mice given exogenous Pro:BMP9 were fixed and sent to Mark Southwood who will stain them to see if BMP9 binds the endothelium and activates signalling here. These samples can be compared to untreated *Gdf2* knockout and wildtype mice to confirm that lungs do not normally accumulate BMP9.

PAH patients carried heterozygous *GDF2* loss-of-function alleles, although two paediatric cases of PAH and HHT carried homozygous mutations. We are collecting samples from wildtype, *Gdf2* knockout and heterozygous mice to assess BMP9 levels and signalling in different organs. It will be interesting to see whether pulmonary vascular signalling is more sensitive to loss of BMP9 than other tissues, and how low plasma levels are in heterozygotes compared to wildtype animals. For the first time, we generated data from humans suggesting neither the wildtype *Gdf2* allele, nor *BMP10*, is sufficient to maintain normal plasma activity.

Some evidence hints long-term loss of BMP9 is partially accommodated, since Addante *et al.* (2018) report hepatic *Id1* expression is reduced by acute ALK1-Fc administration, but not germline *Gdf2* deletion (although BMP10 may be acting here). Similarly, Ricard *et al.* (2012) found anti-BMP9 and ALK1-Fc cause a similar retinal vascularisation defect in neonatal mice, but germline *Gdf2* deletion does not result in any defect. I found *Id* genes were not differently expressed in the livers of wildtype and *Gdf2* knockout mice. However, preliminary data suggested *Gdf2* knockout mice have reduced signalling in the lungs, and we will assess this by qPCR and phospho-SMAD staining in a larger number of samples. Secondly, the Morrell group is undertaking acute and chronic neutralisation studies with anti-BMP9, so the lung transcriptome of these mice could be compared with *Gdf2* knockouts.

We expected the hepatic transcriptome to be dysfunctional in *Gdf2* knockout mice. Reports suggest BMP9 deficiency is weakly inflammatory, not affecting hepatic inflammation in all mouse strains or people, and my data supported this since a few markers were upregulated in our *Gdf2* knockout mice. There is mixed evidence BMP9 deficiency contributes to hepatic fibrosis in healthy mice, since it depends on genetic background and the markers assessed. For example, Addante *et al.* (2018) and Desroches-Castan *et al.* (2019) report no increase in *Col1a1* expression or fibrotic area in the livers of *Gdf2* knockout C57/BL6 mice, but another group reports a small upregulation in *Col4a4*. Similarly, Breitkopf-Heinlein *et al.* (2017) showed BMP9 reverses markers of inflammation and fibrosis of hepatocytes *in vitro*, but find no upregulation of *Col1a1* in *Gdf2* knockout mice. They did however find desmin and vimentin were upregulated. Finally, Desroches-Castan *et al.* show *Gdf2* knockout mice

on an 129/OLA background spontaneously develop severe hepatic fibrosis and inflammation. Using an unbiased approach, I found limited evidence markers of fibrosis were depressed in *Gdf2* knockout C57/BL6 mice.

There is ample evidence BMP9 enhances injury in models of severe hepatic damage, but evidence in humans is mixed (Addante et al. 2018; Breitkopf-Heinlein et al. 2017; Li et al. 2018; Nikolic et al. 2019; John et al. 2018). Therefore, it seems likely BMP9 has complex context dependent roles in liver regeneration. Thorough histological analysis to assess the cell-types, tissue architecture and cell morphology of *Gdf2* knockout livers could be insightful, since current reports only assess specific cell types or use models of severe liver damage.

BMP9 overexpression has been shown to inhibit glucogenesis and lipogenesis in mice (Yang et al. 2019). In contrast Chen *et al.* (2003) found BMP9 upregulates lipogenic genes *in vitro*. Consistent with Chen *et al.*, I found *Gdf2* knockout livers downregulated lipogenic pathways, but I did not implicate the exact same genes. Therefore, BMP9's role in metabolism may also be context, cell-type and concentration dependent. Mice could be placed on different controlled diets and assessed throughout their circadian cycles to investigate this. The transcriptome of *Gdf2* knockout mice will be reanalysed to search for splice variants, since network analysis suggested the spliceosome signature was altered. This could reveal further roles for BMP9 in the liver.

Exogenous BMP9 did not appear to stimulate the livers of mice, which could be useful if supraphysiological doses are to be given to PAH patients without an adverse effect on metabolism. However, longer-term studies could be undertaken, perhaps using markers robustly downregulated in the *Gdf2* knockout transcriptome, such as the cytochrome P450 (*CYP4a*) family. These markers are also likely to be tractable for immunohistochemistry and have been previously reported to be downregulated in the livers of *Gdf2* knockout mice (Truksa et al. 2006; Breitkopf-Heinlein et al. 2017). The *CYP4a* genes may link *Gdf2* deficiency to protection against liver damage, since their ablation has been reported to protect against inflammation and damage, whilst overexpression predisposes to it (Zhang et al. 2017; Ip et al. 2003). Circulating levels of inflammatory cytokines, ALP, AST, ALT and albumin could be monitored to check liver health in in mice and humans administered BMP9.

More work is needed to elucidate which physiological/pathophysiological circumstances, such as infection, diet or toxins lead to downregulation of *Gdf2* in the liver, other than the very severe models used currently. Secondly, if liver expression can be altered in response to certain stimuli, the effect this has on pulmonary vascular signalling could be measured, since there may be compensation. Finally, haemodynamics and histology could be

assessed to see whether this predisposes to pulmonary hypertension. Hence, low BMP9 levels could be established as a causal link between liver disease and pulmonary hypertension.

The lung itself may be a source of BMP9, which may mean it maintains signalling independently of plasma BMP9 levels. I have prepared perfusion fixed samples from wildtype and *Gdf2* knockout mice to carry out RNA-*in situ* hybridisations to assess which cells are expressing *Gdf2*. Counterstains could include von Willebrand factor and smooth-muscle actin to show whether BMP9 acts as an autocrine in pulmonary vessel walls. Tissue-specific (liver, lung, right-atria) conditional knockouts of *Gdf2* and *Bmp10* would be the definitive way to establish from where the activity in different compartments originates, although producing them would be laborious.

Many reports focus on one or other of *Gdf2* or *Bmp10*, but they may have correlated expression levels, circulate together and have similar signalling activity. Unfortunately, we do not have a validated BMP10 ELISA for mouse samples, and BMP10 plasma neutralisations are reported to be unsuccessful, which makes analysis difficult. However, the expression and levels of BMP9 should be assessed in tissues of the inducible *Bmp10* knockout mouse. The plasma activity and pulmonary signalling of *Gdf2* knockout, *Bmp10* knockout and double knockout mice could be compared to see which ligand is most important for quiescing the pulmonary vasculature.

In conclusion, reproducible genetic *in silico* and *in vitro* evidence now shows *GDF2* deficiency causes PAH in some patients. *In vivo* evidence suggests BMP9 administration is likely to be beneficial, and perhaps specifically stimulate protective effects in the lung. *GDF2* deficiency is also likely to disrupt liver metabolism, especially fatty-acid synthesis and oxidative metabolism, although the phenotypic implications of this are unclear. More work is needed to understand the link between BMP9 and BMP10 and whether BMP10 also has roles in PAH and hepatic metabolism. The circulating dynamics of endogenous BMP9 and BMP10, and how their activity on different tissues is regulated, may be more complex than is appreciated in the current literature. There is much still to discover regarding the physiology of BMP9 and BMP10.

References

Abdalla, S A, and M Letarte. 2006. “Hereditary Haemorrhagic Telangiectasia: Current Views on Genetics and Mechanisms of Disease.” *Journal of Medical Genetics* 43 (2): 97–110. https://doi.org/10.1136/jmg.2005.030833.

Abdalla, Salma A., Urszula Cymerman, Diane Rushlow, Ning Chen, Gwendolyn P. Stoeber, Edmond G. Lemire, and Michelle Letarte. 2005. “Novel Mutations and Polymorphisms in Genes Causing Hereditary Hemorrhagic Telangiectasia.” *Human Mutation* 25 (3): 320–21. https://doi.org/10.1002/humu.9312.

Addante, Annalisa, Cesáreo Roncero, Laura Almalé, Nerea Lazcanoiturburu, María García-Álvaro, Margarita Fernández, Julián Sanz, et al. 2018. “Bone Morphogenetic Protein 9 as a Key Regulator of Liver Progenitor Cells in DDC -induced Cholestatic Liver Injury.” *Liver International* 38 (9): 1664–75. https://doi.org/10.1111/liv.13879.

Ades, Edwin W, Francisco J Candal, Robert A Swerlick, Velma G George, Susan. Summers, Diane C Bosse, and Thomas J Lawley. 1992. “HMEC-1: Establishment of an Immortalized Human Microvascular Endothelial Cell Line.” *Journal of Investigative Dermatology* 99 (6): 683–90. https://doi.org/10.1111/1523-1747.ep12613748.

Adzhubei, Ivan A, Steffen Schmidt, Leonid Peshkin, Vasily E Ramensky, Anna Gerasimova, Peer Bork, Alexey S Kondrashov, and Shamil R Sunyaev. 2010. “A Method and Server for Predicting Damaging Missense Mutations.” *Nature Methods* 7 (4): 248–49. https://doi.org/10.1038/nmeth0410-248.

Akla, Naoufal, Claire Viallard, Natalija Popovic, Cindy Lora Gil, Przemyslaw Sapieha, and Bruno Larrivée. 2018. “BMP9 (Bone Morphogenetic Protein-9)/Alk1 (Activin-Like Kinase Receptor Type I) Signaling Prevents Hyperglycemia-Induced Vascular Permeability.” *Arteriosclerosis, Thrombosis, and Vascular Biology* 38 (8): 1821–36. https://doi.org/10.1161/ATVBAHA.118.310733.

Aldred, Micheala A., Suzy A. Comhair, Marileila Varella-Garcia, Kewal Asosingh, Weiling Xu, George P. Noon, Patricia A. Thistlethwaite, et al. 2010. “Somatic Chromosome Abnormalities in the Lungs of Patients with Pulmonary Arterial Hypertension.” *American Journal of Respiratory and Critical Care Medicine* 182 (9): 1153–60. https://doi.org/10.1164/rccm.201003-0491OC.

Aldred, Micheala A., Jairam Vijayakrishnan, Victoria James, Florent Soubrier, Miguel A. Gomez-Sanchez, Gunnar Martensson, Nazzareno Galie, et al. 2006. “BMPR2 Gene Rearrangements Account for a Significant Proportion of Mutations in Familial and Idiopathic Pulmonary Arterial Hypertension.” *Human Mutation* 27 (2): 212–13. https://doi.org/10.1002/humu.9398.

Alt, Aaron, Laura Miguel-Romero, Jordi Donderis, Mikel Aristorena, Francisco J Blanco, Adam Round, Vicente Rubio, Carmelo Bernabeu, and Alberto Marina. 2012. “Structural and Functional Insights into Endoglin Ligand Recognition and Binding.” *PloS One* 7 (2): e29948. https://doi.org/10.1371/journal.pone.0029948.

Archer, Stephen L, E Kenneth Weir, and Martin R Wilkins. 2010. “Basic Science of Pulmonary Arterial Hypertension for Clinicians: New Concepts and Experimental Therapies.” *Circulation* 121 (18): 2045–66. https://doi.org/10.1161/CIRCULATIONAHA.108.847707.

Ashburner, Michael, Catherine A. Ball, Judith A. Blake, David Botstein, Heather Butler, J. Michael Cherry, Allan P. Davis, et al. 2000. “Gene Ontology: Tool for the Unification of Biology.” *Nature Genetics* 25 (1): 25–29. https://doi.org/10.1038/75556.

Ashfaq, M., S. Chinnakotla, L. Rogers, K. Ausloos, S. Saadeh, G. B. Klintmalm, M. Ramsay, and G. L. Davis. 2007. “The Impact of Treatment of Portopulmonary Hypertension on Survival Following Liver Transplantation.” *American Journal of Transplantation* 7 (5): 1258–64. https://doi.org/10.1111/j.1600-6143.2006.01701.x.

Austin, Eric D., Lijiang Ma, Charles LeDuc, Erika Berman Rosenzweig, Alain Borczuk, John A. Phillips, Teresa Palomero, et al. 2012. “Whole Exome Sequencing to Identify a Novel Gene (Caveolin-1) Associated With Human Pulmonary Arterial Hypertension.” *Circulation:*

Cardiovascular Genetics 5 (3): 336–43. https://doi.org/10.1161/CIRCGENETICS.111.961888.
Baardewijk, Laurens J. van, Jacob van der Ende, Suzanne Lissenberg-Thunnissen, Loes M. Romijn, Lukas J. A. C. Hawinkels, Cornelis F. M. Sier, and Inger B. Schipper. 2013. "Circulating Bone Morphogenetic Protein Levels and Delayed Fracture Healing." *International Orthopaedics* 37 (3): 523–27. https://doi.org/10.1007/s00264-012-1750-z.
Baeyens, Nicolas, Bruno Larrivée, Roxana Ola, Brielle Hayward-Piatkowskyi, Alexandre Dubrac, Billy Huang, Tyler D Ross, et al. 2016. "Defective Fluid Shear Stress Mechanotransduction Mediates Hereditary Hemorrhagic Telangiectasia." *The Journal of Cell Biology* 214 (7): 807–16. https://doi.org/10.1083/jcb.201603106.
Barbara, N P, J L Wrana, and M Letarte. 1999. "Endoglin Is an Accessory Protein That Interacts with the Signaling Receptor Complex of Multiple Members of the Transforming Growth Factor-Beta Superfamily." *The Journal of Biological Chemistry* 274 (2): 584–94. http://www.ncbi.nlm.nih.gov/pubmed/9872992.
Barbieri, Michelangela, Antonietta Esposito, Edith Angellotti, Maria Rosaria Rizzo, Raffaele Marfella, and Giuseppe Paolisso. 2013. "Association of Genetic Variation in Adaptor Protein APPL1/APPL2 Loci with Non-Alcoholic Fatty Liver Disease." Edited by Massimo Federici. *PLoS ONE* 8 (8): e71391. https://doi.org/10.1371/journal.pone.0071391.
Barozzi, Chiara, Margherita Galletti, Luciana Tomasi, Sara De Fanti, Massimiliano Palazzini, Alessandra Manes, Marco Sazzini, and Nazzareno Galiè. 2019. "A Combined Targeted and Whole Exome Sequencing Approach Identified Novel Candidate Genes Involved in Heritable Pulmonary Arterial Hypertension." *Scientific Reports* 9 (1): 753. https://doi.org/10.1038/s41598-018-37277-0.
Benza, Raymond L., Dave P. Miller, Robyn J. Barst, David B. Badesch, Adaani E. Frost, and Michael D. McGoon. 2012. "An Evaluation of Long-Term Survival From Time of Diagnosis in Pulmonary Arterial Hypertension From the REVEAL Registry." *Chest* 142 (2): 448–56. https://doi.org/10.1378/chest.11-1460.
Beppu, Hideyuki, Fumito Ichinose, Noriko Kawai, Rosemary C. Jones, Paul B. Yu, Warren M. Zapol, Kohei Miyazono, En Li, and Kenneth D. Bloch. 2004. "*BMPR-II* Heterozygous Mice Have Mild Pulmonary Hypertension and an Impaired Pulmonary Vascular Remodeling Response to Prolonged Hypoxia." *American Journal of Physiology-Lung Cellular and Molecular Physiology* 287 (6): L1241–47. https://doi.org/10.1152/ajplung.00239.2004.
Bi, Jianjun, and Shengfang Ge. 2014. "Potential Roles of BMP9 in Liver Fibrosis." *International Journal of Molecular Sciences* 15 (11): 20656–67. https://doi.org/10.3390/ijms151120656.
Bidart, Marie, Nicolas Ricard, Sandrine Levet, Michel Samson, Christine Mallet, Laurent David, Mariela Subileau, Emmanuelle Tillet, Jean-Jacques Feige, and Sabine Bailly. 2012. "BMP9 Is Produced by Hepatocytes and Circulates Mainly in Its Active Form Complexed to Its Prodomain" 69 (2). https://doi.org/10.1007/s00018-011-0751-1.
Birukova, Anna A., Junjie Xing, Panfeng Fu, Bakhtiyor Yakubov, Oleksii Dubrovskyi, Jennifer A. Fortune, Alexander M. Klibanov, and Konstantin G. Birukov. 2010. "Atrial Natriuretic Peptide Attenuates LPS-Induced Lung Vascular Leak: Role of PAK1." *American Journal of Physiology-Lung Cellular and Molecular Physiology* 299 (5): L652–63. https://doi.org/10.1152/ajplung.00202.2009.
Blanco, Francisco J, Juan F Santibanez, Mercedes Guerrero-Esteo, Carmen Langa, Calvin P H Vary, and Carmelo Bernabeu. 2005. "Interaction and Functional Interplay between Endoglin and ALK-1, Two Components of the Endothelial Transforming Growth Factor-Beta Receptor Complex." *Journal of Cellular Physiology* 204 (2): 574–84. https://doi.org/10.1002/jcp.20311.
Breitkopf-Heinlein, Katja, Christoph Meyer, Courtney König, Haristi Gaitantzi, Annalisa Addante, Maria Thomas, Eliza Wiercinska, et al. 2017. "BMP-9 Interferes with Liver Regeneration and Promotes Liver Fibrosis." *Gut* 66 (5): 939–54. https://doi.org/10.1136/gutjnl-2016-

313314.
Brida, Margarita, and Michael A Gatzoulis. 2018. “Pulmonary Arterial Hypertension in Adult Congenital Heart Disease.” *Heart* 104 (19): 1568–74. https://doi.org/10.1136/heartjnl-2017-312106.
Brown, Monica A., Qinghai Zhao, Kent A. Baker, Chethana Naik, Cecil Chen, Laurie Pukac, Mallika Singh, et al. 2005. “Crystal Structure of BMP-9 and Functional Interactions with Pro-Region and Receptors.” *Journal of Biological Chemistry* 280 (26): 25111–18. https://doi.org/10.1074/jbc.M503328200.
Budhiraja, R., Rubin M Tuder, and Paul M Hassoun. 2004. “Endothelial Dysfunction in Pulmonary Hypertension.” *Circulation* 109 (2): 159–65. https://doi.org/10.1161/01.CIR.0000102381.57477.50.
Burton, Victoria J., Loredana I. Ciuclan, Alan M. Holmes, David M. Rodman, Christoph Walker, and David C. Budd. 2011. “BMPR2 Regulates PAEC Barrier Function.” *Blood* 117 (1). https://doi.org/10.1182/blood-2010-05-285973.
Caperuto, Luciana Chagas, Gabriel Forato Anhê, Tavane David Cambiaghi, Eliana Hiromi Akamine, Daniella do Carmo Buonfiglio, José Cipolla-Neto, Rui Curi, and Silvana Bordin. 2008. “Modulation of Bone Morphogenetic Protein-9 Expression and Processing by Insulin, Glucose, and Glucocorticoids: Possible Candidate for Hepatic Insulin-Sensitizing Substance.” *Endocrinology* 149 (12): 6326–35. https://doi.org/10.1210/en.2008-0655.
Castonguay, Roselyne, Eric D. Werner, Robert G. Matthews, Eleonora Presman, Aaron W. Mulivor, Nicolas Solban, Dianne Sako, et al. 2011. “Soluble Endoglin Specifically Binds Bone Morphogenetic Proteins 9 and 10 via Its Orphan Domain, Inhibits Blood Vessel Formation, and Suppresses Tumor Growth.” *Journal of Biological Chemistry* 286 (34): 30034–46. https://doi.org/10.1074/jbc.M111.260133.
Chaouat, A, F Coulet, C Favre, G Simonneau, E Weitzenblum, F Soubrier, and M Humbert. 2004. “Endoglin Germline Mutation in a Patient with Hereditary Haemorrhagic Telangiectasia and Dexfenfluramine Associated Pulmonary Arterial Hypertension.” *Thorax* 59 (5): 446–48. https://doi.org/10.1136/THX.2003.11890.
Chen, Cecil, Krzysztof J. Grzegorzewski, Steve Barash, Qinghai Zhao, Helmut Schneider, Qi Wang, Mallika Singh, et al. 2003. “An Integrated Functional Genomics Screening Program Reveals a Role for BMP-9 in Glucose Homeostasis.” *Nature Biotechnology* 21 (3): 294–301. https://doi.org/10.1038/nbt795.
Chen, H., Shu Shi, Lourdes Acosta, Weiming Li, Jonathan Lu, Shideng Bao, Zhuang Chen, et al. 2004. “BMP10 Is Essential for Maintaining Cardiac Growth during Murine Cardiogenesis.” *Development* 131 (9): 2219–31. https://doi.org/10.1242/dev.01094.
Chen, Hanying, Wenjun Zhang, Deqiang Li, Tim M. Cordes, R. Mark Payne, and Weinian Shou. 2009. “Analysis of Ventricular Hypertrabeculation and Noncompaction Using Genetically Engineered Mouse Models.” *Pediatric Cardiology* 30 (5): 626–34. https://doi.org/10.1007/s00246-009-9406-5.
Chen, Hao, John Brady Ridgway, Tao Sai, Joyce Lai, Søren Warming, Hanying Chen, Merone Roose-Girma, Gu Zhang, Weinian Shou, and Minhong Yan. 2013. “Context-Dependent Signaling Defines Roles of BMP9 and BMP10 in Embryonic and Postnatal Development.” *Proceedings of the National Academy of Sciences of the United States of America* 110 (29): 11887–92. https://doi.org/10.1073/pnas.1306074110.
Chen, Honglei, Shaoping Wu, Rong Lu, Yong-guo Zhang, Yuanyuan Zheng, and Jun Sun. 2014. “Pulmonary Permeability Assessed by Fluorescent-Labeled Dextran Instilled Intranasally into Mice with LPS-Induced Acute Lung Injury.” Edited by You-Yang Zhao. *PLoS ONE* 9 (7): e101925. https://doi.org/10.1371/journal.pone.0101925.
Chen, Siyu, Wenxiang Zhang, Chunqi Tang, Xiaoli Tang, Li Liu, and Chang Liu. 2014. “Vanin-1 Is a Key Activator for Hepatic Gluconeogenesis.” *Diabetes* 63 (6): 2073–85. https://doi.org/10.2337/db13-0788.
Cheng, HONGWEI, Wei JIANG, Frank M. PHILLIPS, REX C. Haydon, Ying PENG, LAN Zhou, HUE

H. Luu, et al. 2003. “No Title,” no. 8 (August). https://doi.org/10.2106/00004623-200308000-00017.
Cogan, Joy D, Michael W Pauciulo, Amy P Batchman, Melissa A Prince, Ivan M Robbins, Lora K Hedges, Krista C Stanton, et al. 2006. “High Frequency of BMPR2 Exonic Deletions/Duplications in Familial Pulmonary Arterial Hypertension.” *American Journal of Respiratory and Critical Care Medicine* 174 (5): 590–98. https://doi.org/10.1164/rccm.200602-165OC.
Cogan, Joy D, Cindy L Vnencak-Jones, John A Phillips, Kirk B Lane, Lisa A Wheeler, Ivan M Robbins, Gladys Garrison, Lora K Hedges, and James E Loyd. 2005. “Gross BMPR2 Gene Rearrangements Constitute a New Cause for Primary Pulmonary Hypertension.” *Genetics in Medicine : Official Journal of the American College of Medical Genetics* 7 (3): 169–74. https://doi.org/10.109701.GIM.0000156525.09595.E9.
Cool, Carlyne D., J. Scott Stewart, Priya Werahera, Gary J. Miller, Randy L. Williams, Norbert F. Voelkel, and Rubin M. Tuder. 1999. “Three-Dimensional Reconstruction of Pulmonary Arteries in Plexiform Pulmonary Hypertension Using Cell-Specific Markers.” *The American Journal of Pathology* 155 (2): 411–19. https://doi.org/10.1016/S0002-9440(10)65137-1.
Corti, P., S. Young, C.-Y. Chen, M. J. Patrick, E. R. Rochon, K. Pekkan, and B. L. Roman. 2011. “Interaction between Alk1 and Blood Flow in the Development of Arteriovenous Malformations.” *Development* 138 (8): 1573–82. https://doi.org/10.1242/dev.060467.
Crist, Angela M., Xingyan Zhou, Jone Garai, Amanda R. Lee, Janina Thoele, Christoph Ullmer, Christian Klein, Jovanny Zabaleta, and Stryder M. Meadows. 2019. “Angiopoietin-2 Inhibition Rescues Arteriovenous Malformation in a Smad4 Hereditary Hemorrhagic Telangiectasia Mouse Model.” *Circulation* 139 (17): 2049–63. https://doi.org/10.1161/CIRCULATIONAHA.118.036952.
Crosby, Alexi, Mark R. Toshner, Mark R. Southwood, Elaine Soon, Benjamin J. Dunmore, Emily Groves, Stephen Moore, et al. 2018. “Hematopoietic Stem Cell Transplantation Alters Susceptibility to Pulmonary Hypertension in *Bmpr2* -Deficient Mice.” *Pulmonary Circulation* 8 (4): 204589401880164. https://doi.org/10.1177/2045894018801642.
Daher, Raed, Caroline Kannengiesser, Dounia Houamel, Thibaud Lefebvre, Edouard Bardou-Jacquet, Nicolas Ducrot, Caroline de Kerguenec, et al. 2016. “Heterozygous Mutations in BMP6 Pro-Peptide Lead to Inappropriate Hepcidin Synthesis and Moderate Iron Overload in Humans.” *Gastroenterology* 150 (3): 672-683.e4. https://doi.org/10.1053/j.gastro.2015.10.049.
David, Laurent, Christine Mallet, Michelle Keramidas, N. Lamande, J.-M. Jean-Marie Gasc, Sophie Dupuis-Girod, Henri Plauchu, et al. 2008. “BMP9 Is a Circulating Vascular Quiesence Factor.” *Circ.Res.* 102 (8). https://doi.org/10.1161/CIRCRESAHA.107.165530.
David, Laurent, Christine Mallet, Sabine Mazerbourg, Jean-Jacques J.-J. Feige, and Sabine Bailly. 2007. “Identification of BMP9 and BMP10 as Functional Activators of the Orphan Activin Receptor-like Kinase 1 (ALK1) in Endothelial Cells.” *Blood* 109 (5): 1953–61. https://doi.org/10.1182/blood-2006-07-034124.
Deng, Z, J H Morse, S L Slager, N Cuervo, K J Moore, G Venetos, S Kalachikov, et al. 2000. “Familial Primary Pulmonary Hypertension (Gene PPH1) Is Caused by Mutations in the Bone Morphogenetic Protein Receptor-II Gene.” *American Journal of Human Genetics* 67 (3): 737–44. https://doi.org/10.1086/303059.
Derynck, Rik, and Rosemary J Akhurst. 2013. “BMP-9 Balances Endothelial Cell Fate.” *Proceedings of the National Academy of Sciences of the United States of America* 110 (47): 18746–47. https://doi.org/10.1073/pnas.1318346110.
Desroches-Castan, Agnès, Emmanuelle Tillet, Nicolas Ricard, Marie Ouarné, Christine Mallet, Jean-Jacques Feige, and Sabine Bailly. 2019. “Differential Consequences of Bmp9 Deletion on Sinusoidal Endothelial Cell Differentiation and Liver Fibrosis in 129/Ola and C57BL/6 Mice.” *Cells* 8 (9): 1079. https://doi.org/10.3390/cells8091079.
Desroches-Castan, Agnès, Emmanuelle Tillet, Nicolas Ricard, Marie Ouarné, Christine Mallet,

Lucid Belmudes, Yohann Couté, et al. 2019. “Bone Morphogenetic Protein 9 Is a Paracrine Factor Controlling Liver Sinusoidal Endothelial Cell Fenestration and Protecting Against Hepatic Fibrosis.” *Hepatology*, May, hep.30655. https://doi.org/10.1002/hep.30655.
Dhanasekaran, D N, and E P Reddy. 2008. “JNK Signaling in Apoptosis.” *Oncogene* 27 (48): 6245–51. https://doi.org/10.1038/onc.2008.301.
Ding, Bi-Sen, Zhongwei Cao, Raphael Lis, Daniel J. Nolan, Peipei Guo, Michael Simons, Mark E. Penfold, Koji Shido, Sina Y. Rabbany, and Shahin Rafii. 2014. “Divergent Angiocrine Signals from Vascular Niche Balance Liver Regeneration and Fibrosis.” *Nature* 505 (7481): 97–102. https://doi.org/10.1038/nature12681.
Drake, Kylie M., Suzy A. Comhair, Serpil C. Erzurum, Rubin M. Tuder, and Micheala A. Aldred. 2015. “Endothelial Chromosome 13 Deletion in Congenital Heart Disease–Associated Pulmonary Arterial Hypertension Dysregulates *SMAD9* Signaling.” *American Journal of Respiratory and Critical Care Medicine* 191 (7): 850–54. https://doi.org/10.1164/rccm.201411-1985LE.
Drake, Kylie M., Deborah Zygmunt, Lori Mavrakis, Phyllis Harbor, Lingli Wang, Suzy A. Comhair, Serpil C. Erzurum, and Micheala A. Aldred. 2011. “Altered MicroRNA Processing in Heritable Pulmonary Arterial Hypertension An Important Role for Smad-8.” *American Journal of Respiratory and Critical Care Medicine* 184 (12). https://doi.org/10.1164/rccm.201106-1130OC.
Dresdale, D T, R J Michtom, and M Schultz. 1954. “Recent Studies in Primary Pulmonary Hypertension, Including Pharmacodynamic Observations on Pulmonary Vascular Resistance.” *Bulletin of the New York Academy of Medicine* 30 (3): 195–207. http://www.ncbi.nlm.nih.gov/pubmed/13141055.
Droin, Colas, Eric R. Paquet, and Felix Naef. 2019. “Low-Dimensional Dynamics of Two Coupled Biological Oscillators.” *Nature Physics*, August, 1–9. https://doi.org/10.1038/s41567-019-0598-1.
Ducy, P. 2000. “The Family of Bone Morphogenetic Proteins.” *Kidney International* 57 (6): 2207–14. https://doi.org/10.1046/J.1523-1755.2000.00081.X.
Eddahibi, Saadia, Christophe Guignabert, Anne-Marie Barlier-Mur, Laurence Dewachter, Elie Fadel, Philippe Dartevelle, Marc Humbert, et al. 2006. “Cross Talk Between Endothelial and Smooth Muscle Cells in Pulmonary Hypertension.” *Circulation* 113 (15): 1857–64. https://doi.org/10.1161/CIRCULATIONAHA.105.591321.
Elowitz, Michael B, Arnold J Levine, Eric D Siggia, and Peter S Swain. 2002. “Stochastic Gene Expression in a Single Cell.” *Science (New York, N.Y.)* 297 (5584): 1183–86. https://doi.org/10.1126/science.1070919.
Elvevold, Kjetil, Bård Smedsrød, and Inigo Martinez. 2008. “The Liver Sinusoidal Endothelial Cell: A Cell Type of Controversial and Confusing Identity.” *American Journal of Physiology-Gastrointestinal and Liver Physiology* 294 (2): G391–400. https://doi.org/10.1152/ajpgi.00167.2007.
Evans, Jonathan D W, Barbara Girerd, David Montani, Xiao-Jian Wang, Nazzareno Galiè, Eric D Austin, Greg Elliott, et al. 2016. “BMPR2 Mutations and Survival in Pulmonary Arterial Hypertension: An Individual Participant Data Meta-Analysis.” *The Lancet Respiratory Medicine* 4 (2): 129–37. https://doi.org/10.1016/S2213-2600(15)00544-5.
Eyries, Mélanie, David Montani, Sophie Nadaud, Barbara Girerd, Marilyne Levy, Arnaud Bourdin, Romain Trésorier, et al. 2019. “Widening the Landscape of Heritable Pulmonary Hypertension Mutations in Paediatric and Adult Cases.” *European Respiratory Journal* 53 (3): 1801371. https://doi.org/10.1183/13993003.01371-2018.
Faughnan, M. E., J. T. Granton, and L. H. Young. 2009. “The Pulmonary Vascular Complications of Hereditary Haemorrhagic Telangiectasia.” *European Respiratory Journal* 33 (5): 1186–94. https://doi.org/10.1183/09031936.00061308.
Ferreira, Daniel W, Michael J Goedken, Samuel Rommelaere, Lionel Chasson, Franck Galland, Philippe Naquet, and José E Manautou. 2016. “Enhanced Hepatotoxicity by

Acetaminophen in Vanin-1 Knockout Mice Is Associated with Deficient Proliferative and Immune Responses." *Biochimica et Biophysica Acta* 1862 (4): 662–69. https://doi.org/10.1016/j.bbadis.2016.02.001.
Franco, Claudio A., and Holger Gerhardt. 2016. "Blood Flow Boosts BMP Signaling to Keep Vessels in Shape." *The Journal of Cell Biology* 214 (7): 793. https://doi.org/10.1083/JCB.201609038.
Franzoso, G, F Zazzeroni, and S Papa. 2003. "JNK: A Killer on a Transcriptional Leash." *Cell Death and Differentiation* 10 (1): 13–15. https://doi.org/10.1038/sj.cdd.4401154.
Freedman, FB, and JA Johnson. 1969. "Equilibrium and Kinetic Properties of the Evans Blue-Albumin System." *American Journal of Physiology-Legacy Content* 216 (3): 675–81. https://doi.org/10.1152/ajplegacy.1969.216.3.675.
Frevert, Ute, Sabine Engelmann, Sergine Zougbédé, Jörg Stange, Bruce Ng, Kai Matuschewski, Leonard Liebes, and Herman Yee. 2005. "Intravital Observation of Plasmodium Berghei Sporozoite Infection of the Liver." Edited by Thomas Egwang. *PLoS Biology* 3 (6): e192. https://doi.org/10.1371/journal.pbio.0030192.
Fu, Tiwei, Panpan Liang, Jinlin Song, Jinhua Wang, Pengfei Zhou, Yinhong Tang, Jing Li, and Enyi Huang. 2019. "Matrigel Scaffolding Enhances BMP9-Induced Bone Formation in Dental Follicle Stem/Precursor Cells." *International Journal of Medical Sciences* 16 (4): 567–75. https://doi.org/10.7150/ijms.30801.
Fujioka-Kobayashi, Masako, Kosaku Sawada, Eizaburo Kobayashi, Benoit Schaller, Yufeng Zhang, and Richard J. Miron. 2017. "Osteogenic Potential of RhBMP9 Combined with a Bovine-Derived Natural Bone Mineral Scaffold Compared to RhBMP2." *Clinical Oral Implants Research* 28 (4): 381–87. https://doi.org/10.1111/clr.12804.
Gaine, Sean. 2000. "Pulmonary Hypertension." *JAMA* 284 (24): 3160. https://doi.org/10.1001/jama.284.24.3160.
Galambos, Csaba, Sunder Sims-Lucas, Steven H. Abman, and Carlyne D. Cool. 2016. "Intrapulmonary Bronchopulmonary Anastomoses and Plexiform Lesions in Idiopathic Pulmonary Arterial Hypertension." *American Journal of Respiratory and Critical Care Medicine* 193 (5): 574–76. https://doi.org/10.1164/rccm.201507-1508LE.
Galiè, Nazzareno, Marc Humbert, Jean-Luc Vachiery, Simon Gibbs, Irene Lang, Adam Torbicki, Gérald Simonneau, et al. 2016. "2015 ESC/ERS Guidelines for the Diagnosis and Treatment of Pulmonary Hypertension." *European Heart Journal* 37 (1): 67–119. https://doi.org/10.1093/eurheartj/ehv317.
Gallione, C J, J A Richards, T G W Letteboer, D Rushlow, N L Prigoda, T P Leedom, A Ganguly, et al. 2006. "SMAD4 Mutations Found in Unselected HHT Patients." *Journal of Medical Genetics* 43 (10): 793–97. https://doi.org/10.1136/jmg.2006.041517.
Gao, Lili, Teruo Utsumi, Keitaro Tashiro, Bo Liu, Dahai Zhang, E. Scott Swenson, and Yasuko Iwakiri. 2013. "Reticulon 4B (Nogo-B) Facilitates Hepatocyte Proliferation and Liver Regeneration in Mice." *Hepatology* 57 (5): 1992–2003. https://doi.org/10.1002/hep.26235.
Germain, Marine, Mélanie Eyries, David Montani, Odette Poirier, Barbara Girerd, Peter Dorfmüller, Florence Coulet, et al. 2013. "Genome-Wide Association Analysis Identifies a Susceptibility Locus for Pulmonary Arterial Hypertension." *Nature Genetics* 45 (5): 518–21. https://doi.org/10.1038/ng.2581.
Girerd, Barbara, David Montani, Florence Coulet, Benjamin Sztrymf, Azzeddine Yaici, Xavier Jaïs, David Tregouet, et al. 2010. "Clinical Outcomes of Pulmonary Arterial Hypertension in Patients Carrying an *ACVRL1* (*ALK1*) Mutation." *American Journal of Respiratory and Critical Care Medicine* 181 (8): 851–61. https://doi.org/10.1164/rccm.200908-1284OC.
Goetz, Sarah C., and Kathryn V. Anderson. 2010. "The Primary Cilium: A Signalling Centre during Vertebrate Development." *Nature Reviews Genetics* 11 (5): 331–44. https://doi.org/10.1038/nrg2774.
Goumans, M.-J., Gudrun Valdimarsdottir, Susumu Itoh, Alexander Rosendahl, Paschalis

Sideras, and Peter ten Dijke. 2002. “Balancing the Activation State of the Endothelium via Two Distinct TGF-Beta Type I Receptors.” *The EMBO Journal* 21 (7): 1743–53. https://doi.org/10.1093/emboj/21.7.1743.

Gräf, Stefan, Matthias Haimel, Marta Bleda, Charaka Hadinnapola, Laura Southgate, Wei Li, Joshua Hodgson, et al. 2018. “Identification of Rare Sequence Variation Underlying Heritable Pulmonary Arterial Hypertension.” *Nature Communications* 9 (1): 1416. https://doi.org/10.1038/s41467-018-03672-4.

Graham, Kurtis, Joshua I. Murphy, and Gurtej K. Dhoot. 2016. “SULF1/SULF2 Reactivation during Liver Damage and Tumour Growth.” *Histochemistry and Cell Biology* 146 (1): 85–97. https://doi.org/10.1007/s00418-016-1425-8.

Gray, A., and A. Mason. 1990. “Requirement for Activin A and Transforming Growth Factor--Beta 1 pro-Regions in Homodimer Assembly.” *Science* 247 (4948): 1328–30. https://doi.org/10.1126/science.2315700.

Harrison, R E, J A Flanagan, M Sankelo, S A Abdalla, J Rowell, R D Machado, C G Elliott, et al. 2003. “Molecular and Functional Analysis Identifies ALK-1 as the Predominant Cause of Pulmonary Hypertension Related to Hereditary Haemorrhagic Telangiectasia.” *Journal of Medical Genetics* 40 (12): 865–71. http://www.ncbi.nlm.nih.gov/pubmed/14684682.

Heltberg, Mathias L., and Mogens H. Jensen. 2019. “Locked Body Clocks.” *Nature Physics*, August, 1–2. https://doi.org/10.1038/s41567-019-0617-2.

Hernandez, Felicia, Robert Huether, Lester Carter, Tami Johnston, Jennifer Thompson, James R Gossage, Elizabeth Chao, and Aaron M Elliott. 2015. “Mutations in RASA1 and GDF2 Identified in Patients with Clinical Features of Hereditary Hemorrhagic Telangiectasia.” *Human Genome Variation* 2: 15040. https://doi.org/10.1038/hgv.2015.40.

Herrera, Blanca, and Gareth J Inman. 2009. “BMC Cell Biology A Rapid and Sensitive Bioassay for the Simultaneous Measurement of Multiple Bone Morphogenetic Proteins. Identification and Quantification of BMP4, BMP6 and BMP9 in Bovine and Human Serum.” https://doi.org/10.1186/1471-2121-10-20.

Hirono, Keiichi, Kazuyoshi Saito, Undral Munkhsaikhan, Fuyi Xu, Ce Wang, Lu Lu, Fukiko Ichida, Jeffrey A. Towbin, and Enkhsaikhan Purevjav. 2019. “Familial Left Ventricular Non-Compaction Is Associated With a Rare p.V407I Variant in Bone Morphogenetic Protein 10.” *Circulation Journal* 83 (8): 1737–46. https://doi.org/10.1253/circj.CJ-19-0116.

Hodgson, Joshua, Emilia M Swietlik, Richard M Salmon, Charaka Hadinnapola, Ivana Nikolic, John Wharton, Jingxu Guo, et al. 2019. “Characterization of *GDF2* Mutations and Levels of BMP9 and BMP10 in Pulmonary Arterial Hypertension.” *American Journal of Respiratory and Critical Care Medicine*, October, rccm.201906-1141OC. https://doi.org/10.1164/rccm.201906-1141OC.

Hoeper, Marius M., Harm Jan Bogaard, Robin Condliffe, Robert Frantz, Dinesh Khanna, Marcin Kurzyna, David Langleben, et al. 2013. “Definitions and Diagnosis of Pulmonary Hypertension.” *Journal of the American College of Cardiology* 62 (25): D42–50. https://doi.org/10.1016/j.jacc.2013.10.032.

Hollatz, Trina J., Alexandru Musat, Susanne Westphal, Catherine Decker, Anthony M. D’Alessandro, Jon Keevil, Li Zhanhai, and James R. Runo. 2012. “Treatment with Sildenafil and Treprostinil Allows Successful Liver Transplantation of Patients with Moderate to Severe Portopulmonary Hypertension.” *Liver Transplantation* 18 (6): 686–95. https://doi.org/10.1002/lt.23407.

Holmes, AM, E Soon, CM Treacy, NJ Doughty - Circulation, and undefined 2010. n.d. “Elevated Levels of Inflammatory Cytokines Predict Survival in Idiopathic and Familial Pulmonary Arterial Hypertension.” *Discovery.Ucl.Ac.Uk*. Accessed October 5, 2019. http://discovery.ucl.ac.uk/id/eprint/1337254.

Hong, Kwon-Ho, Young Jae Lee, Eunji Lee, Sung Ok Park, Chul Han, Hideyuki Beppu, En Li, Mohan K Raizada, Kenneth D Bloch, and S Paul Oh. 2008. “Genetic Ablation of the BMPR2 Gene in Pulmonary Endothelium Is Sufficient to Predispose to Pulmonary Arterial

Hypertension." *Circulation* 118 (7): 722–30. https://doi.org/10.1161/CIRCULATIONAHA.107.736801.
Huang, Zheng, Degang Wang, Kaori Ihida-Stansbury, Peter Lloyd Jones, and James F Martin. 2009. "Defective Pulmonary Vascular Remodeling in Smad8 Mutant Mice." *Human Molecular Genetics* 18 (15): 2791–2801. https://doi.org/10.1093/hmg/ddp214.
Hurst, Liam A., Benjamin J. Dunmore, Lu Long, Alexi Crosby, Rafia Al-Lamki, John Deighton, Mark Southwood, et al. 2017. "TNFα Drives Pulmonary Arterial Hypertension by Suppressing the BMP Type-II Receptor and Altering NOTCH Signalling." *Nature Communications* 8 (1): 14079. https://doi.org/10.1038/ncomms14079.
International PPH Consortium, Kirk B., K B Lane, R D Machado, M W Pauciulo, J R Thomson, J A Phillips, J E Loyd, W C Nichols, and R C Trembath. 2000. "Heterozygous Germline Mutations in BMPR2, Encoding a TGF-Beta Receptor, Cause Familial Primary Pulmonary Hypertension." *Nature Genetics* 26 (1): 81–84. https://doi.org/10.1038/79226.
Ip, E, Geoffrey C Farrell, Graham Robertson, Pauline Hall, Richard Kirsch, and Isabelle Leclercq. 2003. "Central Role of PPARα-Dependent Hepatic Lipid Turnover in Dietary Steatohepatitis in Mice." *Hepatology* 38 (1): 123–32. https://doi.org/10.1053/jhep.2003.50307.
Israel, D I, J Nove, K M Kerns, I K Moutsatsos, and R J Kaufman. 1992. "Expression and Characterization of Bone Morphogenetic Protein-2 in Chinese Hamster Ovary Cells." *Growth Factors (Chur, Switzerland)* 7 (2): 139–50. http://www.ncbi.nlm.nih.gov/pubmed/1419071.
Jasińska-Stroschein, Magdalena, and Daria Orszulak-Michalak. 2017. "Novel Strategies for Treatment of Pulmonary Arterial Hypertension." *Postepy Higieny i Medycyny Doswiadczalnej (Online)* 71 (0): 577–88. http://www.ncbi.nlm.nih.gov/pubmed/28791952.
Jerkic, Mirjana, Mohammed G Kabir, Adrienne Davies, Lisa X Yu, Brendan A S McIntyre, Nasir W Husain, Masahiro Enomoto, et al. 2011. "Pulmonary Hypertension in Adult Alk1 Heterozygous Mice Due to Oxidative Stress." *Cardiovascular Research* 92 (3): 375–84. https://doi.org/10.1093/cvr/cvr232.
Jiang, He, Richard M. Salmon, Paul D. Upton, Zhenquan Wei, Aleksandra Lawera, Anthony P. Davenport, Nicholas W. Morrell, and Wei Li. 2016. "The Prodomain-Bound Form of BMP10 Is Active on Endothelial Cells." *J.Biol.Chem.* 291 (6). https://doi.org/10.1074/jbc.M115.683292.
John, Miya, Kyung-Jin Kim, Sarah Da Won Bae, Liang Qiao, and Jacob George. 2018. "Role of BMP-9 in Human Liver Disease." *Gut*, October, gutjnl-2018-317543. https://doi.org/10.1136/gutjnl-2018-317543.
Johnson, Katharine E., Yogeshwar Makanji, Peter Temple-Smith, Emily K. Kelly, Peter A. Barton, Sara L. Al-Musawi, Thomas D. Mueller, Kelly L. Walton, and Craig A. Harrison. 2016. "Biological Activity and in Vivo Half-Life of pro-Activin A in Male Rats." *Molecular and Cellular Endocrinology* 422 (February): 84–92. https://doi.org/10.1016/j.mce.2015.12.007.
Jones, W K, E A Richmond, K White, H Sasak, W Kusmik, J Smart, H Oppermann, D C Rueger, and R F Tucker. 1994. "Osteogenic Protein-1 (OP-1) Expression and Processing in Chinese Hamster Ovary Cells: Isolation of a Soluble Complex Containing the Mature and pro-Domains of OP-1." *Growth Factors (Chur, Switzerland)* 11 (3): 215–25. http://www.ncbi.nlm.nih.gov/pubmed/7734147.
Kang, Q, M H Sun, H Cheng, Y Peng, A G Montag, A T Deyrup, W Jiang, et al. 2004. "Characterization of the Distinct Orthotopic Bone-Forming Activity of 14 BMPs Using Recombinant Adenovirus-Mediated Gene Delivery." *Gene Therapy* 11 (17): 1312–20. https://doi.org/10.1038/sj.gt.3302298.
Karczewski, Konrad J., Laurent C. Francioli, Grace Tiao, Beryl B. Cummings, Jessica Alföldi, Qingbo Wang, Ryan L. Collins, et al. 2019. "Variation across 141,456 Human Exomes and

Genomes Reveals the Spectrum of Loss-of-Function Intolerance across Human Protein-Coding Genes." *BioRxiv*, August, 531210. https://doi.org/10.1101/531210.
Kerstjens-Frederikse, Wilhelmina S, Ernie M H F Bongers, Marcus T R Roofthooft, Edward M Leter, J Menno Douwes, Arie Van Dijk, Anton Vonk-Noordegraaf, et al. 2013. "*TBX4* Mutations (Small Patella Syndrome) Are Associated with Childhood-Onset Pulmonary Arterial Hypertension." *Journal of Medical Genetics* 50 (8): 500–506. https://doi.org/10.1136/jmedgenet-2012-101152.
Kienast, Yvonne, Ute Jucknischke, Stefan Scheiblich, Martina Thier, Mariana de Wouters, Alexander Haas, Christian Lehmann, et al. 2016. "Rapid Activation of Bone Morphogenic Protein 9 by Receptor-Mediated Displacement of Pro-Domains." *The Journal of Biological Chemistry* 291 (7): 3395–3410. https://doi.org/10.1074/jbc.M115.680009.
Kim, Jihye, Minhyung Kim, Yoonjeong Jeong, Wook-bin Lee, Hyojin Park, Ja-Young Kwon, Young-Myeong Kim, Daehee Hwang, and Young-Guen Kwon. 2015. "BMP9 Induces Cord Blood–Derived Endothelial Progenitor Cell Differentiation and Ischemic Neovascularization via ALK1." *Arteriosclerosis, Thrombosis, and Vascular Biology* 35 (9): 2020–31. https://doi.org/10.1161/ATVBAHA.115.306142.
Kiskin, FN, CH Chang, … CJZ Huang - American journal of, and Undefined 2018. 2018. "Contributions of BMPR2 Mutations and Extrinsic Factors to Cellular Phenotypes of Pulmonary Arterial Hypertension Revealed by Induced Pluripotent Stem Cell." *Atsjournals.Org*. https://www.atsjournals.org/doi/abs/10.1164/rccm.201801-0049LE.
Kono, Hiroshi, Takehiko Uesugi, Matthias Froh, Ivan Rusyn, Blair U. Bradford, and Ronald G. Thurman. 2001. "ICAM-1 Is Involved in the Mechanism of Alcohol-Induced Liver Injury: Studies with Knockout Mice." *American Journal of Physiology-Gastrointestinal and Liver Physiology* 280 (6): G1289–95. https://doi.org/10.1152/ajpgi.2001.280.6.G1289.
Korchynskyi, Olexander, and Peter ten Dijke. 2002. "Identification and Functional Characterization of Distinct Critically Important Bone Morphogenetic Protein-Specific Response Elements in the Id1 Promoter." *Journal of Biological Chemistry* 277 (7): 4883–91. https://doi.org/10.1074/jbc.M111023200.
Kraehling, Jan R, John H Chidlow, Chitra Rajagopal, Michael G Sugiyama, Joseph W Fowler, Monica Y Lee, Xinbo Zhang, et al. 2016. "Genome-Wide RNAi Screen Reveals ALK1 Mediates LDL Uptake and Transcytosis in Endothelial Cells." *Nature Communications* 7 (November): 13516. https://doi.org/10.1038/ncomms13516.
Kuo, Mario Meng-Chiang, Sooho Kim, Chia-Yun Tseng, Yun-Hui Jeon, Senyon Choe, and Dong Kun Lee. 2014. "BMP-9 as a Potent Brown Adipogenic Inducer with Anti-Obesity Capacity." *Biomaterials* 35 (10): 3172–79. https://doi.org/10.1016/j.biomaterials.2013.12.063.
Lagna, Giorgio, Peter H. Nguyen, Weihua Ni, and Akiko Hata. 2006. "BMP-Dependent Activation of Caspase-9 and Caspase-8 Mediates Apoptosis in Pulmonary Artery Smooth Muscle Cells." *American Journal of Physiology-Lung Cellular and Molecular Physiology* 291 (5): L1059–67. https://doi.org/10.1152/ajplung.00180.2006.
Lamouille, Samy, Christine Mallet, Jean-Jacques Feige, and Sabine Bailly. 2002. "Activin Receptor-like Kinase 1 Is Implicated in the Maturation Phase of Angiogenesis." *Blood* 100 (13): 4495–4501. https://doi.org/10.1182/blood.V100.13.4495.
Larkin, Emma K., John H. Newman, Eric D. Austin, Anna R. Hemnes, Lisa Wheeler, Ivan M. Robbins, James D. West, John A. Phillips, Rizwan Hamid, and James E. Loyd. 2012. "Longitudinal Analysis Casts Doubt on the Presence of Genetic Anticipation in Heritable Pulmonary Arterial Hypertension." *American Journal of Respiratory and Critical Care Medicine* 186 (9): 892–96. https://doi.org/10.1164/rccm.201205-0886OC.
Larrivée, Bruno, Claudia Prahst, Emma Gordon, Raquel del Toro, Thomas Mathivet, Antonio Duarte, Michael Simons, and Anne Eichmann. 2012. "ALK1 Signaling Inhibits Angiogenesis by Cooperating with the Notch Pathway." *Developmental Cell* 22 (3): 489–500. https://doi.org/10.1016/j.devcel.2012.02.005.

Lau, Edmund M. T., Eleni Giannoulatou, David S. Celermajer, and Marc Humbert. 2017. "Epidemiology and Treatment of Pulmonary Arterial Hypertension." *Nature Reviews Cardiology* 14 (10): 603–14. https://doi.org/10.1038/nrcardio.2017.84.

Laux, Derek W, Sarah Young, James P Donovan, Corrine J Mansfield, Paul D Upton, and Beth L Roman. 2013. "Circulating Bmp10 Acts through Endothelial Alk1 to Mediate Flow-Dependent Arterial Quiescence." *Development (Cambridge, England)* 140 (16): 3403–12. https://doi.org/10.1242/dev.095307.

Lawera, Aleksandra, Zhen Tong, Midory Thorikay, Rachael E Redgrave, Jie Cai, Maarten van Dinther, Nicholas W Morrell, et al. 2019. "Role of Soluble Endoglin in BMP9 Signaling." *Proceedings of the National Academy of Sciences of the United States of America* 116 (36): 17800–808. https://doi.org/10.1073/pnas.1816661116.

Levet, S., D. Ciais, G. Merdzhanova, C. Mallet, T. A. Zimmers, S.-J. Lee, F. P. Navarro, et al. 2013. "Bone Morphogenetic Protein 9 (BMP9) Controls Lymphatic Vessel Maturation and Valve Formation." *Blood* 122 (4): 598–607. https://doi.org/10.1182/blood-2012-12-472142.

Levet, Sandrine, Marie Ouarné, Delphine Ciais, Charles Coutton, Mariela Subileau, Christine Mallet, Nicolas Ricard, et al. 2015. "BMP9 and BMP10 Are Necessary for Proper Closure of the Ductus Arteriosus." *Proceedings of the National Academy of Sciences of the United States of America* 112 (25): E3207-15. https://doi.org/10.1073/pnas.1508386112.

Li, D Y, L K Sorensen, B S Brooke, L D Urness, E C Davis, D G Taylor, B B Boak, and D P Wendel. 1999. "Defective Angiogenesis in Mice Lacking Endoglin." *Science (New York, N.Y.)* 284 (5419): 1534–37. http://www.ncbi.nlm.nih.gov/pubmed/10348742.

Li, Peng, Yongyun Li, Liqi Zhu, Zhi Yang, Jie He, Lihua Wang, Qingfeng Shang, et al. 2018. "Targeting Secreted Cytokine BMP9 Gates the Attenuation of Hepatic Fibrosis." *Biochimica et Biophysica Acta (BBA) - Molecular Basis of Disease* 1864 (3): 709–20. https://doi.org/10.1016/J.BBADIS.2017.12.008.

Li, Qi, Xing Gu, Honglei Weng, Shahrouz Ghafoory, Yan Liu, Teng Feng, Johanna Dzieran, et al. 2013. "Bone Morphogenetic Protein-9 Induces Epithelial to Mesenchymal Transition in Hepatocellular Carcinoma Cells." *Cancer Science* 104 (3): 398–408. https://doi.org/10.1111/cas.12093.

Li, Ruifang, Zhengjian Yan, Jixing Ye, He Huang, Zhongliang Wang, Qiang Wei, Jing Wang, et al. 2016. "The Prodomain-Containing BMP9 Produced from a Stable Line Effectively Regulates the Differentiation of Mesenchymal Stem Cells." *International Journal of Medical Sciences* 13 (1): 8–18. https://doi.org/10.7150/ijms.13333.

Li, W., R. M. Salmon, H. Jiang, and N. W. Morrell. 2016. "Regulation of the ALK1 Ligands, BMP9 and BMP10." *Biochemical Society Transactions* 44 (4): 1135–41. https://doi.org/10.1042/BST20160083.

Li, W, L Long, X Yang, R King, M Southwood, Z Tong, P Caruso, et al. 2018. "S39 Endogenous Circulating BMP9 Maintains Endothelial Barrier Function." *Thorax* 73 (Suppl 4): A24–A24. https://doi.org/10.1136/thorax-2018-212555.45.

Liu, Rui, Wenjing Hu, Xiaoqiang Li, Danlan Pu, Gangyi Yang, Hua Liu, Minghong Tan, and Danping Zhu. 2019. "Association of Circulating BMP9 with Coronary Heart Disease and Hypertension in Chinese Populations." *BMC Cardiovascular Disorders* 19 (1): 131. https://doi.org/10.1186/s12872-019-1095-2.

Livak, Kenneth J., and Thomas D. Schmittgen. 2001. "Analysis of Relative Gene Expression Data Using Real-Time Quantitative PCR and the 2−ΔΔCT Method." *Methods* 25 (4): 402–8. https://doi.org/10.1006/meth.2001.1262.

Long, Lu, Mark L Ormiston, Xudong Yang, Mark Southwood, Stefan Gräf, Rajiv D Machado, Matthias Mueller, et al. 2015. "Selective Enhancement of Endothelial BMPR-II with BMP9 Reverses Pulmonary Arterial Hypertension." *Nat Med* 21 (7): 777–85. https://doi.org/10.1038/nm.3877.

Luo, Jinyong, Min Tang, Jiayi Huang, Bai-Cheng He, Jian-Li Gao, Liang Chen, Guo-Wei Zuo, et

al. 2010. “TGFbeta/BMP Type I Receptors ALK1 and ALK2 Are Essential for BMP9-Induced Osteogenic Signaling in Mesenchymal Stem Cells.” *J Biol Chem.* 285 (38). https://doi.org/10.1074/jbc.M110.130518.

Luo, Yong, Ling Li, Xiaohui Xu, Tong Wu, Mengliu Yang, Cheng Zhang, Huaming Mou, et al. 2017. “Decreased Circulating BMP-9 Levels in Patients with Type 2 Diabetes Is a Signature of Insulin Resistance.” *Clinical Science* 131 (3): 239–46. https://doi.org/10.1042/CS20160543.

Luu, Hue H., Wen-Xin Song, Xiaoji Luo, David Manning, Jinyong Luo, Zhong-Liang Deng, Katie A. Sharff, Anthony G. Montag, Rex C. Haydon, and Tong-Chuan He. 2007. “Distinct Roles of Bone Morphogenetic Proteins in Osteogenic Differentiation of Mesenchymal Stem Cells.” *Journal of Orthopaedic Research* 25 (5): 665–77. https://doi.org/10.1002/jor.20359.

Lux, A, L Attisano, and D A Marchuk. 1999. “Assignment of Transforming Growth Factor Beta1 and Beta3 and a Third New Ligand to the Type I Receptor ALK-1.” *The Journal of Biological Chemistry* 274 (15): 9984–92. https://doi.org/10.1074/jbc.274.15.9984.

Ma, Lijiang, and Wendy K Chung. 2017. “The Role of Genetics in Pulmonary Arterial Hypertension.” *The Journal of Pathology* 241 (2): 273–80. https://doi.org/10.1002/path.4833.

Ma, Lijiang, Danilo Roman-Campos, Eric D. Austin, Mélanie Eyries, Kevin S. Sampson, Florent Soubrier, Marine Germain, et al. 2013. “A Novel Channelopathy in Pulmonary Arterial Hypertension.” *New England Journal of Medicine* 369 (4): 351–61. https://doi.org/10.1056/NEJMoa1211097.

Machado, Rajiv D., Oliver Eickelberg, C. Gregory Elliott, Mark W. Geraci, Masayuki Hanaoka, James E. Loyd, John H. Newman, et al. 2009. “Genetics and Genomics of Pulmonary Arterial Hypertension.” *Journal of the American College of Cardiology* 54 (1): S32–42. https://doi.org/10.1016/j.jacc.2009.04.015.

Machado, Rajiv D., Victoria James, Mark Southwood, Rachel E. Harrison, Carl Atkinson, Susan Stewart, Nicholas W. Morrell, Richard C. Trembath, and Micheala A. Aldred. 2005. “Investigation of Second Genetic Hits at the *BMPR2* Locus as a Modulator of Disease Progression in Familial Pulmonary Arterial Hypertension.” *Circulation* 111 (5): 607–13. https://doi.org/10.1161/01.CIR.0000154543.07679.08.

Maguire, Janet J., Rhoda E. Kuc, and Anthony P. Davenport. 2012. “Radioligand Binding Assays and Their Analysis.” In *Methods in Molecular Biology (Clifton, N.J.)*, 897:31–77. https://doi.org/10.1007/978-1-61779-909-9_3.

Mahmoud, Marwa, Gillian M Borthwick, Alison A Hislop, and Helen M Arthur. 2009. “Endoglin and Activin Receptor-like-Kinase 1 Are Co-Expressed in the Distal Vessels of the Lung: Implications for Two Familial Vascular Dysplasias, HHT and PAH.” *Laboratory Investigation; a Journal of Technical Methods and Pathology* 89 (1): 15–25. https://doi.org/10.1038/labinvest.2008.112.

Martin, Harry. 2010. “Role of PPAR-Gamma in Inflammation. Prospects for Therapeutic Intervention by Food Components.” *Mutation Research/Fundamental and Molecular Mechanisms of Mutagenesis* 690 (1–2): 57–63. https://doi.org/10.1016/j.mrfmmm.2009.09.009.

McDonald, Jamie, Whitney Wooderchak-Donahue, Chad VanSant Webb, Kevin Whitehead, David A. Stevenson, and Pinar Bayrak-Toydemir. 2015. “Hereditary Hemorrhagic Telangiectasia: Genetics and Molecular Diagnostics in a New Era.” *Frontiers in Genetics* 6 (January): 1. https://doi.org/10.3389/fgene.2015.00001.

Meurer, Steffen K., Muhammad Alsamman, Hacer Sahin, Hermann E. Wasmuth, Tatiana Kisseleva, David A. Brenner, Christian Trautwein, Ralf Weiskirchen, and David Scholten. 2013. “Overexpression of Endoglin Modulates TGF-B1-Signalling Pathways in a Novel Immortalized Mouse Hepatic Stellate Cell Line.” Edited by Sadashiva Karnik. *PLoS ONE* 8 (2): e56116. https://doi.org/10.1371/journal.pone.0056116.

Mi, Li-Zhi, Christopher T. Brown, Yijie Gao, Yuan Tian, Viet Q. Le, Thomas Walz, and Timothy A. Springer. 2015. "Structure of BMP9 Complex." *Proc.Natl.Acad.Sci.* 112 (12). https://doi.org/10.1073/pnas.1501303112.
Miller, A F, S A Harvey, R S Thies, and M S Olson. 2000. "Bone Morphogenetic Protein-9. An Autocrine/Paracrine Cytokine in the Liver." *The Journal of Biological Chemistry* 275 (24): 17937–45. https://doi.org/10.1074/jbc.275.24.17937.
Miyazono, Kohei, Yuto Kamiya, and Masato Morikawa. 2010. "Bone Morphogenetic Protein Receptors and Signal Transduction." *Journal of Biochemistry* 147 (1): 35–51. https://doi.org/10.1093/jb/mvp148.
Moitra, Jaideep, Saad Sammani, and Joe G.N. Garcia. 2007. "Re-Evaluation of Evans Blue Dye as a Marker of Albumin Clearance in Murine Models of Acute Lung Injury." *Translational Research* 150 (4): 253–65. https://doi.org/10.1016/j.trsl.2007.03.013.
Morrell, Nicholas W., Paul D. Upton, Wei Li, and Paul B. Yu. 2019. "Letter by Morrell et Al Regarding Article, 'Selective BMP-9 Inhibition Partially Protects Against Experimental Pulmonary Hypertension.'" *Circulation Research* 124 (9). https://doi.org/10.1161/CIRCRESAHA.119.314962.
Morrell, Nicholas W., Xudong Yang, Paul D. Upton, Karen B. Jourdan, Neal Morgan, Karen K. Sheares, and Richard C. Trembath. 2001. "Altered Growth Responses of Pulmonary Artery Smooth Muscle Cells From Patients With Primary Pulmonary Hypertension to Transforming Growth Factor-β_1 and Bone Morphogenetic Proteins." *Circulation* 104 (7): 790–95. https://doi.org/10.1161/hc3201.094152.
Morrell, Nicholas W, Micheala A Aldred, Wendy K Chung, C Gregory Elliott, William C Nichols, Florent Soubrier, Richard C Trembath, and James E Loyd. 2019. "Genetics and Genomics of Pulmonary Arterial Hypertension." *The European Respiratory Journal* 53 (1): 1801899. https://doi.org/10.1183/13993003.01899-2018.
Morris, Erin, Izabela Chrobak, Andreea Bujor, Faye Hant, Christine Mummery, Peter Ten Dijke, and Maria Trojanowska. 2011. "Endoglin Promotes TGF-β/Smad1 Signaling in Scleroderma Fibroblasts." *Journal of Cellular Physiology* 226 (12): 3340–48. https://doi.org/10.1002/jcp.22690.
Nasim, Md. Talat, Takeshi Ogo, Mohammad Ahmed, Rebecca Randall, Hasnin M. Chowdhury, Katie M. Snape, Teisha Y. Bradshaw, et al. 2011. "No Title" 32 (12). https://doi.org/10.1002/humu.21605.
Navas, Paula, Jair Tenorio, Carlos Andrés Quezada, Elvira Barrios, Gema Gordo, Pedro Arias, Manuel López Meseguer, et al. 2016. "Molecular Analysis of BMPR2 , TBX4 , and KCNK3 and Genotype-Phenotype Correlations in Spanish Patients and Families With Idiopathic and Hereditary Pulmonary Arterial Hypertension." *Revista Española de Cardiología (English Edition)* 69 (11): 1011–19. https://doi.org/10.1016/j.rec.2016.03.029.
Neuhaus, H, V Rosen, and R S Thies. 1999. "Heart Specific Expression of Mouse BMP-10 a Novel Member of the TGF-Beta Superfamily." *Mechanisms of Development* 80 (2): 181–84. http://www.ncbi.nlm.nih.gov/pubmed/10072785.
Nie, Li, Xia Yang, Liang Duan, Enyi Huang, Zhou Pengfei, Wenping Luo, Yan Zhang, et al. 2017. "The Healing of Alveolar Bone Defects with Novel Bio-Implants Composed of Ad-BMP9-Transfected RDFCs and CHA Scaffolds." *Scientific Reports* 7 (1): 6373. https://doi.org/10.1038/s41598-017-06548-7.
Niessen, K., G. Zhang, J. B. Ridgway, H. Chen, and M. Yan. 2010. "ALK1 Signaling Regulates Early Postnatal Lymphatic Vessel Development." *Blood* 115 (8): 1654–61. https://doi.org/10.1182/blood-2009-07-235655.
Nikolic, Ivana, Lai-Ming Yung, Peiran Yang, Rajeev Malhotra, Samuel D. Paskin-Flerlage, Teresa Dinter, Geoffrey A. Bocobo, et al. 2019. "Bone Morphogenetic Protein 9 Is a Mechanistic Biomarker of Portopulmonary Hypertension." *American Journal of Respiratory and Critical Care Medicine* 199 (7): 891–902. https://doi.org/10.1164/rccm.201807-1236OC.
Ntumba, Kalonji, Naoufal Akla, S Paul Oh, Anne Eichmann, and Bruno Larrivée. 2016.

"BMP9/ALK1 Inhibits Neovascularization in Mouse Models of Age-Related Macular Degeneration." *Oncotarget* 7 (35): 55957–69. https://doi.org/10.18632/oncotarget.11182.

Oh, S P, T Seki, K A Goss, T Imamura, Y Yi, P K Donahoe, L Li, et al. 2000. "Activin Receptor-like Kinase 1 Modulates Transforming Growth Factor-Beta 1 Signaling in the Regulation of Angiogenesis." *Proceedings of the National Academy of Sciences of the United States of America* 97 (6): 2626–31. https://doi.org/10.1073/pnas.97.6.2626.

Oki, Shinya, Tazro Ohta, Go Shioi, Hideki Hatanaka, Osamu Ogasawara, Yoshihiro Okuda, Hideya Kawaji, Ryo Nakaki, Jun Sese, and Chikara Meno. 2018. "Ch IP -Atlas: A Data-mining Suite Powered by Full Integration of Public Ch IP -seq Data." *EMBO Reports* 19 (12). https://doi.org/10.15252/embr.201846255.

Olsen, O E, K F Wader, K Misund, T K Våtsveen, T B Rø, A K Mylin, I Turesson, et al. 2014. "Bone Morphogenetic Protein-9 Suppresses Growth of Myeloma Cells by Signaling through ALK2 but Is Inhibited by Endoglin." *Blood Cancer Journal* 4 (3): e196. https://doi.org/10.1038/bcj.2014.16.

Örem, Cihan. 2017. "Epidemiology of Pulmonary Hypertension in the Elderly." *Journal of Geriatric Cardiology : JGC* 14 (1): 11–16. https://doi.org/10.11909/j.issn.1671-5411.2017.01.001.

Ormiston, Mark L., Chiwen Chang, Lu L. Long, Elaine Soon, Des Jones, Rajiv Machado, Carmen Treacy, et al. 2012. "Impaired Natural Killer Cell Phenotype and Function in Idiopathic and Heritable Pulmonary Arterial Hypertension." *Circulation* 126 (9): 1099–1109. https://doi.org/10.1161/CIRCULATIONAHA.112.110619.

Ormiston, Mark L., Mark R. Toshner, Fedir N. Kiskin, Christopher J. Z. Huang, Emily Groves, Nicholas W. Morrell, and Amer A. Rana. 2015. "Generation and Culture of Blood Outgrowth Endothelial Cells from Human Peripheral Blood." *Journal of Visualized Experiments*, no. 106 (December): e53384. https://doi.org/10.3791/53384.

Ormiston, Mark L, Paul D Upton, Wei Li, and Nicholas W Morrell. 2015. "The Promise of Recombinant BMP Ligands and Other Approaches Targeting BMPR-II in the Treatment of Pulmonary Arterial Hypertension." *Global Cardiology Science & Practice* 2015 (4): 47. https://doi.org/10.5339/gcsp.2015.47.

Ouarné, Marie, Claire Bouvard, Gabriela Boneva, Christine Mallet, Johnny Ribeiro, Agnès Desroches-Castan, Emmanuelle Soleilhac, Emmanuelle Tillet, Olivier Peyruchaud, and Sabine Bailly. 2018. "BMP9, but Not BMP10, Acts as a Quiescence Factor on Tumor Growth, Vessel Normalization and Metastasis in a Mouse Model of Breast Cancer." *Journal of Experimental & Clinical Cancer Research* 37 (1): 209. https://doi.org/10.1186/s13046-018-0885-1.

Panchenko, M. P., M. C. Williams, J. S. Brody, and Q. Yu. 1996. "Type I Receptor Serine-Threonine Kinase Preferentially Expressed in Pulmonary Blood Vessels." *American Journal of Physiology-Lung Cellular and Molecular Physiology* 270 (4): L547–58. https://doi.org/10.1152/ajplung.1996.270.4.L547.

Park, S. O., Y. J. Lee, T. Seki, K.-H. Hong, N. Fliess, Z. Jiang, A. Park, et al. 2008. "ALK5- and TGFBR2-Independent Role of ALK1 in the Pathogenesis of Hereditary Hemorrhagic Telangiectasia Type 2." *Blood* 111 (2): 633–42. https://doi.org/10.1182/blood-2007-08-107359.

Park, Sung Ok, Mamta Wankhede, Young Jae Lee, Eun-Jung Choi, Naime Fliess, Se-Woon Choe, Seh-Hoon Oh, et al. 2009. "Real-Time Imaging of de Novo Arteriovenous Malformation in a Mouse Model of Hereditary Hemorrhagic Telangiectasia." *Journal of Clinical Investigation* 119 (11): 3487–96. https://doi.org/10.1172/JCI39482.

Peacock, A J, N F Murphy, J J V McMurray, L Caballero, and S Stewart. 2007. "An Epidemiological Study of Pulmonary Arterial Hypertension." *The European Respiratory Journal* 30 (1): 104–9. https://doi.org/10.1183/09031936.00092306.

Peng, Ying, Quan Kang, Hongwei Cheng, Xinmin Li, Michael H. Sun, Wei Jiang, Hue H. Luu, Jae

Yoon Park, Rex C. Haydon, and Tong-Chuan He. 2003. “Transcriptional Characterization of Bone Morphogenetic Proteins (BMPs)-Mediated Osteogenic Signaling.” *Journal of Cellular Biochemistry* 90 (6): 1149–65. https://doi.org/10.1002/jcb.10744.

Peng, Ying, Quan Kang, Qing Luo, Wei Jiang, Weike Si, Bernard A Liu, Hue H Luu, et al. 2004. “Inhibitor of DNA Binding/Differentiation Helix-Loop-Helix Proteins Mediate Bone Morphogenetic Protein-Induced Osteoblast Differentiation of Mesenchymal Stem Cells.” *The Journal of Biological Chemistry* 279 (31): 32941–49. https://doi.org/10.1074/jbc.M403344200.

Poduri, Aruna, Andrew H Chang, Brian Raftrey, Siyeon Rhee, Mike Van, and Kristy Red-Horse. 2017. “Endothelial Cells Respond to the Direction of Mechanical Stimuli through SMAD Signaling to Regulate Coronary Artery Size.” *Development (Cambridge, England)* 144 (18): 3241–52. https://doi.org/10.1242/dev.150904.

Porez, Geoffrey, Barbara Gross, Janne Prawitt, Céline Gheeraert, Wahiba Berrabah, Jeremy Alexandre, Bart Staels, and Philippe Lefebvre. 2013. “The Hepatic Orosomucoid/A1-Acid Glycoprotein Gene Cluster Is Regulated by the Nuclear Bile Acid Receptor FXR.” *Endocrinology* 154 (10): 3690–3701. https://doi.org/10.1210/en.2013-1263.

Porres-Aguilar, Mateo, Jose T Altamirano, Aldo Torre-Delgadillo, Michael R Charlton, and Andres Duarte-Rojo. 2012. “Portopulmonary Hypertension and Hepatopulmonary Syndrome: A Clinician-Oriented Overview.” *European Respiratory Review : An Official Journal of the European Respiratory Society* 21 (125): 223–33. https://doi.org/10.1183/09059180.00007211.

Pousada, Guillermo, Adolfo Baloira, and Diana Valverde. 2016. “Complex Inheritance in Pulmonary Arterial Hypertension Patients with Several Mutations.” *Scientific Reports* 6 (1): 33570. https://doi.org/10.1038/srep33570.

Prigoda, N L. 2006. “Hereditary Haemorrhagic Telangiectasia: Mutation Detection, Test Sensitivity and Novel Mutations.” *Journal of Medical Genetics* 43 (9): 722–28. https://doi.org/10.1136/jmg.2006.042606.

Rabinovitch, Marlene. 1999. “EVE and beyond, Retro and Prospective Insights.” *American Journal of Physiology-Lung Cellular and Molecular Physiology* 277 (1): L5–12. https://doi.org/10.1152/ajplung.1999.277.1.L5.

Ramos, Margaret F., Michael W. Lamé, Henry J. Segall, and Dennis W. Wilson. 2008. “Smad Signaling in the Rat Model of Monocrotaline Pulmonary Hypertension.” *Toxicologic Pathology* 36 (2). https://doi.org/10.1177/0192623307311402.

Reinke, Hans, and Gad Asher. 2016. “Circadian Clock Control of Liver Metabolic Functions.” *Gastroenterology* 150 (3): 574–80. https://doi.org/10.1053/j.gastro.2015.11.043.

Rentzsch, Philipp, Daniela Witten, Gregory M Cooper, Jay Shendure, and Martin Kircher. 2019. “CADD: Predicting the Deleteriousness of Variants throughout the Human Genome.” *Nucleic Acids Research* 47 (D1): D886–94. https://doi.org/10.1093/nar/gky1016.

Rhodes, Christopher J, Ken Batai, Marta Bleda, Matthias Haimel, Laura Southgate, Marine Germain, Michael W Pauciulo, et al. 2019. “Genetic Determinants of Risk in Pulmonary Arterial Hypertension: International Genome-Wide Association Studies and Meta-Analysis.” *The Lancet. Respiratory Medicine* 7 (3): 227–38. https://doi.org/10.1016/S2213-2600(18)30409-0.

Rhodes, Christopher J, Pavandeep Ghataorhe, John Wharton, Kevin C Rue-Albrecht, Charaka Hadinnapola, Geoffrey Watson, Marta Bleda, et al. 2017. “Plasma Metabolomics Implicates Modified Transfer RNAs and Altered Bioenergetics in the Outcomes of Pulmonary Arterial Hypertension.” *Circulation* 135 (5): 460–75. https://doi.org/10.1161/CIRCULATIONAHA.116.024602.

Ricard, Nicolas, Delphine Ciais, Sandrine Levet, Mariela Subileau, Christine Mallet, Teresa A Zimmers, Se-Jin Lee, et al. 2012. “BMP9 and BMP10 Are Critical for Postnatal Retinal Vascular Remodeling.” *Blood* 119 (25): 6162–71. https://doi.org/10.1182/blood-2012-01-407593.

Roberts, K.E., J J McElroy, W P K Wong, E Yen, A Widlitz, R J Barst, J A Knowles, and J H Morse. 2004. "BMPR2 Mutations in Pulmonary Arterial Hypertension with Congenital Heart Disease." *European Respiratory Journal* 24 (3): 371–74. https://doi.org/10.1183/09031936.04.00018604.

Rochon, Elizabeth R., Prahlad G. Menon, and Beth L. Roman. 2016. "Alk1 Controls Arterial Endothelial Cell Migration in Lumenized Vessels." *Development* 143 (14): 2593–2602. https://doi.org/10.1242/dev.135392.

Rosenzweig, Erika B., Jane H. Morse, James A. Knowles, Kiran K. Chada, Amar M. Khan, Kari E. Roberts, Jude J. McElroy, et al. 2008. "Clinical Implications of Determining BMPR2 Mutation Status in a Large Cohort of Children and Adults With Pulmonary Arterial Hypertension." *The Journal of Heart and Lung Transplantation* 27 (6): 668–74. https://doi.org/10.1016/j.healun.2008.02.009.

Rostama, Bahman, Jacqueline E. Turner, Guy T. Seavey, Christine R. Norton, Thomas Gridley, Calvin P.H. Vary, and Lucy Liaw. 2015. "DLL4/Notch1 and BMP9 Interdependent Signaling Induces Human Endothelial Cell Quiescence via P27 ^{KIP1} and Thrombospondin-1." *Arteriosclerosis, Thrombosis, and Vascular Biology* 35 (12): 2626–37. https://doi.org/10.1161/ATVBAHA.115.306541.

Rudarakanchana, N., Julia A Flanagan, Hailan Chen, Paul D Upton, Rajiv Machado, D Patel, Richard C Trembath, and Nicholas W Morrell. 2002. "Functional Analysis of Bone Morphogenetic Protein Type II Receptor Mutations Underlying Primary Pulmonary Hypertension." *Human Molecular Genetics* 11 (13): 1517–25. https://doi.org/10.1093/hmg/11.13.1517.

Saito, Takako, Marcel Bokhove, Romina Croci, Sara Zamora-Caballero, Ling Han, Michelle Letarte, Daniele de Sanctis, and Luca Jovine. 2017. "Structural Basis of the Human Endoglin-BMP9 Interaction: Insights into BMP Signaling and HHT1." *Cell Rep.* 19 (9): 1917–28. https://doi.org/10.1016/j.celrep.2017.05.011.

Scharpfenecker, M., M. van Dinther, Z. Liu, R.L. van Bezooijen, Q. Zhao, L. Pukac, C. W. G. M. Lowik, and P. ten Dijke. 2007. "BMP-9 Signals via ALK1 and Inhibits BFGF-Induced Endothelial Cell Proliferation and VEGF-Stimulated Angiogenesis." *Journal of Cell Science* 120 (6): 964–72. https://doi.org/10.1242/jcs.002949.

Schlosser, Kenny, Mohamad Taha, Yupu Deng, Lauralyn A McIntyre, Shirley H J Mei, and Duncan J Stewart. 2018. "High Circulating Angiopoietin-2 Levels Exacerbate Pulmonary Inflammation but Not Vascular Leak or Mortality in Endotoxin-Induced Lung Injury in Mice." *Thorax* 73 (3): 248–61. https://doi.org/10.1136/thoraxjnl-2017-210413.

Schlunegger, Michael P., and Markus G. Grütter. 1992. "An Unusual Feature Revealed by the Crystal Structure at 2.2 Å Resolution of Human Transforming Growth Fact or-B2." *Nature* 358 (6385): 430–34. https://doi.org/10.1038/358430a0.

Schmierer, Bernhard, and Caroline S. Hill. 2007. "TGFβ–SMAD Signal Transduction: Molecular Specificity and Functional Flexibility." *Nature Reviews Molecular Cell Biology* 8 (12): 970–82. https://doi.org/10.1038/nrm2297.

Seki, Tsugio, Jihye Yun, and S. Paul Oh. 2003. "Arterial Endothelium-Specific Activin Receptor-Like Kinase 1 Expression Suggests Its Role in Arterialization and Vascular Remodeling." *Circulation Research* 93 (7): 682–89. https://doi.org/10.1161/01.RES.0000095246.40391.3B.

Selzner, Nazia, Markus Selzner, Bernhard Odermatt, Yinghua Tian, Nico van Rooijen, and Pierre–Alain Clavien. 2003. "ICAM-1 Triggers Liver Regeneration through Leukocyte Recruitment and Kupffer Cell–Dependent Release of TNF-α/IL-6 in Mice." *Gastroenterology* 124 (3): 692–700. https://doi.org/10.1053/gast.2003.50098.

Sengle, Gerhard, Robert N Ono, Takako Sasaki, and Lynn Y Sakai. 2011. "Prodomains of Transforming Growth Factor Beta (TGFbeta) Superfamily Members Specify Different Functions: Extracellular Matrix Interactions and Growth Factor Bioavailability." *The Journal of Biological Chemistry* 286 (7): 5087–99.

https://doi.org/10.1074/jbc.M110.188615.
Shintani, M, H Yagi, T Nakayama, T Saji, and R Matsuoka. 2009. "A New Nonsense Mutation of SMAD8 Associated with Pulmonary Arterial Hypertension." *BMJ* 46 (5). https://doi.org/10.1136/jmg.2008.062703.
Shovlin, Claire L. 2014. "Pulmonary Arteriovenous Malformations." *American Journal of Respiratory and Critical Care Medicine* 190 (11): 1217–28. https://doi.org/10.1164/rccm.201407-1254CI.
Simonneau, Gerald, Michael A. Gatzoulis, Ian Adatia, David Celermajer, Chris Denton, Ardeschir Ghofrani, Miguel Angel Gomez Sanchez, et al. 2013. "Updated Clinical Classification of Pulmonary Hypertension." *Journal of the American College of Cardiology* 62 (25): D34–41. https://doi.org/10.1016/j.jacc.2013.10.029.
Simonneau, Gérald, David Montani, David S Celermajer, Christopher P Denton, Michael A Gatzoulis, Michael Krowka, Paul G Williams, and Rogerio Souza. 2019. "Haemodynamic Definitions and Updated Clinical Classification of Pulmonary Hypertension." *The European Respiratory Journal* 53 (1): 1801913. https://doi.org/10.1183/13993003.01913-2018.
Singer, Mark S, Joanna J Phillips, Hassan Lemjabbar-Alaoui, Yang Qing Wang, Jing Wu, Radoslav Goldman, and Steven D Rosen. 2015. "SULF2, a Heparan Sulfate Endosulfatase, Is Present in the Blood of Healthy Individuals and Increases in Cirrhosis." *Clinica Chimica Acta; International Journal of Clinical Chemistry* 440 (February): 72–78. https://doi.org/10.1016/j.cca.2014.10.038.
Sobolewski, A., N. Rudarakanchana, P. D. Upton, J. Yang, T. K. Crilley, R. C. Trembath, and N. W. Morrell. 2008. "Failure of Bone Morphogenetic Protein Receptor Trafficking in Pulmonary Arterial Hypertension: Potential for Rescue." *Human Molecular Genetics* 17 (20): 3180–90. https://doi.org/10.1093/hmg/ddn214.
Sofianopoulou, Eleni, Stephen Kaptoge, Stefan Gräf, Charaka Hadinnapola, Carmen M Treacy, Colin Church, Gerry Coghlan, et al. 2019. "Traffic Exposures, Air Pollution and Outcomes in Pulmonary Arterial Hypertension: A UK Cohort Study Analysis." *The European Respiratory Journal* 53 (5). https://doi.org/10.1183/13993003.01429-2018.
Song, J J, A J Celeste, F M Kong, R L Jirtle, V Rosen, and R S Thies. 1995. "Bone Morphogenetic Protein-9 Binds to Liver Cells and Stimulates Proliferation." *Endocrinology* 136 (10). https://doi.org/10.1210/endo.136.10.7664647.
Song, Yanli, John E. Jones, Hideyuki Beppu, John F. Keaney, Joseph Loscalzo, and Ying-Yi Zhang. 2005. "Increased Susceptibility to Pulmonary Hypertension in Heterozygous BMPR2-Mutant Mice." *Circulation* 112 (4): 553–62. https://doi.org/10.1161/CIRCULATIONAHA.104.492488.
Soon, Elaine, Alexi Crosby, Mark Southwood, Peiran Yang, Tamara Tajsic, Mark Toshner, Sarah Appleby, et al. 2015. "Bone Morphogenetic Protein Receptor Type II Deficiency and Increased Inflammatory Cytokine Production. A Gateway to Pulmonary Arterial Hypertension." *American Journal of Respiratory and Critical Care Medicine* 192 (7): 859–72. https://doi.org/10.1164/rccm.201408-1509OC.
Soubrier, Florent, Wendy K. Chung, Rajiv Machado, Ekkehard Grünig, Micheala Aldred, Mark Geraci, James E. Loyd, et al. 2013. "Genetics and Genomics of Pulmonary Arterial Hypertension." *Journal of the American College of Cardiology* 62 (25): D13–21. https://doi.org/10.1016/j.jacc.2013.10.035.
Susan-Resiga, Delia, Rachid Essalmani, Josée Hamelin, Marie-Claude Asselin, Suzanne Benjannet, Ann Chamberland, Robert Day, et al. 2011. "Furin Is the Major Processing Enzyme of the Cardiac-Specific Growth Factor Bone Morphogenetic Protein 10." *Journal of Biological Chemistry* 286 (26): 22785–94. https://doi.org/10.1074/JBC.M111.233577.
Sutendra, G., and E. D. Michelakis. 2013. "Pulmonary Arterial Hypertension: Challenges in Translational Research and a Vision for Change." *Science Translational Medicine* 5 (208): 208sr5-208sr5. https://doi.org/10.1126/scitranslmed.3005428.

Suzuki, Yuka, Noritaka Ohga, Yasuyuki Morishita, Kyoko Hida, Kohei Miyazono, and Tetsuro Watabe. 2010. "BMP-9 Induces Proliferation of Multiple Types of Endothelial Cells in Vitro and in Vivo." *Journal of Cell Science* 123 (Pt 10): 1684–92. https://doi.org/10.1242/jcs.061556.

Szklarczyk, Damian, Annika L Gable, David Lyon, Alexander Junge, Stefan Wyder, Jaime Huerta-Cepas, Milan Simonovic, et al. 2019. "STRING V11: Protein–Protein Association Networks with Increased Coverage, Supporting Functional Discovery in Genome-Wide Experimental Datasets." *Nucleic Acids Research* 47 (D1): D607–13. https://doi.org/10.1093/nar/gky1131.

Tajsic, Tamara, and Nicholas W Morrell. 2011. "Smooth Muscle Cell Hypertrophy, Proliferation, Migration and Apoptosis in Pulmonary Hypertension." *Comprehensive Physiology* 1 (1): 295–317. https://doi.org/10.1002/cphy.c100026.

Tate, Jill, and Greg Ward. 2004. "Interferences in Immunoassay." *The Clinical Biochemist. Reviews* 25 (2): 105–20. http://www.ncbi.nlm.nih.gov/pubmed/18458713.

Teichert-Kuliszewska, Krystyna, Michael J B Kutryk, Michael A Kuliszewski, Golnaz Karoubi, David W Courtman, Liana Zucco, John Granton, and Duncan J Stewart. 2006. "Bone Morphogenetic Protein Receptor-2 Signaling Promotes Pulmonary Arterial Endothelial Cell Survival: Implications for Loss-of-Function Mutations in the Pathogenesis of Pulmonary Hypertension." *Circulation Research* 98 (2): 209–17. https://doi.org/10.1161/01.RES.0000200180.01710.e6.

The Gene Ontology Consortium. 2019. "The Gene Ontology Resource: 20 Years and Still GOing Strong." *Nucleic Acids Research* 47 (D1): D330–38. https://doi.org/10.1093/nar/gky1055.

Thenappan, T, S J Shah, S Rich, and M Gomberg-Maitland. 2007. "A USA-Based Registry for Pulmonary Arterial Hypertension: 1982-2006." *The European Respiratory Journal* 30 (6): 1103–10. https://doi.org/10.1183/09031936.00042107.

Theruvath, Tom P., Venkat K. Ramshesh, Zhi Zhong, Robert T. Currin, Thomas Karrasch, and John J. Lemasters. 2012. "ICAM-1 Upregulation in Ethanol-Induced Fatty Murine Livers Promotes Injury and Sinusoidal Leukocyte Adherence after Transplantation." *HPB Surgery* 2012 (June): 1–10. https://doi.org/10.1155/2012/480893.

Thomas, Gary. 2002. "Furin at the Cutting Edge: From Protein Traffic to Embryogenesis and Disease." *Nature Reviews Molecular Cell Biology* 3 (10): 753–66. https://doi.org/10.1038/nrm934.

Thomson, J R, R D Machado, M W Pauciulo, N V Morgan, M Humbert, G C Elliott, K Ward, et al. 2000. "Sporadic Primary Pulmonary Hypertension Is Associated with Germline Mutations of the Gene Encoding BMPR-II, a Receptor Member of the TGF-Beta Family." *Journal of Medical Genetics* 37 (10): 741–45. https://doi.org/10.1136/jmg.37.10.741.

Tian, Sun. 2009. "A 20 Residue Motif Delineates the Furin Cleavage Site." http://www.expasy.

Tian, Wen, Xinguo Jiang, Yon K. Sung, Eric Shuffle, Ting-Hsuan Wu, Peter N. Kao, Allen B. Tu, et al. 2019. "Phenotypically Silent Bone Morphogenetic Protein Receptor 2 Mutations Predispose Rats to Inflammation-Induced Pulmonary Arterial Hypertension by Enhancing the Risk for Neointimal Transformation." *Circulation* 140 (17): 1409–25. https://doi.org/10.1161/CIRCULATIONAHA.119.040629.

Tillet, Emmanuelle, and Sabine Bailly. 2015. "Emerging Roles of BMP9 and BMP10 in Hereditary Hemorrhagic Telangiectasia." *Frontiers in Genetics* 5 (January). https://doi.org/10.3389/fgene.2014.00456.

Tillet, Emmanuelle, Marie Ouarné, Agnès Desroches-Castan, Christine Mallet, Mariela Subileau, Robin Didier, Anna Lioutsko, Guillaume Belthier, Jean-Jacques Feige, and Sabine Bailly. 2018. "A Heterodimer Formed by Bone Morphogenetic Protein 9 (BMP9) and BMP10 Provides Most BMP Biological Activity in Plasma." *The Journal of Biological Chemistry* 293 (28): 10963–74. https://doi.org/10.1074/jbc.RA118.002968.

Tørring, P., S. Dupuis-Girod, S. Giraud, K. Brusgaard, L. Ousager, and A. Kjeldsen. 2016. "Germline Mutations in BMP9 Are Not Identified in a Series of Danish and French Patients

with Hereditary Hemorrhagic Telangiectasia." *Gene Reports* 5 (December): 30–33. https://doi.org/10.1016/J.GENREP.2016.08.005.
Tørring, P.M., K. Brusgaard, L.B. Ousager, P.E. Andersen, and A.D. Kjeldsen. 2014. "National Mutation Study among Danish Patients with Hereditary Haemorrhagic Telangiectasia." *Clinical Genetics* 86 (2): 123–33. https://doi.org/10.1111/cge.12269.
Toshner, Mark, Robert Voswinckel, Mark Southwood, Rafia Al-Lamki, Luke S. G. Howard, Denis Marchesan, Jun Yang, et al. 2009. "Evidence of Dysfunction of Endothelial Progenitors in Pulmonary Arterial Hypertension." *American Journal of Respiratory and Critical Care Medicine* 180 (8): 780–87. https://doi.org/10.1164/rccm.200810-1662OC.
Townson, Sharon A., Erik Martinez-Hackert, Chloe Greppi, Patricia Lowden, Dianne Sako, June Liu, Jeffrey A. Ucran, et al. 2012. "Specificity and Structure of a High Affinity ALK1 Complex." *J.Biol.Chem.* 287 (33). https://doi.org/10.1074/jbc.M112.377960.
Truksa, Jaroslav, Hongfan Peng, Pauline Lee, and Ernest Beutler. 2006. "Bone Morphogenetic Proteins 2, 4, and 9 Stimulate Murine Hepcidin 1 Expression Independently of Hfe, Transferrin Receptor 2 (Tfr2), and IL-6." *Proceedings of the National Academy of Sciences of the United States of America* 103 (27): 10289–93. https://doi.org/10.1073/pnas.0603124103.
Tu, Ly, Agnès Desroches-Castan, Christine Mallet, Laurent Guyon, Amélie Cumont, Carole Phan, Florian Robert, et al. 2019. "Selective BMP-9 Inhibition Partially Protects Against Experimental Pulmonary Hypertension." *Circulation Research* 124 (6): 846–55. https://doi.org/10.1161/CIRCRESAHA.118.313356.
Tuder, Rubin M., John C. Marecki, Amy Richter, Iwona Fijalkowska, and Sonia Flores. 2007. "Pathology of Pulmonary Hypertension." *Clinics in Chest Medicine* 28 (1): 23–42. https://doi.org/10.1016/j.ccm.2006.11.010.
Upton, Paul D, Rachel J Davies, Richard C Trembath, and Nicholas W Morrell. 2009. "Bone Morphogenetic Protein (BMP) and Activin Type II Receptors Balance BMP9 Signals Mediated by Activin Receptor-like Kinase-1 in Human Pulmonary Artery Endothelial Cells." *The Journal of Biological Chemistry* 284 (23): 15794–804. https://doi.org/10.1074/jbc.M109.002881.
Upton, Paul D, Lu Long, Richard C Trembath, and Nicholas W Morrell. 2008. "Functional Characterization of Bone Morphogenetic Protein Binding Sites and Smad1/5 Activation in Human Vascular Cells." *Molecular Pharmacology* 73 (2): 539–52. https://doi.org/10.1124/mol.107.041673.
Urness, Lisa D., Lise K. Sorensen, and Dean Y. Li. 2000. "Arteriovenous Malformations in Mice Lacking Activin Receptor-like Kinase-1." *Nature Genetics* 26 (3): 328–31. https://doi.org/10.1038/81634.
Vaser, Robert, Swarnaseetha Adusumalli, Sim Ngak Leng, Mile Sikic, and Pauline C Ng. 2016. "SIFT Missense Predictions for Genomes." *Nature Protocols* 11 (1): 1–9. https://doi.org/10.1038/nprot.2015.123.
Verhoven, B, R A Schlegel, and P Williamson. 1995. "Mechanisms of Phosphatidylserine Exposure, a Phagocyte Recognition Signal, on Apoptotic T Lymphocytes." *The Journal of Experimental Medicine* 182 (5): 1597–1601. http://www.ncbi.nlm.nih.gov/pubmed/7595231.
Vinuesa, A. G. de, M. Bocci, K. Pietras, and P. ten Dijke. 2016. "Targeting Tumour Vasculature by Inhibiting Activin Receptor-like Kinase (ALK)1 Function." *Biochemical Society Transactions* 44 (4): 1142–49. https://doi.org/10.1042/BST20160093.
Vion, Anne-Clémence, Silvanus Alt, Alexandra Klaus-Bergmann, Anna Szymborska, Tuyu Zheng, Tijana Perovic, Adel Hammoutene, et al. 2018. "Primary Cilia Sensitize Endothelial Cells to BMP and Prevent Excessive Vascular Regression." *The Journal of Cell Biology* 217 (5): 1651–65. https://doi.org/10.1083/jcb.201706151.
Vorselaars, Veronique MM, Sebastiaan Velthuis, Repke J Snijder, Jan Albert Vos, Johannes J Mager, and Martijn C Post. 2015. "Pulmonary Hypertension in Hereditary Haemorrhagic

Telangiectasia." *World Journal of Cardiology* 7 (5): 230. https://doi.org/10.4330/wjc.v7.i5.230.
Wakefield, L M, T S Winokur, R S Hollands, K Christopherson, A D Levinson, and M B Sporn. 1990. "Recombinant Latent Transforming Growth Factor Beta 1 Has a Longer Plasma Half-Life in Rats than Active Transforming Growth Factor Beta 1, and a Different Tissue Distribution." *Journal of Clinical Investigation* 86 (6): 1976–84. https://doi.org/10.1172/JCI114932.
Walton, Kelly L., Yogeshwar Makanji, Matthew C. Wilce, Karen L. Chan, David M. Robertson, and Craig A. Harrison. 2009. "A Common Biosynthetic Pathway Governs the Dimerization and Secretion of Inhibin and Related Transforming Growth Factor β (TGFβ) Ligands." *Journal of Biological Chemistry* 284 (14): 9311–20. https://doi.org/10.1074/jbc.M808763200.
Wang, Guoliang, Rui Fan, Ruirui Ji, Wenxin Zou, Daniel J Penny, Nidhy P Varghese, and Yuxin Fan. 2016. "Novel Homozygous BMP9 Nonsense Mutation Causes Pulmonary Arterial Hypertension: A Case Report." *BMC Pulmonary Medicine* 16: 17. https://doi.org/10.1186/s12890-016-0183-7.
Wang, Xiao-Jian, Tian-Yu Lian, Xin Jiang, Shao-Fei Liu, Su-Qi Li, Rong Jiang, Wen-Hui Wu, et al. 2019. "Germline *BMP9* Mutation Causes Idiopathic Pulmonary Arterial Hypertension." *European Respiratory Journal* 53 (3): 1801609. https://doi.org/10.1183/13993003.01609-2018.
Wang, Yufeng, Qiaoling Feng, Caixia Ji, Xiaohua Liu, Li Li, and Jinyong Luo. 2017. "RUNX3 Plays an Important Role in Mediating the BMP9-Induced Osteogenic Differentiation of Mesenchymal Stem Cells." *International Journal of Molecular Medicine* 40 (6): 1991–99. https://doi.org/10.3892/ijmm.2017.3155.
Wei, Zhenquan, Richard M Salmon, Paul D Upton, Nicholas W Morrell, and Wei Li. 2014. "Regulation of Bone Morphogenetic Protein 9 (BMP9) by Redox-Dependent Proteolysis." *The Journal of Biological Chemistry* 289 (45): 31150–59. https://doi.org/10.1074/jbc.M114.579771.
West, James, Julie Harral, Kirk Lane, Yupu Deng, Brian Ickes, Daniel Crona, Sebastian Albu, Duncan Stewart, and Karen Fagan. 2008. "Mice Expressing BMPR2R899X Transgene in Smooth Muscle Develop Pulmonary Vascular Lesions." *American Journal of Physiology. Lung Cellular and Molecular Physiology* 295 (5): L744-55. https://doi.org/10.1152/ajplung.90255.2008.
Wick, Marilee J., Julie W. Harral, Zoe L. Loomis, and Edward C. Dempsey. 2018. "An Optimized Evans Blue Protocol to Assess Vascular Leak in the Mouse." *Journal of Visualized Experiments*, no. 139 (September). https://doi.org/10.3791/57037.
Wiercinska, Eliza, Lucia Wickert, Bernd Denecke, Harun M. Said, Jafar Hamzavi, A. M. Gressner, Midori Thorikay, et al. 2006. "Id1 Is a Critical Mediator in TGF-β-Induced Transdifferentiation of Rat Hepatic Stellate Cells." *Hepatology* 43 (5): 1032–41. https://doi.org/10.1002/hep.21135.
Wood, Jennifer H., Jingxu Guo, Nicholas W. Morrell, and Wei Li. 2019. "Advances in the Molecular Regulation of Endothelial BMP9 Signalling Complexes and Implications for Cardiovascular Disease." *Biochemical Society Transactions* 47 (3): 779–91. https://doi.org/10.1042/BST20180137.
Wooderchak-Donahue, Whitney L, Jamie McDonald, Brendan O'Fallon, Paul D Upton, Wei Li, Beth L Roman, Sarah Young, et al. 2013. "BMP9 Mutations Cause a Vascular-Anomaly Syndrome with Phenotypic Overlap with Hereditary Hemorrhagic Telangiectasia." *American Journal of Human Genetics* 93 (3): 530–37. https://doi.org/10.1016/j.ajhg.2013.07.004.
Wu, N., Y. Zhao, Y. Yin, Y. Zhang, and J. Luo. 2010. "Identification and Analysis of Type II TGF- Receptors in BMP-9-Induced Osteogenic Differentiation of C3H10T1/2 Mesenchymal Stem Cells." *Acta Biochimica et Biophysica Sinica* 42 (10): 699–708.

https://doi.org/10.1093/abbs/gmq075.
Xu, Weiling, and Serpil C. Erzurum. 2010. "Endothelial Cell Energy Metabolism, Proliferation, and Apoptosis in Pulmonary Hypertension." In *Comprehensive Physiology*, 1:357–72. Hoboken, NJ, USA: John Wiley & Sons, Inc. https://doi.org/10.1002/cphy.c090005.
Yang, Min, Zerong Liang, Mengliu Yang, Yanjun Jia, Gangyi Yang, Yirui He, Xinrun Li, et al. 2019. "Role of Bone Morphogenetic Protein-9 in the Regulation of Glucose and Lipid Metabolism." *The FASEB Journal* 33 (9): 10077–88. https://doi.org/10.1096/fj.201802544RR.
Yao, Yucheng, Medet Jumabay, Albert Ly, Melina Radparvar, Anthony H. Wang, Raushan Abdmaulen, Kristina I Boström, and K. I. Bostrom. 2012. "CV2 Regulates BMP9 in Mouse and Human Endothelium." *Blood* 119 (21). https://doi.org/10.1182/blood-2011-10-385906.
Yoshimatsu, Yasuhiro, Yulia G Lee, Yuichi Akatsu, Luna Taguchi, Hiroshi I Suzuki, Sara I Cunha, Kazuichi Maruyama, et al. 2013. "Bone Morphogenetic Protein-9 Inhibits Lymphatic Vessel Formation via Activin Receptor-like Kinase 1 during Development and Cancer Progression." *Proceedings of the National Academy of Sciences of the United States of America* 110 (47): 18940–45. https://doi.org/10.1073/pnas.1310479110.
Young, Kira, Barbara Conley, Diana Romero, Eric Tweedie, Christine O'Neill, Ilka Pinz, Louise Brogan, Volkhard Lindner, Lucy Liaw, and Calvin P H Vary. 2012. "BMP9 Regulates Endoglin-Dependent Chemokine Responses in Endothelial Cells." *Blood* 120 (20): 4263–73. https://doi.org/10.1182/blood-2012-07-440784.
Yu, Paul B., Donna Y. Deng, Hideyuki Beppu, Charles C. Hong, Carol Lai, Stefan A. Hoyng, Noriko Kawai, and Kenneth D. Bloch. 2008. "Bone Morphogenetic Protein (BMP) Type II Receptor Is Required for BMP-Mediated Growth Arrest and Differentiation in Pulmonary Artery Smooth Muscle Cells." *Journal of Biological Chemistry* 283 (7): 3877–88. https://doi.org/10.1074/jbc.M706797200.
Zhang, Dahai, Teruo Utsumi, Hui-Chun Huang, Lili Gao, Panjamaporn Sangwung, Chuhan Chung, Kazunori Shibao, et al. 2011. "Reticulon 4B (Nogo-B) Is a Novel Regulator of Hepatic Fibrosis." *Hepatology* 53 (4): 1306–15. https://doi.org/10.1002/hep.24200.
Zhang, Xiaoyan, Sha Li, Yunfeng Zhou, Wen Su, Xiongzhong Ruan, Bing Wang, Feng Zheng, Margaret Warner, Jan-Åke Gustafsson, and Youfei Guan. 2017. "Ablation of Cytochrome P450 Omega-Hydroxylase 4A14 Gene Attenuates Hepatic Steatosis and Fibrosis." *Proceedings of the National Academy of Sciences of the United States of America* 114 (12): 3181–85. https://doi.org/10.1073/pnas.1700172114.
Zhou, J., P.-L. Lee, C.-S. Tsai, C.-I. Lee, T.-L. Yang, H.-S. Chuang, W.-W. Lin, et al. 2012. "Force-Specific Activation of Smad1/5 Regulates Vascular Endothelial Cell Cycle Progression in Response to Disturbed Flow." *Proceedings of the National Academy of Sciences* 109 (20): 7770–75. https://doi.org/10.1073/pnas.1205476109.
Zhu, Jia-Hui, Yun-Peng Liao, Fu-Shu Li, Ying Hu, Qin Li, Yan Ma, Han Wang, Ya Zhou, Bai-Cheng He, and Yu-Xi Su. 2018. "Wnt11 Promotes BMP9-Induced Osteogenic Differentiation through BMPs/Smads and P38 MAPK in Mesenchymal Stem Cells." *Journal of Cellular Biochemistry* 119 (11): 9462–73. https://doi.org/10.1002/jcb.27262.
Zhu, Na, Michael W Pauciulo, Carrie L Welch, Katie A Lutz, Anna W Coleman, Claudia Gonzaga-Jauregui, Jiayao Wang, et al. 2019. "Novel Risk Genes and Mechanisms Implicated by Exome Sequencing of 2,572 Individuals with Pulmonary Arterial Hypertension." *BioRxiv*, February, 550327. https://doi.org/10.1101/550327.

Acknowledgements

Dr. Paul Upton and Prof. Nicholas Morrell helped design this project, advised on experimental technique and data analysis, and reviewed this thesis. Dr. Paul Upton also helped create many of the reagents and protocols used herein, including the *BRE*-hMEC cells, ELISA protocols, chromatography reagents, solutions administered to animals, ALK1 luciferase signalling protocol etc. All animal work was undertaken with Dr. Alexi Crosby and Stephen Moore, who carried out regulated procedures. Mark Southwood carried out histological analyses of samples. Dr. Rick Salmon created BMP9 variant expression vectors and transfected HEK-EBNA cells. Dr. Wei Li advised on structural biology, and her group, Dr. Aleksandra Lawera, He Jiang and Dr. Jingxu Guo, supplied reagents such as Pro:BMP10, Pro:BMP9 and peristaltic pumps. Dr. Lydia Ruiz Llorente (Centro de Investigaciones Biológicas Madrdrid) prepared expression vectors for nonsense variants of BMP9 and Drs. Jamie Bentham, Robin Condliffe, Rebecca Mason, Oliver Quarrell, Kelechi Ugonna, Pinar Bayrak-Toyndemir, and Jamie McDonald collected samples from patient carriers and relatives. Dr. Stefan Gräf and his group, including Drs. Marta Bleda and Matthias Haimel, carried out the *in silico* analysis which identified pathogenic BMP9 variants. Dr. James Liley helped advise on statistical testing. Dr. Emilia Swietlik assessed clinical characteristics in PAH patients according to their *GDF2* mutation status or circulating BMP9 levels, which informed experiments herein. Dr. Swietlik, also helped supply plasma samples collected from different blood vessels, as did Drs. Joanna Pepke-Zaba, Gary Polwarth, Kasia Zalewska and Sonja Boyle. Dr. Mattia Frontini (Department of Haematology, University of Cambridge) carried out RNA sequencing and data analysis. PhD students Emily Groves, Jennifer Wood, Joy Sih, and Bin Liu, and Drs. Benjamin Dunmore and Ian Horan provided advice, assistance, reagents and support.

This PhD was funded by the British Heart Foundation (Grant № FS/14/59/31282). Additional resources, including animals were from the British Heart Foundation programme grant awarded to Prof. Morrell.

British Heart Foundation